

**COLUMN-SUPPORTED EMBANKMENTS: FULL-SCALE TESTS AND
DESIGN RECOMMENDATIONS**

Joel A. Sloan

Dissertation submitted to the faculty of the Virginia Polytechnic Institute and State
University in partial fulfillment of the requirements for the degree of

Doctor of Philosophy
In
Civil Engineering

George M. Filz (Chair)
James G. Collin
Russell A. Green
James K. Mitchell
Erik C. Westman

May 26, 2011
Blacksburg, VA

Keywords:
Bridging layers
Column-supported embankment
Geosynthetic reinforcement
Load transfer platform
Settlement

COLUMN-SUPPORTED EMBANKMENTS: FULL-SCALE TESTS AND DESIGN RECOMMENDATIONS

Joel A. Sloan

ABSTRACT

When an embankment is to be constructed over ground that is too soft or compressible to adequately support the embankment, columns of strong material can be placed in the soft ground to provide the necessary support by transferring the embankment load to a firm stratum. This technology is known as column-supported embankments (CSEs). A geosynthetic-reinforced load transfer platform (LTP) or bridging layer may be constructed immediately above the columns to help transfer the load from the embankment to the columns. There are two principal reasons to use CSEs: 1) accelerated construction compared to more conventional construction methods such as prefabricated vertical drains (PVDs) or staged construction, and 2) protection of adjacent facilities from distress, such as settlement of existing pavements when a roadway is being widened. One of the most significant obstacles limiting the use of CSEs is the lack of a standard design procedure which has been properly validated.

This report and the testing described herein were undertaken to help resolve some of the uncertainty regarding CSE design procedures in light of the advantages of the CSE technology and potential for significant contributions to the Strategic Highway Research Program, which include accelerated construction and long-lived facilities. Twelve design/analysis procedures are described in this report, and ratings are assigned based on information available in the literature.

A test facility was constructed and the facility, instrumentation, materials, equipment, and test procedures are described. A total of 5 CSE tests were conducted with 2 ft diameter columns in a square array. The first test had a column center-to-center spacing of 10 ft and the remaining four tests had center-to-center spacings of 6 ft. The Adapted Terzaghi Method of determining the vertical stress on the geosynthetic reinforcement and the Parabolic Method of determining the tension in the geosynthetic reinforcement provide the best agreement with the test results. The tests also illustrate the importance of soft soil support in CSE performance and behavior.

A generalized formulation of the Adapted Terzaghi Method for any column/unit cell geometry and two layers of embankment fill is presented, and two new formulations of the Parabolic Method for triangular arrangements is described. A recommended design

procedure is presented which includes use of the GeogridBridge Excel workbook described by Filz and Smith (2006, 2007), which was adapted for both square and triangular column arrangements. GeogridBridge uses the Adapted Terzaghi Method and the Parabolic Method in a load-displacement compatibility design approach. For completeness, recommended quality control and quality assurance procedures are also provided, and a new guide specification is presented.

ACKNOWLEDGEMENTS

I would like to thank my co-advisors Drs. George Filz and Jim Collin for the guidance they provided during this research. Both provided valuable insights to this research and served as great examples of engineering professionals and researchers.

I would also like to thank the other members of my committee, Professors Russell Green, Jim Mitchell, and Erik Westman, for the direction they provided to the research. Drs. Vern Schaefer, Jie Han, and Barry Christopher of the Strategic Highway Research Program 2 Project R02 (SHRP2 R02) team, also provided valuable support and input to this research.

I would like to thank all of the students who assisted in the CSE field work: Steve Adamchak, Amanda Barngrover, Kolleen Carlson, Conrad Cho, Peter Duvigneaud, Bernadette McManamon, Alex Reeb, Evan Ruggles, and Lisa Vanhoute. The five embankments totaled over 2,100 tons of gravel, 3,250 ft³ of geof foam, 24 rolls of geogrid, and countless hours in the Bobcat. Without the help of these students, the field work would not have been possible.

I would also like to thank Bonnie Franklin of the Department of Civil and Environmental Engineering. Her efforts to procure the materials necessary for completion of the field work made this research possible.

Dwight Paulette, Jon Wooge, and Chad Keith of Virginia Tech's Kentland Farm assisted in selection and provision of a suitable site for the CSE test facility, excavation of the site for the test facility, and assisted in unloading materials used in the CSE tests.

I would like to thank and the Department of Civil and Environmental Engineering at the U.S. Air Force Academy, for sponsoring me for this degree.

Support for this research was provided by the SHRP2 R02 project and the Exploring Interfaces through Graduate Education and Research (EIGER) program. Tensar® Corporation generously donated all of the geogrid used in the embankment tests.

Finally, and most importantly, I would especially like to thank my wife, Nancy, for the support and companionship that she has provided me during our 10 years of marriage and during the completion of this work.

DISCLAIMER: The views expressed in this dissertation are those of the author and do not necessarily reflect the official policy or position of the United States Air Force, the Department of Defense or the U.S. Government.

TABLE OF CONTENTS

ACKNOWLEDGEMENTS.....	iii
TABLE OF CONTENTS.....	v
LIST OF FIGURES	ix
LIST OF TABLES.....	xiii
LIST OF SYMBOLS	xv
Chapter 1 INTRODUCTION.....	1
1.1 SHRP2 R02 PROJECT AND THIS DISSERTATION	1
1.2 OVERVIEW OF THE REMAINDER OF THIS DISSERTATION	2
Chapter 2 CSE BACKGROUND AND OVERVIEW OF DESIGN METHODS	3
2.1 CSE DESCRIPTION.....	3
2.1.1 SHRP2 Applicability.....	4
2.1.2 Geologic and Geometric Applicability	5
2.1.3 Competing Technologies.....	5
2.1.4 Advantages and Disadvantages.....	5
2.1.5 Time and Cost Considerations	6
2.1.6 Complimentary Technologies	6
2.1.7 Case Histories.....	6
2.2 DESIGN AND ANALYSIS METHODS.....	7
Chapter 3 DESCRIPTION AND PRELIMINARY RATING OF CSE DESIGN AND ANALYSIS PROCEDURES	15
3.1 DESCRIPTION OF RATING METHODS	15
3.2 DESCRIPTION OF CSE DESIGN AND ANALYSIS PROCEDURES, AND DISCUSSION OF PRELIMINARY RATINGS.....	19
3.2.1 Adapted Guido Method.....	19
3.2.2 Adapted Terzaghi Method.....	21
3.2.3 British Standard 8006 Method	24

3.2.4	Cao et al. Method	29
3.2.5	Chen et al. Method	31
3.2.6	Collin Method	33
3.2.7	Filz and Smith Method.....	36
3.2.8	Hewlett and Randolph Method	39
3.2.9	Japanese PWRC Method.....	42
3.2.10	Kempfert et al. (EBGO 6.9) Method.....	44
3.2.11	Naughton Method.....	47
3.2.12	Swedish Method.....	50
3.3	METHODS TO DETERMINE TENSION AND STRAIN IN THE GEOSYNTHETIC REINFORCEMENT	52
3.3.1	Parabolic Method	53
3.3.2	Tensioned Membrane Method	53
3.3.3	Kempfert et al. (EBGEO 6.9) Method	54
Chapter 4 DESCRIPTION OF CSE TEST FACILITY AND INSTRUMENTATION		
		55
4.1	MOTIVATION FOR CSE TESTS	55
4.2	DESCRIPTION OF THE CSE TEST FACILITY	58
4.3	TEST CONCEPT	59
4.4	ALTERNATIVE METHODS CONSIDERED.....	63
4.5	GEOFOAM DISSOLVER DELIVERY SYSTEM	64
4.6	INSTRUMENTATION.....	66
Chapter 5 MATERIALS, EQUIPMENT, AND PROCEDURES USED IN CSE TESTS.....		
		75
5.1	MATERIAL PROPERTIES.....	75
5.1.1	Properties of Gravel Fill.....	75
5.1.2	Geogrid.....	79
5.1.3	Geofoam	79
5.1.4	Geofoam Dissolver and Geonet	81
5.2	EQUIPMENT AND FILL PLACEMENT	83
5.3	TRAFFICKING PROCEDURES	85
5.4	CSE TEST PROCEDURES	87

Chapter 6 GOALS, DESCRIPTIONS, AND RESULTS OF CSE TESTS	91
6.1 TEST PROGRAM GOALS	91
6.2 TEST PROGRAM OVERVIEW	91
6.3 DESCRIPTION AND RESULTS OF CSE TEST #1	92
6.4 DESCRIPTION AND RESULTS OF CSE TEST #2	99
6.5 DESCRIPTION AND RESULTS OF CSE TEST #3	111
6.6 DESCRIPTION AND RESULTS OF CSE TEST #4	118
6.7 DESCRIPTION AND RESULTS OF CSE TEST #5	129
6.8 SUMMARY OF RESULTS AND CONCLUSIONS FROM CSE #2 TO #5	137
Chapter 7 ANALYSIS OF CSE TEST RESULTS	146
7.1 COMPARISON OF STRESS REDUCTION RATIOS BEFORE DISSOLVING GEOFOAM	146
7.2 COMPARISON OF DATA TO METHODS FOR DETERMINING THE TENSION/STRAIN IN THE GEOSYNTHETIC	148
7.3 COMPARISON OF DATA TO METHODS FOR DETERMINING THE VERTICAL STRESS ON THE GEOSYNTHETIC	155
7.4 OBSERVATIONS FOR CRITICAL HEIGHT	161
7.5 TOTAL SETTLEMENT MAGNITUDE FOR EMBANKMENTS ABOVE THE CRITICAL HEIGHT	163
Chapter 8 CSE DESIGN IMPROVEMENTS AND RECOMMENDATIONS	165
8.1 DESIGN IMPROVEMENTS	165
8.1.1 Generalized Formulation of the Adapted Terzaghi Method of Arching	165
8.1.2 Parabolic Method for Other Column Arrangements	170
8.1.2a Axisymmetric Parabolic Method with Radially-Isotropic Reinforcement	171
8.1.2b Parabolic Method for Triangular Column Arrangements and Bidirectional Geosynthetic	175
8.1.3 Comparison of Parabolic Method with Numerical Modeling	178
8.2 RECOMMENDED DESIGN PROCEDURE	180

Chapter 9 QC/QA AND SPECIFICATIONS FOR CSE.....	196
9.1 QUALITY CONTROL AND QUALITY ASSURANCE.....	196
9.1.1 QC/QA Method Description: Embankment Test Section.....	198
9.1.2 QC/QA Method Description: Geosynthetics Verification	199
9.1.3 QC/QA Method Summary: Testing of Embankment Fill Materials	200
9.1.4 QC/QA Method Summary: Monitoring	201
9.2 CSE PERFORMANCE GUIDE SPECIFICATION	201
Chapter 10 SUMMARY, CONCLUSIONS, AND RECOMMENDATIONS.....	216
10.1 SUMMARY OF WORK ACCOMPLISHED.....	216
10.2 CONCLUSIONS	217
10.3 SUMMARY OF RECOMMENDATIONS FOR CSE DESIGN.....	218
10.4 RECOMMENDATIONS FOR FURTHER RESEARCH	218
REFERENCES	221
APPENDIX A: FOIL STRAIN GAGE CALIBRATION	229
APPENDIX B: GEOGRID TESTING	244

LIST OF FIGURES

Figure 2.1: Diagram of a geosynthetic-reinforced column-supported embankment.	4
Figure 2.2: CSE cross-section showing relevant parameters.	8
Figure 2.3: Unit cells for square and equilateral triangular column arrangements.	8
Figure 4.1: Picture of the CSE test facility.	59
Figure 4.2: CSE plan and cross-section views with 4 precast moveable columns and sample embankment.	59
Figure 4.3: Simplified cross-section of test facility and embankment.	60
Figure 4.4: CSE test facility with base layer of polyethylene plastic, geonet, and 9-column array.	61
Figure 4.5: CSE test facility with geofoam and geofoam dissolver delivery system.	61
Figure 4.6: Reinforced fill placement.	62
Figure 4.7: Column and geofoam dissolver distribution system for CSE Tests #2 to #5.	65
Figure 4.8: Geofoam dissolver distribution system installation and calibration with water.	65
Figure 4.9: Central column with load cells and webcams. The steel plate at the top of the picture is placed over the load cells prior to placing fill.	68
Figure 4.10: Earth pressure cell installation.	68
Figure 4.11: Stainless steel wire and nylon tubing (top left), draw-wire sensors (top right), and aluminum housing for lead-wire extensometers (bottom) used in CSE tests.	69
Figure 4.12: Mounting bracket, aluminum housing, and protective tubing for lead-wire extensometers.	70
Figure 4.13: Lead-wire extensometers, instrumentation wiring, geofoam dissolver piping, and geogrid placement.	70
Figure 4.14: Settlement profiler and data acquisition system.	71
Figure 4.15: Plot of corrected gage strain ($CF = 1.22$) and machine strain during single-rib load test on Tensar® BX1500 geogrid.	73
Figure 4.16: Picture of survey grid and total station on the embankment surface.	74
Figure 5.1: Modified Proctor compaction results for WVDOT Class 1 shown with ZAV for $G_s = 2.74$	77
Figure 5.2: Pre- and post-testing gradations of fill in CSE tests along with WVDOT Class 1 Requirements.	77
Figure 5.3: Typical stress-strain curves for geofoam in CSE #1 and CSEs #2 - #5.	80
Figure 5.4: Creep test results of geofoam used in CSE #1.	81
Figure 5.5: Typical creep test results of geofoam used in CSEs #2 - #5 for applied stress in psi and percentage of geofoam compressive strength at 5% strain.	82
Figure 5.6: Fill placement with Bobcat 643 from one side of the embankment to the other in order to tension the geogrid and prevent slack.	84
Figure 5.7: Bobcat 643 and Wacker RD11A used for placement and compaction of gravel fill.	85
Figure 5.8: Moisture-density testing with the Troxler 3440 gauge.	85
Figure 5.9: Pictures showing the trafficking process and the additional settlement induced by trafficking loads.	87
Figure 6.1: Instrumentation locations for CSE Test #1.	93
Figure 6.2: Cross-section of CSE #1.	93

Figure 6.3: Picture of CSE #1 prior to dissolving the geofoam to remove support.....	94
Figure 6.4: Picture of the differential settlement in CSE #1 after dissolving the geofoam.	95
Figure 6.5: Plots of surface deformations in CSE #1 from total station survey (top) and LIDAR scan (bottom).	96
Figure 6.6: EPC results from CSE #1.	97
Figure 6.7: Load cell results from CSE #1.	97
Figure 6.8: Strain measurements from CSE #1 (LWEs 55, 56, 57, 58).....	98
Figure 6.9: Strain measurements from CSE #1 (LWEs 59, 60, 97, 98).....	98
Figure 6.10: Surface settlement locations and terminology for CSE tests.	100
Figure 6.11: EPC, load cell, and settlement profiler tube locations for CSE #2.	104
Figure 6.12: Strain gage locations on geogrid layer #1 at Elev = 0 ft.	105
Figure 6.13: Strain gage locations on geogrid layer #2 at Elev = 0.5 ft.	105
Figure 6.14: EPC results from CSE #2.	106
Figure 6.15: Load cell results from CSE #2.	106
Figure 6.16: Datalogger panel, EPC, and load cell temperatures from CSE #2.	107
Figure 6.17: Lead-wire extensometer strain for CSE #2 (Sensors 59, 60, 97, 98).	107
Figure 6.18: Foil strain gage data from CSE #2 for geogrid layer #2, Elev = 0.5 ft.	108
Figure 6.19: Plot of before-trafficking (top) and after-trafficking (bottom) elevations for CSE #2 showing differential surface settlement between columns.	109
Figure 6.20: Settlements from profiler tubes #1 and #2 for CSE #2.	110
Figure 6.21: Webcam photo shortly after pumping in the geofoam dissolver, showing partial dissolution of the geofoam in CSE #2.	111
Figure 6.22: Picture of CSE #3.	113
Figure 6.23: Location of instrumentation for CSE #3.	113
Figure 6.24: Webcam picture from CSE #3 showing partially dissolved geofoam, geogrid, and select fill.	114
Figure 6.25: Webcam picture from CSE #3 showing deflected geogrid and select fill after geofoam is fully dissolved.	114
Figure 6.26: EPC data from CSE #3.	115
Figure 6.27: Load cell data from CSE #3.	115
Figure 6.28: Strain data from CSE #3 (Sensors 56, 58).....	116
Figure 6.29: Strain data from CSE #3 (Sensors 60, 97, 98).....	116
Figure 6.30: Surface settlement of CSE #3 before (top) and after (bottom) trafficking.	117
Figure 6.31: Settlement from profiler tube #2 before and after trafficking.	118
Figure 6.32: Picture of CSE #4, note instrumentation panel, settlement profiler and tubes, and total station.	122
Figure 6.33: Plan and cross-section drawings of CSE #4.	123
Figure 6.34: Instrumentation locations for CSE #4.	124
Figure 6.35: EPC data from CSE #4.	124
Figure 6.36: Load cell readings from CSE #4 along with hourly rainfall.	125
Figure 6.37: Lead-wire extensometer strain from CSE #4 (Sensors 55, 56, 57, 58).	125
Figure 6.38: Lead-wire extensometer strain from CSE #4 (Sensors 60, 97, 98).	126
Figure 6.39: Foil strain gage data from geogrid layer #1 (Elev = 0.0) from CSE #4.	126
Figure 6.40: Foil strain gage data from geogrid layer #2 (Elev = 0.5 ft) from CSE #4.	127

Figure 6.41: After-trafficking total settlement within unit cell from CSE #4 (average settlement = 1.2 in.).	127
Figure 6.42: Tube #1 settlement from CSE #4 as a function of days after dissolving geof foam.	128
Figure 6.43: Tube #2 settlement from CSE #4 as a function of days after dissolving geof foam.	128
Figure 6.44: Picture of CSE #5 upon embankment completion.	131
Figure 6.45: Instrumentation locations for CSE #5.	132
Figure 6.46: EPC data from CSE #5.	132
Figure 6.47: Load cell data from CSE #5.	133
Figure 6.48: Panel, EPC, and Load Cell temperature from CSE #5.	133
Figure 6.49: Strain data from CSE #5 (Sensors 55, 56, 47, 58).	134
Figure 6.50: Strain from CSE #5 (Sensors 14, 97, 60).	134
Figure 6.51: Picture of CSE #5 differential settlement after trafficking.	135
Figure 6.52: Settlement plot of CSE #5 after trafficking.	135
Figure 6.53: Tube #1 settlement from CSE #5.	136
Figure 6.54: Tube #2 settlement from CSE #5.	136
Figure 6.55: Locations of geogrid strain measurements reported in Table 6.13.	140
Figure 6.56: Maximum differential settlement vs embankment height (CSEs #2 to #5).	143
Figure 6.57: $DSBR_d$ vs normalized embankment height (CSEs #2 to #5).	143
Figure 7.1: SRRs measured in CSE tests versus SRRs calculated with GeogridBridge.	148
Figure 7.2: Comparison of measured and calculated strains (4 – 24 hr).	153
Figure 7.3: Comparison of measured and calculated strains (7 – 14 day).	153
Figure 7.4: Comparison of measured and calculated vertical deflections (7 to 14 day).	154
Figure 7.5: Possible distributions of vertical stress on the geosynthetic reinforcement.	156
Figure 7.6: Comparison of predicted and measured vertical loads on the geosynthetic reinforcement (CSEs #2 to #5).	157
Figure 7.7: Unit cell geometries and definition of s' .	162
Figure 7.8: Comparison of critical height from McGuire (2011) and the current study.	162
Figure 8.1: Cross-sectional geometry for generalized Adapted Terzaghi Method.	167
Figure 8.2: Plan view of CSE unit cell and column/pile areas.	169
Figure 8.3: Conceptual illustration of biaxial and radially-isotropic geosynthetic stiffness.	170
Figure 8.4: Area contributing to the load on the geosynthetic reinforcement in the Parabolic Method for a square arrangement of square columns.	171
Figure 8.5: Definition sketch for Axisymmetric Parabolic Method with radially-isotropic reinforcement.	172
Figure 8.6: Square/rectangular and triangular geometries for radially-isotropic geosynthetics and the axisymmetric parabolic method.	175
Figure 8.7: Diagram of triangular column arrangements with biaxial geogrid.	177
Figure 8.8: Strain from numerical analyses (Filz and Plaut 2009) compared to strain from the Parabolic Method for square column arrangements.	179

Figure 8.9: Strain from numerical analyses (Filz and Plaut 2009) compared to strain from the Parabolic Method for triangular column arrangements	180
Figure 8.10: Definition sketch for a geosynthetic reinforced column supported embankment.....	193
Figure 8.11: Column geometries (round or square) and unit cell areas for square/rectangular or triangular arrangements.....	193
Figure 8.12: Effective column width for competent upper layer.....	195
Figure 8.13: Definition of L_e , L_b , and L_p	195
Figure A1: Instron 4411 – constant rate of strain geogrid tensile testing machine	232
Figure A2: Example of rubber distribution system below a geogrid layer.....	233
Figure A3: Strain gage connected to external terminals with strain relief	234
Figure A4: Strain gage encased in M-Coat J-3 Protective Coating	234
Figure A5: Strain gage encased in protective coating and wrapped in electrical tape	235
Figure A6: Calibration of EP-230DS foil strain gages for CSE #2	239
Figure A7: Calibration of EP-230DS foil strain gages for CSE #2	239
Figure A8: Calibration of EP-230DS foil strain gages for CSE #2	240
Figure A9: Calibration of EP-230DS foil strain gages for CSE #2	240
Figure A10: Calibration of EP-230DS foil strain gages for CSE #2	241
Figure A11: Calibration of EP-125AD foil strain gages for CSE #4	241
Figure A12: Calibration of EP-125AD foil strain gages for CSE #4	242
Figure A13: Calibration of EP-125AD foil strain gages for CSE #4	242
Figure A14: Calibration of EP-125AD foil strain gages for CSE #4	243
Figure A15: Calibration of EP-125AD foil strain gages for CSE #4	243
Figure B1: Instron 4411, constant rate of strain testing machine	244
Figure B2: Example of ruptured geogrid sample.....	248

LIST OF TABLES

Table 2.1: Typical CSE design/analysis procedure inputs and outputs.	9
Table 2.2: List of CSE design/analysis procedures and their primary references.	12
Table 2.3: Design/Analysis procedure characterization matrix.	14
Table 3.1: Preliminary ratings of the CSE design/analysis procedures.	18
Table 4.1: Instrumentation used in CSE tests.	67
Table 5.1: Gradation requirements of VDOT 21B and WVDOT Class 1.	76
Table 5.2: Properties of WVDOT Class 1 gravel as-delivered and post-testing.	78
Table 5.3: Summary of peak and large-strain friction angles for triaxial tests of high density 21B from Duncan et al. (2007).	78
Table 5.4: Properties of geofoam used in CSE tests.	80
Table 5.5: Comparison of the fluid properties of d-limonene (from Clara et al. 2009) and water.	83
Table 5.6: Properties of geonet used in CSE tests.	83
Table 5.7: Bobcat 643 specifications.	84
Table 6.1: CSE test characteristics.	91
Table 6.2: CSE geometry and material properties.	92
Table 6.3: Timeline and properties for CSE #1.	94
Table 6.4: Timeline and properties of CSE #2.	104
Table 6.5: Summary of surface and base settlements from CSE #2.	110
Table 6.6: Timeline and properties of CSE #3.	112
Table 6.7: Summary of surface and base settlements from CSE #3.	118
Table 6.8: Timeline and properties of CSE #4.	122
Table 6.9: Summary of surface and base settlements from CSE #4.	129
Table 6.10: Timeline and properties of CSE #5.	131
Table 6.11: Summary of surface and base settlements from CSE #5.	137
Table 6.12: Calculated SRRs from CSEs #2 to #5 from EPCs and load cells before dissolving geofoam.	138
Table 6.13: Geogrid strains and EPC stresses after dissolving geofoam.	139
Table 6.14: Summary of average CSE settlements before trafficking (BT).	141
Table 6.15: Summary of average CSE settlements after trafficking (AT).	141
Table 7.1: properties used in GeogridBridge soft soil support analysis.	147
Table 7.2: Calculated strains (%) for a given deflection.	149
Table 7.3: Values of geogrid stiffness used to determine approximate value for analysis.	150
Table 7.4: Recommendations and findings for design/analysis procedures to determine the tension in the geosynthetic reinforcement.	154
Table 7.5: Parameters for comparison of EPC readings to design methods.	157
Table 7.6: Recommendations and findings for design/analysis procedures to determine the load on the geosynthetic reinforcement.	160
Table 7.7: Summary of measured and predicted values of settlement ratios for embankments above the critical height.	164
Table 8.1: Column types, capacities, lengths, diameters and approximate embankment heights based on column capacity and spacing.	194

Table A1: Summary of foil strain gage performance in CSEs #2 and #4.....	238
Table B1: List of Geogrid Rolls Tested for Tensile Strength.....	245
Table B2: Summary of geogrid testing, machine direction	246
Table B3: Summary of geogrid testing, transverse machine direction.....	247
Table B4: Approximate Number of Ribs per Linear Foot for Material Type and Testing Direction	248
Table B5: Summary of Average Percent Increase in Strength above MARV for Each Material Type Tested	249

LIST OF SYMBOLS

a	Square column width
A	Column tributary area (total plan view area within the unit cell)
A_c	Column cross-sectional area
A_p	Plan view area contributing to the vertical stress on the geosynthetic reinforcement
a_s	Area replacement ratio
A_s	Plan view area of soil with the unit cell
c	Clear span between columns
C_c	Arching coefficient used in BS8006 (1995)
d	Geosynthetic deflection at mid-span between columns
d_b	Maximum base deflection of the geosynthetic
d_c	Round column diameter
d_s	Total surface settlement for embankments above the critical height
d_w	Depth to water table
E	Young's modulus or pile efficacy
H	Embankment height
H_{crit}	Critical height (minimum height with zero differential settlement)
$H_{crit,AT}$	Critical height after trafficking
$H_{crit,BT}$	Critical height before trafficking
h_g	Parameter used in the Kempfert et al. (2004) method
J	Stiffness of the geosynthetic reinforcement
K	Lateral earth pressure coefficient
K_p	Passive lateral earth pressure coefficient
p	Vertical stress on the geosynthetic reinforcement or column perimeter distance
p_c	Vertical stress on the column tops from Marston's equation
q	Embankment surcharge
s	Column center-to-center spacing
S	Settlement
s_g	Parameter used in the Kempfert et al. (2004) method
SRR	Stress reduction ratio
T	Tension in the geosynthetic reinforcement between columns
w	Roll width of geosynthetic
W_T	Vertical line load between columns
γ	Soil unit weight
ε	Average strain in the geosynthetic reinforcement between columns

$\lambda_{1,2}$	Parameters used in the Kempfert et al. (2004) method
ν	Poisson's ratio
σ_{soil}	Vertical stress on the geosynthetic reinforcement
φ	Friction angle
χ	Parameter used in the Kempfert et al. (2004) method

CHAPTER 1

INTRODUCTION

1.1 SHRP2 R02 PROJECT AND THIS DISSERTATION

Many geoconstruction technologies, including some that have been in existence for several decades, face both technical and non-technical obstacles preventing broader utilization in transportation infrastructure projects. The research team for Strategic Highway Research Program 2, Project Number R02 (SHRP2 R02) *Geotechnical Solutions for Soil Improvement, Rapid Embankment Construction, and Stabilization of the Pavement Working Platform* is investigating the state of practices of transportation project engineering, geotechnical engineering, and earthwork construction to identify and assess methods to advance the use of geoconstruction technologies. Such technologies are often underutilized in current practice, and they offer significant potential to achieve one or more of the SHRP2 Renewal objectives, which are rapid renewal of transportation facilities, minimal disruption of traffic, and production of long-lived facilities. Project R02 encompasses a broad spectrum of materials, processes, and technologies within geotechnical engineering and geoconstruction that are applicable to one or more of the following “elements” of construction (as defined in the project scope): (1) new embankment and roadway construction over unstable soils; (2) roadway and embankment widening; and (3) stabilization of pavement working platforms.

Column-supported embankments (CSEs) apply to elements 1 and 2 of the SHRP2 R02 project and are ranked highly for use in new embankments and widening of existing embankments. CSEs have the potential for significant contributions to the SHRP2 renewal objectives of rapid renewal of transportation facilities and production of long-lived facilities. One of the most significant obstacles limiting the use of CSEs is the lack of a standard design procedure which has been properly validated. At least 12 different procedures were identified in the course of this research, and the literature documents the widely varying results produced by the procedures (e.g. Love and Milligan 2003, McGuire and Filz 2008). Due the variation in design procedures, field tests were required in addition to a review of the literature in order to make reliable recommendations for CSE design procedures.

This dissertation describes the literature review and field tests conducted for the SHRP2 R02 development project for CSE design, design improvements made, and the resulting design recommendations. Guidelines for specifications and QC/QA procedures are also provided for completeness.

Some of the formatting and content in this dissertation is common to other technologies in SHRP2 R02, such as the rating format for design methods in Chapter 3 and the liquefaction statement contained in the recommended design procedure in Chapter 8. The strong link between the SHRP2 R02 project and this dissertation research resulted in a synergistic use of resources which will hopefully advance both the state-of-the-art and state-of-practice for CSEs.

1.2 OVERVIEW OF THE REMAINDER OF THIS DISSERTATION

Chapter 2 provides an overview of the column-supported embankments technology, summarizes some of the background information found in the SHRP2 R02 Comprehensive Technology Summary (CTS) on CSEs, and provides an introduction to the design principles for CSEs. Chapter 3 provides a description and preliminary ratings of the design and analysis procedures identified in this dissertation. These descriptions and preliminary ratings are taken directly from the SHRP2 R02 Task 10 Assessment of CSEs. The ratings are termed “preliminary” in this dissertation since they were assigned based only on the information about the procedures available in the literature, and before the field testing phase of this research was complete. The final design recommendations, which incorporate results from the field testing, are found in Chapter 8.

Chapter 4 describes the CSE test facility constructed at Virginia Tech and the instrumentation used in the CSE tests. Chapter 5 describes the materials, equipment, and CSE test procedures. Chapter 6 lists the goals of the CSE tests, provides a description of the CSE test parameter variations, and presents the results of the CSE tests. Chapter 7 analyzes the results of the CSE tests and compares data with the CSE design and analysis procedures presented in Chapter 3.

Chapter 8 presents CSE design improvements to include: a generalized formulation of the Adapted Terzaghi method of arching for two layers of embankment fill, Parabolic Methods for determining tension and strain in the geosynthetic reinforcement for triangular column arrangements, and comparison of numerical modeling data to calculations from the Parabolic Methods. Following the design improvements, Chapter 8 also contains the recommended design procedure for CSEs based on the CSE tests and a review of the CSE literature. For completeness, Chapter 9 provides the QC/QA guidance and guide specification for CSEs developed for the SHRP2 R02 project. The recommended design procedure, QC/QA procedures, and specification are also found within CSE products of the SHRP2 R02 Guidance and Selection System. Chapter 10 provides a summary of work accomplished, a summary of conclusions, a summary of design recommendations, and recommendations for further research.

CHAPTER 2

CSE BACKGROUND AND OVERVIEW OF DESIGN METHODS

2.1 CSE DESCRIPTION

When an embankment is to be constructed over ground that is too soft or compressible to adequately support the embankment, columns of strong material can be placed in the soft ground to provide the necessary support by transferring the embankment load to a firm stratum. There are numerous types of columns that may be used for this technology (e.g., aggregate columns, vibro-concrete columns, deep mixing method columns, continuous flight auger piles, driven piles (steel, concrete or timber) with or without pile caps, geotextile encased columns, combined soil stabilization with vertical columns (CSV), or other types of columns). A load transfer platform (LTP) or bridging layer may be constructed immediately above the columns to help transfer the load from the embankment to the columns and also prevent a “bearing capacity” type of failure above the columns. Load transfer platforms generally consist of compacted soil, and they may include geosynthetic reinforcement, in which case, the technology may be referred to as geosynthetic-reinforced column-supported embankments (GRCSE). In this dissertation, GRCSEs and CSEs are both referred to as CSEs.

The important details of soil type and geosynthetic reinforcement used in the load transfer platform depend on the design procedure employed. Load transfer platforms are used more often when the spacing between columns is relatively large, which requires higher load carrying capacity from the columns (e.g., vibro-concrete columns, continuous flight auger piles, or driven piles). Load transfer platforms are also used to minimize differential settlement when the embankment height is low. Stone columns and rammed aggregate piers, because of their lower vertical load capacity, are often spaced close enough together that a load transfer platform or geosynthetic reinforcement may not be necessary. A cross-section view of a GRCSE is shown in Figure 2.1.

There have been many successful installations of column-supported embankments, and case histories with references are listed in Section 2.1.7. There have also been some failures, including excessive deformation and geosynthetic rupture such as described by Camp and Siegel (2006). Success of column-supported embankments is enhanced when existing near-surface soils are competent, the embankment is not excessively thin, and care is exercised in design and construction.

The principal design considerations for column-supported embankments are total settlement, differential settlement, stability, lateral spreading, and tensile capacity of geosynthetic reinforcement, if used. At present, there are at least twelve different design procedures for column-supported embankments. These procedures produce widely varying loads on geosynthetic reinforcement, and most do not include any procedure for calculating differential settlement. One of the principal needs for the future growth of this technology is to develop one or more FHWA endorsed design procedures.

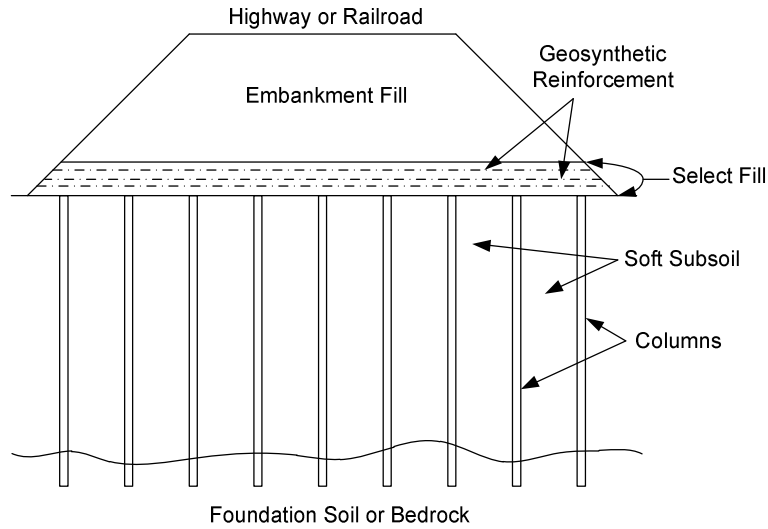


Figure 2.1: Diagram of a geosynthetic-reinforced column-supported embankment.

2.1.1 SHRP2 Applicability

Column-supported embankments apply to Elements 1 and 2 of SHRP2 R02 because they can reduce settlements and improve stability of new embankments over unstable soil, and can reduce differential settlements between new roadway widenings and existing pavements. This technology does not ordinarily apply to Element 3 because columns within the pavement working platform would be too close to the pavement to avoid differential settlements. Column-supported embankments help achieve the SHRP2 renewal objectives of rapid renewal and long-lived facilities because they eliminate the need to wait for settlement to occur and can reduce long-term total and differential settlements. This technology does not help achieve minimal disruption of traffic because it is a technology for new construction, not rehabilitation.

2.1.2 Geologic and Geometric Applicability

Column-supported embankments are typically used on soft compressible clay, peats, and organic soils where large settlements and/or global stability are concerns. Column-supported embankments are most cost-effective on deposits with thicknesses from 15 to 70 feet (5 to 21 m). FHWA (2004) reports depth limits of 10 to 130 ft (3 to 40 m). Dumas et al. (2003) report a depth limit of 120 ft (36 m). Other methods are typically used when the depth of the compressible layer is shallower or deeper than this range. The columns can be floating or end-bearing depending on the site geology and the type of column used. For many CSE applications, the columns are end-bearing.

2.1.3 Competing Technologies

Other technologies for similar applications include preloading with or without PVDs, lightweight fill, removal and replacement, staged construction, geosynthetic reinforcement embankments, and vacuum consolidation (Collin 2004, FHWA 2004, Almeida et al. 2007).

2.1.4 Advantages and Disadvantages

There are two principal reasons to use column-supported embankments. One is to accelerate construction compared to more conventional construction methods (i.e., installing prefabricated vertical drains and constructing the embankment in stages). The other is to protect adjacent facilities from distress, such as settlement of existing pavements when a roadway is being widened. The key obstacles preventing more widespread use of this technology are (1) lack of standard design procedures and (2) lack of knowledge about technology benefits, design procedures, and construction techniques (FHWA 2004, Filz and Smith 2006, Abdullah and Edil 2007b). Also, utilities or inclusions cannot be included within the lower portion of the embankment that may experience large differential settlements (Shiells, personal communication 2009). These obstacles can be overcome by developing a suitable integrated design procedure and expanded training. According to Han and Gabr (2002), Collin (2004), and Abdullah and Edil (2007b), properly designed geosynthetic reinforcement reduces the tendency for lateral spreading and eliminates the need for battered piles supporting the edges of the embankment. The pile type can be chosen based on local economic and environmental considerations (Whyte 2005).

2.1.5 Time and Cost Considerations

Column-supported embankments are typically more expensive than conventional solutions such as preloading with or without PVDs and geosynthetic-reinforced embankments, but CSEs may be less expensive than geofoam. However, considerable time can be saved over PVDs when using column-supported embankments since follow on construction can proceed immediately after the columns are installed. The time savings when using column-supported embankments may outweigh the additional construction cost for time sensitive projects.

2.1.6 Complimentary Technologies

Many of the column technologies from Elements 1 and 2 of SHRP2 R02, such as sand compaction piles, aggregate columns, vibro-concrete columns, continuous flight auger (CFA) piles, combined soil stabilization with vertical columns (CSV), geotextile encased columns (GEC), and deep mixing methods (DMM) are suitable column types for column-supported embankments. Some applications may use lightweight fills in combination with column-supported embankments. A white paper on combining technologies for embankments on soft ground can be found within the SHRP2 R02 guidance and selection system.

2.1.7 Case Histories

Select case histories in the literature include:

- Rancocas Creek Railroad Bridge, New Jersey, reported by Young et al. (2004) and Young et al. (2008)
- I-95/Route 1 Interchange, Virginia, and associated test embankment, reported by Stewart et al. (2004), Navin (2005), Smith (2005), Shiells et al. (2003), Lambrechts and Layhee (2003), and Lambrechts et al. (2003)
- Minnesota Trunk Highway 241 reported by Wachman and Labuz (2008), and Wachman et al. (2010)
- High-Speed Railway Embankment, Germany, as described by Gartung et al. (1996), Brandl et al. (1997), Zanzinger and Gartung (2002), Collin et al. (2006)
- GRCSE Roadway Embankment, Hertsby Finland, as described by Forsman et al. (1999), Forsman (2000), and Huang et al. (2009).

2.2 DESIGN AND ANALYSIS METHODS

Design of CSEs involves calculating the portion of embankment load transferred to the columns through arching and the portion carried by the soft foundation soil. For GRCSEs, the vertical stress on the geosynthetic is used to calculate the tension and strain in the geosynthetic based on an assumed deformed shape.

GRCSEs are complex systems whose performance is influenced by a number of materials and variables, including:

- Strength and compressibility of the soft soil
- Strength and compressibility of the bearing layer on which the columns are founded
- Strength, compressibility, cross-sectional area, length, spacing, and arrangement of the columns or piles and pile caps
- Strength, stiffness, quantity (# of layers), vertical spacing, lateral extent, and type (geogrid, geotextile) of the geosynthetic reinforcement
- Strength and gradation of select fill material in the load transfer platform, if used
- Strength and gradation of general embankment fill material
- Height of the embankment above the tops of the columns
- Surcharge or traffic loading

Comprehensive analysis of these complex systems requires that the effect of each variable is well-understood. Some of these variables (column strength and compressibility, consolidation of soft-soil, strength of the bearing layer) are well-understood independently, but neither the integrated system performance nor the arching and load transfer within the GRCSE are as well understood. Some of the key variables and design parameters are illustrated in Figure 2.2 and Figure 2.3. Typical inputs and outputs for CSE design and analysis procedures are shown, and variables are defined, in Table 2.1.

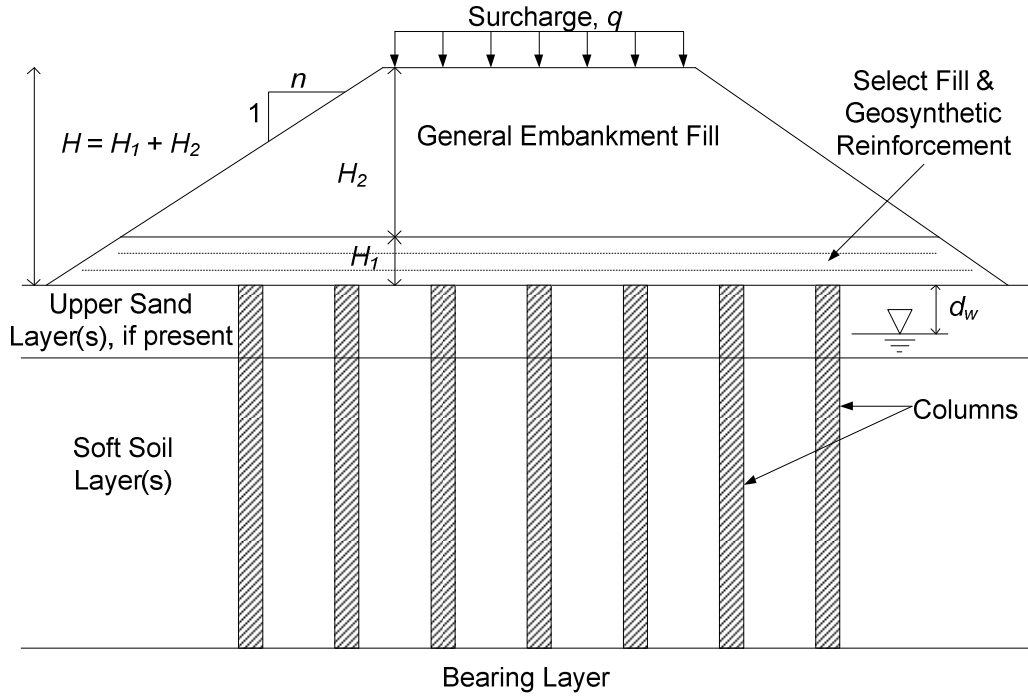


Figure 2.2: CSE cross-section showing relevant parameters.

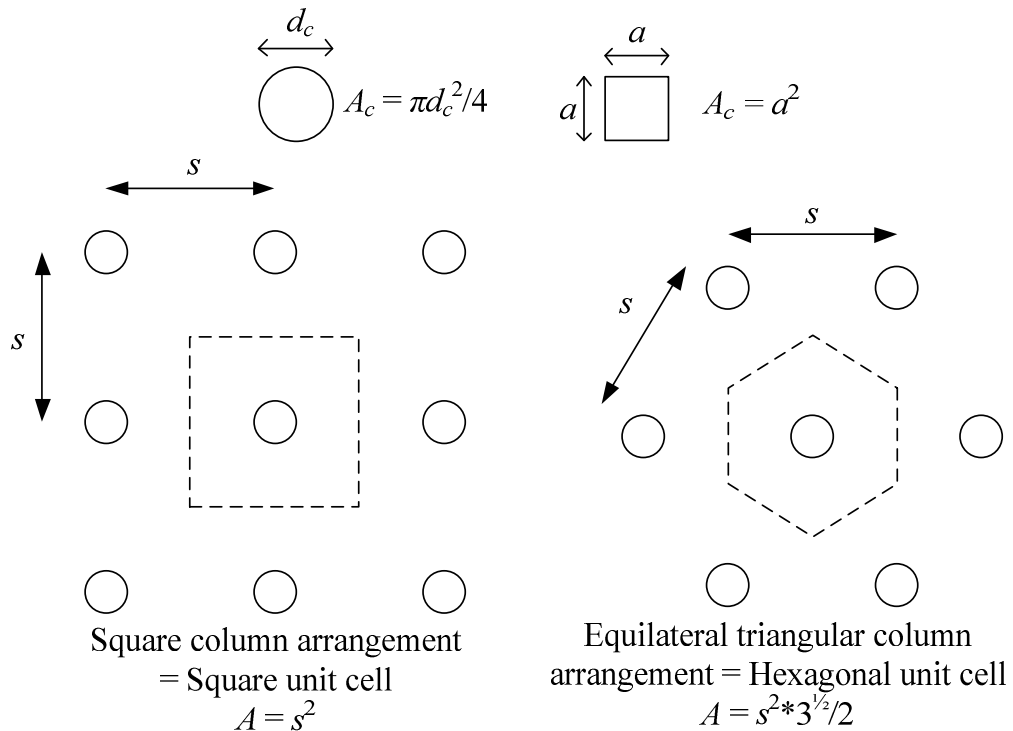


Figure 2.3: Unit cells for square and equilateral triangular column arrangements.

Table 2.1: Typical CSE design/analysis procedure inputs and outputs.

Performance Criteria / Indicators	Allowable total settlement (S)
	Allowable differential settlement
	Factor of safety for stability
	Factor of safety for lateral spreading
	Geosynthetic reduction factors of safety for damage (RF_{ID}), creep (RF_{CR}), degradation (RF_D), and overall factor of safety (FS_{UNC})
Subsurface Conditions	Site stratigraphy
	Compressibility, unit weight (γ), Poisson's ratio (ν), lateral earth pressure coefficient (K_o) of soft soil, and interface friction angle (δ) between columns and soil
	Depth to bearing layer for column design
	Surface desiccated crust or surface sand layer
	Depth to groundwater table (d_w)
	Liquefiable soil
Loading Conditions	Traffic surcharge, q
	Embankment load
	Embankment height (H) to meet grade of road
	Structure load, including MSE walls or other structures, if applicable
	Embankment side slope inclination (n , as in $nH:1V$)
Material Characteristics	Column type (e.g. steel/concrete/timber pile, ground improvement column, etc)
	Column properties (compressive strength, flexural strength, stiffness)
	Allowable column load ($q_{all,col}$)
	Load transfer platform (LTP) or bridging layer unit weight (γ), large-strain friction angle (ϕ), Young's Modulus (E), and Poisson's ratio (ν)
	General embankment fill unit weight (γ), large-strain friction angle (ϕ), Young's Modulus (E), lateral earth pressure coefficient (K), and Poisson's ratio (ν)
	Geosynthetic ultimate tensile strength (T_{ult})
	Geosynthetic stiffness (J)
	Geosynthetic allowable design/creep-limited strength ($T_{cr@5\%e}$)
	Interaction coefficient between geosynthetic and fill (c_{iemb})
Properties of geosynthetics (uniaxial or biaxial or radially-isotropic)	
Construction Techniques	Orientation of geosynthetics
	Overlap (ν) or seaming of geosynthetics
Geometry	Column spacing (s)
	Column layout (square/rectangular or triangular)
	Column tributary area (A)
	Thickness of load transfer platform (LTP) or bridging layer (H_b), and thickness of general embankment fill ($H_{Emb\#2}$)
	Number, vertical spacing, and roll width (w) of geosynthetic
	Diameter (d_{col}) or width (a) of column, column cross-sectional area (A_{col})
	Pile cap (if used) diameter (d_c) or width (a), thickness, and shape

The mechanism of load transfer and arching within column-supported embankments can be described by the arching theory proposed by Terzaghi (1943) for a two-dimensional trap-door arrangement. Terzaghi (1943) based his work on the efforts of Cain (1916), Völlmy (1937), Ohde (1938), and others. If support is removed from one part of a soil mass, the relative movement within the soil is opposed by shear resistance at the contact between the stationary and moving masses of soil. This resistance tends to keep the moving mass in its original position, reduces the stresses at the base of the moving mass, and increases the stress at the adjoining stationary mass. The transfer of stress from a yielding mass of soil to the stationary mass of soil is what Terzaghi termed the “arching effect.”

The premise of column-supported embankments is that the soil arches above the columns to bridge the gap between columns and thereby transfer much of the embankment load and surcharge to the columns, rather than to the soft foundation soil. Han and Gabr (2002) show that the area replacement ratio (area of columns divided by total embankment area) for column-supported embankment case histories is consistently lower than 20%. The embankment load is then transferred through the columns to a more competent bearing stratum, reducing the load applied to the soft foundation soil, which reduces the settlement of the embankment.

There are several theories regarding the shape and nature of the arching above the columns. In column-supported embankments without geosynthetic reinforcement, the soft foundation soil carries a reduced load due to arching in the embankment fill. In geosynthetic-reinforced column-supported embankments, the geosynthetic reinforcement may be designed to carry all or a portion of the reduced load from arching. The Collin or Beam Method (Collin 2004, 2007) includes several layers of geogrid with select fill material which create a stiffened beam to enhance the arching and load transfer to the columns. Several procedures directly or indirectly consider some support from the underlying soil when specifying the required strength of the geosynthetic reinforcement.

The design of geosynthetic-reinforced column-supported embankments involves calculating the vertical stress on the geosynthetic reinforcement and using the stress on the geosynthetic to calculate the strain and tension developed in the geosynthetic. There are at least 12 methods for directly calculating the vertical stress on the geosynthetic reinforcement. Many of these arching theories can be used to predict the reduced stress on the soft foundation soil for column-supported embankments without geosynthetic reinforcement. These 12 procedures and their primary references are listed in Table 2.2.

There are at least three methods for calculating the strain and tension developed in the geosynthetic reinforcement: the Parabolic, Tensioned Membrane, and Kempfert et al. (2004) Methods. The Parabolic Method is described in John (1987), Giroud (1995), BS8006 (1995), Rogbeck et al. (1998), and others. The Tensioned Membrane Method is described in Collin (2004, 2007) and is an adaptation of the work of Giroud (1990). The Kempfert et al. (2004) method uses a theory of elastic embedded membranes to evaluate the strain and tension in the geosynthetic. Many design methods limit the strain in the geosynthetic to 5 or 6% and allow an additional 2% for creep (e.g. BS8006 and Rogbeck et al. 1998).

Design of column-supported embankments should also consider differential settlement at the surface of the embankment, the tendency of the embankment to spread laterally at the side slopes (and the resulting additional tension in the geosynthetic if used), the development length or anchoring of the geosynthetic at the side slopes to resist pullout, and global stability. Some methods state that the differential settlement at the surface will be zero if a critical height of the embankment is exceeded. The BS8006 and Swedish methods include provisions for the additional tension in the geosynthetic due to lateral spreading. Other documents provide recommendations for global stability calculations such as BS8006 (1995), Collin (2004), and Filz and Navin (2006).

Some methods only apply for certain column arrangements. Twelve design and analysis procedures for CSEs and GRCSEs are categorized according to the design features they address in Table 2.3 and are discussed in greater detail in Chapter 3.

Other technology summaries or literature reviews of column-supported embankments and design methods are found in Han (1999), Rogbeck et al. (2003), FHWA (2004), Collin et al. (2005a), Smith (2005), Whyte (2005), Collin et al. (2006), Elias et al. (2006), Filz and Smith (2006), Serridge and Synac (2007), and McGuire and Filz (2008).

Table 2.2: List of CSE design/analysis procedures and their primary references.

		Design/Analysis Procedure											
		Adapted Guido Method	Adapted Terzaghi Method	British Standard 8006	Cao Min. Potential Energy Mthd	Chen et al. 1-D Method	Collin/Beam Method	Filz and Smith Method	Hewlett and Randolph Method	Japanese PWRC Method	Kempfert Method	Naughton Method	Swedish Method
REFERENCES	Bell et al. (1994)	✓											
	BS8006 (1995)			✓									
	Elias et al. (2006b)			✓			✓				✓		✓
	Jones et al. (1990)			✓									
	Cao et al. (2006)				✓								
	Carlson (1987)												✓
	Chen et al. (2008a, 2009)					✓							
	Chen et al. (2008b)		✓	✓					✓				
	Collin (2004, 2005b, 2007)			✓			✓		✓				✓
	EBGEO 6.9 (2004)										✓		
	Ellis and Aslam (2009a)	✓	✓	✓					✓		✓		✓
	Ellis and Aslam (2009b)	✓	✓	✓					✓		✓		✓
	Filz and Navin (2006)	✓							✓				
	Filz and Smith (2006, 2007)	✓							✓				
	Guido et al. (1987)	✓											
	Habib et al. (2002)	✓	✓	✓					✓				
	Han and Huang (2005)			✓			✓		✓	✓			✓
	Hewlett and Randolph (1988)								✓				
	Horgan and Sarsby (2002)	✓	✓	✓					✓				✓
	Jenner et al. (1998)	✓											
	Kempfert et al. (2004a/b)										✓		
	Kempton and Naughton (2002)	✓	✓	✓					✓				
	Liu et al. (2007)		✓						✓				
	Love and Milligan (2003)	✓		✓					✓				
	Low et al. (1994)								✓				
	McGuire and Filz (2008)	✓	✓				✓	✓	✓		✓	✓	✓
	Miki (1997)									✓			
	Naughton (2007)		✓	✓					✓			✓	✓
Raithel et al. (2008)										✓			
Rogbeck et al. (1998)			✓									✓	

		Design/Analysis Procedure											
		Adapted Guido Method	Adapted Terzaghi Method	British Standard 8006	Cao Min. Potential Energy Mthd	Chen et al. 1-D Method	Collin/Beam Method	Filz and Smith Method	Hewlett and Randolph Method	Japanese PWRC Method	Kempfert Method	Naughton Method	Swedish Method
	Rogbeck et al. (2003)												✓
	Russell et al. (2003)		✓										
	Russell and Pierpoint (1997)	✓	✓										
	Sloan et al. (2011)		✓										
	Svano et al. (2000)			✓									✓
	van Eekelen et al. (2003)			✓									✓
	van Eekelen et al. (2008a)			✓							✓		
	van Eekelen et al. (2008b)			✓							✓		

Table 2.3: Design/Analysis procedure characterization matrix.

Design or Analysis Method	Analysis Approach	Column Arrangement	Geosynthetic Included	Stress On Soil or Geosynthetic	Tension In Geo-Synthetic If Used	Tension due to Lateral Spreading	Global Stability	Soft Soil Support Considered	Settlement Considered
Adapted Guido	3D	S	✓	✓					
Adapted Terzaghi	3D	S	✓	✓	✓			✓	✓
BS8006	2D	S	✓	✓	✓	✓	✓		✓
Cao et al.	A	A	✓	✓				✓	✓
Chen et al.	A	A		✓				✓	✓
Collin	3D	S / T	✓	✓	✓	✓	✓		✓
Filz & Smith	3D	S	✓	✓	✓		✓	✓	✓
Hewlett & Randolph	3D	S	✓	✓					
Japanese PWRC	3D	S		✓			✓	✓	✓
Kempfert	3D	S / T	✓	✓	✓	✓	✓	✓	✓
Naughton	3D	S	✓	✓					✓
Swedish	2D / 3D	S	✓	✓	✓	✓	✓		✓

S = Square, T = triangular, A = axisymmetric

CHAPTER 3

DESCRIPTION AND PRELIMINARY RATING OF CSE DESIGN AND ANALYSIS PROCEDURES

3.1 DESCRIPTION OF RATING METHODS

This section contains the preliminary ratings for the twelve design/analysis procedures listed in Table 2.2. The procedures are rated for the appropriate use of performance criteria/indicators, subsurface conditions, loading conditions, material characteristics, construction techniques, and geometry. The performance criteria/indicators, subsurface conditions, loading conditions, material characteristics, construction techniques, and geometry applicable to CSEs were listed previously in Table 2.1. The procedures are further rated based on the validation of the procedure, whether the procedure is rational or empirical, its ease of use, and its LRFD status. In general, the procedures are given high, medium, or low ratings in each of these areas.

The rating system described herein is a generic system developed for, and applied to, a wide variety of soil improvement technologies in the SHRP2 R02 project. Most of the ratings are subjective judgments made by the authors based on the information available about a design procedure in the literature, e.g. whether the degree of validation for a particular procedure is high, medium, or low. Some of the ratings are objective, e.g. whether or not a procedure uses LRFD. All of the ratings for CSE design and analysis procedures in this chapter were reviewed by a member of the SHRP2 R02 advisory board. The rating criteria for each category are described below:

Performance Criteria/Indicators

- H: The design procedure appropriately uses performance criteria, and/or the analysis procedure generates appropriate performance indicators.
- M: The design procedure uses appropriate performance criteria to a limited extent, and/or the analysis procedure generates appropriate performance indicators to a limited extent.
- L: The design procedure does not appropriately use performance criteria, and/or the analysis procedure does not generate appropriate performance indicators.
- N: Performance criteria/indicators are not applicable to the design/analysis procedure.

Subsurface Conditions

- H: The design/analysis procedure appropriately uses relevant information about subsurface conditions.
- M: The design/analysis procedure uses relevant information about subsurface conditions to a limited extent.
- L: The design/analysis procedure does not adequately use relevant information about subsurface conditions.
- N: Subsurface conditions are not applicable to the design/analysis procedure.

Loading Conditions

- H: The design/analysis procedure appropriately uses relevant information about loading conditions.
- M: The design/analysis procedure uses relevant information about loading conditions to a limited extent.
- L: The design/analysis procedure does not adequately use relevant information about loading conditions.

Material Characteristics

- H: The design/analysis procedure appropriately uses relevant construction material characteristics.
- M: The design/analysis procedure uses relevant construction material characteristics to a limited extent.
- L: The design/analysis procedure does not adequately use relevant construction material characteristics.

Construction Techniques

- H: The design/analysis procedure appropriately incorporates relevant considerations of construction technique.
- M: The design/analysis procedure incorporates relevant considerations of construction technique to a limited extent.
- L: The design/analysis procedure does not incorporate relevant considerations of construction technique.
- N: Differences in construction techniques are not applicable to the design/analysis procedure.

Geometry

- H: The design/analysis procedure produces the geometric information that should be included in the plans and specifications for construction.

- M: The design/analysis procedure produces most of the geometric information that should be included in the plans and specifications for construction.
- L: The design/analysis procedure does not produce sufficient geometric information for developing plans and specifications for construction.
- U: References for this design/analysis procedure do not provide sufficient information to enable a rating.

Validation of Procedure

- H: The design/analysis procedure has been validated to a great extent. Methods of validation may include instrumented case histories; the absence of known failures due to inadequacy of the design/analysis procedure; long-term performance data; extensive numerical; and/or physical modeling.
- M: The design/analysis procedure has been validated with limited case histories and limited numerical and/or physical modeling.
- L: The design/analysis procedure has not been validated, or there are failures due to inadequacy of the design/analysis procedure.

Rational-Empirical Basis

- R: The design/analysis procedure is based primarily on rational principles of soil mechanics, mechanics of materials, and methods of analysis.
- S: The design/analysis procedure is semi-mechanical and semi-empirical.
- E: The design/analysis procedure is primarily empirical.

Ease of Use

- H: The design/analysis procedure can be implemented by practicing engineers with tools readily available to them in an amount of time consistent with the degree of complexity and importance of the application (if intricate analyses are required, user-friendly software is available to perform these analyses). Procedure is highly standardized and can easily be applied to a variety of different site and loading conditions.
- M: The design/analysis procedure can be implemented by practicing engineers, but implementation requires an excessive amount of time, it involves analysis methods not typically used in geotechnical practice, and/or the procedure cannot be easily applied to a variety of site and loading conditions.
- L: The design/analysis procedure is complex and cannot be implemented by most practicing geotechnical engineers.

LRFD Status

- Y: The design/analysis procedure is an LRFD procedure.
 N: The design/analysis procedure is not an LRFD procedure.

The ratings for each of the design/analysis methods are summarized in Table 3.1 below, and supporting information for the ratings is presented in Section 3.2. It is important to note that the ratings are based on an analysis of the information available in the literature and these ratings were assigned prior to conducting the field tests described in Chapter 6. The design/analysis methods are compared with the results from the field tests in Chapter 7, and the final design recommendations are made in Chapter 8.

Table 3.1: Preliminary ratings of the CSE design/analysis procedures.

		Design/Analysis Procedure											
		Adapted Guido Method	Adapted Terzaghi Method	British Standard 8006	Cao Min. Potential Energy Method	Chen et al. 1-D Method	Collin/Beam Method	Filz and Smith Method	Hewlett and Randolph Method	Japanese PWRC Method	Kempfert Method	Naughton Method	Swedish Method
APPLIC ATIONS	SUPPORT OF EMBANKMENTS	✓	✓	✓	✓	✓	✓	✓	✓	✓	✓	✓	✓
	SUPPORT OF STRUCTURES						✓						
	EARTH RETENTION												
	SLOPE STABILIZATION												
ASSESSMENT	PERFORMANCE CRITERIA/INDICATORS	N	M	H	N	M	H	H	N	H	H	M	H
	SUBSURFACE CONDITIONS	N	L	N	M	H	N	H	N	N	M	N	N
	LOADING CONDITIONS	H	H	H	H	H	H	H	H	H	H	H	H
	MATERIAL CHARACTERISTICS	L	H	M	M	H	M	H	H	M	H	H	M
	CONSTRUCTION TECHNIQUES	N	N	N	N	N	N	N	N	H	N	N	N
	GEOMETRY	L	M	H	M	H	H	H	H	M	H	M	H
	VALIDATION OF PROCEDURE	L	M	L	L	M	H	M	M	L	M	L	M
	RATIONAL-EMPIRICAL BASIS	E	S	S	R	R	S	R	R	S	R	R	S
	EASE OF USE	H	H	M	L	L	H	M	H	H	M	H	H
	LRFD STATUS	N	Y	Y	N	N	N	N	N	N	Y	N	Y

3.2 DESCRIPTION OF CSE DESIGN AND ANALYSIS PROCEDURES, AND DISCUSSION OF PRELIMINARY RATINGS

Each of the CSE design and analysis methods are described below. The material used to describe and rate each procedure is taken from all of the references pertaining to that procedure, as listed in Table 2.2.

3.2.1 Adapted Guido Method

Guido et al. (1987) showed that stiff geogrid in granular layers beneath shallow foundations can improve bearing capacity. According to Bell et al. (1994), the work of Guido et al. (1987) shows that the angle of load spread through the geogrid-reinforced cohesionless soil is at least 45 degrees from vertical. Bell et al. (1994) applied this information to geosynthetic-reinforced column-supported embankments on vibro-concrete columns. Russell and Pierpoint (1997) expanded on this work to determine a stress reduction ratio (SRR) based on a single layer of reinforcement supporting an embankment over columns. The SRR is equal to the reduced stress on the geosynthetic or soft soil due to arching, divided by the total overburden stress. They assumed that the wedge of soil supported by the geogrid takes the form of a pyramid with the ridge lines of the pyramid forming an angle of 45 degrees with the horizontal. The final expression for the stress reduction ratio included in Russell and Pierpoint (1997) is commonly referred to as the Adapted Guido Method. Jenner et al. (1998) notes that the “load spread through the fill can be conservatively taken as 45 degrees providing that the peak internal angle of friction of the fill is at least this value.” Jenner et al. (1998) reports a case history of a roadway embankment where a simplifying assumption was made that half of the fill under the arch would be supported by the soft foundation soil and half by the geogrid layers.

According to the Adapted Guido Method, the vertical stress on the geosynthetic reinforcement, p , can be found according to,

$$p = \frac{\gamma(s - a)}{3\sqrt{2}} \quad (3.1)$$

Performance Criteria/Indicators

Comments: This procedure calculates the stress on the geosynthetic reinforcement or soft soil based on the height of the embankment. It does not consider

performance criteria such as settlement, global stability, or factors of safety for the geosynthetic reinforcement.

Rating: N

Subsurface Conditions

Comments: This method does not consider support provided by the foundation soil.

Rating: N

Loading Condition

Comments: This method provides an expression to calculate the stress on the geosynthetic reinforcement. The variables in the expression are the column diameter and column spacing (used to calculate the clear span of the geosynthetic) and the unit weight of the fill material. The area over which the load acts is assumed to be the interior area between columns or pile caps (i.e., a square with sides $s - a$) rather than the cruciform area.

Rating: H

Material Characteristics

Comments: The unit weight of the fill is used to calculate the vertical stress on the geosynthetic layer. The designer can select a geosynthetic with sufficient strength and stiffness to withstand the tensile forces imposed by the embankment load for a given column spacing. There is very limited information on the minimum strength of the embankment fill, although Jenner et al. (1998) state that “the load spread through the fill can be conservatively taken as 45 degrees providing that the peak internal angle of friction of the fill is at least this value.”

Rating: L

Construction Techniques

Comments:

Rating: N

Geometry

Comments: Using this procedure to determine the vertical stress on the geosynthetic reinforcement and one of the methods for determining the tension in the geosynthetic (Parabolic Method, Tension Membrane Theory, or Kempfert Method), the designer can select spacing and diameter of the columns such that an adequate factor of safety for ultimate strength of the geosynthetic reinforcement is obtained. The geosynthetic details (number of layers and vertical spacing) are not fully developed in this method. Russell and Pierpoint's (1997) expression applies for a single geosynthetic layer whereas Guido's work was based on an optimum of three layers. Bell et al. (1994) and Maddison et al. (1996) report the use of 2 layers of geogrid in the Second Severn River crossing and Jenner et al. (1997) reports 2 layers of geogrid in the Rhuddlan bypass load transfer platform.

Rating: L

Validation of Procedure

Comments: Love and Milligan (2003) point out that gravity acts in the opposite direction in Guido et al.'s (1987) foundation analysis problem to that in the column-supported embankment problem. Therefore, settlement of the soil under the arch acts to reduce confinement within the arch, not increase it. Russell and Pierpoint (1997) and Kempton and Naughton (2002) note that the Adapted Guido Method consistently underpredicts the value of stress reduction ratio when compared with results from numerical modeling, although the Adapted Guido Method was used successfully in the design of several case histories as reported by Bell et al. (1994), Madison et al. (1996), and Jenner et al. (1997).

Rating: L

Rational-Empirical Basis

Comments: This method is based on an empirical modeling of foundation test results indicating that the geosynthetic reinforcement carries a pyramid of soil that is not supported by the piles or pile caps. The ridges of this pyramid of soil form a 45 degree angle with the horizontal.

Rating: E

Ease of Use

Comments: The method is straightforward and easy to use.

Rating: H

LRFD Status

Comments: This analysis procedure for determining the vertical stress on the geosynthetic reinforcement is not LRFD-based.

Rating: N

3.2.2 Adapted Terzaghi Method

This method is a modification of Terzaghi's (1943) arching analysis to account for the three dimensional shape of the settling soil mass in the embankment above the foundation soil between columns. Russell and Pierpoint (1997) use a lateral earth pressure coefficient of 1 in their Adapted Terzaghi Method. Russell et al. (2003) present a method where the lateral earth pressure coefficient is 0.5 in the arching portion of the embankment (lower 80%) and the upper 20% of the embankment is considered to be a surcharge. Both of these modifications increase the vertical stress on the geosynthetic. Russell et al. (2003) also provide a method for including the supporting capacity of the soil between columns based on a total stress analysis of load transfer from the soil to the columns. Given that the consolidation of clay soils is based on the change in effective stress and effective pre-consolidation pressure, the total stress analysis for the soft soil

support by Russell et al. (2003) does not seem appropriate for analyzing the column-supported embankment problem. The expression included in Russell and Pierpoint (1997) for the stress reduction ratio depends on the column spacing and diameter, height of embankment, lateral earth pressure coefficient, and friction angle of the embankment. This method considers a square column arrangement and the sliding mass of soil is assumed to be cruciform in shape when viewed in plan. Russell et al. (2003) include a method for inclusion of primary and secondary reinforcement. The high-strength primary reinforcement runs between columns and the secondary reinforcement covers the entire plan area and serves to transfer the load in the areas between columns to the primary reinforcement. Russell et al. (2003) also include a method for calculating the average settlement at the embankment surface based on the average deflection between piles (using the parabolic method) and the assumption that there is no volume change. They state that the assumption of no volume change is conservative since the well-compacted frictional embankment fill is likely to dilate.

SRR for the ultimate limit state as presented in Russell and Pierpoint (2003), can be calculated according to:

$$SRR = \frac{(s^2 - a^2)\gamma}{(\gamma H + q)4aK \tan \varphi} \left(1 - e^{-\frac{4aHK \tan \varphi}{(s^2 - a^2)}} \right) + \frac{q}{\gamma H + q} e^{-\frac{4aHK \tan \varphi}{(s^2 - a^2)}} \quad (3.2)$$

The vertical stress on the geosynthetic reinforcement, p , can then be calculated according to,

$$p = SRR(\gamma H + q) \quad (3.3)$$

Performance Criteria/Indicators

Comments: This procedure calculates the vertical load on the geosynthetic reinforcement or soft soil based on the height of the embankment and allowable strength of the geosynthetic, after suitable reduction factors are applied to the geosynthetic ultimate strength. It does not consider settlement of the embankment or global stability.

Rating: M

Subsurface Conditions

Comments: This method as presented by Russell and Pierpoint (1997) does not consider subgrade support. Russell et al. (2003) include a simplified method for including the resistance of the subsoil based on a total stress analysis of the soft soil.

However, consolidation is inherently an effective stress problem so this method of incorporating subsoil support does not seem consistent with sound soil mechanics.

Rating: L

Loading Conditions

Comments: The stress reduction ratio is dependent on the column spacing and diameter, height of embankment, lateral earth pressure coefficient, and friction angle of embankment fill. The stress on the geosynthetic or soft soil also depends on the unit weight of the fill material.

Rating: H

Material Characteristics

Comments: This method includes an expression for the stress on the geosynthetic in terms of the column diameter and spacing, friction angle and unit weight of the fill, surcharge, an empirical lateral earth pressure coefficient, and height of the embankment. The designer can select a geosynthetic with sufficient strength and stiffness to withstand the tensile forces imposed by the embankment load for a given column spacing. Russell et al. (2003) use the parabolic method for determining the tension and strain in the geosynthetic, and they impose stress-strain compatibility based on the stiffness of the geosynthetic. Russell and Pierpoint (1997) use an empirical lateral earth pressure coefficient of 1.0 and Russell et al. (2003) use an empirical lateral earth pressure coefficient of 0.5 in the embankment fill. Russell et al. (2003) state that the coefficient of earth pressure can approach passive values on the yielding surface but is unlikely to do so because of the limited magnitude of the movement and the lack of lateral support to the failing soil mass. Therefore, Russell et al. (2003) used a conservative value of 0.5, which was verified in their numerical analyses.

Rating: H

Construction Techniques

Comments:

Rating: N

Geometry

Comments: The procedure is iterative and begins with selecting trial column spacing and diameter. The geometry can be adjusted until an adequate factor of safety for ultimate strength of the geosynthetic reinforcement is found. The final geometry of the geosynthetic reinforcement includes the location of both the primary and secondary reinforcement.

Rating: M

Validation of Procedure

Comments: According to Filz and Smith (2006), this method is used to determine the limiting value of stress reduction ratio since it provides reasonably good fit to the results of the verified numerical analyses they reported when a lateral earth coefficient of

0.75 was used. Russell and Pierpoint (1997) found that the Adapted Terzaghi Method was consistent with the results of three-dimensional numerical analyses. Russell and Pierpoint (1997) found that this method provided relatively consistent results when compared with numerical modeling. In some cases it did under-predict the stress reduction ratio and they recommended that it be used with care. Russell et al. (2003) base their method on 3-dimensional FLAC analysis. Liu et al. (2007) state that the expression in Russell and Pierpoint (1997) provides results consistent with measured values from an instrumented case history and values from three-dimensional finite element analysis. Kempton and Naughton (2002) show that the Adapted Terzaghi and Hewlett and Randolph methods are consistent with one another and consistent with 3D finite difference modeling for two example embankments.

Rating: M

Rational-Empirical Basis

Comments: The derivation of the expression for vertical stress on the geosynthetic is based on rational mechanics analysis. The method uses an empirical lateral earth pressure coefficient of 1.0 as proposed by Russell and Pierpoint (1997), which was modified to be 0.5 by Russell et al. (2003).

Rating: S

Ease of Use

Comments: The method is simple and easy to use.

Rating: H

LRFD Status

Comments: This analysis procedure for determining the vertical stress on the geosynthetic reinforcement or soft subsoil is LRFD-based as presented in Russell et al. (2003) which is compatible with Eurocode 7, ENV 1997-1. The Eurocode LRFD method differs from that used in the US as the Eurocode resistance factors are greater than 1 and therefore the unfactored resistance is divided by the resistance factors.

Rating: Y

3.2.3 British Standard 8006 Method

This method was originally published by Jones et al. (1990) and was adopted as British Standard BS8006 (1995). An updated draft version of BS8006 was released on 30 June 2009. This draft version includes three methods for analyzing the vertical stress on the geosynthetic reinforcement. For a three-dimensional analysis, the method listed is the Hewlett and Randolph (1988) method. For two-dimensional analyses, the draft version recommends the designer “consider” the Marston formula method if permanent partial soil support is available and the “enhanced arching method” if permanent partial support is not available. The draft BS8006 (2009) contains the equations for the Hewlett and

Randolph (1988) method and for the Marston formula method, which is the method presented in BS8006 (1995). BS8006 (2009) contains references to Guido et al. (1987), Jenner et al. (1998), and Collin (2004) for the “enhanced arching method” but does not contain equations for implementation. Since the Hewlett and Randolph, Adapted Guido, and Collin methods are discussed and rated elsewhere in this document, the following discussion and ratings pertain to the Marston formula method that is contained in BS8006 (1995).

The procedure in BS8006 (1995) includes methods for incorporating the two-dimensional line load on the geosynthetic as well as for calculating the strain and tension in the geosynthetic. This method applies to a square arrangement of columns. The method for determining the strain and tension in BS8006 assumes a parabolic shape of the deflected geosynthetic and assumes a practical upper limit on strain in the geosynthetic of 6%. BS8006 allows a maximum creep strain of 2% over the design life of the reinforcement. The uniform load on the geosynthetic and therefore the stress reduction ratio are dependent on the height of the embankment, unit weight of the embankment fill, column spacing and diameter, and an arching coefficient. Two expressions are provided: one for embankments with a height between 0.7 and 1.4 times the clear spacing, and one for embankments with height greater than 1.4 times the clear spacing. An expression is also included for determining if the geosynthetic reinforcement can resist the tendency of the embankment to slide laterally, including a recommended minimum bond length for the geosynthetic beyond the outermost piles/columns. Recommendations are also provided for overall stability analysis.

van Eekelen et al. (2008b) present a modified BS8006 (1995) method which satisfies vertical equilibrium and is fully three-dimensional.

In the BS8006 (1995) Method, the uniform vertical line load between columns, W_T , can be calculated according to:

$$\begin{aligned}
 W_T &= \frac{s(\gamma H + q)}{s^2 - a^2} \left[s^2 - a^2 \left(\frac{p_c}{\gamma H + q} \right) \right] \text{ for } H \leq 1.4(s - a) \\
 W_T &= \frac{1.4s\gamma(s - a)}{s^2 - a^2} \left[s^2 - a^2 \left(\frac{p_c}{\gamma H + q} \right) \right] \text{ for } H > 1.4(s - a)
 \end{aligned} \tag{3.4}$$

where $p_c/(\gamma H + q) = (C_c/H)^2$ and where p_c is the vertical stress on the column tops determined by Marston’s equation. The term C_c is the arching coefficient determined by

$$\begin{aligned}
C_c &= 1.95 \frac{H}{a} - 0.18 \text{ for non-yielding steel or concrete piles} \\
C_c &= 1.70 \frac{H}{a} - 0.12 \text{ for steel or concrete friction piles or timber piles} \\
C_c &= 1.5 \frac{H}{a} - 0.07 \text{ for stone columns, lime columns, or sand compaction piles}
\end{aligned}
\tag{3.5}$$

The vertical stress on the geosynthetic, p , can be calculated according to:

$$p = \frac{2W_T}{s + a} \tag{3.6}$$

Performance Criteria/Indicators

Comments: The embankment height should be at least 1.4 times the clear span of the columns for full arching to occur and avoid differential settlement at the surface of the embankment. The expression for $H < 1.4$ is provided for partial arching below the critical height. Partial factors of safety for the geosynthetic reinforcement strength can be incorporated in this method. BS8006 includes provisions for calculating increased geosynthetic tension due to lateral spreading of the embankment, recommendations for global stability, settlement calculations, and recommendations for ensuring adequate factor of safety for geosynthetic pullout at the embankment edges.

Rating: H

Subsurface Conditions

Comments: This method does not consider the support provided by the soft foundation soil.

Rating: N

Loading Conditions

Comments: In this method, the vertical stress on the geosynthetic is a function of the column diameter and spacing, unit weight of the fill material, height of the embankment, and an arching coefficient. The expression for the tension in the reinforcement is based on the assumed strain in the reinforcement, the column spacing and diameter, and the uniformly distributed load acting on the geosynthetic reinforcement.

Rating: H

Material Characteristics

Comments: This method is based on a recommendation of one layer of geosynthetic reinforcement that acts as a structural element and deforms in a parabolic

shape. Rowe and Li (2003) state that where varying strengths of reinforcement are used, and settlements are relatively large, the stronger reinforcement attracts a disproportionately higher percentage of the tensile stresses. Blume et al. (2006) report that when multiple layers of reinforcement with the same strength are used, the layer located lower within the embankment carries a higher percentage of the tensile stresses. Therefore, BS8006 (1995) recommends only one layer of reinforcement, but does allow for multiple layers of similar strengths when the total required strength cannot be met by a single layer. This method includes two expressions for calculating the line load on the geosynthetic reinforcement depending on the height of the embankment (greater or less than 1.4 times the column clear span). These expressions depend on the column spacing and diameter, unit weight of the fill, height of the embankment, surcharge load, and an arching coefficient. The arching coefficient depends on the height of the embankment fill, width of the pile caps, and the rigidity of the piles or columns. The stress on the geosynthetic is calculated from the vertical line load and the clear span. The BS8006 method also includes a provision for calculating the tension in the reinforcement based on an assumed strain, the spacing and diameter of the columns, and the line load on the geosynthetic. Stress-strain compatibility based on the stiffness of the geosynthetic is not imposed. The stress concentration on the piles, and consequently the stress remaining to be carried by the geosynthetic, depends on the pile type and pile support condition. The material output in this procedure is the required ultimate strength of the geosynthetic. Since only one layer of geosynthetic is recommended for use in the BS8006 method, and because the method produces high stresses on the geosynthetic for some conditions, the required ultimate strength of the geosynthetic is typically higher for the same design conditions than for other methods that use multiple layers of geosynthetic (Collin 2007).

Rating: M

Construction Techniques

Comments:

Rating: N

Geometry

Comments: The designer can select a geosynthetic reinforcement layer with sufficient strength and stiffness based on the embankment load and the column diameter and spacing. Reinforcement details include the anchoring of the reinforcement at the side slopes with a gabion anchor and periphery trench.

Rating: H

Validation of Procedure

Comments: Rogbeck et al. (1998) note that the BS8006 method for determining the stress on the geosynthetic is not continuous at $H = 1.4(s - a)$ because q is included in one of the expressions for W_T but not the other, and that relatively small changes in embankment heights can produce large changes in the calculated stress on the

reinforcement. Similar trends are also noted by van Eekelen et al. (2003). Van Eekelen et al. (2008b) also note that the BS8006 (1995) method does not satisfy vertical equilibrium: the total load does not equal the sum of the loads on the geosynthetic reinforcement and on the piles. Chen et al. (2008b) states that the BS8006 method significantly underestimates the stress concentration ratio in bench-scale tests. Love and Milligan (2003) show that the BS8006 method does not satisfy vertical equilibrium. For high values of the ratio of pile cap width to pile spacing, the BS8006 method can give negative values of strength reduction ratio. The Marston formula seems to work for certain situations and provide erratic results for others. Kempton and Naughton (2002) state that the method is inconsistent—it underpredicted the stress reduction ratio in one comparison with 3D finite difference modeling and overpredicted the stress reduction ratio for another case. However, the parabolic method for determining the tension in the geosynthetic (if stress-strain compatibility is imposed) does provide results consistent with numerical methods (see Section 8.1.3) and results from full-scale tests (see Section 7.2).

Rating: L

Rational-Empirical Basis

Comments: This method is an empirical method developed by Jones et al. (1990) which is based on Marston’s equation for a positive projecting conduit.

Rating: S

Ease of Use

Comments: The Marston procedure as presented in BS8006 (1995) is straightforward and easy to use. However, the draft 2009 version is very confusing regarding which of the three methods to use. As described above, the choice of method is dependent on whether the system is analyzed as a 2-D or 3-D system and whether or not there is permanent partial support available from the soft ground. However, it does not provide any guidance on when a 2-D analysis should be used as opposed to a 3-D analysis or on what types of conditions would allow consideration of partial support of the soft soil.

Rating: M

LRFD Status

Comments: This method employs a form of LRFD that is consistent with Eurocode 7, version ENV 1997-1. In this method, the “load” and “resistance” factors are all greater than or equal to 1.0. The resistance (R) is divided by the resistance factors (γ_R) and the action effect (E) is multiplied by the partial factors for action effects (γ_S). The result must satisfy the inequality $R/\gamma_R - \gamma_S E \geq 0$.

Rating: Y

3.2.4 Cao et al. Method

This axisymmetric analytical model with equivalent circular area estimates the pile efficacy based on the principle of minimum potential energy which considers the interaction among the embankment fill, geotextile, pile or pile cap, and subsoil. Pile efficacy is equal to the load on the pile cap divided by the total load imparted by the embankment and surcharge over the tributary area of the pile. The pile and subsoil are modeled by pile-springs and soil-springs. A single layer of geotextile is used and the embankment soil is modeled by an inner column above the pile and an outer cylinder above the geotextile and subsoil. The embankment cannot displace laterally. The inner column and the outer cylinder move downwards under the embankment load but the vertical displacement of the inner column is less than that of the outer cylinder due to the higher stiffness of the column/pile springs. Equations are provided for the radial and vertical displacement of the geotextile which contain three unknown constants. The deflected shape of the geotextile is assumed to be parabolic. All system components are represented as having linear elastic material properties without a failure criteria which means that (1) there is no limit to the capacity of the embankment to arch as deformations increase and (2) the non-linear and stress-history behavior of the soft subsoil is not incorporated. The magnitude of the spring stiffness modeling the soft foundation soil is unaffected by the size of the loaded area. Based on the boundary conditions, the equations are solved and the pile efficacy can be determined. The effects of pile spacing, embankment height, cap size, shear modulus of embankment fill, geotextile stiffness, and pile-subsoil stiffness ratio on pile efficacy are studied. Cao et al. (2006) found that based on this method, pile efficacy is significantly affected by pile spacing, embankment height, cap size, and pile-subsoil stiffness ratio, while shear modulus of the embankment fill and geotextile stiffness have lesser effects.

The equations necessary to use the Cao et al. (2006) Method are not included in this report, but can be found in the paper by Cao et al. (2006).

Performance Criteria/Indicators

Comments: This procedure does not explicitly include provisions for the factor of safety for the reinforcement, embankment stability, or settlement. Presumably, allowable values can be obtained based on the reduction of ultimate values by an adequate factor of safety.

Rating: N

Subsurface Conditions

Comments: This method considers the support of the subsoil through the use of soil-springs in the model. The linear elastic springs contain no failure criteria or nonlinear consolidation parameters.

Rating: M

Loading Conditions

Comments: This procedure does not appear to include a provision for surcharge loading.

Rating: H

Material Characteristics

Comments: The height, Young's modulus, Poisson's ratio, and unit weight of the fill are used in this procedure, along with the diameter, length, and Young's modulus of the pile, and the Young's modulus, Poisson's ratio, and unit weight of the foundation soil. Filz and Smith (2007) note that all system components are represented as having linear elastic material properties which means that (1) the capacity of the embankment to arch is unlimited as deformations increase, and (2) the nonlinear and stress-history dependent response of soft clay soils to compressive load is not incorporated. Since no failure criterion or strength parameters are specified, there is no limit on the capacity of the soil in the embankment to arch. There is no slippage allowed between the columns and soft soil. The magnitude of the spring stiffness representing the soft soil is unaffected by the size of the loaded area. This is an iterative procedure based on the Young's modulus and Poisson's ratio of the embankment fill. Stress-strain compatibility of the geosynthetic is imposed.

Rating: M

Construction Techniques

Comments:

Rating: N

Geometry

Comments: This is an iterative procedure starting with an assumed column diameter and spacing. This method does not appear to have a way to ensure that there is no differential settlement at the embankment surface.

Rating: M

Validation of Procedure

Comments: Cao et al. (2006) present results from the Hangzhou-Ningbo highway embankment case history in southeastern China which shows good agreement with the method. Results from the Hewlett and Randolph method are also shown; the Cao et al. (2006) method shows better agreement with the field measurements than the Hewlett and Randolph method for this case history. This method received a low rating since there is

only one case history and since the materials are linear-elastic so there is no yielding of the embankment fill.

Rating: L

Rational-Empirical Basis

Comments: This is a rational model based on minimizing the potential energy of the system components.

Rating: R

Ease of Use

Comments: This procedure involves solving a system of three equations and three unknowns using numerical methods of the designer's choice. It is more complicated than most of the other methods presented in this design summary.

Rating: L

LRFD Status

Comments: This analysis procedure for determining the vertical stress on the geosynthetic reinforcement is not LRFD-based.

Rating: N

3.2.5 Chen et al. Method

This method is a closed-form solution for one-dimensional loading which considers the soil arching in the embankment fill, the negative skin friction along the pile shaft, and the settlement of the foundation soil. The piles, the embankment fill, and the foundation soil deform one-dimensionally. There is no geosynthetic reinforcement included in the model. This method should only be applied to piles near the centerline of the embankment due to the two-dimensional loading near the toe of an embankment. The method solves for the location of the plane of equal settlement, the proportion of load carried by the pile, the distribution of skin friction along the pile, and the settlement of the embankment. The method is based on an axisymmetric unit cell model, and 17 nonlinear equations with 17 unknowns are developed. The system of equations is solved with a Newton Raphson method. Comparisons with FEM results from PLAXIS are made by Chen et al. (2008a) for two case histories (one with floating piles and one with end-bearing piles). The comparisons show good agreement for settlement contours within the embankment fill, axial force in the pile vs depth, and skin friction along the pile shaft vs depth. The foundation soils and embankment fill were modeled as linearly elastic, perfectly plastic materials with Mohr-Coulomb failure criteria. A case history from the SJZA highway in China is presented in Chen et al. (2009), and the method shows good agreement with field measurements of the pile efficacy and settlement.

The equations necessary to solve the Chen et al. Method are not included in this dissertation but can be found in the paper by Chen et al. (2008a).

Performance Criteria/Indicators

Comments: This procedure results in plots of settlement above the pile caps at various heights, it and can be run iteratively so that there will be no differential settlement at the embankment surface. There do not appear to be any factors of safety or load/resistance factors included, therefore, the method seeks an exact solution to the problem.

Rating: M

Subsurface Conditions

Comments: This procedure incorporates the negative skin friction along the piles using the beta method, but does not include the preconsolidation pressure and compression index of the foundation soil. It can incorporate one layer of soft soil.

Rating: H

Loading Conditions

Comments: The embankment fill is homogeneous, isotropic, and cohesionless with internal friction angle, unit weight, and Young's modulus.

Rating: H

Material Characteristics

Comments: The elastic properties (friction angle, cohesion, Young's modulus, constrained modulus, Poisson's ratio, unit weight, and coefficient of skin friction) of the embankment, soft soil, firm foundation soil, pile, and pile cap are used in this procedure. The pile length, spacing, and cap size are adjusted iteratively. This method does not use geosynthetic reinforcement.

Rating: H

Construction Techniques

Comments:

Rating: N

Geometry

Comments: The pile length, spacing and cap size are adjusted iteratively. This method solves for the plane of equal settlement within the embankment based on the differential settlement that occurs between the top of the pile caps and the soft soil between the pile caps.

Rating: H

Validation of Procedure

Comments: The results of this procedure show reasonable agreement with results from PLAXIS in the paper by Chen et al. (2008a). The method also shows good agreement with the case history presented in the paper by Chen et al. (2009).

Rating: M

Rational-Empirical Basis

Comments: This is a rational procedure based on elastic theory. It contains an arching coefficient, n , which varies from $n = 1$ for no arching to $n = 0$ for complete arching and n is calculated as a part of the procedure.

Rating: R

Ease of Use

Comments: This procedure requires use of advanced numerical techniques to solve the 17 non-linear equations.

Rating: L

LRFD Status

Comments: This is not an LRFD-based procedure.

Rating: N

3.2.6 Collin Method

The Collin Method is a refinement of the Adapted Guido method. The geosynthetic layers in a geosynthetic-reinforced column-supported embankment support a pyramid of soil where the sides of the pyramid (rather than the ridge lines) form a 45 degree angle. The method calls for a minimum of three layers of geosynthetic and is developed for both square and triangular column arrangements. Each geosynthetic layer provides lateral confinement of the select fill to facilitate soil arching, and it supports the weight of soil in the section of the pyramid between it and the next geosynthetic layer. This load is used to calculate the tension in the geosynthetic layers using tensioned membrane theory and assuming a maximum value of strain in the geosynthetic. This method is fundamentally different from many other methods, and it is based on the premise that the geosynthetic reinforcement and select reinforced fill within the load transfer platform creates a stiffened beam of reinforced soil that distributes the load from the embankment above the load transfer platform to the columns below the platform (Collin 2007). The uniform load on the reinforcement (and therefore the stress reduction ratio) is dependent on the clear spacing and diameter of columns, vertical spacing of geosynthetic layers, and the unit weight of the embankment fill. Expressions are provided for both square and triangular arrangement of columns. The Collin (2004, 2007) method includes a provision for calculating the tension in the geosynthetic reinforcement which is dependent on the area load on the geosynthetic, column spacing and diameter, column layout (square or triangular), the vertical spacing of the reinforcement, and a dimensionless factor from tensioned membrane theory. The dimensionless tension membrane factor is dependent on the reinforcement strain. The allowable strength of the geosynthetic reinforcement is calculated based on the required tensile strength, an overall factor of safety, and reduction

factors for durability, installation damage, and creep. For serviceability, the creep limited strength of the geosynthetic at a strain of 5% must be equal to or greater than the required strength. In order to ensure that the geosynthetic provides the required confinement to the select fill, the aperture stability of the geogrid must be greater than 3.0 kg-cm/deg. Collin (2004) presents an 11-step procedure summarizing the method, including checks for lateral spreading and global stability based on BS8006 (1995). Collin et al. (2004b) describe a case history for an MSE-wall support project.

Collin (2004, 2007) and Elias et al. (2006b) present the equations to solve for the vertical stress on each individual layer of geosynthetic reinforcement. The stress on each reinforcement layer is equal to the volume of soil below the arch at angle 45 degrees which is not supported by the layer above it. Collectively, the total vertical stress on all of the geosynthetic reinforcement layers, p , is equal to,

$$p = \frac{\gamma(s - a)}{6} \quad (3.7)$$

Performance Criteria/Indicators

Comments: This procedure calculates the stress on the geosynthetic reinforcement or soft soil based on the height of the embankment and factor of safety for ultimate strength of the geosynthetic. Stability and lateral spreading calculations from Collin (2004) are performed in accordance with BS8006 (1995). The settlement calculations are performed in accordance with the design procedures for the type of column used in the design.

Rating: H

Subsurface Conditions

Comments: This method does not directly consider support of the soft foundation soil. It does state that if the subgrade soil is strong enough to support the first layer of fill, the first layer of reinforcement can be located 6 to 10 inches above the subgrade. An alternative approach described by Collin (2007) is the Modified Beam Method where a layer of “catenary” reinforcement is used directly above the columns or pile caps in addition to the 3 or more layers of “beam” reinforcement.

Rating: N

Loading Conditions

Comments: The distributed load acting on the reinforcement is calculated for each layer of reinforcement based on the column diameter and spacing, vertical spacing of the reinforcement layers, and the fill unit weight. The tension in the geosynthetic is calculated based on tensioned membrane theory and depends on the distributed load

acting on the geosynthetic, the column spacing and diameter, and a dimensionless factor from tensioned membrane theory.

Rating: H

Material Characteristics

Comments: The method considers a minimum of three layers of geosynthetic reinforcement with 6 to 18 in. of vertical spacing between the reinforcing layers. This method requires the use of a well graded select granular fill with an effective friction angle ≥ 34 degrees for the load transfer platform. This method results in the required allowable strength of the geosynthetic reinforcing layers and a fill material with effective friction angle ≥ 34 degrees. The strain in the geosynthetic is assumed to be 5% and the creep-limited strength of the geosynthetic at 5% strain must be greater than the required allowable tension in the geosynthetic, for each layer used.

Rating: M

Construction Techniques

Comments:

Rating: N

Geometry

Comments: The column diameter and spacing are selected based on the guidance that the thickness of the load transfer platform must be greater than or equal to half of the clear span between columns or pile caps. The Collin or Beam method will generally allow for larger column spacings than the BS8006 method since multiple layers of geosynthetic reinforcement are used to enhance the arching of the soil resulting in a 45 degree arch angle from the horizontal, which is lower than the arch angle for other design methods (Collin 2007). This procedure is developed for both square and triangular column arrangements.

Rating: H

Validation of Procedure

Comments: Collin (2007) notes that the beam and modified beam methods have been used on several projects in the U.S. Collin (2007) also notes that numerical modeling of the procedure was performed which resulted in adding the “catenary” layer of reinforcement in the modified beam method. Several case histories are provided in the literature. Abdullah and Edil (2007a) present results from an instrumented test embankment which compares an LTP based on the BS8006 method with a beam LTP (Collin Method) over Geopiers. They note that although construction costs vary with location, the beam LTP appears to offer a less costly approach with enhanced performance. Collin et al. (2005b) contains a case history.

Rating: H

Rational-Empirical Basis

Comments: This method is based on an empirical model where arching occurs at a 45 degree angle from the horizontal. The geosynthetic reinforcement carries a pyramid of soil with sides inclined at 45 degrees from the horizontal. The base of the pyramid is the interior area of soil that is not supported by the piles or pile caps. The model is supported by the findings of Guido et al. (1987), Bell et al. (1994), Jenner et al. (1998), and case histories.

Rating: S

Ease of Use

Comments: The method is straightforward and easy to use.

Rating: H

LRFD Status

Comments: This analysis procedure for determining the vertical stress on the geosynthetic reinforcement is not LRFD-based.

Rating: N

3.2.7 Filz and Smith Method

This method satisfies force equilibrium and displacement compatibility of the embankment, geosynthetic reinforcement, columns, and foundation soil. Nonlinear response of the soil components is incorporated in the analysis.

Load-deflection relationships are developed for 1) the column or pile cap penetrating up, relatively, into the embankment, 2) the geosynthetic reinforcement deflecting down on the soft soil between columns, and 3) the soil settling down between columns.

The load-deflection relationship for the column or pile cap penetrating up into the embankment is linear up to a maximum and is approximated using the linear-elastic solution for displacement of a circular loaded area on a semi-infinite mass by Poulos and Davis (1974). The limiting stress condition in the embankment above the geosynthetic reinforcement is established by using the Adapted Terzaghi Method (Russell and Pierpoint 1997) with a lateral earth pressure coefficient of 0.75.

The load-deflection relationship for the geosynthetic deflecting down on the soft soil was approximated by performing axisymmetric numerical analyses of a uniformly loaded annulus of membrane material in Smith (2005). An equation given in Filz and Smith (2006) approximates the numerical results.

The settlements of the columns and subgrade soil are determined based on the vertical stress applied to the top of the column or pile and the vertical stress applied to the subgrade soil. The column compression is calculated based on a constant value of the column modulus. The one-dimensional compression of clay soil located between columns is calculated using the compression ratio, re-compression ratio, and preconsolidation pressure of the soil. As the soft soil settles down between the columns, load is transferred to the columns until the depth at which the column and soil settlements are equal.

An Excel® spreadsheet called GeogridBridge solves the three nonlinear equations and requires that the calculated values of the maximum differential settlement at subgrade level must be the same for the base of the embankment, the geosynthetic, and the underlying foundation soil. The method is summarized in a 10-step procedure outlined by Filz and Smith (2006) which includes calculating the average embankment settlement.

Performance Criteria/Indicators

Comments: This procedure calculates the stress on the geosynthetic reinforcement or soft soil based on the height of the embankment and allowable strength of the geosynthetic reinforcement, and other factors. The procedure includes provisions for calculating the embankment surface settlement. This procedure is documented in a Virginia Transportation Research Council (VTRC) report by Filz and Smith (2006) that focuses on the design of the bridging layers for column-supported embankments. Another VTRC report completed by Filz and Navin (2006) at about the same time contains recommendations for global stability calculations for a variety of column types, although it does not include procedures for incorporating geosynthetic reinforcement to improve stability.

Rating: H

Subsurface Conditions

Comments: This method considers support of the subgrade when calculating the vertical stress on the geosynthetic layer(s). It includes up to two soft clay layers with input parameters for layer thickness, unit weight, Poisson's ratio, lateral earth pressure coefficient, interface friction angle between soil and columns, compression ratio, recompression ratio, initial effective stress, and preconsolidation pressure.

Rating: H

Loading Conditions

Comments: The embankment surcharge due to pavement and traffic is an input to this method. Use of preloading to reduce settlement of the embankment is also considered.

Rating: H

Material Characteristics

Comments: The unit weight and friction of the embankment fill are used in this procedure. The method can also distinguish between the properties of the bridging or LTP fill and the additional embankment fill placed on the bridging layer. A preload layer can also be included. This method employs the method of BS8006 (1995) for calculating the strain and tension in the geosynthetic reinforcement. The BS8006 (1995) method assumes a parabolic deflection of the reinforcement. This method modifies the strain and tension calculation from BS8005 (1995) by imposing stress-strain compatibility in the geogrid reinforcement by using the sum of the stiffness of up to three geogrid reinforcing layers placed in the lower part of the embankment.

Rating: H

Construction Techniques

Comments: This method includes a procedure for reduction of the load transfer platform thickness based on an upper sand layer (above the soft clay layer) or working platform.

Rating: N

Geometry

Comments: The spacing and diameter of columns are selected based on the maximum allowable settlement. The design process is iterative—if settlement is too high, then the process is repeated using a closer column spacing, larger area replacement ratio, stiffer geosynthetic reinforcement, stiffer columns, and/or a preload. This method was developed for a square column arrangement with round column tops or square pile caps.

Rating: H

Validation of Procedure

Comments: This method is verified with the results of a large numerical parameter study, for which the numerical procedures were verified against closed-form solutions for membranes, pilot-scale experiments, and field case histories. The net strength reduction ratios from this method are compared with FLAC analyses. The net strength reduction ratios from this method are greater than those from FLAC which is conservative for strain and tension in the geosynthetic. The foundation strength reduction ratios are typically less than those from FLAC which is unconservative for calculating the settlement magnitude of column-supported embankments without geosynthetics, however, this is countered by the conservatism believed to exist in the method that was adopted for estimating the settlement due to embankment compliance (Russell et al. (2003).

Rating: M

Rational-Empirical Basis

Comments: This method is based on load-displacement compatibility between the embankment, columns, geosynthetic reinforcement, and foundation soil. The load-deflection relationship for the column or pile cap penetrating up, relatively, into the embankment is assumed to be linear up to the maximum loading condition and is approximated using the linear-elastic solution provided by Poulos and Davis (1974). The limiting stress condition in the embankment above the geosynthetic reinforcement is established by setting a lower limit on the value of the embankment stress reduction ratio using the Adapted Terzaghi Method. An empirical lateral earth pressure coefficient of 0.75 is used, which is between the values of 1.0 used in Russel and Pierpoint (1997) and 0.5 used by Russell et al. (2003). The lateral earth pressure coefficient value of 0.75 was validated by numerical analyses which were, in turn, validated with instrumented case histories and bench scale tests. The load-deflection response of the geosynthetic reinforcement is approximated by an expression fitting the results of axisymmetric numerical analyses of a uniformly loaded annulus of membrane material with the inner boundary pinned, which represents the support of the column, and with the outer boundary free to move vertically but not laterally, which represents the axisymmetric approximation of the lines of symmetry in the actual three-dimensional configuration of a column-supported embankment. The settlements of the column and the subgrade soil are determined based on the vertical stress applied to the top of the column or pile and the vertical stress applied to the subgrade soil using a solution in Poulos and Davis (1974) for an elastic solid cylinder (column) surrounded by a concentric and laterally constrained thick-walled cylinder (soil).

Rating: R

Ease of Use

Comments: This method is presented in a Microsoft Excel® spreadsheet which is relatively easy to use. Filz and Smith (2006) include two design examples along with instructions for using the spreadsheet. The spreadsheet is incorporated into a 10-step design procedure.

Rating: M

LRFD Status

Comments: This analysis procedure for determining the vertical stress on the geosynthetic reinforcement or soft subsoil is not LRFD-based.

Rating: N

3.2.8 Hewlett and Randolph Method

Hewlett and Randolph (1988) derived theoretical solutions for granular, free-draining soil based on mechanisms observed in model tests. The method is based on a limit

equilibrium analysis of a hemispherical domed region of sand above the square columns or pile caps in a square array. The stress reduction ratio is calculated assuming limiting plastic stress states in the arch. The critical failure location is either at the top of the column for high embankments or at the crown of the arch for low embankments. The lower of the two estimates of pile efficacy can be converted to a stress reduction ratio. The stress reduction ratio is dependent on the column width and spacing, passive earth pressure coefficient (which is dependent on the friction angle of the fill), and height of the embankment.

Low et al. (1994) present a refinement of the Hewlett and Randolph method for a 2-dimensional case where piles have cap beams. The refinements include a body force in the 2D equilibrium equations and a parameter to account for non-uniform vertical stress on the soft ground.

Using Hewlett and Randolph's (1988) method, the pile efficacy at the crown of the arch and the top of the column can be determined by Equation (3.8) and (3.9), respectively.

$$E = 1 - \left[1 - \left(\frac{a}{s} \right)^2 \right] \left[\left(1 - \frac{a}{s} \right)^{2(K_p - 1)} \left(1 - \frac{2s(K_p - 1)}{\sqrt{2}H(2K_p - 3)} \right) + \left(\frac{(s - a)2(K_p - 1)}{\sqrt{2}H(2K_p - 3)} \right) \right] \quad (3.8)$$

$$E = \frac{\beta}{1 + \beta} \text{ where } \beta = \left(\frac{2K_p}{K_p + 1} \right) \left(\frac{1}{1 + \frac{a}{s}} \right) \left[\left(1 - \frac{a}{s} \right)^{-K_p} - \left(1 + \frac{a}{s} K_p \right) \right] \quad (3.9)$$

where K_p is the passive earth pressure coefficient. The critical pile efficacy is the lower of the two values, which can be used to determine the vertical stress on the geosynthetic reinforcement, p , according to

$$p = \frac{(1 - E)(\gamma H + q)}{1 - a_s} \quad (3.10)$$

Performance Criteria/Indicators

Comments: This method is primarily focused on the arching action which occurs in the soil above the columns and the resulting soil load below the arch which is transferred to the geosynthetic or soft foundation soil. This procedure calculates the

stress on the geosynthetic reinforcement or soft soil based on the height of the embankment. It does not consider settlement of the embankment or global stability.

Rating: N

Subsurface Conditions

Comments: This method does not consider support of the foundation soil.

Rating: N

Loading Conditions

Comments: The unit weight of the embankment load and the surcharge pressure are used to calculate the vertical stress on the geosynthetic reinforcement.

Rating: H

Material Characteristics

Comments: This method recommends a well-compacted, high grade fill, with a Rankine passive earth pressure coefficient greater than 3 (a friction angle greater than 30 degrees), which should be installed to a height above the pile caps equal to or greater than the column center-to-center spacing. A lower grade fill can be used in the upper portion of the embankment. Therefore, this method only applies to relatively high embankments. The column width and spacing are used to calculate the vertical stress on the geosynthetic. The geosynthetic is chosen such that it can support the load due to the reduction in stress due to arching. This method produces the vertical stress on the geosynthetic, but it requires use of another method (BS8006/Parabolic, Tension Membrane, or Kempfert et al. [2004]) to get the strains and tension in the geosynthetic, if used. Hewlett and Randolph (1988) note that the geosynthetic reinforcement at the tops of the columns will increase the efficacy of the support and help to prevent lateral spreading of the piles, but these effects are not accounted for explicitly in their analysis procedure.

Rating: H

Construction Techniques

Comments:

Rating: N

Geometry

Comments: The pile spacing should not be greater than 3 times the pile cap width. The ratio of column center-to-center spacing to the total embankment height must be less than 0.5. This requirement combined with the requirement that the high grade fill be installed to a height above the pile caps equal to or greater than the center-to-center spacing, means that this method results in a relatively high embankment. The column spacing and width can be varied iteratively such that the stress on the soil between columns is sufficiently low that it can be supported by the geosynthetic or soft foundation soil. This method of calculating the pile/column efficacy is valid only for a square column arrangement.

Rating: H

Validation of Procedure

Comments: Hewlett and Randolph (1988) present results from field and bench-scale model tests which show good agreement with their method. Russell and Pierpoint (1997) found that the Hewlett and Randolph Method was consistent with the results of three-dimensional numerical analyses. In some cases, it did underpredict the strength reduction ratio and they recommended that it be used with care. Liu et al. (2007) state that the Hewlett and Randolph method is consistent with measured values from an instrumented case history and three-dimensional finite element analysis provided that the embankment height is high. Kempton and Naughton (2002) show that the Adapted Terzaghi and Hewlett and Randolph methods are consistent with one another and consistent with 3D finite difference modeling for two example embankments.

Rating: M

Rational-Empirical Basis

Comments: This method for determining the vertical stress on the geosynthetic is based on the assumption that the arching pattern in the embankment takes the shape of a hemispherical dome. The analysis is based on limiting equilibrium of stresses in the domed region and assumes failure at the crown of the arch or at the top of the column. The load concentration is evaluated in terms of efficacy, which depends on the column width and spacing, the Rankine lateral earth pressure coefficient, and the height of the embankment. The vertical stress on the geosynthetic reinforcement is then calculated based on the efficacy, unit weight of the embankment, embankment height, surcharge pressure, and the column width and spacing (area replacement ratio). Ellis and Aslam (2009a/b) note that the Hewlett and Randolph method is one of the most rational methods as it account for all of the geometrical parameters and the soil strength.

Rating: R

Ease of Use

Comments: The procedure is straightforward and easy to use.

Rating: H

LRFD Status

Comments: This procedure is not LRFD-based.

Rating: N

3.2.9 Japanese PWRC Method

This method was proposed by Miki (1997) for embankments on deep mixing method columns. The total embankment volume is divided into the volume of embankment that acts on the improved ground (DMM columns) and the unimproved ground or geosynthetic. The shape of the volume of soil supported by the unimproved ground is

complex. A formula to calculate this volume is provided in Miki (1997) in terms of the column center-to-center spacing (s), column diameter (d_c), and arch angle ($\theta = 45 + \varphi/2$). A formula for the stress reduction ratio for this method is provided in Han and Huang (2005) in terms of column center-to-center spacing, column diameter, arch angle, and embankment height.

Based on Miki (1997), the expression for the vertical stress, p , on the unimproved soil for a square arrangement of round columns is,

$$p = \gamma \frac{\frac{\pi}{96} (s - d_c)^2 \tan \theta (5d_c + 4s) + (4 - \pi) \left(\frac{s}{2}\right)^2 \left[\frac{s - d_c}{2} \tan \theta + \frac{s}{6}\right] (\sqrt{2} - 1) \tan \theta}{s^2 - \frac{\pi d_c^2}{4}} \quad (3.11)$$

Performance Criteria/Indicators

Comments: This method includes a settlement analysis specific to deep mixing method columns. The settlement analysis includes analysis of both the column and unimproved soil settlement. A factor of safety for bearing capacity of the deep mixing method columns is included. Recommendations for calculating a factor of safety for global stability are included.

Rating: H

Subsurface Conditions

Comments: Soft soil properties are used in calculating settlement of the unimproved ground. The load carried by the soft soil is independent of the soft soil properties and depends only on the column diameter, column spacing, and friction angle of embankment fill.

Rating: N

Loading Conditions

Comments: Embankment unit weight is used to calculate the load on columns and unimproved soil.

Rating: H

Material Characteristics

Comments: The friction angle of the fill material is used in the arching calculations to determine the vertical stress on the soft soil.

Rating: M

Construction Techniques

Comments: This method was developed specifically for embankments on deep mixing method columns and may or may not be applicable to other types of columns.

Rating: H

Geometry

Comments: Column diameter and spacing affect the vertical stress on the soft soil. The minimum height to avoid differential settlement is not addressed although there are calculations for the differential settlement of improved and unimproved ground at the elevation of the column tops.

Rating: M

Validation of Procedure

Comments: Three case histories are provided by Miki (1997). The procedure is based on three model tests of a 2 m high embankment constructed in a 1 m by 8 m test facility with three different improvement ratios. The dimensions of the facility suggest that it is essentially a 2D test and the limited width of the facility may make it subject to significant boundary influences. Numerical modeling results by an unspecified method are presented by Miki (1997). This method was adopted by the Japanese Public Works Research Center (PWRC), and other case histories and supporting information may be available in Japanese.

Rating: L

Rational-Empirical Basis

Comments: The arching method does depend on the friction angle of the fill material, but the shape of the volume of embankment fill carried by the soft soil is empirically based.

Rating: S

Ease of Use

Comments: This method is straightforward and relatively easy to implement.

Rating: H

LRFD Status

Comments: This is not an LRFD procedure.

Rating: N

3.2.10 Kempfert et al. (EBGO 6.9) Method

The Kempfert et al. (2004) method is based on lower bound plasticity theory, pilot-scale tests, and numerical analyses. Like the Hewlett and Randolph (1988) method, this method considers a hemispherical domed arch between columns or pile caps. The method accounts for subgrade support of the geosynthetic reinforcement through use of a modulus of subgrade reaction.

Equations are provided for the stress on the reinforcement in terms of the column diameter and spacing, friction angle of the embankment fill, height of embankment, unit weight of the fill, and embankment live load surcharge. A dimensionless design chart for

a friction angle of embankment fill equal to 30 degrees is provided in Kempfert et al. (2004a), and other charts are included in German in EBGeo 6.9 (2004).

The Kempfert et al. (2004a) method employs a theory of elastic embedded membranes to evaluate the strain and tension in the geosynthetic. The results are also presented in the form of a dimensionless design chart. The strain in the geosynthetic is multiplied by the geosynthetic stiffness to obtain the tension in the geosynthetic.

In addition to the design charts, this procedure includes several other recommendations. The maximum clear spacing should be less than 3 m for static loads and less than 2.5 m for heavy live loads. The ratio of column width to column center-to-center spacing should be greater than 0.15. The ratio between modulus of the column and modulus of subgrade reaction of the soft soil should be greater than 100 to ensure full arching. Most piles fulfill this criteria, but some soil improvement columns may not fulfill the criteria, in which case, the Kempfert et al. (2004a) procedure should not be used. When using a single layer of reinforcement, the reinforcement should be located 6 in. (0.15 m) or less above the tops of the columns. When two layers of reinforcement are used, the vertical centroid between the two layers should be 12 in. (0.30 m) or less above the tops of the columns. Overlapping of reinforcement layers is allowed only above the pile caps and must be overlapped by a length greater than or equal to the width of the pile cap or column.

In the Kempfert et al. (2004) method, the vertical stress on the geosynthetic, p , can be calculated according to:

$$p = \lambda_1^\chi \left(\gamma + \frac{q}{H} \right) \left[H(\lambda_1 + h_g^2 \lambda_2)^{-\chi} + h_g \left(\left(\lambda_1 + \frac{h_g^2 \lambda_2}{4} \right)^{-\chi} - (\lambda_1 + h_g^2 \lambda_2)^{-\chi} \right) \right] \quad (3.12)$$

where $s_g = 1.414s$, $\lambda_1 = (s_g - d_c)^2/8$, $\lambda_2 = (s_g + 2d_c s_g - d_c^2)/(2s_g^2)$, $\chi = d_c(K_p - 1)/(\lambda_2 s_g)$, $h_g = s_g/2$ for $H > s_g/2$, and $h_g = H$ for $H > s_g/2$.

Performance Criteria/Indicators

Comments: This procedure is compatible with using factors of safety for the strength of geosynthetic reinforcement. It can be used to compute the deflection at the base of the reinforcement between columns.

Rating: H

Subsurface Conditions

Comments: The influence of subgrade support is accounted for through a modulus of subgrade reaction of the soft foundation soil during the calculation of the tension in the geosynthetic layer. There is no recommended method for determining the modulus of subgrade reaction, although, the modulus of subgrade reaction may be determined by correlation with laboratory strength/stiffness tests or determined *in situ* by a plate load test. Recommendations are provided for combining as many as three soft soil layers into a single value of the modulus of subgrade reaction. The approach of using a modulus of subgrade reaction is a better approach than the total stress approach by Russell and Pierpoint (2003), but still does not capture the consolidation behavior of the soft soil in terms of the effective pre-consolidation pressure and compression index.

Rating: M

Loading Conditions

Comments: The stress acting on the geosynthetic incorporates the effects of stress reduction due to soil arching within the embankment and depends on the unit weight of the fill, surcharge load, height of the embankment, diameter and spacing of the columns, and an empirical coefficient. Kempfert et al. (2004) also presents a method for evaluating the tension in the geosynthetic reinforcement. The strain in the geosynthetic is determined using design charts and the tension is determined by compatibility of stress-strain. This method incorporates the additional tension in the geosynthetic due to the tendency of the embankment to spread laterally.

Rating: H

Material Characteristics

Comments: The column diameter/spacing and friction angle of embankment fill are used to compute the stress on the geosynthetic or soft soil. This procedure applies to one or two geosynthetic layers and will confirm if the geosynthetic is stiff and strong enough for the given column spacing, modulus of subgrade soil, and height of embankment.

Rating: H

Construction Techniques

Comments:

Rating: N

Geometry

Comments: Applying this procedure iteratively will result in an acceptable combination of column diameter and spacing for a given type of geosynthetic.

Rating: H

Validation of Procedure

Comments: The procedure is compared with 1/3 scale experimental results and finite element numerical modeling by Kempfert et al. (2004a). The Kempfert et al

(2004a) procedure is a summary of the procedure in the draft EBGEO (German Recommendations for Geosynthetic Reinforcement) Chapter 6.9. Kempfert et al. (2004b) provides a case history. van Eekelen et al. (2004) provides an instrumented case history with 2 years of data which show that the method results in more accurate predictions of the load distribution in the embankment than BS8006 (1995). van Eekelen et al. (2008a) shows reasonable agreement between this method and results from an instrumented test embankment for the vertical stress on the geosynthetic reinforcement; however, the load transferred directly to the pile is over-predicted and the vertical stress on the soft soil is under-predicted.

Rating: M

Rational-Empirical Basis

Comments: This method employs a domed analytical model based on plasticity theory. It also includes the Rankine lateral earth pressure empirical coefficient.

Rating: R

Ease of Use

Comments: The procedure for calculating the stress on the geosynthetic involves solving a differential equation. Kempfert et al. (2004a) provides a dimensionless design chart for $\phi' = 30$ degrees (in English). EBGEO 6.9 (2004) provides dimensionless design charts for $\phi' = 30, 32.5, 35,$ and 37.5 degrees (in German). A dimensionless design chart is included which relates the strain in the geosynthetic to the force on the geosynthetic. Properties necessary to use the chart are the column diameter, clear span, stiffness of the geogrid, and modulus of subgrade reaction. The complete method is included in EBGEO 6.9 (2004) in German, which is an obstacle to the use of this method in the U.S.

Rating: M

LRFD Status

Comments: Kempfert et al. (2004a) does not discuss LRFD. Paragraph 6.9.7.1 of EBGEO 6.9 (2004) describes a general format with partial safety factors where the resistance is greater than or equal to the action effects. This method appears to fit within the framework of Eurocode 7, ENV 1997-1, which is also used in the BS8006 method, the Adapted Terzaghi method as described in Russell et al. (2003), and the Swedish method.

Rating: Y

3.2.11 Naughton Method

The Naughton Method calculates the critical height of an embankment assuming that:

- 1) the vertical shear plane in the embankment fill due to arching is log spiral in shape with initial radius equal to half the clear spacing between columns and final radius equal to the critical height,

- 2) the piles are arranged in a square grid, and
- 3) no support is given by the foundation soil to the yielding embankment fill.

The critical height is the plane above which there is equal settlement within the embankment, and according to this method, it is a function of the friction angle of the embankment fill and the clear spacing between pile caps or columns. For friction angles from 30 to 45 degrees, the critical height varies from 1.24 to 2.40 times the clear spacing between columns, and a higher friction angle of the fill results in a higher value of critical height. For high embankments, the stress reduction ratio is expressed as the ratio of critical height to height of the embankment. For low embankments, the stress reduction ratio is equal to one. The stress reduction ratio is defined as the ratio of the actual stress at the base of the embankment to the theoretical stress if no arching occurred.

In this method, higher quality fill material (i.e., higher friction angle) results in a higher value of critical height and a higher value of stress reduction ratio for an embankment height greater than the critical height. These results do not seem logical, and consequently, this method will not be pursued further in the SHRP2 R02 project.

According to the Naughton Method, for an embankment above the critical height, the vertical stress on the geosynthetic reinforcement, p , can be calculated according to

$$p = \frac{(s - a)(\gamma H + q)}{2H} e^{\left(\frac{\pi}{2} \tan \varphi\right)} \quad (3.13)$$

According to this expression, the vertical stress on the geosynthetic increases as the frictional increases, which is an unexpected result.

Performance Criteria/Indicators

Comments: This procedure calculates the vertical stress on the geosynthetic reinforcement or soft soil based on the height of the embankment. It can then be combined with one of the methods for determining the strain and tension in the geosynthetic reinforcement (if used) which would employ the factor of safety for ultimate strength of the geosynthetic. It does not consider settlement of the embankment or global stability.

Rating: M

Subsurface Conditions

Comments: This method does not consider support from the foundation subgrade.

Rating: N

Loading Conditions

Comments: The stress on the geosynthetic in this method depends on the column diameter and spacing (clear span between columns or pile caps), unit weight of the fill material, height of the embankment, surcharge load, and the friction angle of the embankment fill.

Rating: H

Material Characteristics

Comments: The unit weight and friction angle of the fill material are used to calculate the stress reduction ratio. The geosynthetic can be selected by applying one of the three methods to calculate the strain and tension in the geosynthetic.

Rating: H

Construction Techniques

Comments:

Rating: N

Geometry

Comments: A designer using this method would iterate with column spacing and diameter until the degree of arching was significant enough such that the soft foundation soil or geosynthetic could carry the load not supported by the columns.

Rating: M

Validation of Procedure

Comments: This procedure applies only to square column layouts. This method is compared with the BS8006 (1995), Carlsson (1987), Hewlett and Randolph (1988), Kempfert et al. (2004a), Russell et al. (2003), and Terzaghi (1943) methods along with results from numerical analysis for three embankments by Naughton (2007). The calculated stress reduction ratio for this method is higher than for some of the comparison methods and lower than for others, but in none of the three tests embankments analyzed does it yield the highest or lowest value of stress reduction ratio. According to Naughton's method, higher friction angles result in a larger value of the critical height of the embankment. McGuire and Filz (2008) note that a higher friction angle of the embankment fill results in a greater vertical stress on the geosynthetic, according to Naughton's method. Both of these items seem counterintuitive. Instead, it seems fundamental that, as the quality of the fill in the embankment increases, the value of critical height decreases and more load would be transferred to the columns (e.g., consider the case of a concrete slab spanning the columns where virtually no load would be transferred to the soft soil and the critical height would be the height of the top of the slab assuming it deflected minimally).

Rating: L

Rational-Empirical Basis

Comments: This method is based on Terzaghi's assertion that the shear planes formed by arching soil in a trap door opening are log-spiral in shape. This method applies the log-spiral shape to the shear planes developed in the embankment fill due to arching for a square array of columns.

Rating: R

Ease of Use

Comments: The expression for the critical height is very straightforward and depends only on the clear span and the friction angle of the fill. This procedure must be combined with one of the three methods for calculating the strain and tension in the geosynthetic reinforcement (if used).

Rating: H

LRFD Status

Comments: This procedure is not LRFD-based.

Rating: N

3.2.12 Swedish Method

Carlsson (1987) presents a method (in Swedish) for calculating the vertical stress on geosynthetic layers in a geosynthetic-reinforced column-supported embankment. Rogbeck et al. (1998) describe the method in English, and they include expressions for the tension in the geosynthetic for both 2D and 3D cases. The Carlsson Method considers a wedge of soil under the arch formed between columns where the internal angle at the apex of the wedge is 30 degrees (i.e. the angle of arching within the soil is 75 degrees from horizontal). It adopts a critical height approach such that any additional overburden above the top of the wedge (above the critical height) is transferred directly to the columns. In this method, the critical height is 1.87 times the clear spacing between pile caps. Rogbeck et al. (1998) include an expression for the force in the reinforcement per unit meter which is dependent on the column spacing and diameter, unit weight of the fill, and the strain in the reinforcement. The minimum area replacement ratio for this method is 10 percent.

Svano et al. (2000) present a method developed at SINTEF, a large independent research organization in Scandinavia. The method considers a three-dimensional wedge of soil with slope of the sides of the wedge equal to $\beta:1$ (V:H). The slope β has values between 2.5 and 3.5, and the precise value must be calibrated, presumably with physical model tests using the embankment soil or with numerical modeling. The precise value of β depends on the column width, column spacing, and height of the embankment. Svano et al. (2000) also state that further calibration is required for determining precise values of β

to use for design. For the purposes of this assessment, the method of Svano et al. (2000) is considered to be an extension of the Swedish method since it also considers a 3D wedge of soil above the pile caps. The Swedish method considers the angle of the wedge to be 75 degrees from the horizontal, whereas the angle is variable within the range from 68 to 74 degrees in the Svano method, depending on the geometry of the pile caps, spacing, and height of embankment.

In the Swedish Method, the vertical stress on the geosynthetic reinforcement, p , for the 2D case is equal to

$$p = \frac{\gamma(s - a)}{4 \tan 15} \quad (3.14)$$

Performance Criteria/Indicators

Comments: Partial factors of safety for the geosynthetic are used. General guidelines for global stability are provided by Rogbeck et al. (2003). Guidance is provided for calculating the additional tension in the geosynthetic due to the tendency of the embankment to spread laterally.

Rating: H

Subsurface Conditions

Comments: This method does not include support by the lower foundation soil.

Rating: N

Loading Conditions

Comments: The pressure acting on the geosynthetic reinforcement depends on the column diameter and spacing, and the unit weight of the embankment fill. Rogbeck et al. (2003) include a calculation for bond length of the reinforcement to ensure it will not pull out at the embankment side slopes.

Rating: H

Material Characteristics

Comments: The unit weight of the fill is used to calculate the vertical stress on the geosynthetic. This method uses only one layer of geosynthetic. The friction angle of the fill must be at least 35 degrees. The maximum strain in the geosynthetic is 6% with an additional 2 percent allowance for creep. Rogbeck et al. (2003) includes the parabolic method for calculating the tension and based on an assumed strain in the reinforcement. Rogbeck et al. (2003) also include procedures for the additional tension in the reinforcement due to the tendency of the embankment to spread laterally, as well as the required bond length of the reinforcement.

Rating: M

Construction Techniques

Comments:

Rating: N

Geometry

Comments: The column diameter and spacing are chosen such that the factor of safety for the geosynthetic reinforcement is adequate. The function of the reinforcement is greatest if it is placed directly on the pile caps, but it should for practical reasons be about 0.1 m above the pile caps.

Rating: H

Validation of Procedure

Comments: Rogbeck et al. (2003) state that finite element modeling support the assumption of a 30 degree top angle of the arch when the friction angle of the fill is 35 degrees.

Rating: M

Rational-Empirical Basis

Comments: This method assumes that the soil supported by the geosynthetic takes the form of a two-dimensional triangular wedge with an internal angle at the apex equal to 30 degrees and a base equal to the clear spacing of the columns.

Rating: S

Ease of Use

Comments: This procedure is straightforward and easy to use.

Rating: H

LRFD Status

Comments: This method employs a form of LRFD which is consistent with Eurocode 7, version ENV 1997-1. In this method, the “load” and “resistance” factors are all greater than or equal to 1.0. The resistance (R) is divided by the resistance factors (γ_R) and the action effect (E) is multiplied by the partial factors for action effects (γ_S). The result must satisfy the inequality $R/\gamma_R - \gamma_S E \geq 0$.

Rating: Y

3.3 METHODS TO DETERMINE TENSION AND STRAIN IN THE GEOSYNTHETIC REINFORCEMENT

There are at least three methods to determine the tension and strain in the geosynthetic reinforcement. These three methods are used by some of the 12 methods reviewed in Section 3.2. The Parabolic Method is used in the BS8006 (1995), Filz and Smith (2006), and the Swedish Methods. The Tensioned Membrane Method is used by Collin (2004, 2007). Although there are no preliminary ratings assigned to the methods to determine

the tension and strain in the geosynthetic reinforcement, they are presented here for completeness. The methods are compared with results from the CSE tests in Section 7.2.

3.3.1 Parabolic Method

The Parabolic Method assumes a parabolic deflection between columns. According to Giroud (1995), the exact solution for strain, ε , in terms of the deflection, d , center-to-center spacing, s , and pile cap width, a , is equal to

$$\varepsilon = \frac{1}{2} \sqrt{1 + 16 \left(\frac{d}{s-a} \right)^2} + \frac{s-a}{8d} \ln \left[\frac{4d}{s-a} + \sqrt{1 + 16 \left(\frac{d}{s-a} \right)^2} \right] - 1 \quad (3.15)$$

Giroud (1995) also showed that when the strains are small, the strain for a parabolic deflection can be approximated by $\varepsilon \approx 8d^2/[3(s-a)^2]$. Using this approximation, for a square array of square columns, the tension in the geosynthetic, T , is calculated according to:

$$T = \frac{p(s^2 - a^2)}{4a} \sqrt{1 + \frac{1}{6\varepsilon}} \quad (3.16)$$

Equation (3.16) is the Parabolic Method equation that appears in BS8006 (1995), Robgeck (2003), and many others. McGuire and Filz (2008) present a solution which imposes stress-strain compatibility by substituting $\varepsilon = T/J$ into Equation (3.16), resulting in:

$$96T^3 - 6K_g^2T - K_g^2J = 0 \text{ where } K_g = \left(\frac{p(s^2 - a^2)}{a} \right) \quad (3.17)$$

3.3.2 Tensioned Membrane Method

For the Tensioned Membrane Method, as described by Collin (2004, 2007),

$$T = \frac{p(s-a)\Omega}{\sqrt{2}} \quad (3.18)$$

where Ω is a dimensionless coefficient determined by:

$$1 + \varepsilon = 2\Omega \sin^{-1} \left(\frac{1}{2\Omega} \right) \quad (3.19)$$

Stress-strain compatibility can be imposed for the Tensioned Membrane Method (McGuire and Filz 2008), by combining Equations (3.18) and (3.19) and by substituting $\Omega = T/J$, which results in:

$$\left(\frac{2\sqrt{2}TJ}{p(s-a)} \right) \sin^{-1} \left(\frac{p(s-a)}{2\sqrt{2}T} \right) - T - J = 0 \quad (3.20)$$

3.3.3 Kempfert et al. (EBGEO 6.9) Method

Kempfert et al. (2004) present an analytic model based on the theory of elastically embedded membranes to determine the tension and strain in the geosynthetic. The method imposes stress-strain compatibility, and the resulting strain can be determined from a dimensionless design chart presented by Kempfert et al. (2004a) and in EBGEO 6.9 (2004).

CHAPTER 4

DESCRIPTION OF CSE TEST FACILITY AND INSTRUMENTATION

4.1 MOTIVATION FOR CSE TESTS

Research and documentation of CSE performance falls into one of several categories: bench-scale tests, centrifuge tests, case histories, numerical modeling, and pilot- or full-scale test results. Each of these categories is discussed below.

Hewlett and Randolph (1988), Low et al. (1994), Horgan and Sarsby (2002), van Eekelen et al. (2003), Chen et al. (2008), work in progress by McGuire (2011), and others have performed bench-scale tests to investigate CSE behavior. Centrifuge modeling results are presented by Ellis and Aslam (2009a/b). Bench-scale tests and centrifuge modeling provide valuable insight into the performance of CSEs, and many of the bench-scale tests provided data upon which some of the design methods in Chapter 2 were based. In any bench-scale test, it is important that the results be verified at full scale since size effects may influence the outcome of the bench-scale testing. This is particularly true with regards to the soil-geosynthetic interaction and possible stiffening effect of geogrids, which is difficult to model at bench-scale.

Case histories are reported by authors such as Forsman et al. (1999), Alexiew et al. (2000), Collin et al. (2005), Almeida et al. (2007), Whyte (2007), Batista et al. (2008), Bergado et al. (2008), Young et al. (2004, 2008), and many others. Some full-scale instrumented tests or trial sections associated with larger projects have been performed such as those described by Habib et al. (2002), Hossain and Rao (2006), Stewart et al. (2004), Abdullah and Edil (2007a/b), Wachman et al. (2010), and Chen et al. (2010). Case histories also provide valuable insight into CSE and GRCSE performance; however, many case histories have uncertain or ill-defined boundary conditions, undefined material properties, and/or inadequate instrumentation, which complicate the interpretation of the results.

Numerical results of GRCSE analyses are presented by Han and Gabr (2002), Collin et al. (2006), Smith and Filz (2007), Filz and Plaut (2009), and others. Numerical analyses also provide valuable insight into CSE and GRCSE behavior, but they should be calibrated with field measurements to provide more reliable results. Numerical methods are often time-consuming and are difficult to implement in routine geotechnical practice.

Villard et al. (2004) and Le Hello and Villard (2009) describe a CSE test facility where temporary support is provided from compacted sand which is removed from a side-opening door after the embankment is constructed on top. The test pit has dimensions of 9.8 ft (3 m) wide, 15.6 ft (4.75 m) long, and 6.6 ft (2 m) high. The columns are 3.3 ft (1 m) in length with a center-to-center spacing of 3.9 ft (1.2 m) in a fixed triangular arrangement. The columns have round pile caps with a diameter of 8.1 in. (0.205 m). The reported embankment heights ranged from 1.6 to 4.9 ft (0.5 m to 1.5 m) and included 2 layers of geotextile reinforcement that were fixed at the perimeter of the facility. These boundary conditions may not be realistic, and this test facility permits investigation of only a few of the variables relevant to GRCSE design.

Kempfert et al. (2004) briefly describe the test arrangement for 1:3 scale tests that are described further by Zaeske (2001) in German. The test setup consists of four 6.3 in. (16 cm) square piles with 1.3 ft (40 cm) length in a 3.6 ft (110 cm) square facility. Embankment heights shown in Kempfert et al. (2004) are up to 2.3 ft (70 cm). The soft soil between the piles is described as a weak peat. Reinforced and unreinforced sand fill of varying heights was placed above the piles and soft soil. Instrumentation included load cells in the piles, earth pressure cells within the fill, and strain gages on the reinforcement. The results of this study were used to develop the Kempfert et al. (2004) design procedure, which is also incorporated in EBGEO 6.9 (2004).

Oh and Shin (2007) report a series of five “pilot-scale” tests with 4 in. (0.1 m) round concrete piles and 6 in. (0.15 m) diameter pile caps. The column center-to-center spacing varied from 2.0 to 3.1 ft (0.6 to 0.95 m). Of the five test sections, four contained piles and one contained no piles for comparison. Three of the piled sections also contained one layer of geogrid reinforcement. The five test sections were tested simultaneously in a 13 m x 3 m test site with a soft soil depth of 5.2 ft (1.6 m). Embankments were constructed of poorly graded silty sand (SP-SM according to USCS) on marine soft clays (CL), and the settlement, earth pressures, and geogrid strains were monitored over time. The boundary conditions are unknown, but an embankment height of 2.9 m and a 3 m width of soft soil suggest that the boundary conditions would be extremely important to the interpretation of results from these tests.

Many of the 12 distinct design or analysis procedures documented in Table 2.2 also contain subvariations within them, so the overwhelming number of design or analysis procedures can be confusing to the practicing geotechnical engineer. Habib et al. (2002), Love and Milligan (2003), and McGuire and Filz (2008) among others, document the widely varying results produced by these design procedures.

In an FHWA document on CSE design procedures, Collin et al. (2006) perform numerical analysis and parametric studies based on an instrumented CSE case history reported by Gartung et al. (1996). Collin et al. (2006) recommends the following for further research into CSE design:

“Instrumentation of full scale structures to evaluate strain in the reinforcement, settlement profiles, arch angle, etc. These studies may include instrumented CSE projects and research projects (i.e., where an air bag is employed below the LTP and deflated to evaluate the case where no support is provided from subgrade.)”

A review of the CSE technology completed by Gabr et al. (2006) for the Central Federal Lands Highway Division (CFLHD), a Core Business Unit of FHWA, labels the CSE technology as “Developing.” Gabr et al. (2006) notes that “there is no current guidance or overwhelming field verification regarding which of the ... design methods to use” and further states that “the current design methods should be validated by full scale, well instrumented field measurements investigating strains in the geosynthetic, deformation characteristics, and stress distribution between column and native soil.” It also states that “the confinement benefits from the geosynthetic on the granular LTP material (if applicable for a particular grid or textile product) are not addressed in the design methods.”

A comprehensive suite of full-scale CSE or GRCSE tests has rarely been performed. The facility described in Section 4.2 will provide a means to do so and may answer many of the questions about CSEs and GRCSEs that remain unanswered. Use of this facility will enable engineering and science investigations not otherwise possible since nothing else like this facility exists to the author’s knowledge. It may provide a means to tie together the results of bench-scale tests, centrifuge modeling, case histories, numerical modeling, and results from other instrumented CSE tests. The facility and the results of the current study may also have application to other areas of reinforced soil arching such as sinkhole mitigation, tunneling, and mining engineering.

Currently, design engineers are left with a decision to choose traditional solutions, such as preloading with wick drains, which take a long time and could damage adjacent facilities, or to take a risk and select one of twelve design/analysis procedures with unknown reliability. Neither choice is an acceptable solution. This research will investigate the factors affecting the performance of GRCSE and result in improved design recommendations for GRCSE projects. The objective is to enable more widespread use of this technology for new embankments and widening of existing embankments for highway and railroad infrastructure. The potential payoff for this

project is high because it may increase the reliability of design procedures for this technology.

4.2 DESCRIPTION OF THE CSE TEST FACILITY

In order to fully evaluate the load transfer and arching that occurs within a CSE, a test facility was designed and constructed at Virginia Tech. The facility is located at the Kentland Farm property which is approximately 10 miles west of Blacksburg and the main campus.

The test facility consists of a 12 in. thick, 32 ft by 32 ft reinforced concrete mat foundation, with a 12 in. wide and 16 in. high concrete masonry unit (CMU) wall around the perimeter. The result is a 30 ft by 30 ft interior area for CSE testing. The surface of the mat foundation was made as level as possible and the maximum differential elevation is approximately 0.7 in.

The mat foundation was constructed using 4,000 psi 28-day compressive strength concrete and contains 2 grids (for both positive and negative bending moments) of ASTM A615 Grade 60 #6 rebar spaced 12 in. on center. The mat foundation is designed to support a minimum of four 16 in. diameter round columns with a maximum load on each column of 150 kips.

The perimeter wall is tied into the foundation with #4 rebar grouted into the slab to a depth of 6 in. at 2 ft intervals. Additional wall reinforcement is located at the corners of the facility. The interior cells of the CMU wall are grouted with the exception of a 10 ft section of the perimeter wall which is left open to permit equipment to enter the facility. The ground surrounding the facility is graded level with the top of the perimeter wall, 16 in. above the top of the slab.

The size of the facility was selected as a reasonable size based on the time and labor available to complete the testing phase of this research. The 16 in. height also allows for significant deflection of the CSE but also minimizes the volume of material required for temporary support. A picture of the completed CSE facility is shown in Figure 4.1. Plan and elevation views of the facility with a sample embankment are shown Figure 4.2.

Precast moveable concrete columns, also 16 in. in height, are placed on the slab in the desired arrangement. Since the columns are not permanently fixed to the slab, a variety of column sizes, clear spacings, and arrangements (square or triangular) can be investigated. The columns used in this study were 2 ft diameter. The columns were

fabricated with round cardboard tube forms and concrete with a minimum compressive strength of 4,000 psi.



Figure 4.1: Picture of the CSE test facility.

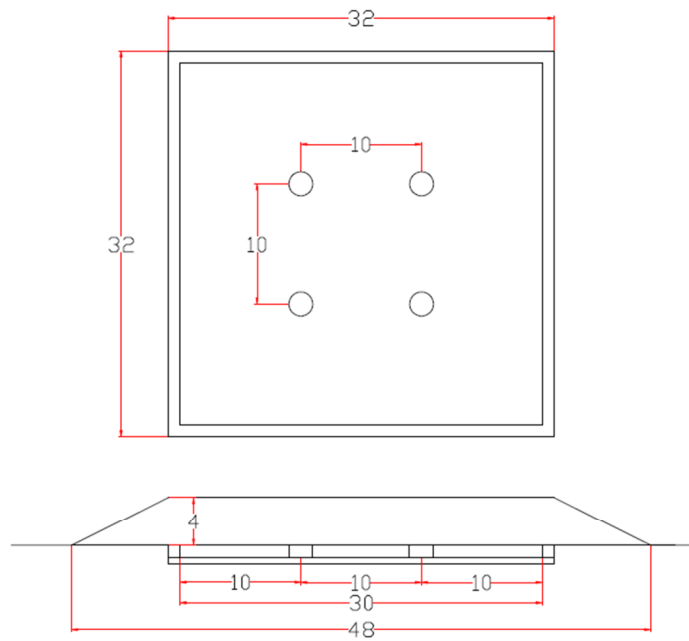


Figure 4.2: CSE plan and cross-section views with 4 precast moveable columns and sample embankment.

4.3 TEST CONCEPT

The full procedure for conducting a CSE test is found later in Section 5.4, but an introduction to the test concept is provided here. Figure 4.3 shows a simplified cross-section illustrating the components of the facility and embankment. To begin a CSE test, a layer of 6 mil polyethylene plastic is placed on top of the mat foundation. The

polyethylene plastic serves to contain the fluid that will be pumped into the facility later in the procedure and prevent the fluid from permeating through the walls of the facility. Rubber mats, approximately 0.25 in. in thickness are placed at the locations of the columns to help distribute the load from the columns to the mat foundation and to prevent point loads. Precast concrete columns of the desired shape and size are then placed on the rubber mats.

A layer of geonet is placed on top of the polythene plastic over the entire base of the slab inside the perimeter wall, except where the columns are positioned (see Figure 4.4). The purpose of the geonet is to conduct a fluid to all parts of the slab which will then dissolve the geofoam used for temporary support. The areas between columns are filled with 16 in. high geofoam blocks, cut to fit, and placed over the layer of geonet (see Figure 4.5). Another layer of 6 mil polyethylene plastic is then placed on top of the geofoam and holes are cut around the columns so the plastic will settle down on top of the geofoam. Small pieces of geotextile are placed above the perimeter wall and columns to avoid damage to the geogrid by the concrete edges. The top of the columns, the geofoam blocks, the perimeter wall, and surrounding backfill soil are all at the same elevation and form a level platform for construction of the CSE (see Figure 4.6).

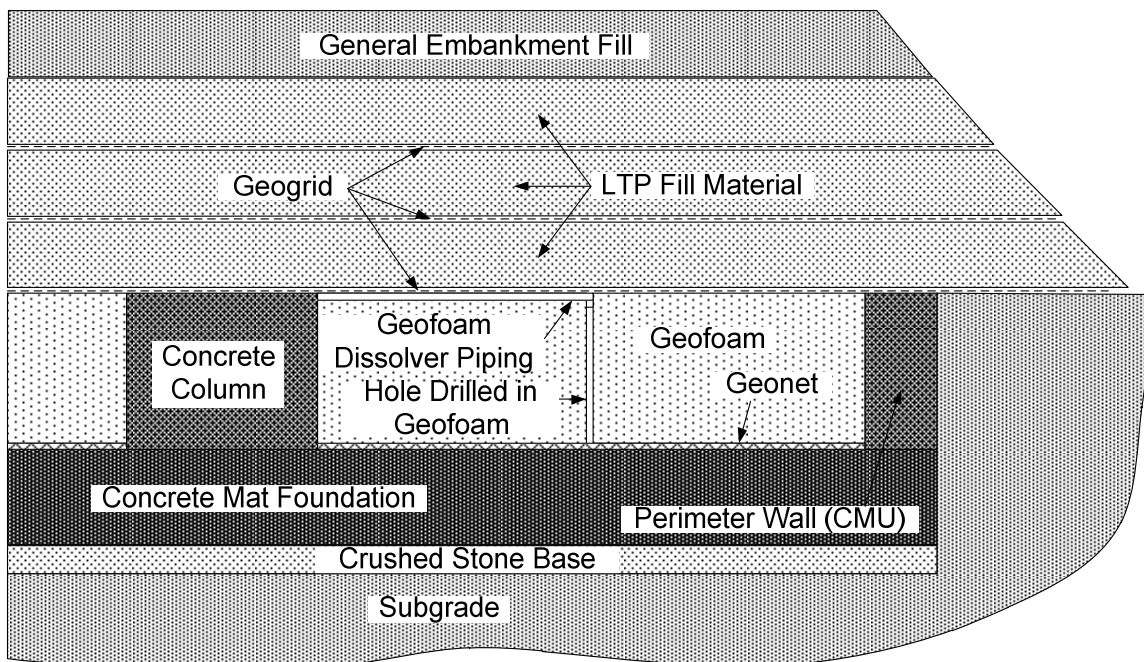


Figure 4.3: Simplified cross-section of test facility and embankment.



Figure 4.4: CSE test facility with base layer of polyethylene plastic, geonet, and 9-column array.

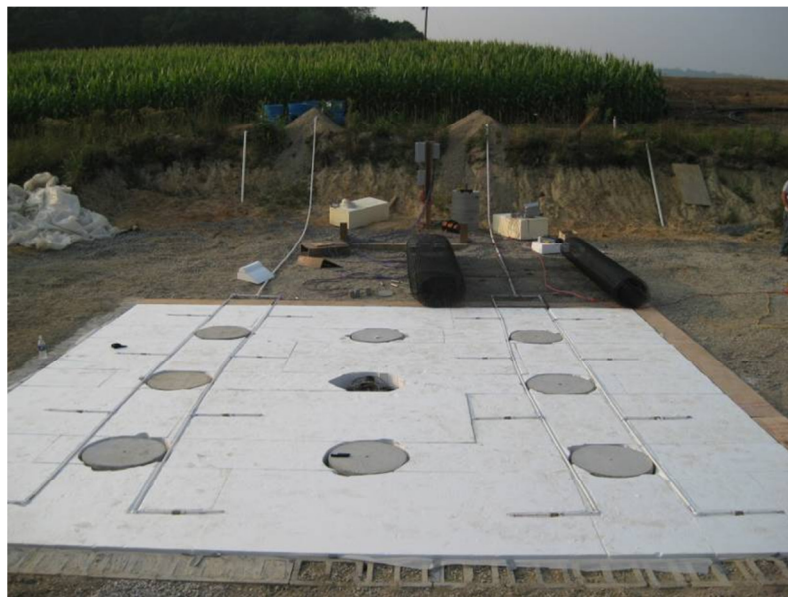


Figure 4.5: CSE test facility with geofoam and geofoam dissolver delivery system.

The geonet underneath the geofoam is then flooded with d-limonene through a network of PVC pipes. D-limonene is a natural oil obtained from orange peels that dissolves expanded polystyrene (EPS) on contact. Noguchi et al. (1998) and Shin and Chase (2005) note that d-limonene is an effective dissolver of expanded polystyrene and is used in recycling applications to minimize the volume of foam products placed in landfills. Clara et al. (2009) provide properties of d-limonene such as density and viscosity at various temperatures.

Dissolving the geof foam removes the support from under the embankment so that the entire weight of the embankment is resting on the perimeter walls and the interior columns. The embankment is free to deflect between these structural supports and the response is measured with the instrumentation described in Section 4.6.



Figure 4.6: Reinforced fill placement.

It is important to note that documentation for the use of geof foam as a lightweight fill and a compressible inclusion exist in the literature, but there do not appear to be any cases where geof foam is used for temporary support and is then dissolved. Ellis and Aslam (2009a/b) report the use of EPS as soft subsoil in centrifuge tests. As the g-level increases, the stress increases on the EPS until yielding. Nowhere in the literature was an example found where geof foam was dissolved in order to completely remove support from beneath an embankment.

The variables that can be evaluated with this facility include:

- Column geometry (square, round, diamond), size, and spacing (area replacement ratio)
- Column arrangement pattern (square, rectangular, equilateral triangular, isosceles triangle)
- Geosynthetic reinforcement type (geogrid, geotextile), number of layers, vertical spacing between layers, and stiffness of each layer
- Embankment material type and density, including layers of different soil types
- Embankment height

For a proper understanding of GRCSEs, it is helpful to quantify the variables and isolate each in succession to ultimately understand the load transfer and arching that occurs within the geosynthetic-reinforced fill material at the top of the columns. Such analysis can only be accomplished through a facility like the one described where repeated tests can be performed. Other effects not captured in this facility, such as the influence of the soft soil between columns, can be addressed with geotechnical analyses, but the load-transfer, arching, and confinement effects of the geosynthetic are not fully understood, and they can be studied most effectively when investigated independently from soft soil support.

Other parameters relating to CSE design that are not investigated with this facility include:

- Stiffness of the piles
- Pile installation method (e.g. driven piles may increase pore pressures)
- Column permeability (e.g. stone columns can increase the drainage of the soft subsoil)
- Subsoil compressibility

The influence of these parameters are better understood than the load transfer and arching within the embankment, and they can be analyzed with other geotechnical methods. Once the load transfer and arching is better understood, CSE system performance can be analyzed completely.

Data gathered from this facility will be compared with results from the twelve analytic methods in Table 2.2. Procedures which do not accurately predict the embankment performance can be ruled out, and one or more successful procedures will be recommended for widespread use in transportation projects.

4.4 ALTERNATIVE METHODS CONSIDERED

Geofoam was selected as a means to provide temporary support to the CSE during construction. Other methods to remove support, such as airbags or water bladders were considered. Fluet et al. (1986) report a geosynthetic reinforced embankment test where temporary support was provided by airbags. Chen et al. (2008b) also report the use of water-filled bladders in a bench-scale application.

Airbags offer the flexibility of varying the pressure within the bags to gradually and uniformly remove support. However, many airbags would be required and the interface between the bags would require additional material such as urethane foam to fill in the gaps at the interface between bags. The support condition may therefore be variable. The bags may have required a solid surface to permit walking on them for installation of the instrumentation and compaction on top of the airbags would be difficult.

Geofoam is used in transportation situations for fill placement, and it permits operation of equipment once a minimum cover is placed. Due to the uniform support that the geofoam provided and the availability of an environmentally friendly solvent to dissolve the geofoam, it was deemed the best solution to provide temporary support for the embankment.

4.5 GEOFOAM DISSOLVER DELIVERY SYSTEM

The initial geofoam dissolver delivery system for CSE #1 was constructed of 1.5 in. diameter PVC pipe. The pipes were run along two sides of the facility at the base of the slab on top of the geonet. Holes were drilled at even intervals along each section of pipe resulting in a flow rate of approximately 4.5 gpm per side when calibrated with water. In the first CSE test, it was noticed that the dissolving of the geofoam, and therefore the settlements, proceeded from the sides of the facility toward the center. In order to more realistically model how settlement would occur in the field, the delivery system was modified for subsequent CSE tests.

In an actual CSE, the stress on the soft soil is highest in the centroid of the column arrangement, and settlement will progress from this point. In order to model this behavior, a dissolver distribution system was designed with delivery points at the centroid of column arrays, or between the columns and the perimeter wall. For a 9-column array, this results in 16 delivery points as shown in Figure 4.7. In order to provide even flow to each delivery point, valves were added to control the flow. Prior to construction of CSEs #2 - #5, the flow was calibrated using water, as in Figure 4.8.

The pumping point was elevated above the slab approximately 6 ft and the fluid was pumped with two rotary hand pumps. After calibration was complete, the flow rate at each delivery point was approximately 0.5 gpm, resulting in a flow rate of 4 gpm for each side of the distribution system, and 8 gpm total. Trial tests revealed that application of 110 gallons of d-limonene was sufficient to dissolve the 16 in. thick geofoam in a 22 ft square test area as used in CSEs #2 to #5. Two rotary hand pumps capable of 8 to 10 gpm were used to pump d-limonene from 55 gallon drums into the distribution system.

The pumping process lasted approximately 7 minutes total for each test, and the geofoam dissolved over a period of several hours following the pumping.

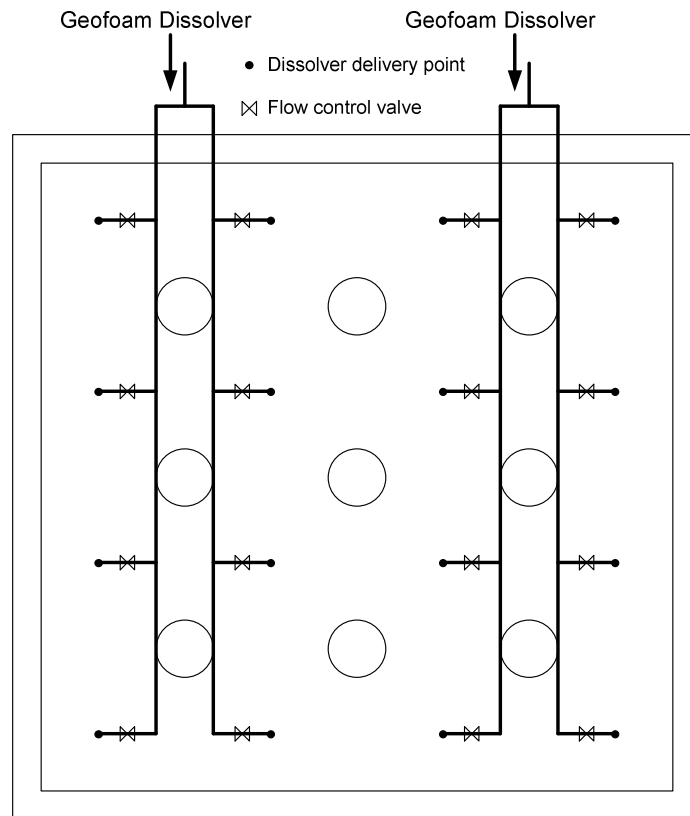


Figure 4.7: Column and geofoam dissolver distribution system for CSE Tests #2 to #5.



Figure 4.8: Geofoam dissolver distribution system installation and calibration with water.

4.6 INSTRUMENTATION

During construction of a CSE above the test facility, instrumentation is placed at key locations. The instrumentation includes load cells on one column, earth pressure cells at various points within the embankment, lead-wire extensometers to measure geosynthetic strain, foil strain gages on the geosynthetic reinforcement as a redundant geosynthetic strain measurement, and settlement profilers to obtain cross-sections of settlement at the base of the geosynthetic reinforcement. Traditional survey techniques with a total station were used to measure surface settlement. Table 4.1 lists the CSE test instrumentation, which is described in more detail below.

In the CSE tests, three load cells were used in a triangular arrangement in one of the columns to measure the load in the column. The load cells were placed between steel plates on top of a concrete column that is shorter than the other columns used in the tests. The top steel plate is at the same elevation as the other precast concrete columns. Three steel pipe sections cut slightly shorter than the height of the load cells were also placed in the central column so that the column would remain stable in the event of an eccentric load. The central column with load cells is shown in Figure 4.9.

Webcams were also placed in the void between the two steel plates housing the load cells. The webcams were not continually monitored, but were connected by USB cables to a laptop to take still photos at key times. The primary purpose of the webcams was to evaluate the dissolution of the geofilm and to view the unsupported geogrid and gravel. Some of the webcam pictures are shown along with the CSE test descriptions and results in Chapter 6. Figure 4.9 shows the central column (without the top steel plate) with the load cells and webcams inside.

Up to three earth pressure cells were placed in the test embankments. In most cases, the earth pressure cells were placed near the base of the embankment, approximately 3 in. above the base layer of geogrid. Figure 4.10 shows a picture of an earth pressure cell during installation.

Table 4.1: Instrumentation used in CSE tests.

Type of Instrument	Quantity	Purpose	Model Number
Load cell	3	measure load on column	Geokon 4900-100-1 vibrating wire load cell, 100 kip capacity
Earth pressure cell	3	measure earth pressure within embankment	Geokon 4800-1-170KPA vibrating wire earth pressure cell, 170 kPa (25 psi) range
Lead-wire extensometer	8	measure extension of the geogrid, calculate strain from differential extension	Micro-Epsilon WPS-1000-MK46-P10 draw-wire sensors (1000 mm range), stainless steel wire and protective tubing
Strain gage	16	measure strain in geogrid	Vishay EP-08-230DS-120 or EP-08-125AD-120 strain gages with Vishay MR1-120-133 bridge completion module
Datalogger	1	data storage and collection	Geokon 8021 MICRO-1000 datalogger
Multiplexer	3	provide additional input channels for datalogger and separate excitation voltages for the different types of instrumentation	Geokon 8032 16X4 multiplexer
Settlement profiler	1	measure settlement within the embankment	VW 4651-1-170KPA settlement profiler 170 (25 psi)
Vibrating wire readout	1	handheld data readout for settlement profiler	Geokon GK 404
Total station	1	measure surface profiles before and after removing embankment support	Leica TC605L



Figure 4.9: Central column with load cells and webcams. The steel plate at the top of the picture is placed over the load cells prior to placing fill.



Figure 4.10: Earth pressure cell installation.

Strain in the geosynthetic was measured in two ways: using lead-wire extensometers and foil strain gages. The lead-wire extensometers were used on all of the CSE tests and the foil strain gages were only used on CSEs #2 and #4 due to the time required to prewire and glue the gages onto the geogrid.

The lead-wire extensometers (LWEs) were fabricated using Micro-Epsilon WPS-1000-MK46-P10 draw-wire sensors (also known as string potentiometers or “string pots”), stainless steel wire, and protective nylon tubing (see Figure 4.11). The manufacturer’s calibration of the draw-wire sensors was checked in the lab and found to be accurate to 1 mm or less. The stainless steel wire is type 302/304 stainless steel, 0.020” diameter, with

spring temper and bright finish, and has a published tensile strength of 210,000 to 340,000 psi according to the manufacturer. The stainless steel wire is protected by a high-strength nylon tubing with outside diameter (OD) = 5/32", inside diameter (ID) = 0.106", and wall thickness of 0.025". Graphite powder was used to reduce the friction between the stainless steel wire and the inside of the conduit. The ends of the stainless steel wires were fixed to the geogrid by drilling small holes through the grid and attaching the wire. The wires and conduit were then run out of the embankment a distance of approximately 28 ft to the lead-wire extensometers. The conduit was held in place on the geogrid with cable ties. These parameters and installation procedures generally follow the recommendations of Cuelho et al. (2008). Figure 4.12 and Figure 4.13 show the lead-wire extensometers used to measure strain in the CSE tests.

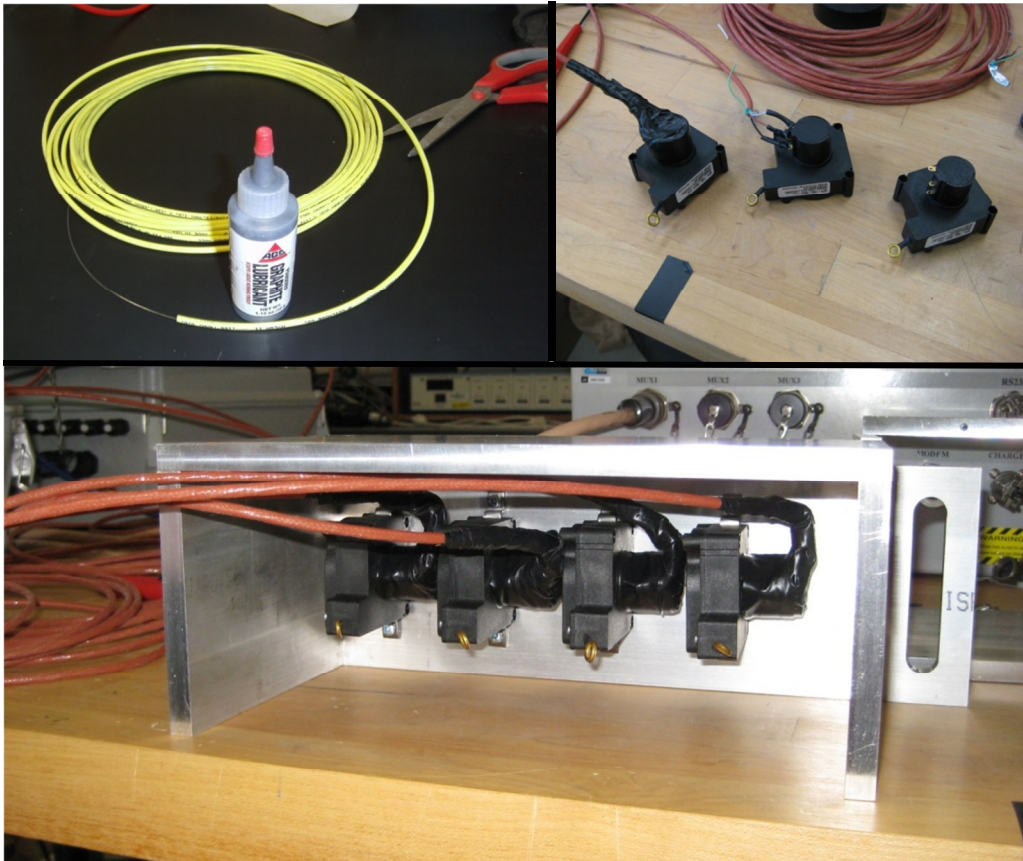


Figure 4.11: Stainless steel wire and nylon tubing (top left), draw-wire sensors (top right), and aluminum housing for lead-wire extensometers (bottom) used in CSE tests.



Figure 4.12: Mounting bracket, aluminum housing, and protective tubing for lead-wire extensometers.



Figure 4.13: Lead-wire extensometers, instrumentation wiring, geofabric, geogrid placement, and geofabric placement.

The settlement within each embankment was measured with a Geokon 4651 vibrating wire settlement profiler pulled through 2-in. inside-diameter polyethylene pipes placed

within the embankment. A Geokon GK-404 handheld device is used to collect data from the settlement profiler. A picture of the settlement profiler is shown in Figure 4.14. Ground penetrating radar was also considered as a means of measuring base settlement but cost and time considerations prevented exploration of its use on this project.

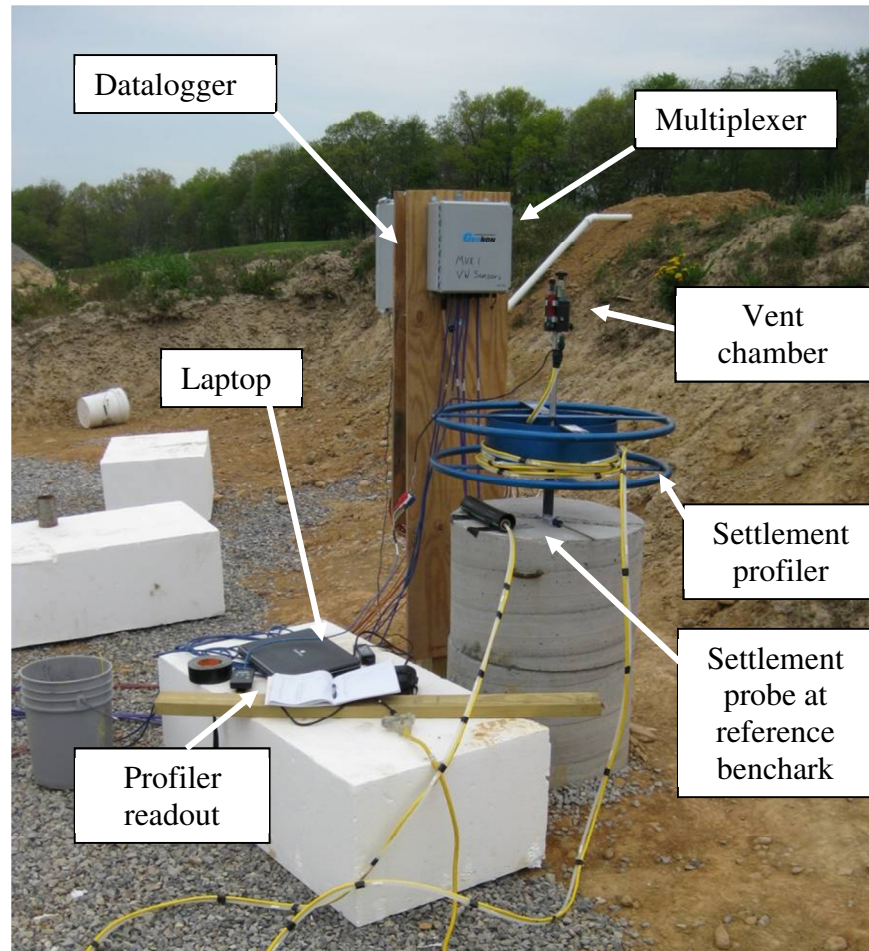


Figure 4.14: Settlement profiler and data acquisition system.

The foil strain gages are Vishay EP-08-230DS-120 (used in CSE #2) and EP-08-125AD-120 (used in CSE #4). Both types can function up to a strain of 20% according to the manufacturer, but all gages debonded at strains less than 10% in the lab and field tests. The 230DS gages have a gage length of 0.23 in. and the 125AD gages have a gage length of 0.125 in. The gages are installed according to the manufacturer's specifications, which are similar to procedures described in Warren et al. (2006) and Warren et al. (2010). Vishay GA-2 adhesive is used to bond the gages to the geogrid and Vishay MCOATJ water-proofer was used as a moisture barrier. The gages are connected to Vishay MR1-120-133 bridge completion modules, which are wired into a dedicated multiplexer.

An extensive laboratory testing program with the strain gages was undertaken to determine calibration factors for the gages based on the gage properties and installation location on the geogrid. The strain measured by a foil gauge glued to a rib is generally less than the overall strain of the geogrid specimen since the rib is stretched the most in the manufacturing process and has a locally higher modulus as compared to the junction. The calibration factor is defined as:

$$\varepsilon_{machine} = CF * \varepsilon_{FSG}$$

where $\varepsilon_{machine}$ is the strain of the entire specimen in the lab measured by the tensile testing machine, CF is the calibration factor, and ε_{FSG} is the strain measured by the foil strain gage in the lab. The machine strain may slightly overestimate the total strain in the specimen due to compliance at the machine grips. For the 230DS gages used in CSE #2, a calibration factor of 1.25 was determined based on five single-rib tensile tests on Tensar® BX1500 comparing the gage strain to the machine strain. Similarly, a calibration constant of 1.40 was determined based on five single rib tests on the 125AD gages. A sample test result comparing corrected gage strain to machine strain is shown in Figure 4.15. A description of the testing process and the results comparing gage strain to machine strain are shown in APPENDIX A.

Other methods of measuring strain in the geosynthetic were considered, such as fiber optic methods. Wang et al. (2009) describes the use of Brillouin Optical Time Domain Reflectometry (BOTDR) for measuring strain in geogrid reinforcement in a retaining wall application. In this case, the strain is purely 1-D and strains are relatively small. BOTDR has capability to measure up to +/- 1.5% strain and the data acquisition equipment is expensive. There is also a lack of prior documentation of BOTDR used for CSE applications. Since there is a horizontal and vertical component to the deflection of the geosynthetic and typical design strains are 5 – 6%, BOTDR was not used.

Geosynthetics with fiber optic strain gages installed within them by the geosynthetic manufacturer were also considered. Most of the fiber optic systems have strain limits of 5%. The strain limits combined with time and cost considerations prevented their use in the CSE tests in this report.

Data collection was performed with a Geokon Micro-1000 datalogger, which is based on the Campbell Scientific Model CR1000 Measurement and Control System. Three Geokon 8032 multiplexers are used: one for the vibrating wire instruments (load cells and earth pressure cells), one for the Vishay strain gages, and one for the Micro-Epsilon

draw-wire sensors. Portions of the data acquisition system were shown in Figure 4.14. In general, readings of all of the instruments were taken every hour during the CSE tests.

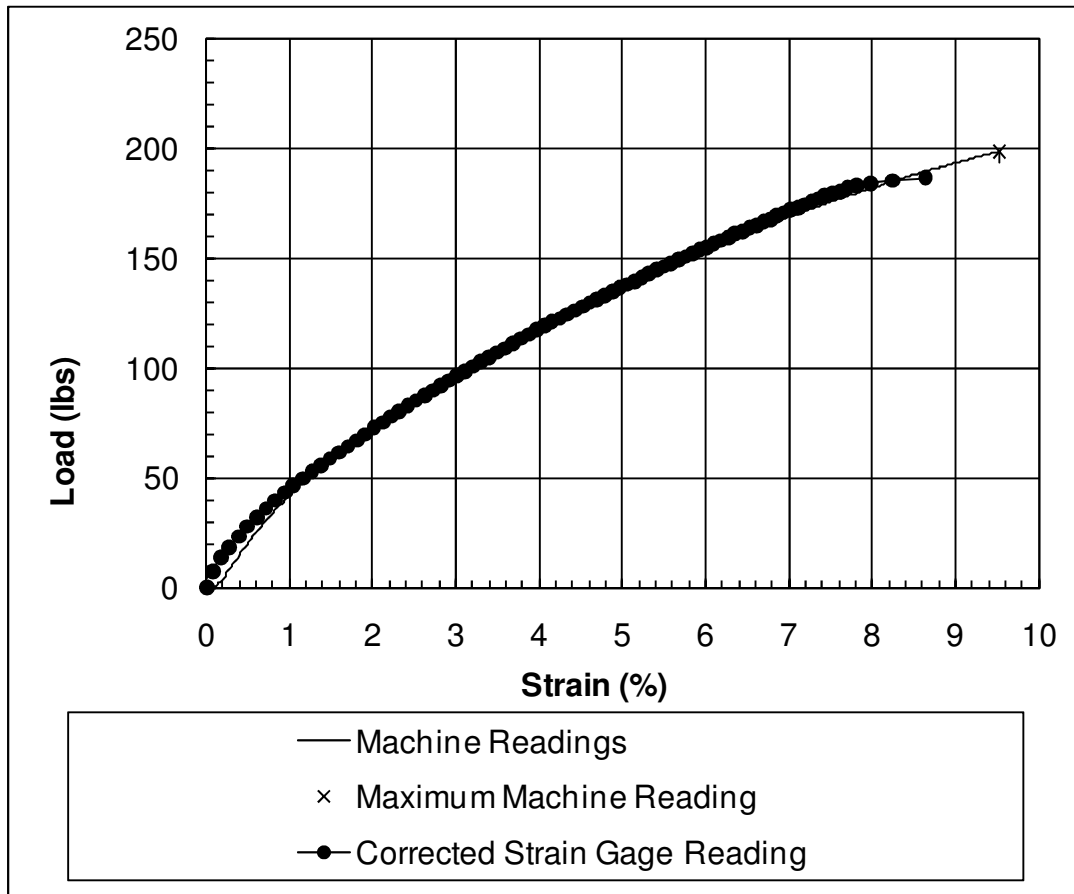


Figure 4.15: Plot of corrected gage strain (CF = 1.22) and machine strain during single-rib load test on Tensar® BX1500 geogrid.

A set of four survey benchmarks were installed at the site and a coordinate system was established. Surveys using a Leica TC605L total station were performed on each layer during construction to ensure proper elevation. Surveys were performed on the embankment surfaces before and after dissolution of the geofoam to measure total and differential settlement. Survey grids as shown in Figure 4.16 were painted on the surface of the completed embankment to facilitate measurement of elevations before and after dissolving the geofoam in each CSE test. The distance between survey points was typically 1 ft within the area of the columns and a coarser mesh of 2 to 3 ft was used elsewhere.



Figure 4.16: Picture of survey grid and total station on the embankment surface.

CHAPTER 5

MATERIALS, EQUIPMENT, AND PROCEDURES USED IN CSE TESTS

5.1 MATERIAL PROPERTIES

Properties for the gravel, geofoam, and geogrid used in the CSE tests are discussed below.

5.1.1 Properties of Gravel Fill

Two types of gravel were used in the tests. The first gravel meets the 21B gradation requirements of VDOT (2007) and was delivered from Acco Stone in Blacksburg VA. The gradation requirements of VDOT 21B are provided in Table 5.1, which includes a range of 4% to 7% passing the #200 sieve when tested according to Virginia Test Method (VTM) 25. VTM 25 requires that only the material passing the #10 sieve be washed. Therefore, any fines clinging to the material coarser than the #10 are counted as coarser materials, and the fines content may be artificially low when determined by the VTM 25 method. Gradations on the VDOT 21B from Acco Stone revealed an average fines content of approximately 11% when the entire gradation sample was washed.

A different source of gravel was sought with a lower fines content due to concern about the high fines content leading to artificially high strength due to negative pore water pressures, which may limit the application of the findings from the CSE tests. The result was the selection of the WVDOT (2000) Class 1 gravel from Pounding Mill's Mercer Plant, which has an average fines content of 5% in washed sieve analyses. The gradation requirements for VDOT 21B and WVDOT Class 1 are shown in Table 5.1.

Duncan et al. (2007) report a modified proctor maximum dry density of 150 pcf and an optimum water content of 6.0% for VDOT 21B. Modified Proctor compaction tests were conducted on the WVDOT Class 1 in accordance with ASTM D 1557, and they revealed a maximum dry density of 145 pcf and an optimum moisture content of 6.0%, as shown in Figure 5.1. Gravel was sieved on a $\frac{3}{4}$ in. sieve and the material passing was used for the modified proctor results in a 6 in. mold. The oversize correction was completed in accordance with ASTM D 4718.

CSE #1 was constructed using both VDOT 21B and WVDOT Class 1, but CSE Tests #2 through #5 were constructed completely of the WVDOT Class 1 gravel. A total of 665 tons of WVDOT Class 1 was delivered to the test site: 350 tons during construction of

CSE #1, 200 tons during construction of CSE #2, and 115 tons during construction of CSE #4. The same WVDOT Class 1 gravel was re-used from test-to-test, although these additional deliveries provided fresh material for use in some tests. The average gradation as-delivered from the quarry and after completion of Test #5 are shown in Figure 5.2 below. The grain-size distributions were determined in accordance with ASTM C117 and C136. The gradation was slightly finer after testing due to the placement, compaction, and removal processes, and possibly due to some mixing with the finer VDOT 21B in CSE #1.

Table 5.1: Gradation requirements of VDOT 21B and WVDOT Class 1.

Sieve Size	Percent Passing by Weight			
	VDOT 21B Coarse	VDOT 21B Fine	WVDOT Class 1 Coarse	WVDOT Class 1 Fine
2 in.	100	-	-	-
1.5 in.	-	-	100	-
1 in.	85	95	-	-
3/4 in.	-	-	50	90
3/8 in.	50	69	-	-
No. 4	-	-	20	50
No. 10	20	36	-	-
No. 40	9	19	5	20
No. 200	4	7	0	7

The plastic and liquid limit of the WVDOT Class 1 material passing the #40 sieve were found to be 13 and 20 respectively, when determined in accordance ASTM D 4318. The resulting plasticity index is 7 which falls in the transition zone between silt and clay for PI's of 4 to 7%. The resulting classification of the fines is CL-ML.

Table 5.2 summarizes the properties of the WVDOT Class 1 gravel and the resulting USCS classification for gravel as-delivered from the quarry and the gravel after CSE testing was complete. The gradation of the WVDOT Class 1 gravel according to the Unified Soil Classification system (ASTM D 2487) in both cases is GP-GC.

Following CSE #1, the VDOT 21B gravel was used to construct the ramps necessary to construct the embankments.

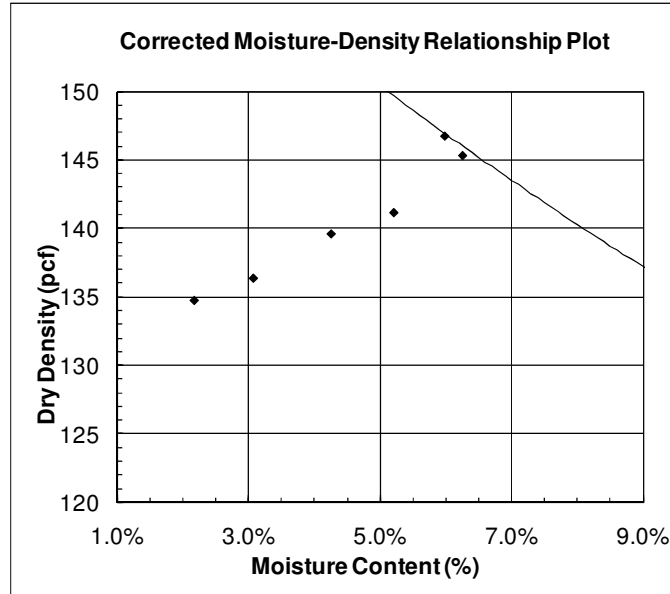


Figure 5.1: Modified Proctor compaction results for WVDOT Class 1 shown with ZAV for $G_s = 2.74$.

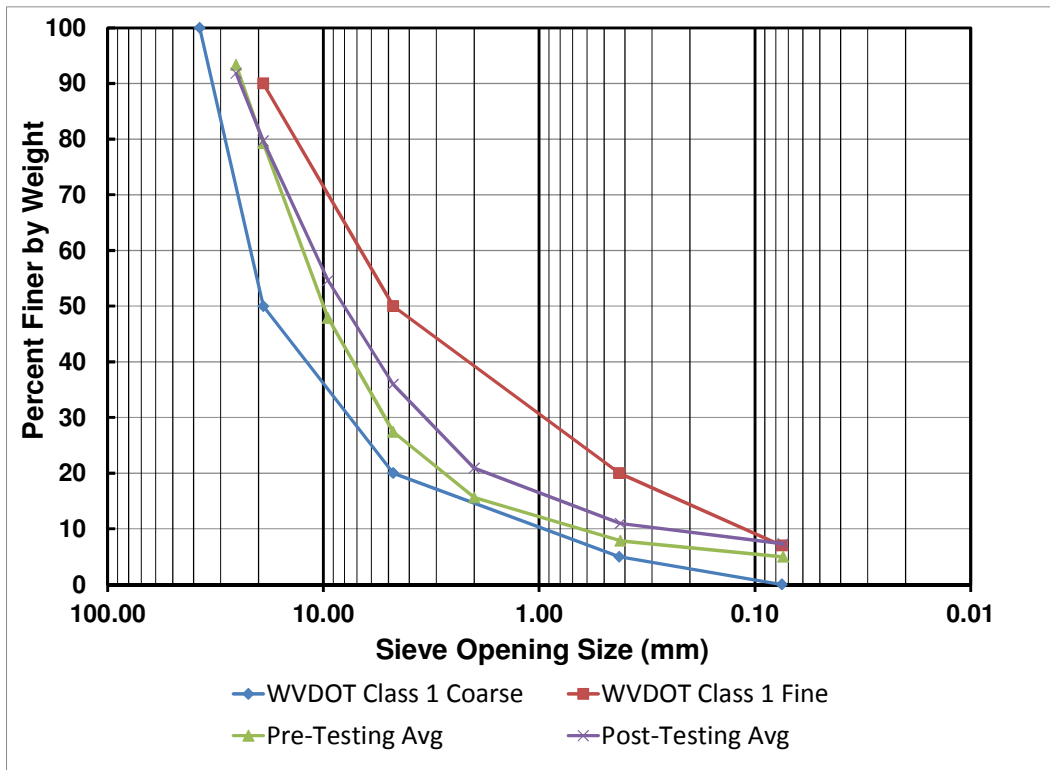


Figure 5.2: Pre- and post-testing gradations of fill in CSE tests along with WVDOT Class 1 Requirements.

Table 5.2: Properties of WVDOT Class 1 gravel as-delivered and post-testing.

Property	WVDOT Class 1 Properties	
	As-delivered	Post-testing
Percent passing #4	27.4	35.9
Percent passing #200	5.0	7.3
Coefficient of uniformity	18.8	39.3
Coefficient of curvature	3.4	3.5
Atterberg limits	PL = 13, LL = 20, PI = 7	
USCS classification	GP-GC	GP-GC

Duncan et al. (2007) report a series of consolidated drained (CD) triaxial tests performed on the VDOT 21B gradation for two mineralogies: limestone and granite. The limestone gradation tested by Duncan et al. (2007) came from the same quarry as the VDOT 21B for CSE #1. The triaxial tests were performed at two densities, termed “high” and “low” in the report. The gravel in the high density tests was compacted using 100% standard proctor energy, which represents the energy used for compaction in the CSE tests more closely than the low density tests. Duncan et al. (2007) found no significant difference in the strengths between the limestone and granite mineralogies. Table 5.3 summarizes the peak and large-strain friction angles calculated from the data contained in the Duncan et al. (2007) report.

Table 5.3: Summary of peak and large-strain friction angles for triaxial tests of high density 21B from Duncan et al. (2007).

Test #	Mineral-ogy	Effective Confining Stress (psi)	Peak			Large-Strain		
			Deviator Stress (psi)	Axial Strain (%)	ϕ' (deg)	Deviator Stress (psi)	Axial Strain (%)	ϕ' (deg)
9	Limestone	6.43	62.35	2.92	56.0	44.06	8.74	50.7
10	Limestone	10.08	97.77	2.59	56.0	66.21	9.71	50.0
11	Limestone	19.95	130.97	3.69	50.0	116.93	8.23	48.2
12	Limestone	30.11	178.64	4.77	48.4	157.91	10.8	46.4
13	Granite	6.07	68.57	2.01	58.2	50.71	8.02	53.8
14	Granite	6.14	73.07	2.92	58.9	48.46	9.61	52.9
15	Granite	30.09	192.12	4.92	49.6	178.63	8.63	48.4

The confining pressures in Table 5.3 vary from 6 to 30 psi, which are typical stresses for most of the embankment heights where CSEs are used. The lower confining pressures represent low-height embankments or the stress above the subsoil, and the higher stresses may represent the stress concentration above a column for higher embankments. For

these confining pressures, the peak friction angles vary from approximately 48 to 59 degrees, with the higher friction angles occurring at the lower confining stresses. The peak deviator stresses used to compute the peak friction angle occurred at axial strains of approximately 2 to 5%. It is important to note that even at axial strains as large as 8 to 11%, the gravel still had friction angles from 46 to 54 degrees which is only a slight reduction from the peak values and is still quite high.

Although there is no triaxial test data available for the WVDOT Class 1 gravel, the friction angles are believed to be similar to those in the Duncan et al. (2007) report for the VDOT 21B.

5.1.2 Geogrid

Samples from each roll of geogrid used in the embankments were tested using the single-rib tensile test for geogrid in accordance with ASTM D 6637. Approximately five single-rib tensile tests were performed in both the machine and transverse directions on each roll used in the CSE tests. The average strengths from each roll ranged from approximately 3% to 35% above the minimum average role value (MARV) reported by the manufacturer for the type of geogrid tested. More information on the geogrid testing program is found in APPENDIX A.

5.1.3 Geof foam

The grade of geof foam used in the CSE tests was selected based on several factors. The first consideration was the ability to withstand construction traffic from the skid-steer loader with shallow lift thicknesses of approximately 6 in. during initial construction of the embankment. Several ASTM D6817 grades of expanded polystyrene (EPS) geof foam were analyzed using a simplified Boussinesq model for a circular loaded area and a layered elastic solution from Poulos and Davis (1974).

The second consideration concerned the reaction of the geof foam to the embankment load. A stiff foam would ensure that very little compression occurred under the construction and embankment loads until the geof foam is dissolved. A more compressible geof foam would allow for more deflection of the base layer of geosynthetic to occur during the construction of the embankment. Using a stiff geof foam provides more rigorous data for evaluation of CSE design methods since deflection of the base layer of geof foam (as with a more compressible geof foam) during construction of the embankment will enhance the arching that takes place in the embankment as placement of each successive lift smooths out any total and differential settlement that occurs during construction. The stiff

geofoam ensures that very little base deflection of the embankment occurs until the geofoam is dissolved.

Compressive strength testing for geofoam used in all five tests was completed in accordance with ASTM D 1621. The density and compressive strength results for the geofoam used in each test are summarized in Table 5.4. Typical stress-strain curves from CSE #1 and CSEs #2 to #5 are shown in Figure 5.3. The stress-strain curves were re-zeroed in accordance with ASTM D 1621 such that a tangent to the initial straight portion of the curve intersects the origin.

Table 5.4: Properties of geofoam used in CSE tests.

CSE Test	ASTM D 6817 Grade Ordered	Number of Samples Tested	Average Measured Properties			
			Density (pcf)	Compressive Resistance at 1% Strain (psi)	Compressive Resistance at 5% Strain (psi)	Compressive Resistance at 10% Strain (psi)
1	EPS12	7	0.99	2.4	9.6	12.1
2	EPS19	6	1.33	3.4	13.0	15.8
3	EPS19	8	1.58	5.4	16.8	19.6
4	EPS19	8	1.22	4.7	14.0	15.8
5	EPS19	10	1.20	3.7	13.2	15.4
ASTM D6817 EPS12 Min.			0.70	2.2	5.1	5.8
ASTM D6817 EPS19 Min.			1.15	5.8	13.1	16.0

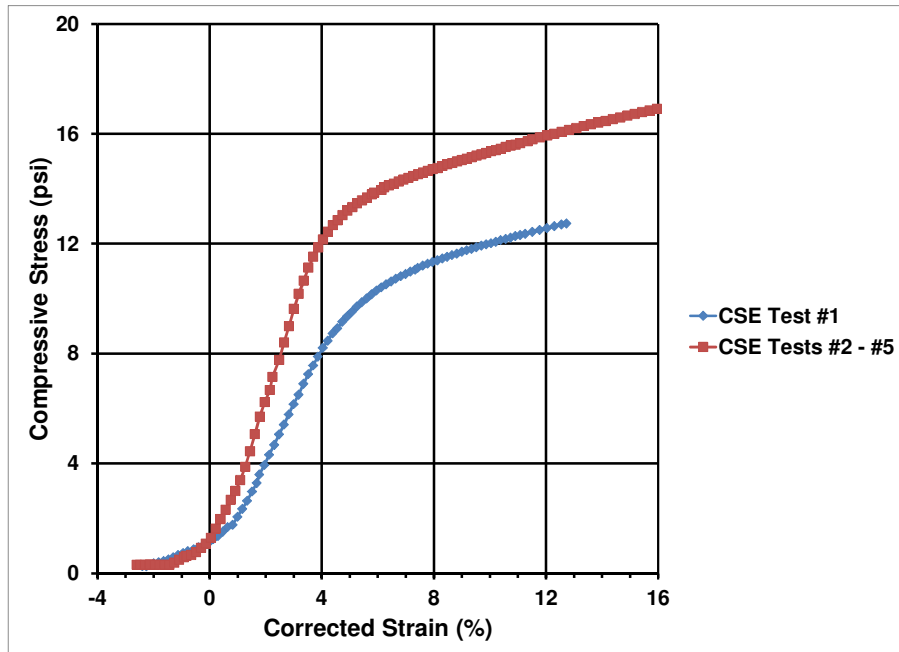


Figure 5.3: Typical stress-strain curves for geofoam in CSE #1 and CSEs #2 - #5.

Creep testing of the geofoam was also completed for each CSE at loads approximating the expected embankment loads with no arching. These results are shown in Figure 5.4 and Figure 5.5 along with the percentage of the compressive stress at 5% strain. The significant creep strains from the EPS12 geofoam in CSE #1 at 6.2 psi resulted in the selection of EPS19 geofoam for CSEs #2 - #5 so a consistent grade of geofoam could be used for this series of tests, including the tests at greater embankment heights, without significant creep strains prior to dissolving the geofoam.

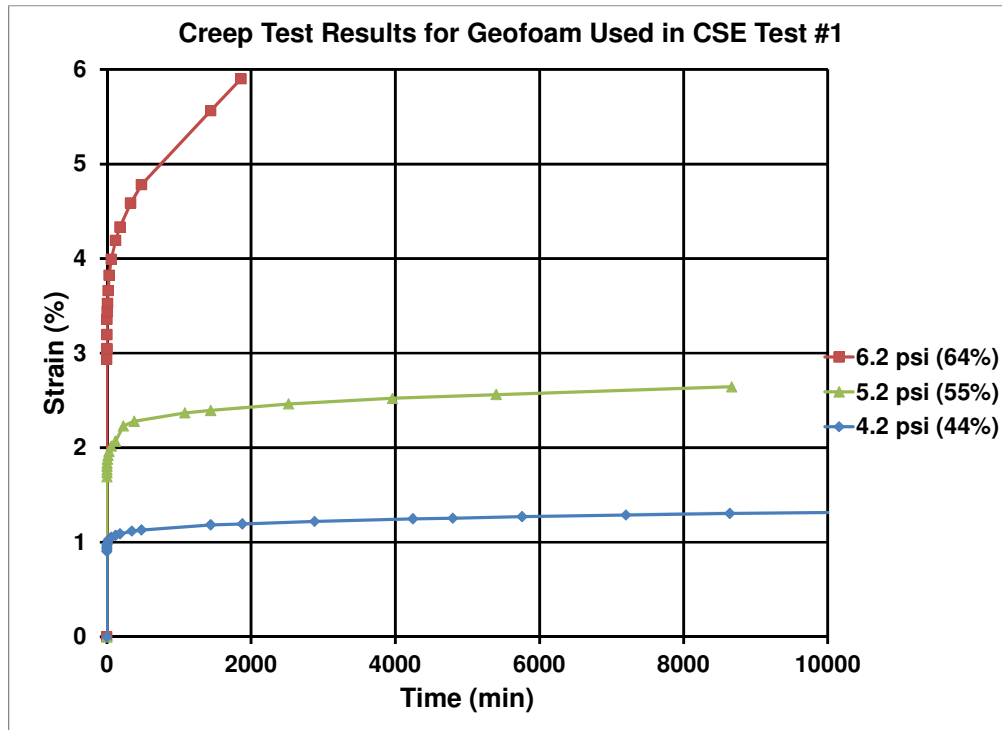


Figure 5.4: Creep test results of geofoam used in CSE #1.

5.1.4 Geofoam Dissolver and Geonet

The fluid used to dissolve the geofoam is d-limonene. Several types of geofoam dissolvers were investigated, including acetone, proprietary products, and d-limonene. Noguchi et al. (1998) and Shin and Chase (2005) note that d-limonene effectively dissolves EPS and is used in recycling applications to reduce volume of EPS in landfills. The flash point of d-limonene is approximately 47° C which is significantly higher than that of acetone (-18° C), making it much safer.

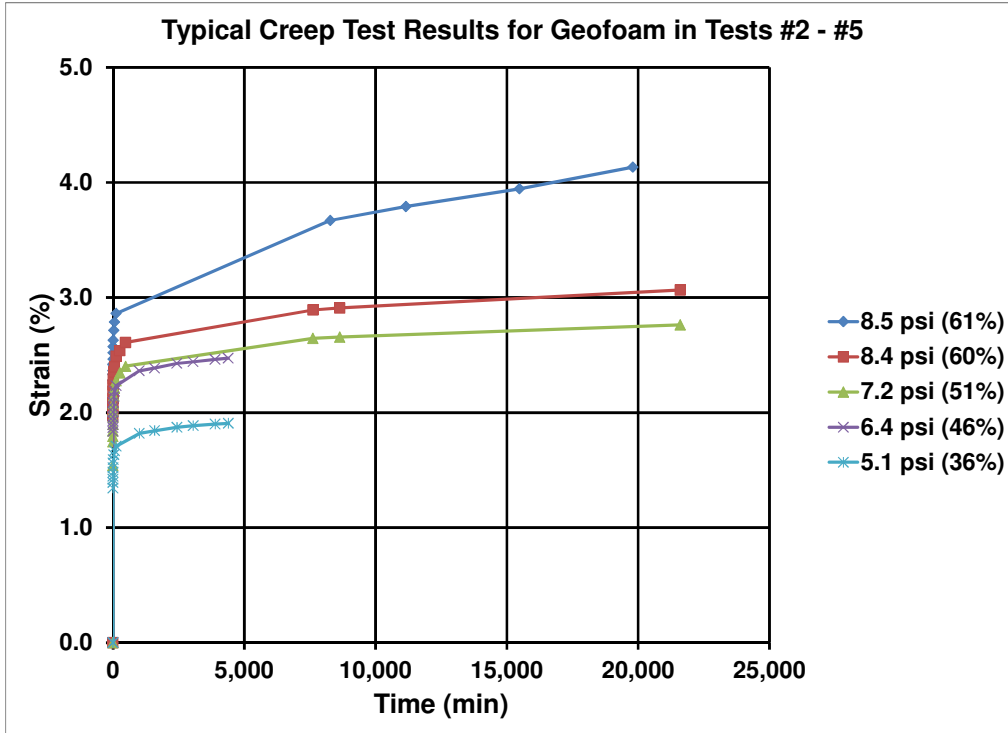


Figure 5.5: Typical creep test results of geofoam used in CSEs #2 - #5 for applied stress in psi and percentage of geofoam compressive strength at 5% strain.

Due to the cost of d-limonene (approximately \$700 per 55-gallon drum) and the closeness to which water approximates the intrinsic permeability of d-limonene, the geofoam dissolver delivery system was calibrated with water prior to construction of each embankment to ensure even flow at each delivery point. Mitchell and Soga (2005) report the intrinsic permeability as:

$$K = k_h \frac{\mu}{\gamma_p} \quad (5.1)$$

where k_h = hydraulic conductivity, μ = viscosity of the fluid, γ_p = unit weight of the fluid. The two properties related to the fluid are the viscosity and unit weight. The viscosity and unit weight of water are approximately 1.02×10^{-3} Pa*s and 9.80 kN/m^3 resulting in a ratio of 1.04×10^{-4} m-s. Clara et al. (2009) report the viscosity of d-limonene at 20°C as 0.932×10^{-3} Pa*s. The specific gravity of d-limonene is approximately 0.83 resulting in a unit weight of 8.13 kN/m^3 . This results in a μ/γ_p ratio of 1.15×10^{-4} m-s, which is within approximately 10% of the value for water.

Table 5.5: Comparison of the fluid properties of d-limonene (from Clara et al. 2009) and water.

Property	D-Limonene	Water
Viscosity (Pa*s)	0.932×10^{-3}	1.02×10^{-3}
Unit weight (kN/m ³)	8.13	9.80
Viscosity/Unit weight (m-s)	1.15×10^{-4}	1.04×10^{-4}

The geonet used in the CSE tests was GeoSyntec’s Tendrain 3 or UBXC Biaxial geonet. The properties of these geonets reported by the manufacturer are summarized in Table 5.6.

Table 5.6: Properties of geonet used in CSE tests.

Property	Syntec Tendrain 3	Syntec UBXC
Thickness (mil)	250	200
Tensile Strength – MD (lb/ft)	625	540
Transmissivity – MD (m ² /sec)	2×10^{-3}	2×10^{-3}
Roll Dimensions (ft)	12.75 x 200	13 x 250

5.2 EQUIPMENT AND FILL PLACEMENT

Fill placed directly on top of geogrid was placed from one side of the embankment to the other, in the direction of the geogrid roll, to tension the geogrid and prevent slack during placement. Fill was placed using a Bobcat 643 skid-steer loader. The manufacturer’s specifications for the Bobcat 643 are shown in Table 5.7.

In all of the CSE tests, the gravel was placed in a relatively dry manner. In most cases, no water was added during the compaction process. In some cases, a small amount of water was added to the gravel to enhance compaction. A low moisture content was desired in order to minimize the additional strength that may be present due to negative pore water pressures. Dry densities from the CSE tests averaged approximately 93% of the maximum modified Proctor dry density for WVDOT Class 1 from Figure 5.1.

In general, the gravel was placed in lifts such that the compacted lift height was approximately 6 in. Rollers used to compact the fill were 1.5 ton dual-drum vibratory rollers such as the Wacker RD11A or 12A. A Troxler 3440 Moisture-Density gauge was

used to verify the dry density and moisture content of each lift. Pictures of the fill placement, compaction, and density measurements are shown in Figure 5.6, Figure 5.7, and Figure 5.8.

Table 5.7: Bobcat 643 specifications.

Item	Value
Model Year	1981
Horsepower	28.5
Rated Operating Capacity (lbs)	1,000
Operating Weight (lbs)	4,140
Height (in.)	78.5
Length (in.)	120.1
Width (in.)	55.1
Wheelbase (in.)	35.2
Tire pressure (psi)	35



Figure 5.6: Fill placement with Bobcat 643 from one side of the embankment to the other in order to tension the geogrid and prevent slack.



Figure 5.7: Bobcat 643 and Wacker RD11A used for placement and compaction of gravel fill.



Figure 5.8: Moisture-density testing with the Troxler 3440 gauge.

5.3 TRAFFICKING PROCEDURES

Fill soils within CSEs may undergo significant shear strains, particularly near the base of the embankment where there is little or no subgrade support. Thus, the soil in some portions of the embankment may be in a relatively loose state. In CSE applications for

highways and railways, densification of the soil in a loose state may occur due to the vehicular or rail traffic loading. In an effort to measure some of this additional settlement, each embankment after CSE #1 was trafficked with the Bobcat 643 to measure the additional total and differential settlements induced by the trafficking process. CSE #1 was not trafficked due to the large amount of differential settlement that occurred by dissolving the geofoam.

The issue of trafficking is particularly important when determining the critical height for a given column diameter and spacing. Bench-scale studies reporting the critical height as a function of the column spacing and diameter are not able to assess the additional differential settlement that may be induced by the application of traffic loading.

In the embankment tests, the “before-trafficking” or “BT” settlements were measured 7 to 10 days after dissolving the geofoam, but before the embankment experienced any additional loading other than the light foot traffic necessary to survey the embankment surface elevations. Care was also taken to minimize the volume of foot traffic on the surface of the embankments since even this light traffic may cause additional settlement to occur. For cases where the embankment was below the critical height, the gravel on the embankment surface was noticeably loose and even light foot traffic may have induced additional differential settlements for some embankments. This is discussed in further detail in the description of each embankment in Chapter 6.

At 7 to 10 days after dissolving the geofoam, each embankment following CSE #1 was trafficked with the Bobcat 643 and the surface and base settlements were measured again. These settlements are referred to as the “after-trafficking” or “AT” settlements in Chapter 6. Figure 5.9 shows several pictures of the trafficking process and the additional differential settlement induced by trafficking.



Figure 5.9: Pictures showing the trafficking process and the additional settlement induced by trafficking loads.

5.4 CSE TEST PROCEDURES

The CSEs and results are described fully in Chapter 6. The general steps employed in each CSE test are listed below. Note that safety on the worksite is extremely important when working with the skid-steer loader and compaction equipment on site, particularly as the embankment height increases.

1. Install the PVC piping network for the geofoam dissolver delivery system.
2. Calibrate the geofoam dissolver delivery system with water by adjusting the valve at each delivery point so that the flow rate is equal at all 16 delivery points.
3. Move the geofoam dissolver delivery system out of the way to facilitate cleaning of the slab (the PVC pipe is flexible enough that this can be done while the piping remains connected).
4. Clean the test area of all debris and water.
5. Install a PVC plug in the drain at the base of the mat foundation.

6. Place a layer of 6 mil polythelyene plastic at the base of the test facility so that it extends up the inside of the perimeter wall. Tape the plastic to the facility walls as required.
7. Place rubber at the column locations to prevent point loads due to column irregularities. Sequentially install the columns without driving on or damaging the base plastic layer. Column installation is a delicate process since the columns weigh over 600 lbs each. Care should be taken to be sure that this step is completed safely.
8. Cut the geonet and install it around the columns and on top of the polyethylene plastic layer.
9. Cut and fit the geofoam blocks between the perimeter walls and columns. Ensure that there is a small gap (at least ¼ in.) between the columns/walls and the geofoam blocks so that there will not be any friction to prevent the geofoam from settling and dissolving down to the base of the slab once the dissolution process begins.
10. Drill holes in the geofoam blocks at the location of the geofoam dissolver delivery points. This is best done by removing the geofoam blocks to ensure there is no damage to the geonet or polyethylene plastic from the drill bit.
11. Place the bottom steel plate in the center column and install shims to ensure that it is level and stable.
12. Put the geofoam dissolver delivery system piping back into place and ensure that the PVC elbows from the delivery points are pointing downward into the drilled holes. Cut small channels in the surface of the geofoam so that the tops of the PVC pipes are flush with the top of the geofoam to prevent any unnecessary slack in the base layer of reinforcement.
13. Install another layer of 6 mil polyethylene plastic on top of the geofoam and cut holes in the plastic around the columns and perimeter wall, so the plastic will move downward on the top of the geofoam as it is dissolved.
14. Place the webcams and load cells in the center column and place the second steel plate on top.
15. Connect all instrumentation to the datalogger and begin monitoring. Monitoring of the load cells with the top steel plate in place for 24 hours is recommended to get an accurate zero reading. Zero readings for the EPCs can also be taken during this period.
16. Place small sections of geotextile on top of the columns and the perimeter wall to prevent abrasion of the base layer of geogrid.
17. Place first layer of geogrid. The geogrid should extend at least 5 ft beyond the edges of the facility on all sides to prevent pullout. Roll widths of 13 ft were

- used, so three roll widths were required across the facility for CSEs #2 to #5 with a 22 ft wide facility. Edges of the rolls should be overlapped a minimum of 3 ft.
18. Attach the ends of the lead-wire extensometers to the base layer of geogrid in the desired locations. Measure and record the distance between the attachment locations for use in the strain calculations. Secure the tubing to the geogrid with cable ties. Configure the datalogger and begin monitoring of the lead-wire extensometers if not already done.
 19. Begin placing gravel from one side of the facility to the next to tension the geogrid and remove any slack. After the first "row" of gravel is placed, begin placing gravel on top of the existing gravel and then push it onto the geogrid. Do not dump the gravel directly on the geogrid after the first "row" as this may cause unnecessary slack in the geogrid.
 20. Install 2 in. ID polyethylene pipe for the settlement profiler in the desired location(s) and elevation(s). Survey and record the locations.
 21. Install EPCs in the desired locations and elevations. Survey and record the locations.
 22. Finish placing the first lift of fill material. Compact the lift using the 1.5 ton dual-drum vibratory roller.
 23. Check the density and moisture content with the nuclear gauge. Generally, 4 to 5 measurements were made on each lift. The goal for compaction of the gravel fill in the CSE tests was a relative compaction of approximately 93% of the modified Proctor maximum. Continue compaction if necessary. In most cases, no water was applied during compaction in order to limit the apparent cohesion in the partially saturated fill.
 24. Survey the elevation of the lift once compaction is complete. Generally, a 9-point grid was used to survey each lift. The survey elevations and the density of each lift are used to calculate the stress at the base of the embankment during construction for comparison with EPC and load cell measurements.
 25. Continue placing geogrid and lifts of gravel as required based on the design number of reinforcement layers and embankment height. The compacted lift thicknesses for the CSE tests were generally 6 in. The machine direction of each layer of geogrid should be rotated 90 degrees from the layer below it.
 26. Take settlement profiler measurements as desired during construction.
 27. Establish a survey grid on the completed embankment surface with spray paint. Survey the grid and record the elevations.
 28. Cover the embankment with 6 mil polyethylene plastic as required to prevent rain infiltration into the embankment.
 29. Take the final settlement profiler measurements in each polyethylene pipe.

30. Download files from the datalogger and plot the results during construction to make sure there are no abnormalities prior to dissolving the geofoam.
31. Install the hand pumps on 55-gallon drums and connect the pumps to the geofoam dissolver delivery system. Pump in the geofoam dissolver.
32. Take surface and base settlement readings at 1, 3, and 7 days after dissolving geofoam.
33. After 7 to 10 days have passed since dissolving the geofoam, take the final “before-trafficking” surface and base settlement readings.
34. Traffic the embankment and take “after-trafficking” surface and base settlement readings.
35. When after-trafficking measurements are complete, remove embankment materials for the next test, taking care not to damage the instrumentation within the embankment.

CHAPTER 6

GOALS, DESCRIPTIONS, AND RESULTS OF CSE TESTS

6.1 TEST PROGRAM GOALS

The goals of the test program were to:

- Construct the facility (described in Chapter 4) and validate its performance (CSE #1 discussed in Section 6.3)
- Evaluate performance of low-height embankments with large column spacings (CSE #1 discussed in Section 6.3)
- Find critical height for one column arrangement (CSEs #2 to #4 discussed in Sections 6.4 to 6.6)
- Evaluate the influence of geogrid quantity and spacing (CSE #5 discussed in Section 6.7)
- Analyze the test results using existing design/analysis procedures (Chapter 7)
- Make CSE design recommendations based on the test results, information in the literature, and selected design improvements (Chapter 8)

6.2 TEST PROGRAM OVERVIEW

A total of five CSE tests were performed as a part of the testing program. Each test is described in the sequence in which it was performed, and the results are presented, beginning in Section 6.3. The test characteristics and geometry from the five tests are summarized in Table 6.1 and Table 6.2 below. The test embankments ranged in height from 4.0 to 7.5 ft, and each test used from approximately 300 to 500 tons of gravel select fill. All tests used 2 ft diameter round concrete columns.

Table 6.1: CSE test characteristics.

CSE Test No.	Column Diameter (ft)/No. of Columns	C-to-C Column Spacing (ft)	Fill Height (ft)	Fill Material	Geofoam Grade for Base Support	Tensar® Geogrid: No. Layers / Type
1	2 / 4	10	4.1	2 ft VDOT 21B 2.1 ft WVDOT Class 1	EPS12	2 / BX1500 2 / BX1200 1 / BX1100
2	2 / 9	6	5.1	WVDOT Class 1	EPS19	3 / BX1500
3	2 / 9	6	6.1	WVDOT Class 1	EPS19	3 / BX1500
4	2 / 9	6	7.5	WVDOT Class 1	EPS19	3 / BX1500
5	2 / 9	6	4.0	WVDOT Class 1	EPS19	5 / BX1500

Table 6.2: CSE geometry and material properties.

CSE Test No.	Square Embankment Geometry			Gravel Fill Properties			Approx. Material Used (tons)
	Height (ft)	Base Width (ft)	Crest Width (ft)	Avg Dry Unit Wt (pcf)	Avg Moisture Content (%)	Avg Moist Unit Weight (pcf)	
1	4.1	45	37	136	4.0	141	473
2	5.1	42	28	135	1.7	137	447
3	6.1	36	24	137	2.1	140	391
4	7.5	38	24	135	1.8	137	511
5	4.0	38	28	137	2.2	140	305

6.3 DESCRIPTION AND RESULTS OF CSE TEST #1

The first embankment test used four, 2 ft diameter round columns placed in a square arrangement on 10 ft center-to-center spacing as shown below in Figure 6.1 which also shows the location of the instrumentation. The embankment consisted of 4.1 ft of select fill and five layers of geogrid (2 layers of Tensar® BX1500, 2 layers of Tensar® BX1200, and 1 layer of Tensar® BX1100) as shown in Figure 6.2. The stiffness and spacing of the five layers of geogrid were designed using the Collin Method. The material used as the select fill for the first two feet of the embankment meets the 21B gradation requirements of VDOT (2007). The remaining 2.1 ft were constructed of WVDOT Class 1. Table 6.3 shows the construction timeline and properties of the fill material.

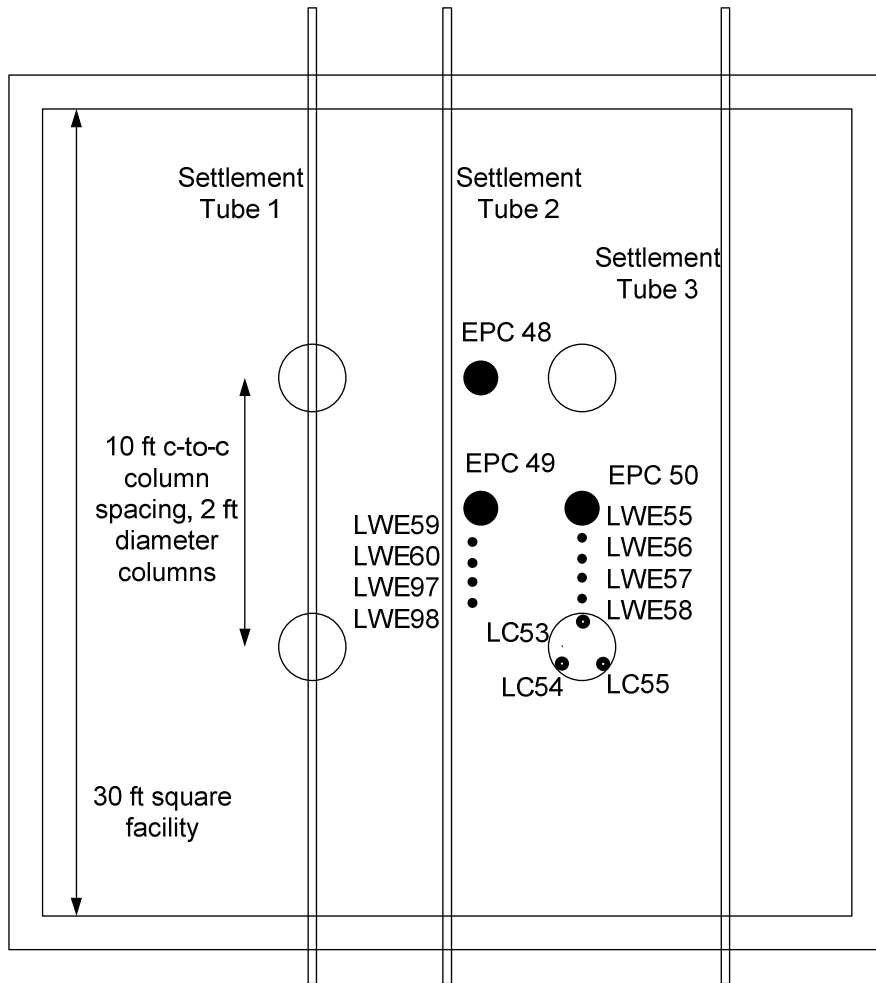


Figure 6.1: Instrumentation locations for CSE Test #1.

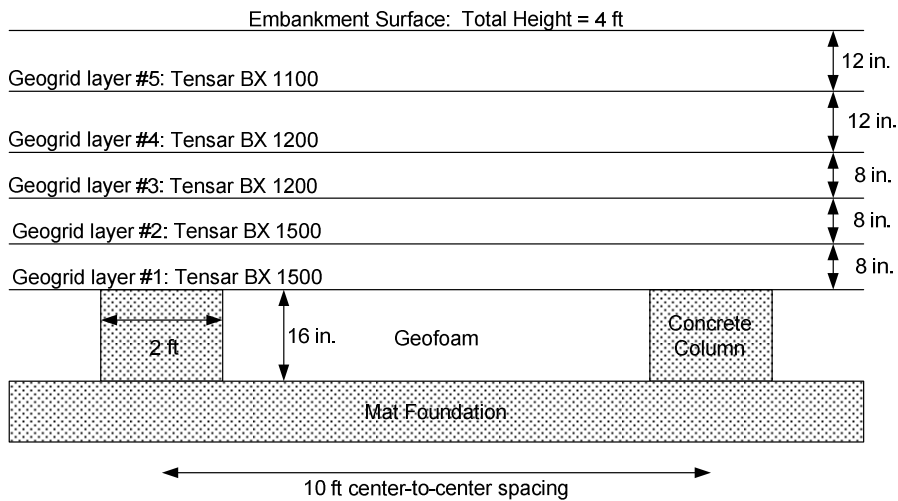


Figure 6.2: Cross-section of CSE #1.

Table 6.3: Timeline and properties for CSE #1.

Date in 2010	Start Elev. (in.)	Finish Elev. (in.)	Avg Nuclear Dry Density (pcf)	Avg Moisture Content (%)
April 14 – 15	0	8	133	3.9
April 16	8	16	139	4.5
April 20 – 21	16	24	140	4.5
May 19 – 20	24	30	136	3.5
May 20 – 21	30	36	134	3.5
May 21	36	42	n/a	n/a
May 25	42	48	n/a	n/a
Average			136	4.0
Geofoam dissolved on June 1, 2010				

Embankment construction for the first test started on April 14, 2010 and was completed on May 25, 2010 as shown in Table 6.3. Figure 6.3 shows a picture of the completed embankment. Approximately 180 gallons of d-limonene were pumped into the geonet on June 1, 2010 in the span of 50 minutes using two rotary hand pumps. There was noticeable surface settlement approximately 2 hours after starting to pump the d-limonene into the embankment. Figure 6.4 shows the embankment surface profile after settlement had occurred (approximately 8 days after dissolving the geofoam) by total station and LIDAR. The LIDAR technique is described further by Dove et al. (2008).



Figure 6.3: Picture of CSE #1 prior to dissolving the geofoam to remove support.



Figure 6.4: Picture of the differential settlement in CSE #1 after dissolving the geofoam.

The instrumentation results from CSE #1 are provided in Figure 6.6, Figure 6.7, Figure 6.8, and Figure 6.9. The EPC and load cell readings are corrected using the manufacturer's temperature correction factors.

The EPC readings increased as the embankment was constructed and approximated the calculated values based on overburden pressure. The EPC readings dropped as the geofoam was dissolved but started to increase shortly thereafter, which indicated that the base of the embankment deflected downward until it came into contact with the concrete slab below.

The load cell readings also increased during construction and reached a maximum of about 33,000 lbs after the geofoam was dissolved and then began to decrease. The load based on the tributary area of the column and unit weights of the fill materials is approximately 55,000 lbs. The fact that the loads decreased and that they were significantly less than those calculated based on the tributary area of the column also indicate that the base of the embankment was resting on the slab shortly after the geofoam was dissolved.

The strain measurements ranged from 11% to 15% in the geogrid directly between two columns but were lower (0.75% to 2.0%) in the centerline of the embankment. The measured strains are consistent with the base of the embankment resting on the slab. For

instance, a deflection of 16 in. for a clear span of 8 ft results in a strain of 11.9% according to the exact solution for the Parabolic Method.

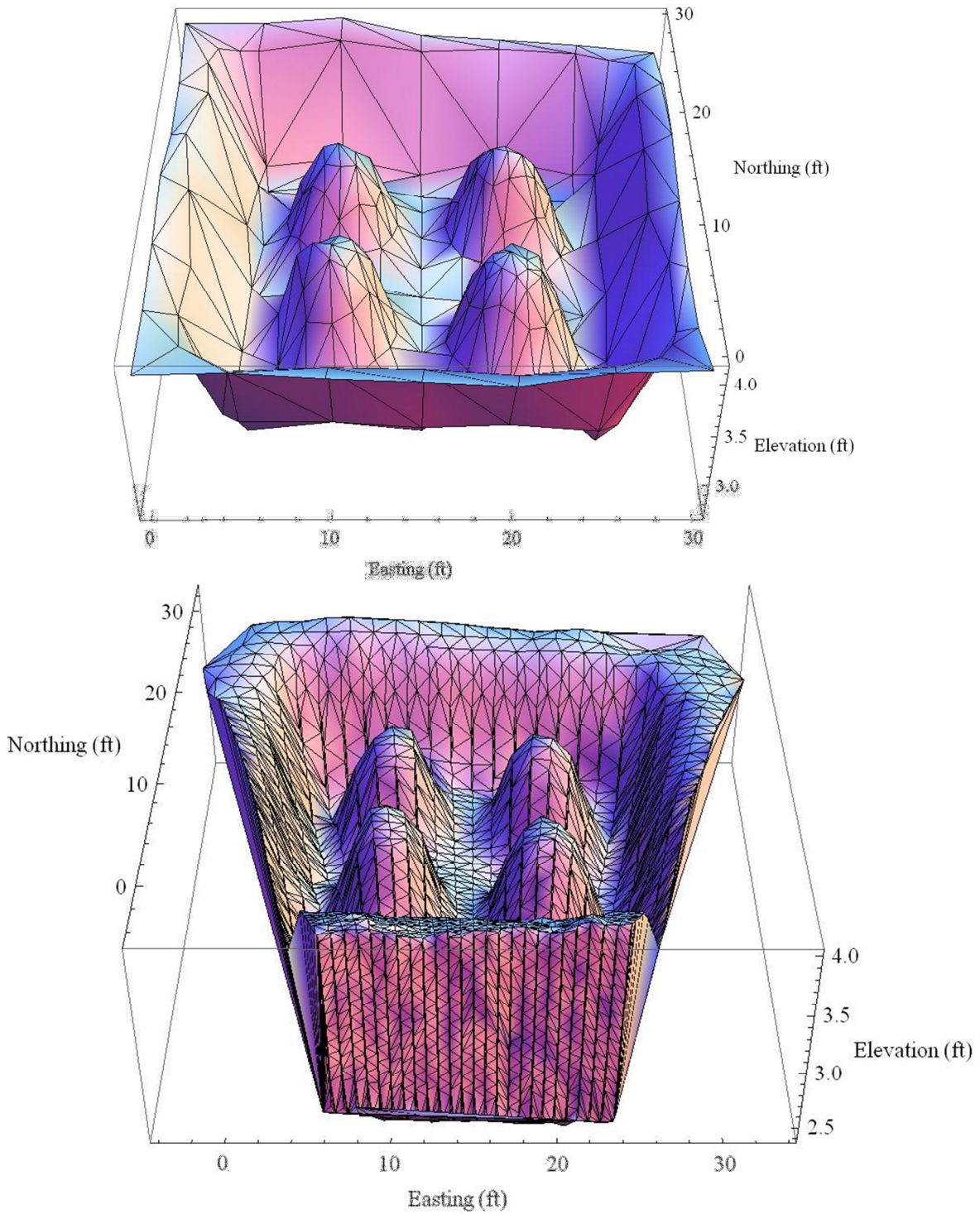


Figure 6.5: Plots of surface deformations in CSE #1 from total station survey (top) and LIDAR scan (bottom).

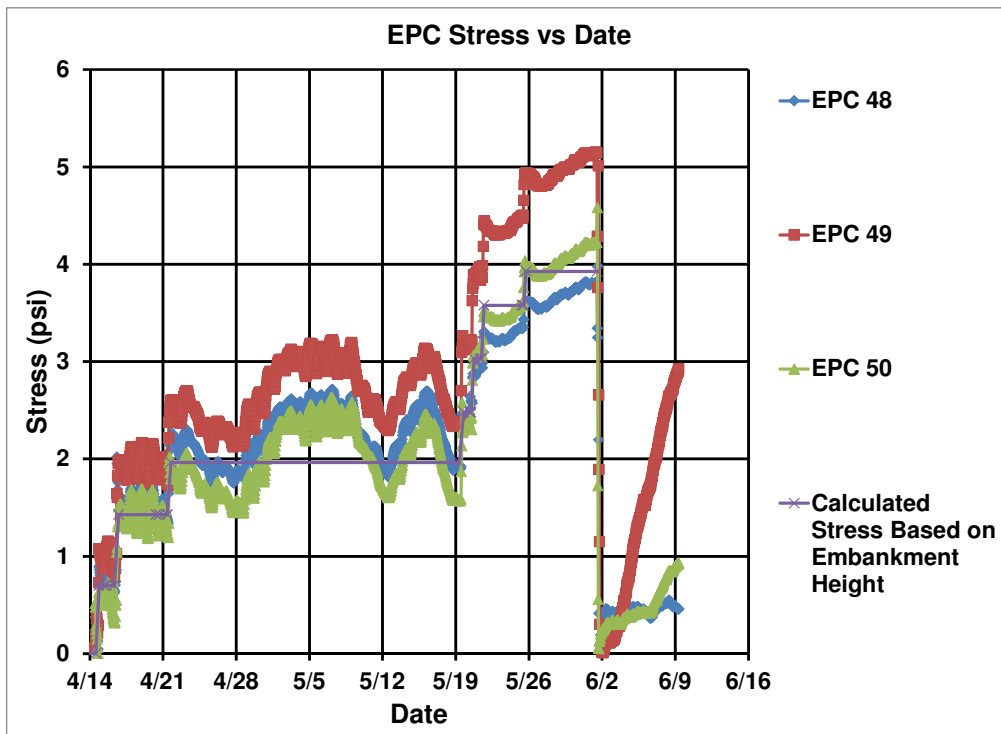


Figure 6.6: EPC results from CSE #1.

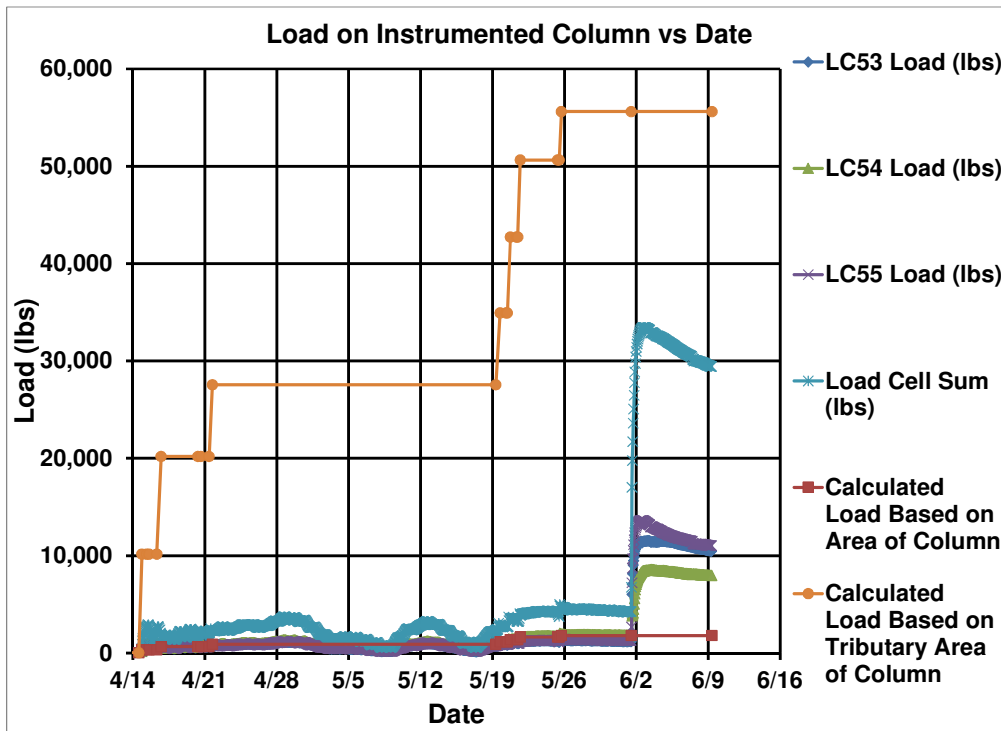


Figure 6.7: Load cell results from CSE #1.

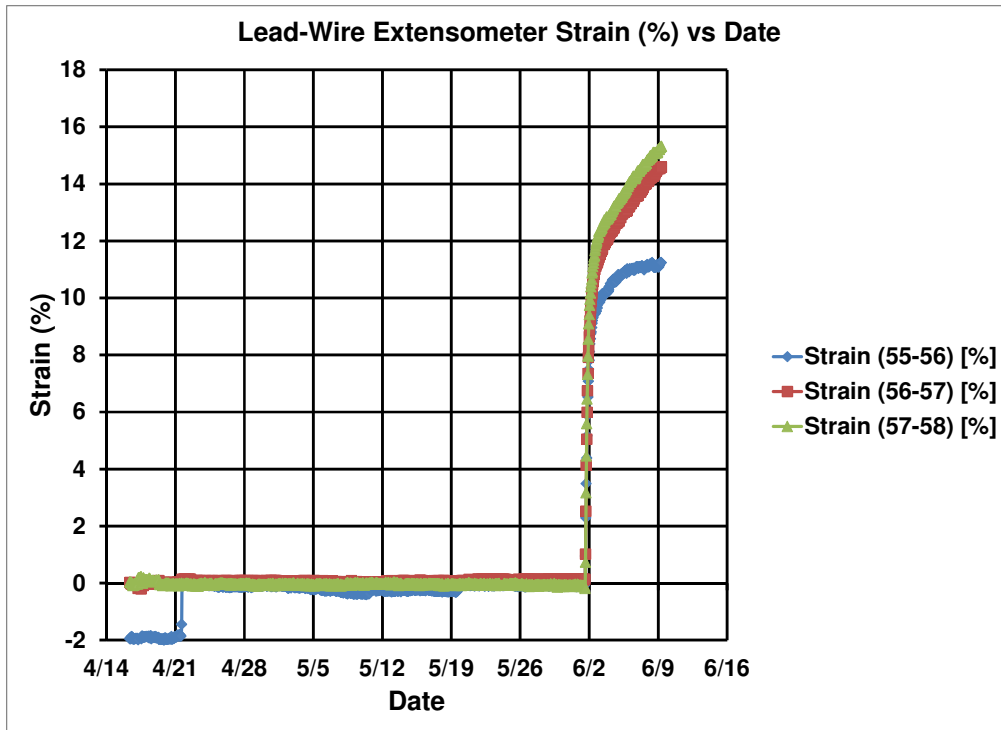


Figure 6.8: Strain measurements from CSE #1 (LWEs 55, 56, 57, 58).

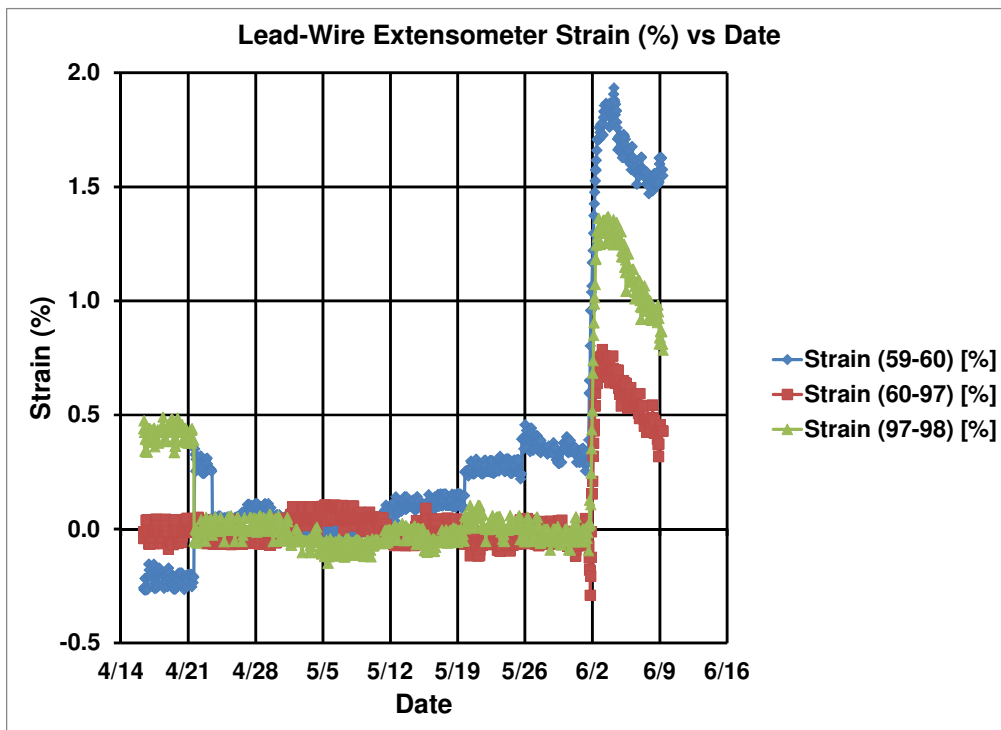


Figure 6.9: Strain measurements from CSE #1 (LWEs 59, 60, 97, 98).

The surface settlement at the centroid between the four columns was 13.5 in. The initial gap between the slab and the base of the embankment was 16 in. The dense gravel most

likely dilated which explains the difference in surface and base settlements. None of the three settlement profiler tubes were passable after the geofoam was dissolved, which confirms that significant settlement occurred at the base of the embankment.

The large differential settlements measured in CSE #1 indicate that the embankment height was too low to provide complete arching and load transfer to the columns given column spacing, height of the embankment, and quantity of reinforcement.

Because of the large differential settlements from CSE Test #1, a smaller clear span was used for the subsequent CSE tests.

6.4 DESCRIPTION AND RESULTS OF CSE TEST #2

A center-to-center spacing of 6 ft was used on CSE Tests #2 - #5 with 2 ft diameter columns in a square array of 9 columns. This geometry was chosen since 2 ft is a reasonable diameter that is close to the column diameter produced by many ground improvement methods. The center-to-center spacing was selected by balancing the costs of labor and materials with the desire to conduct the tests at spacings that represent typical spacings for full-scale CSE applications. A center-to-center spacing of 6 ft is significantly smaller than the maximum reported on CSE projects (approximately 12 ft), but may be a reasonable spacing for full-scale CSE applications for some combinations of column type and embankment height.

The goal of CSE Tests #2 - #4 was to find the critical height for this arrangement of $s = 6$ ft and $d_c = 2$ ft. Studies have shown that a plot of the differential settlement versus embankment height is approximately linear when the embankment height is below the critical height, e.g. work in progress by McGuire (2011). The approach used in CSEs #2 and #3 was to conduct at least two tests below the critical height so that a trendline could be used to estimate the critical height for both the before-trafficking (BT) and after-trafficking (AT) cases. CSE #4 would then confirm the trendline and may be above the critical height for this column geometry.

An array of 9 columns was used in CSEs #2 to #5 with $s = 6$ ft and $d_c = 2$ ft. Three layers of Tensar® BX1500 geogrid were used in CSEs #2 to #4, and all three layers were located low within the embankment. One layer was located directly above the columns, and two layers, placed transverse to one another, were located at an elevation of 6 in. above the columns. The only variable in CSEs #2 to #4 was the embankment height.

Figure 6.10 shows the notation used to report the surface settlements in the CSEs #2 to #5. S_{col} is defined as the surface settlement above the center column, $S_{soil,d}$ is the surface settlement at the unit cell perimeter at the centroid of four columns, and $S_{soil,i}$ is the surface settlement on the unit cell perimeter directly between two columns. Note that there are four measurement locations for both $S_{soil,d}$ and $S_{soil,i}$.

The base settlements can also be defined as follows: $S_{base,d}$ and $S_{base,i}$ are the settlements at the base of the embankment corresponding to the surface locations of $S_{soil,d}$ and $S_{soil,i}$, respectively. Since only one settlement tube was used within the first 6 in. of embankment fill, there are generally two measurement locations for $S_{base,d}$ and one measurement location for $S_{base,i}$ from each CSE test. Differential surface settlement can also be defined as $DS_d = S_{soil,d} - S_{col}$ and $DS_i = S_{soil,i} - S_{col}$. The differential settlement ratio can be defined as $DSBR_d = DS_d/S_{base,d}$ and $DSBR_i = DS_i/S_{base,i}$.

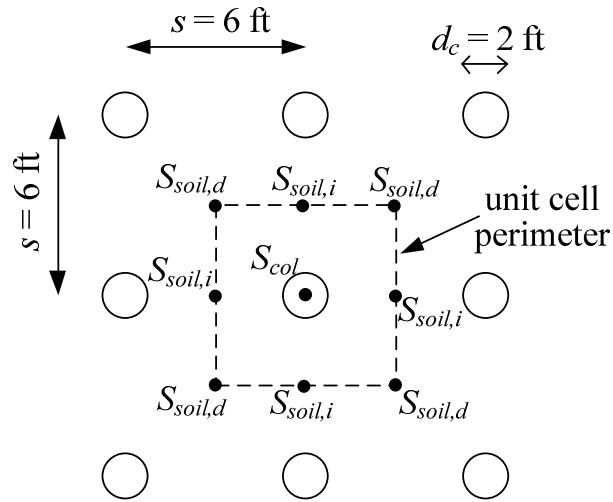


Figure 6.10: Surface settlement locations and terminology for CSE tests.

The construction sequence for CSE #2 is found in Table 6.4. Upon completion, CSE #2 had an average height above the column tops of 5.1 ft. The instrumentation locations for CSE #2 are shown in Figure 6.11, Figure 6.12, and Figure 6.13. Note that CSE #2 included the use of foil strain gages on the geogrid in addition to the lead-wire extensometers. The data from the earth pressure cells, load cells, and both types of strain gages are shown in Figure 6.14, Figure 6.15, Figure 6.16, Figure 6.17, and Figure 6.18. Note that the foil strain gages on the base layer of geogrid (Layer 1) are not shown since all of the gages experienced electrical problems or debonded from the geogrid shortly after dissolving the geofoam. The settlements from CSE #2 are summarized in Table 6.5.

During construction of the embankment, two of the three EPCs indicated stresses below the calculated stress based on the embankment height (Figure 6.14). The load in the central column was above calculated load for the area of the column itself, but below the tributary area of the column (Figure 6.15). These observations indicate that there was some arching occurring due to the compression of the geofoam during construction of the embankment and prior to dissolution of the geofoam.

The EPC readings generally decreased with time for a given load increment (see Figure 6.14). This indicates the compression of the geofoam after a load increment was applied and the accompanying load transfer to the stiff columns through tension in the geogrid and arching in the gravel fill.

After pumping in the geofoam dissolver, the EPC readings quickly dropped and stayed very low at stresses less than 1 psi as in Figure 6.14. The difference in readings between EPC 49 and EPC 50 are consistent with the vertical distance between them, with EPC 49 being 1.1 ft below EPC 50. The EPC 49 reading is approximately 1 psi greater than EPC 50 before dissolving the geofoam and approximately 0.4 psi greater after dissolving the geofoam as shown in Figure 6.14.

The load in the central column increased to a value very close to the calculated load based on the tributary area of the center column as shown in Figure 6.15. This indicates that the geofoam dissolved completely and that the embankment was supported by the columns (not resting on the mat foundation below).

The strain in both layers of geogrid was minimal during construction of the embankment and prior to dissolving the geofoam as shown in Figure 6.17 and Figure 6.18. Note that the increase in readings of FSG9 and FSG10 in Figure 6.18 prior to dissolving the geofoam is believed to be due to electrical drift, and not due to measureable strain, since none of the other gages experienced significant strains during construction. After dissolution of the geofoam, the strains quickly increased as shown in Figure 6.17 and Figure 6.18. Although not shown, FSG1 and FSG2 debonded from the geogrid at strains of approximately 3% and 4% respectively. This indicates that the strains were at least a magnitude of 4% and were probably significantly higher than this (perhaps as high as 9% to 10%), based on the strains measured by the lead-wire extensometers. The low strains during embankment construction, followed by the rapid increase in strain when the geofoam is dissolved (see Figure 6.17 and Figure 6.18), indicate the importance of the soft soil, or in this case geofoam, support to CSE performance.

Note also that the settlement profiler measurements (base deflections) from Tube #2 in Figure 6.20 and Table 6.5 can be used to calculate the strain using one of the three methods from Section 3.3. For example, a deflection of 8.9 in. between columns results in a strain of 9.2% for a clear span of 4 ft using the Parabolic Method from Section 3.3.1. This suggests that strains significantly higher than 9% may be unreasonable based on the measured deflection.

The strains from lead-wire extensometers LWE55 to LWE58 are not shown since the strains from these gages were up to 22% and are believed to be significantly higher than the actual strains in the geogrid, due to the placement of the wires and conduit for this test. These measured strains are not consistent with the measured deflections when using the Parabolic Method, as demonstrated previously. Modifications to the lead-wire extensometer placement for strain measurements directly between two columns were made for subsequent CSE tests and these modifications are believed to result in accurate strain measurements from the lead-wire extensometers in CSEs #3 to #5.

Additional observations from CSE #2 include:

- The WVDOT Class 1 gravel fill has a relatively high dry density of 135 pcf and a low water content of 1.7 % (see Table 6.4). The fill was compacted dry to avoid capillarity and increased strength due to negative pore water pressures.
- Load cells and EPCs are temperature sensitive, even with the use of the manufacturer's temperature correction factors (see Figure 6.14 and Figure 6.15). However, the temperature is relatively constant (see Figure 6.16) within the embankment after 2 to 3 ft of fill is placed for the timeframe in which the test was conducted. Therefore, temperature is not deemed to have affected the EPC and load cell readings.
- The individual load cell readings are within approximately 1,000 lbs of one another as shown in Figure 6.15. This indicates that the load distribution on the center column is relatively uniform (i.e. the load on the center column has a low eccentricity).
- Some arching is occurring in the fill prior to dissolving of the geofoam based on the EPC (Figure 6.14) and load cell (Figure 6.15) readings during construction.
- Strains in the geogrid are minimal prior to dissolving the geofoam (see Figure 6.17 and Figure 6.18).
- The combination of the previous two observations suggest that there is relatively little vertical deformation in the soft soil (or geofoam) required for at least some arching to occur.

- The geogrid strains are higher directly between two columns than in the center of four columns (see Figure 6.17 and Figure 6.18). This observation agrees with other results in the literature and numerical modeling.
- The foil strain gages experienced significant problems to include electrical connection issues, drift, and debonding at strains significantly lower than the manufacturer’s reported strain capacity of 20%. More information on the foil strain gage performance is found in APPENDIX A.
- Surface settlements followed a profile similar to what would be expected, with four noticeable depressions located at the four centroids between columns in the 9-column array (see Figure 6.19). As expected, settlements at the $S_{soil,d}$ locations were greater than the $S_{soil,i}$ locations. The settlements at each of the four measurement locations for both $S_{soil,d}$ and $S_{soil,i}$ were relatively uniform (i.e. the difference between the maximum and minimum measurements is relatively small).
- The trafficking process did not have a significant effect on S_{col} , but $S_{soil,d}$ and $S_{soil,i}$ increased significantly with trafficking (see Table 6.5). Therefore, the differential surface settlements (DS_d , DS_i) increased significantly with trafficking.
- The base settlements followed the expected profile for a CSE with no base support: local maxima were observed at the column locations and local minima were observed between columns (see Figure 6.20).
- The base deflections between columns ($S_{base,d}$) are greater than the deflections between the facility walls and the outermost columns (see Figure 6.20).
- For this embankment height, which was below the critical height, the soil at the surface of the embankment, after dissolving the geofoam, was very loose. This is consistent with the recommendation of BS8006 (1995) to use the large-strain friction angle in design and analysis of CSEs. Because the soil at the surface was loose, the “before-trafficking” settlements in Figure 6.19 may be subject to scatter since even the foot traffic required to take the survey measurements may have induced additional settlement. The after-trafficking settlements are believed to be more robust measurements.
- The webcam photos in Figure 6.21 were useful to provide a visual reference for the geofoam and the geogrid under the embankment.

Table 6.4: Timeline and properties of CSE #2.

Date	Start Elev. (ft)	Finish Elev. (ft)	Avg Nuclear Dry Density (pcf)	Avg Moisture Content (%)
July 10, 2010	0.0	0.6	137	1.0
July 13, 2010	0.6	1.2	132	2.1
July 14, 2010	1.2	1.7	136	1.8
July 14, 2010	1.7	2.2	134	1.4
July 15, 2010	2.2	2.8	136	1.4
July 15, 2010	2.8	3.5	133	1.7
July 16, 2010	3.5	4.1	134	1.6
July 16, 2010	4.1	4.5	133	1.4
July 19, 2010	4.5	5.1	137	2.9
Average			135	1.7
Geofoam dissolved on July 20				
Trafficking on July 28				

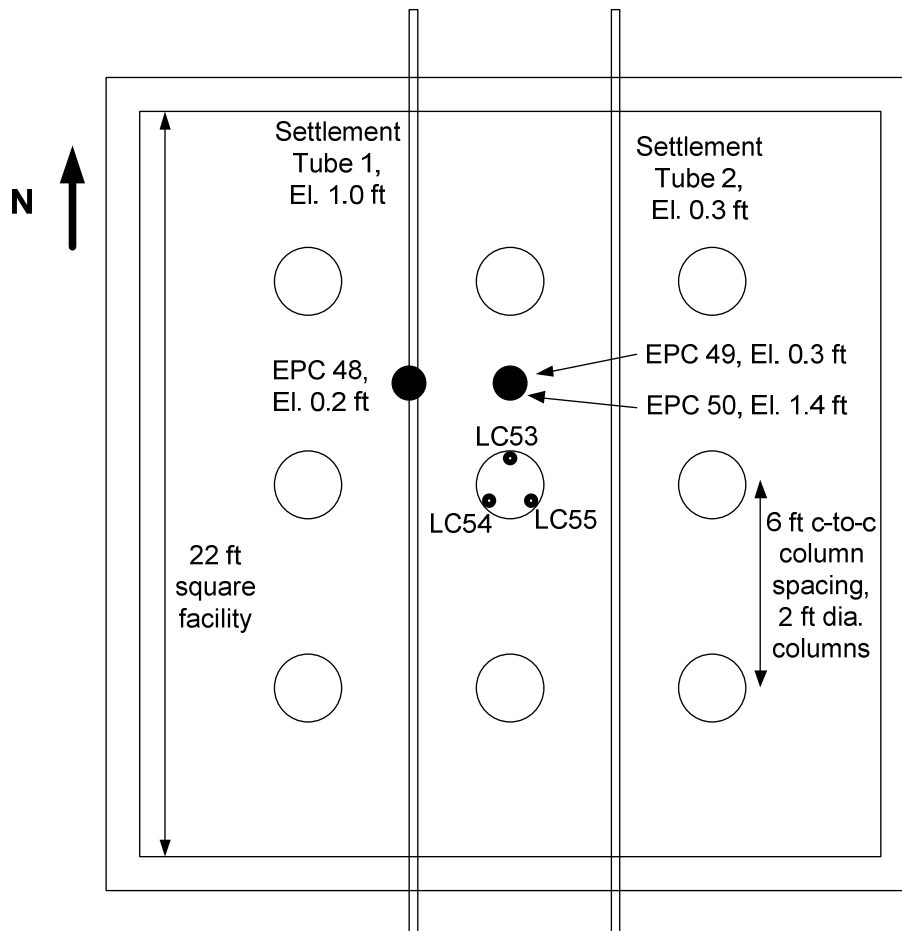


Figure 6.11: EPC, load cell, and settlement profiler tube locations for CSE #2.

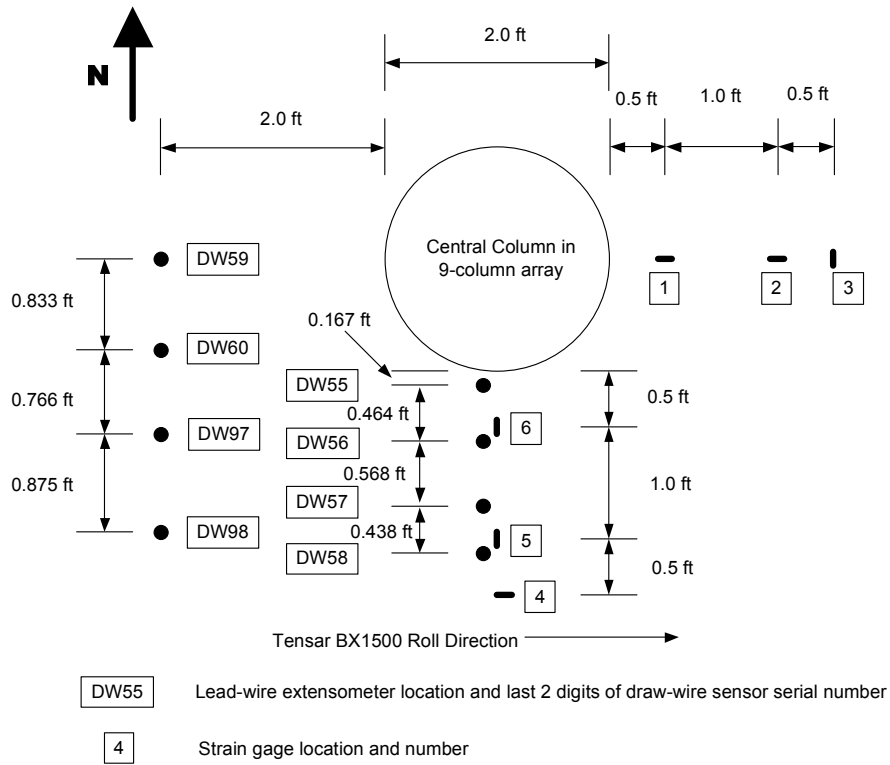


Figure 6.12: Strain gage locations on geogrid layer #1 at Elev = 0 ft.

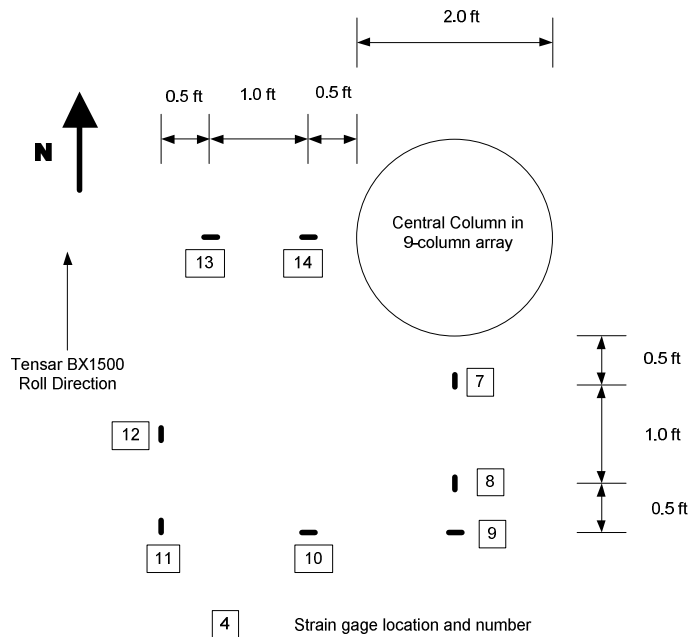


Figure 6.13: Strain gage locations on geogrid layer #2 at Elev = 0.5 ft.

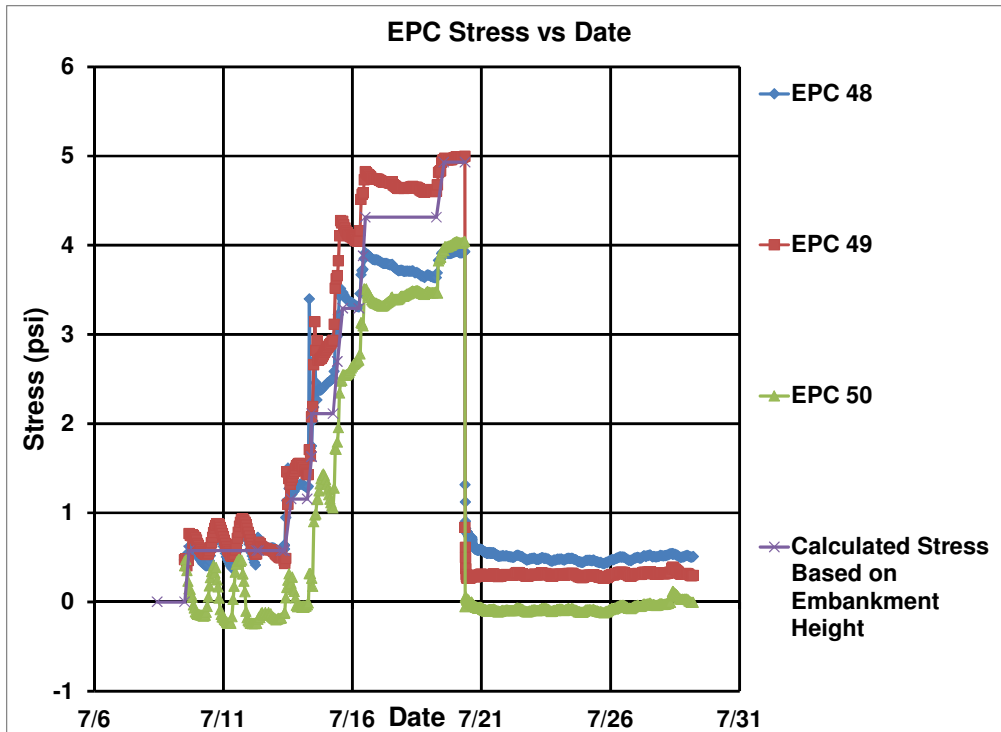


Figure 6.14: EPC results from CSE #2.

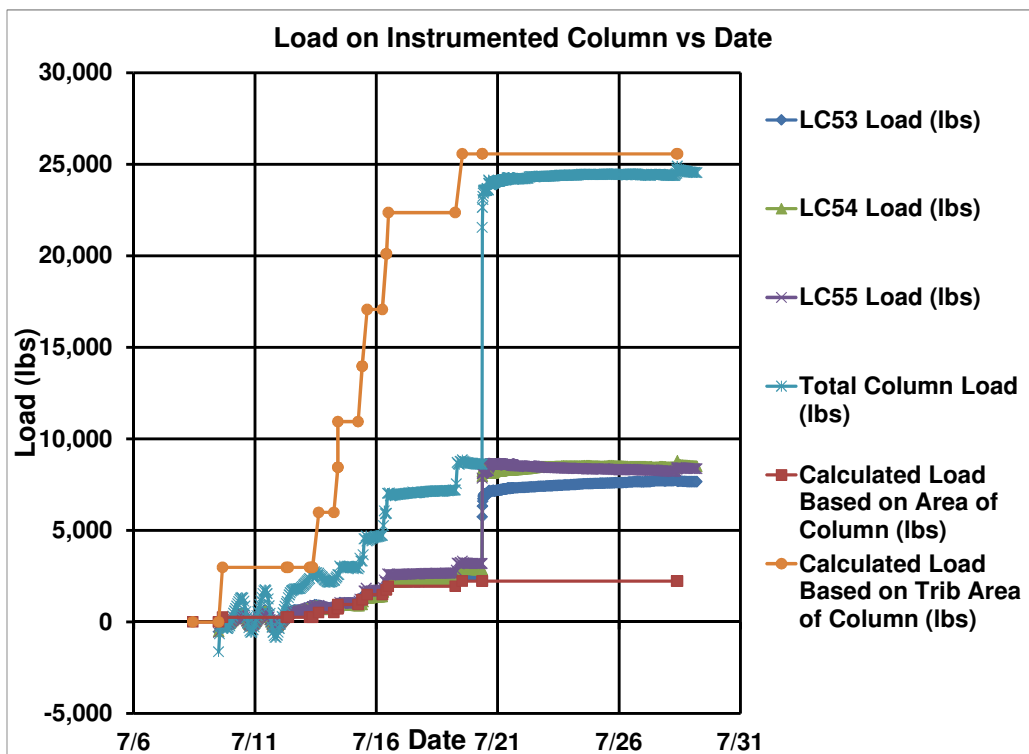


Figure 6.15: Load cell results from CSE #2.

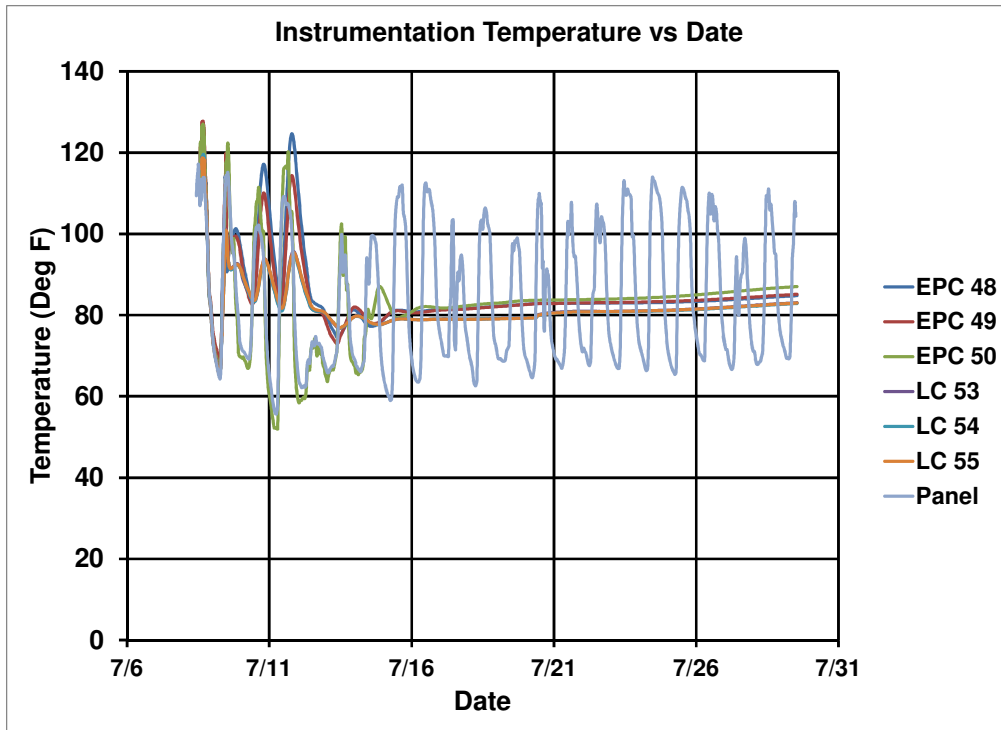


Figure 6.16: Datalogger panel, EPC, and load cell temperatures from CSE #2.

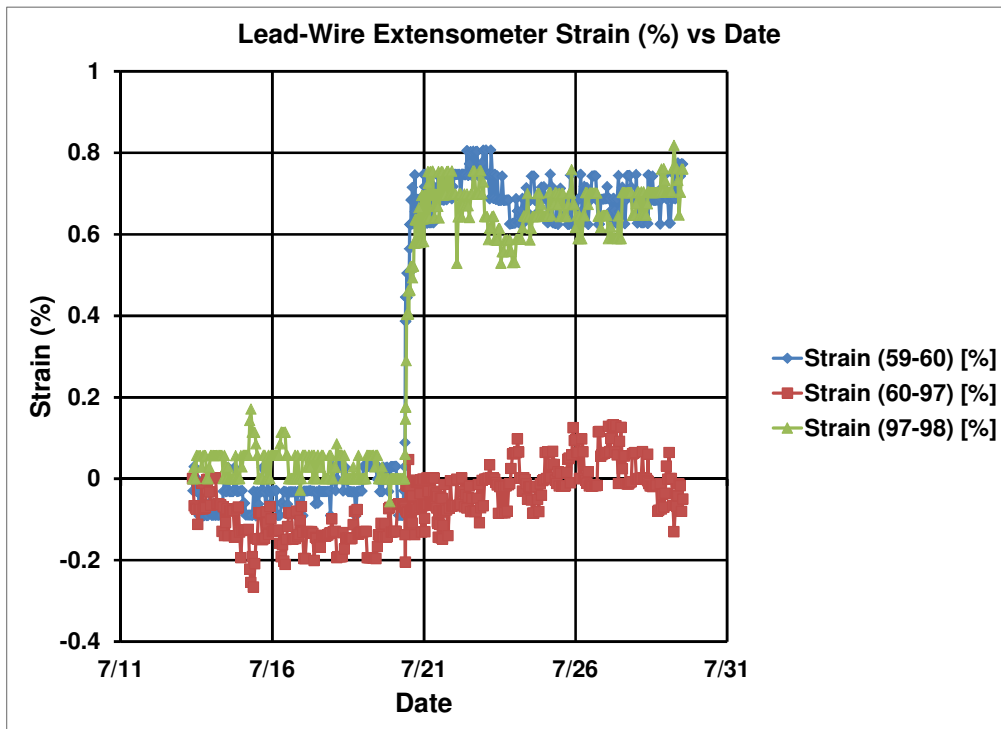


Figure 6.17: Lead-wire extensometer strain for CSE #2 (Sensors 59, 60, 97, 98).

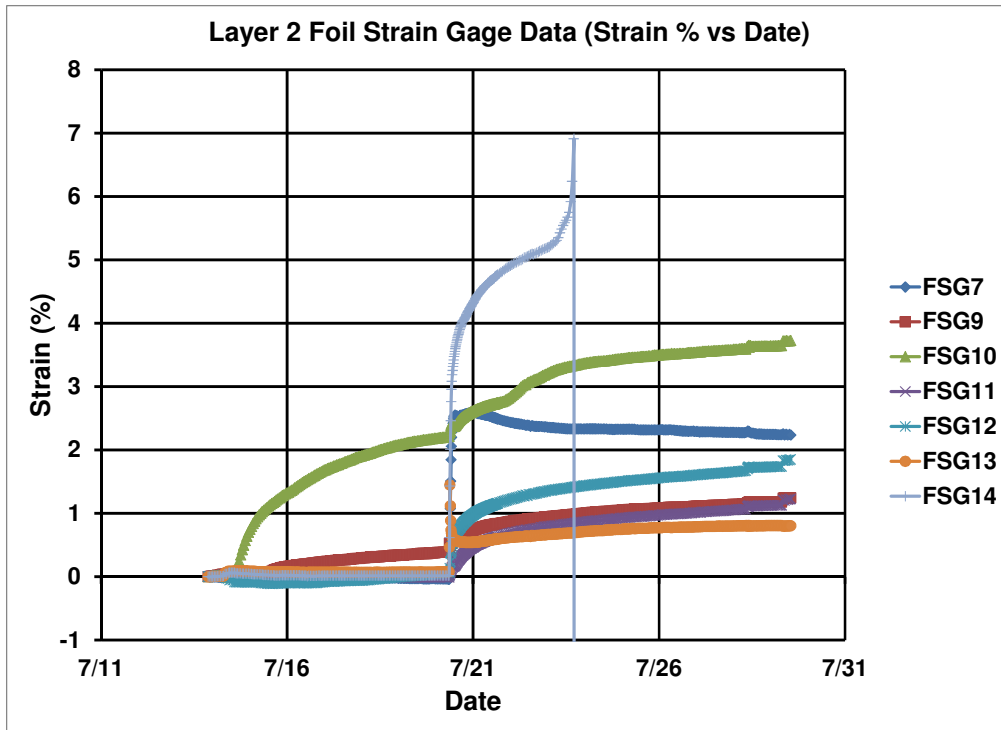


Figure 6.18: Foil strain gage data from CSE #2 for geogrid layer #2, Elev = 0.5 ft.

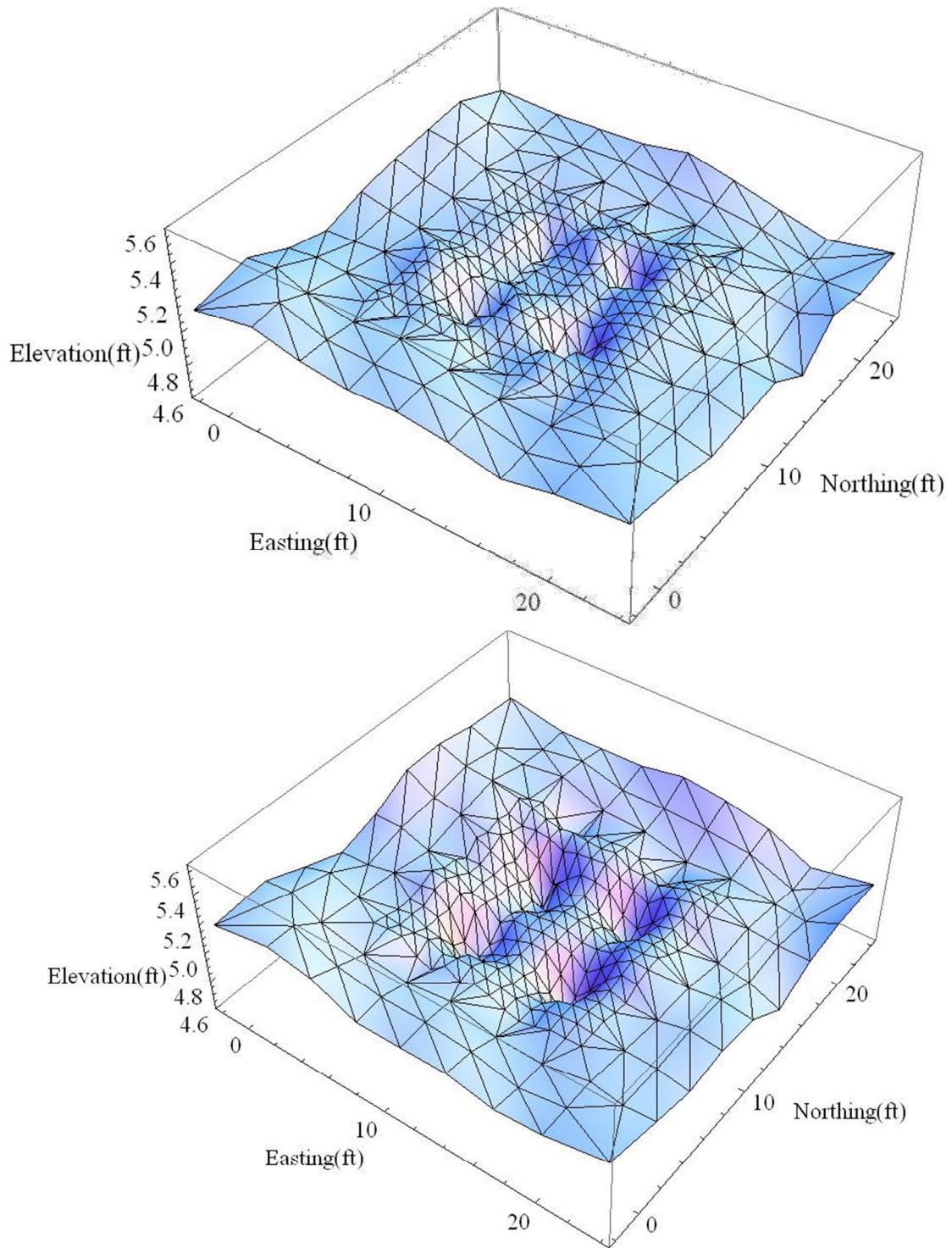


Figure 6.19: Plot of before-trafficking (top) and after-trafficking (bottom) elevations for CSE #2 showing differential surface settlement between columns.

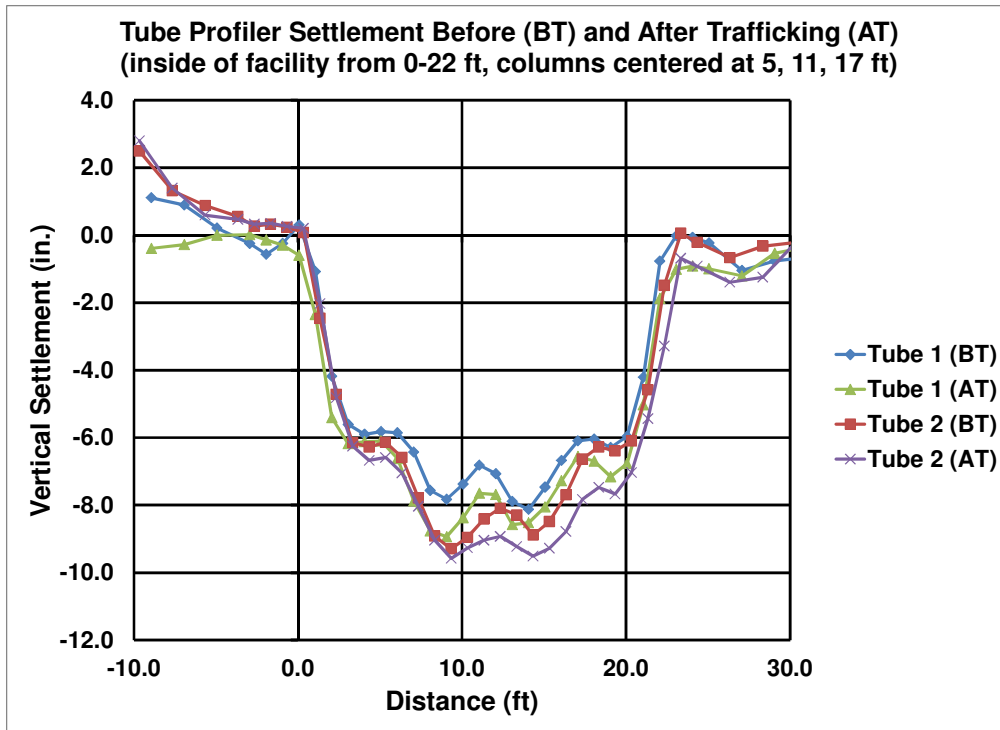


Figure 6.20: Settlements from profiler tubes #1 and #2 for CSE #2.

Table 6.5: Summary of surface and base settlements from CSE #2.

Settlement	BT Value (8 days after dissolving geofom)			AT Value (9 days after dissolving geofom)		
	Min	Max	Avg	Min	Max	Avg
S_{col} (in.)	n/a	n/a	0.6	n/a	n/a	0.6
$S_{soil,d}$ (in.)	2.3	2.6	2.5	3.9	5.0	4.4
$S_{soil,i}$ (in.)	0.3	1.2	0.9	1.5	1.6	1.6
$S_{base,d}$ (in.)	8.9	9.3	9.1	9.5	9.6	9.5
$S_{base,i}$ (in.)	n/a	n/a	8.1	n/a	n/a	8.9



Figure 6.21: Webcam photo shortly after pumping in the geof foam dissolver, showing partial dissolution of the geof foam in CSE #2.

6.5 DESCRIPTION AND RESULTS OF CSE TEST #3

Like CSE #2, CSE #3 consisted of a 9-column square array of 2 ft diameter columns with 6 ft center-to-center spacing. The construction timeline and properties of CSE #3 are shown in Table 6.6. CSE #3 had an average height of 6.1 ft, which was 1.0 ft higher than CSE #2. Figure 6.22 shows a picture of CSE #3. Note the significant amount of gravel required for the ramp at the side of CSE #3. Figure 6.23 shows the instrumentation locations for CSE #3.

Figure 6.24 shows a webcam photo with partial dissolution of the geof foam and Figure 6.25 shows a webcam photo where the geof foam is fully dissolved.

Figure 6.26 to Figure 6.31 show the instrumentation results from CSE #3. Note that settlement Tube #1 was impassable after dissolving geof foam. Foil strain gages were not used in CSE #3.

Many of the same observations from CSE #2 also apply to CSE #3. Additional observations from CSE #3 are as follows:

- One of the EPCs was located above a column. The higher reading in this EPC, as compared to the other two EPCs, further indicates that arching is occurring during

- construction of the embankment as the geofoam compresses (see Figure 6.26). This is reinforced by the fact that the load in the center column is more than the load based on the area of the column times the average embankment pressure, γH (see Figure 6.27). Upon dissolving the geofoam, the stress in this EPC increased significantly and quickly, and it exceeded the rated capacity of the instrument, so an exact measurement of the stress after dissolving the geofoam is not available.
- The eccentricity in the load cell readings (difference of approximately 6,000 lbs) shown in Figure 6.27 may be explained by the eccentric location of EPC 49 above the center column. The eccentric location of this EPC above the column is believed to affect the arching and load transfer to the column resulting in the higher eccentricity of the load cell readings for this test than for CSE #2.
 - The load in the center column is approximately equal to the calculated load based on the tributary area of the column times the average embankment pressure, γH , after dissolving the geofoam (see Figure 6.27). The load transfer took a longer period of time to occur than for CSE #2, and this may be due to the higher embankment height and a longer time for the greater number of embankment soil particles to shift to equilibrium positions.
 - The strain in the geogrid between two columns is highest closer to the column, i.e., Figure 6.29 shows that the LWE 60-97 strain is higher than the LWE 97-98 strain. This is consistent with numerical modeling such as Russell et al. (2003), Jones et al. (2010), and others.

Table 6.6: Timeline and properties of CSE #3.

Date	Start Elev. (ft)	Finish Elev. (ft)	Avg Nuclear Dry Density (pcf)	Avg Moisture Content (%)
Aug 9, 2010	0.0	0.5	139	1.5
Aug 10, 2010	0.5	1.2	135	1.7
Aug 10, 2010	1.2	1.7	135	1.8
Aug 11, 2010	1.7	2.3	135	1.8
Aug 11, 2010	2.3	2.9	134	1.8
Aug 12, 2010	2.9	3.4	138	2.9
Aug 12, 2010	3.4	4.0	137	2.7
Aug 13, 2010	4.0	4.7	139	2.3
Aug 13, 2010	4.7	5.4	136	2.0
Aug 16, 2010	5.4	5.9	137	2.2
Aug 16, 2010	5.9	6.2	140	2.2
Average			137	2.1
Geofoam dissolved on Aug 17				
Trafficking on Aug 25				



Figure 6.22: Picture of CSE #3.

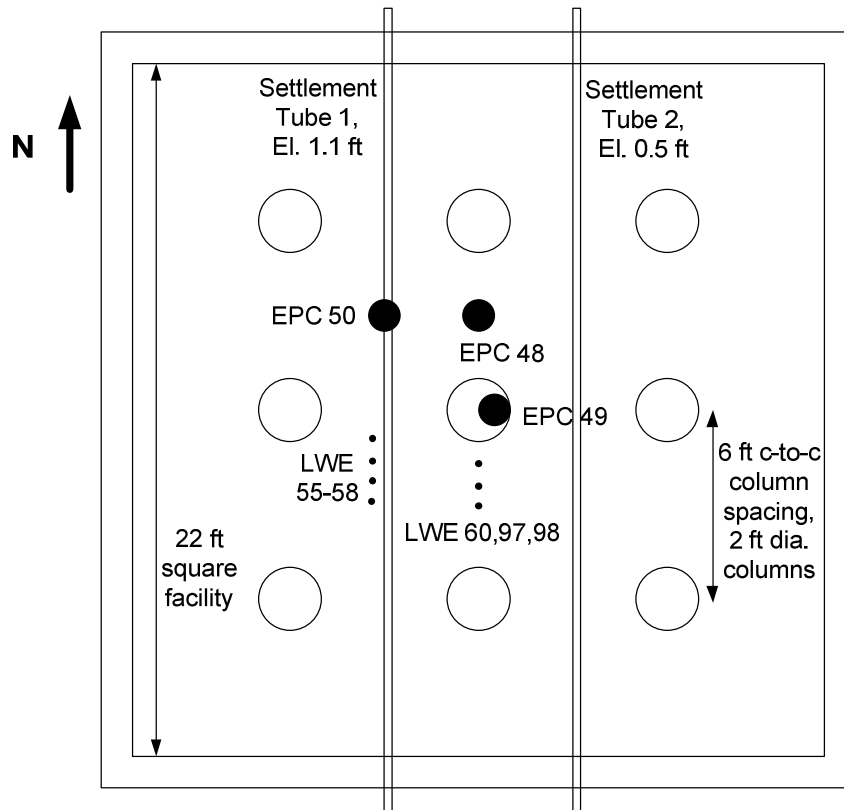


Figure 6.23: Location of instrumentation for CSE #3.

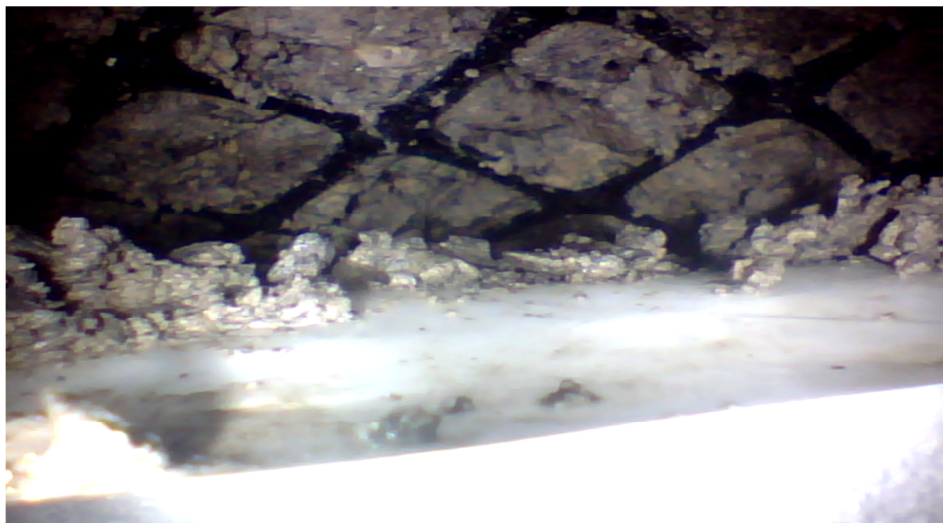


Figure 6.24: Webcam picture from CSE #3 showing partially dissolved geofilm, geogrid, and select fill.

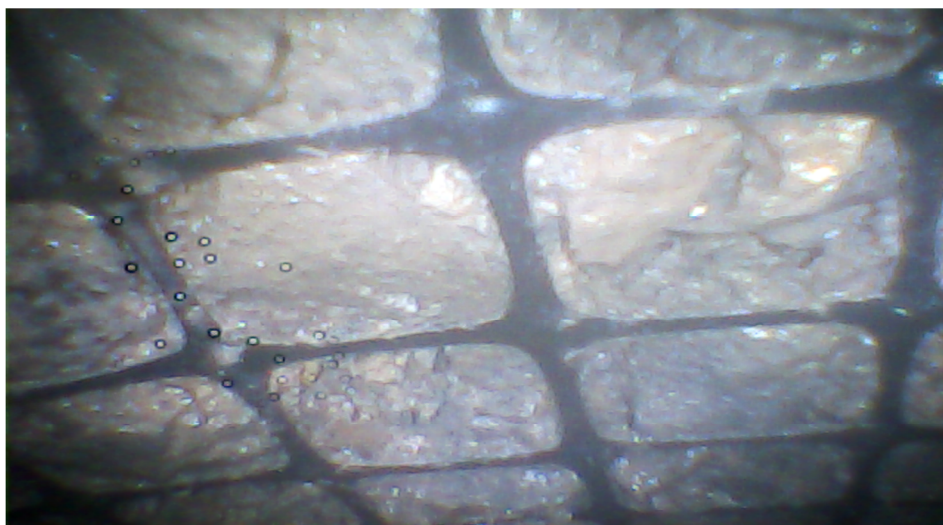


Figure 6.25: Webcam picture from CSE #3 showing deflected geogrid and select fill after geofilm is fully dissolved.

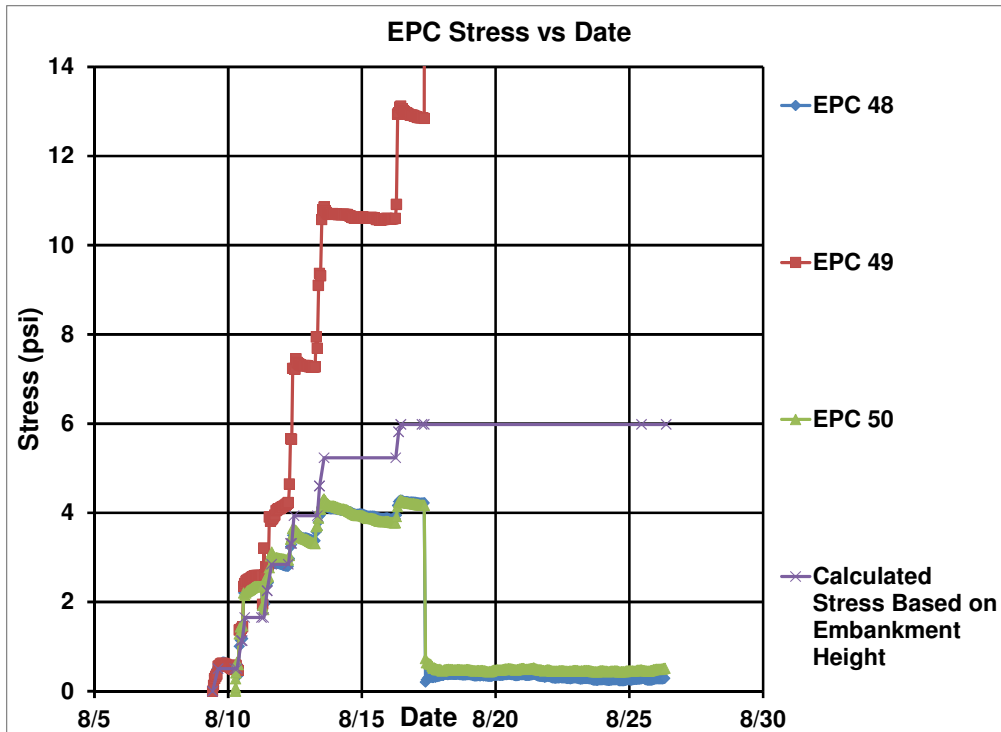


Figure 6.26: EPC data from CSE #3.

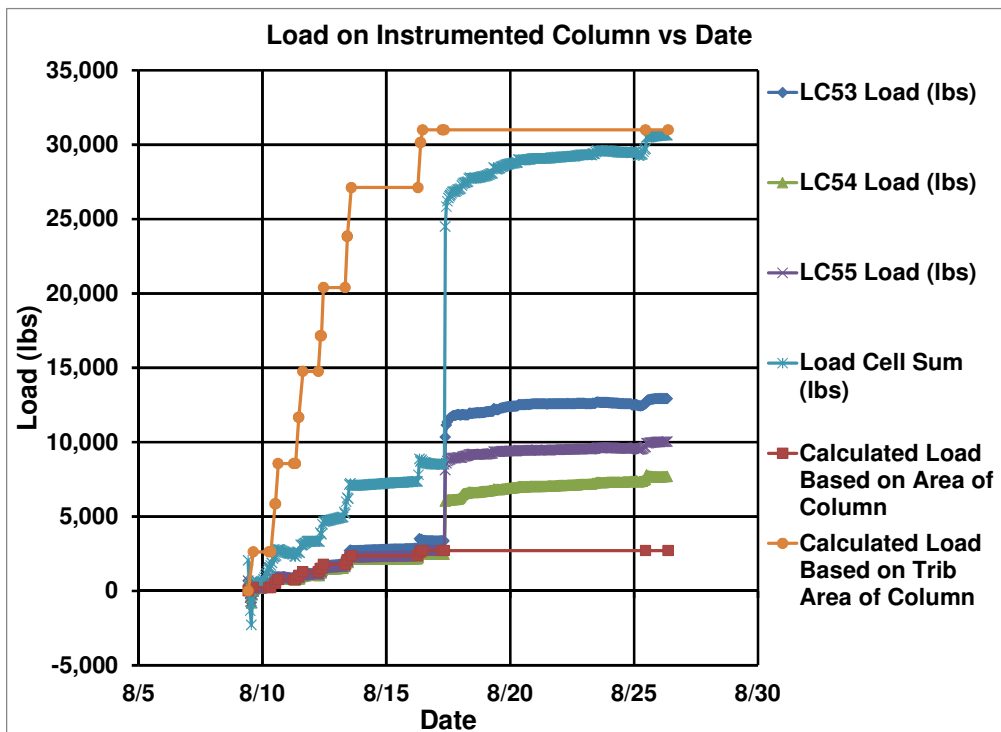


Figure 6.27: Load cell data from CSE #3.

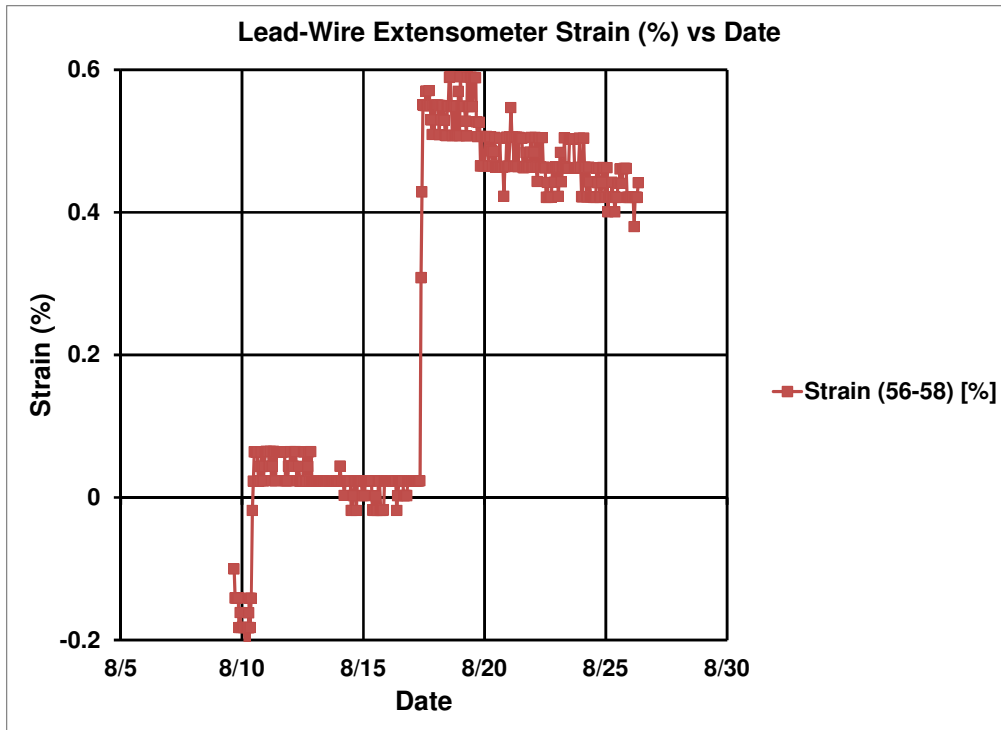


Figure 6.28: Strain data from CSE #3 (Sensors 56, 58).

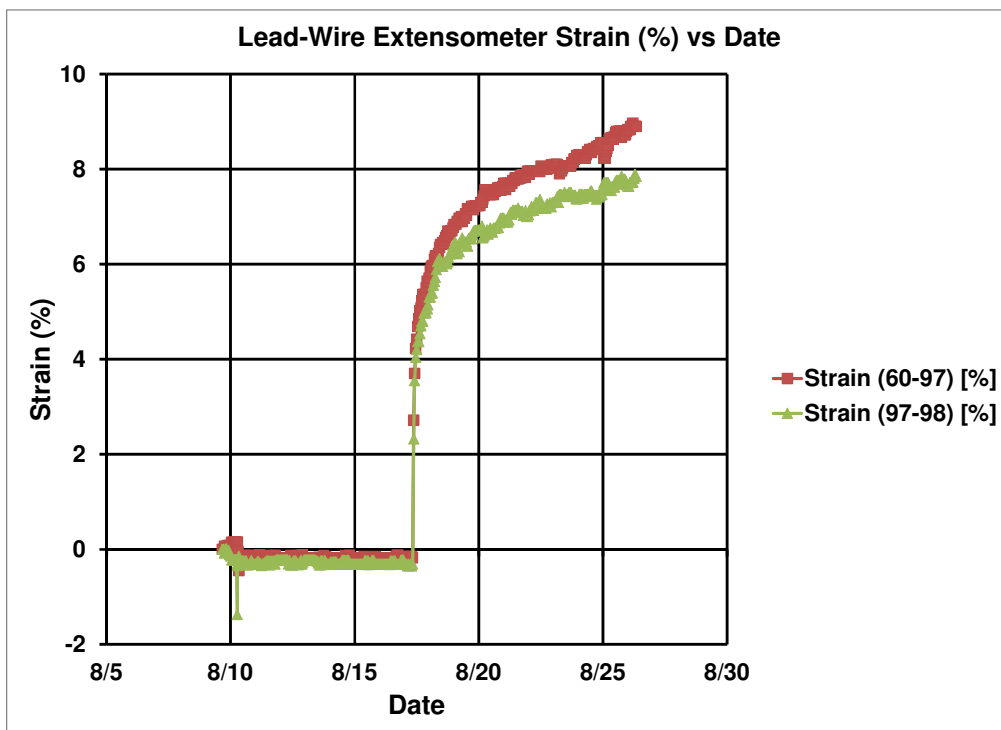


Figure 6.29: Strain data from CSE #3 (Sensors 60, 97, 98).

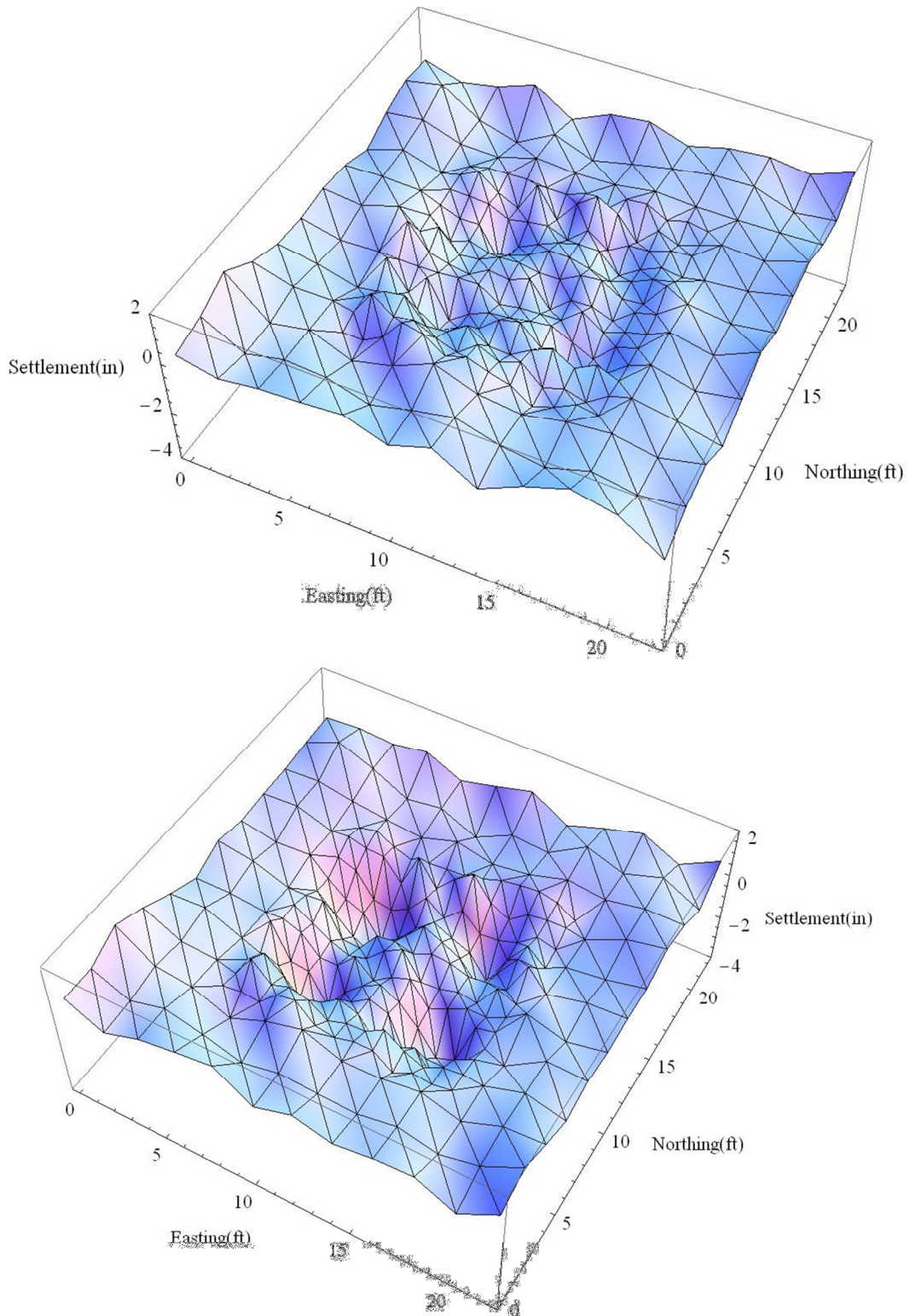


Figure 6.30: Surface settlement of CSE #3 before (top) and after (bottom) trafficking.

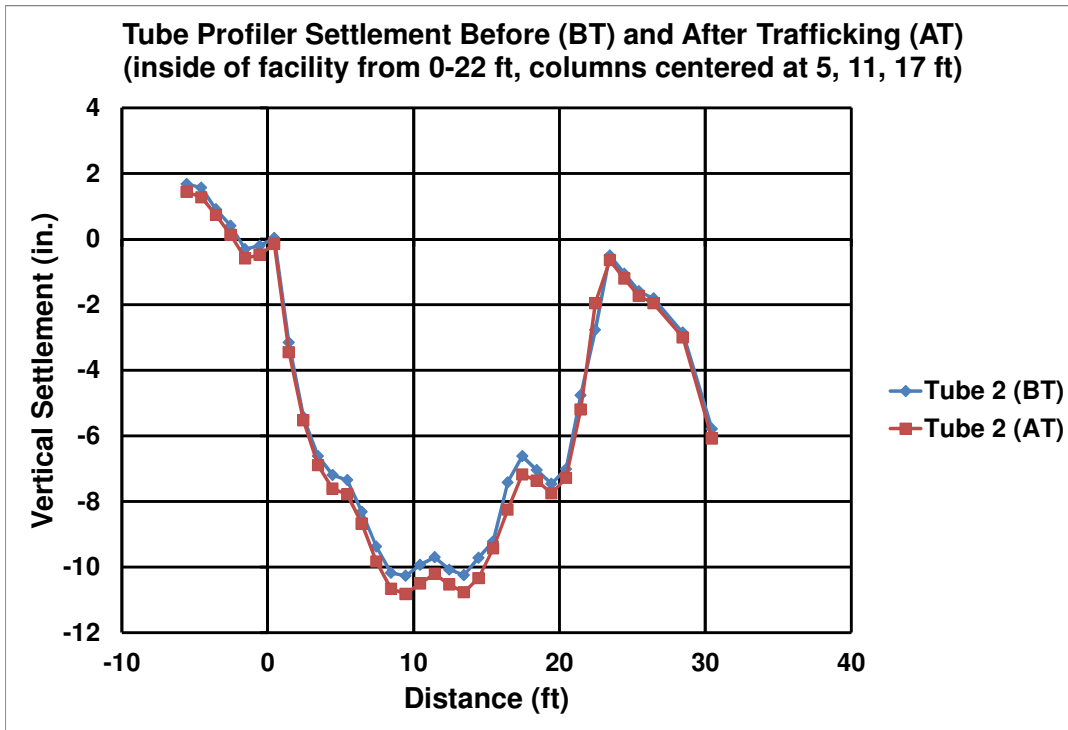


Figure 6.31: Settlement from profiler tube #2 before and after trafficking.

Table 6.7: Summary of surface and base settlements from CSE #3.

Settlement	BT Value (7 days after dissolving geofoam)			AT Value (7 days after dissolving geofoam)		
	Min	Max	Avg	Min	Max	Avg
S_{col} (in.)	n/a	n/a	0.1	n/a	n/a	0.0
$S_{soil,d}$ (in.)	0.7	1.7	1.0	2.4	3.2	2.9
$S_{soil,i}$ (in.)	0.2	0.7	0.4	0.7	1.9	1.2
$S_{base,d}$ (in.)	10.3	10.3	10.3	10.8	10.8	10.8
$S_{base,i}$ (in.)	n/a	n/a	9.7	n/a	n/a	10.2

6.6 DESCRIPTION AND RESULTS OF CSE TEST #4

CSE #4 had the same configuration as CSEs #2 and #3: 6 ft center-to-center spacing of 9 each, 2 ft diameter columns, with 3 layers of Tensar® BX1500 geogrid in the first 6 in. of fill (one layer directly above the columns and two layers placed transverse to one another at an elevation of 6 in. above the columns). Whereas CSEs #2 and #3 had heights of 5.1 ft and 6.2 ft respectively, CSE #4 had an average embankment height of 7.5 ft which is the highest embankment constructed in this test program. The only variable in CSEs #2 to #4 was the embankment height.

A height of 7.5 ft was initially chosen for CSE #4 since it was believed to be above the BT critical height but below the AT critical height based on the results of CSEs #2 and #3. Based on the results of CSE #4, the height of 7.5 ft is certainly above the BT critical height and either at or slightly above the AT critical height for this geometry.

Figure 6.32 shows a picture of CSE #4 and Figure 6.33 shows the as-built plan and cross-sectional views of the embankment. The CSE #4 timeline is shown in Table 6.8. Figure 6.34 shows the locations of the instrumentation in CSE #4, and the instrumentation results are presented in Figure 6.35 to Figure 6.43. The surface and base settlements from CSE #4 are listed in Table 6.9.

The load in the center column increased significantly after pumping in the geofoam dissolver as shown in Figure 6.36, but the load did not reach the full calculated load based on the tributary area around the center column. The load continued to increase over the next several weeks before demolition of the embankment. The extended length of time for load transfer is believed to be caused by the high embankment height relative to the column spacing and the size of the CSE facility for this test (22 ft square). Some “global arching” from the edges of the facility is believed to have occurred, at least temporarily. As this arch broke down, the load was transferred to the columns, hence, the gradual increase in load measured in the center column. This mechanism is consistent with the fact that the deflections between the walls of the facility and the outermost columns are less than the deflections between columns (7 to 8 in. as opposed to 10 to 11 in.), as shown in Figure 6.43 for CSE #4, Tube #2, on Day 19 (AT). This indicates that arching is sensitive to the base deflection and support conditions, and that some time may be necessary for global arching to break down and transfer the load to the center column for the configuration of CSE #4. Creep of the geosynthetic reinforcement could also be a factor, but the creep strains and deflections over two to three weeks are smaller than the immediate strain and base deflections that occur when the geofoam is dissolved.

Although some time-dependent global arching from the facility walls is believed to have occurred in CSE #4, the embankment is still believed to be at or slightly above the critical height, even after the trafficking since: 1) the highest measured load of 33,160 lbs is approximately 90% of the calculated load, so a majority of the load transfer was complete, especially considering the potential variation in material properties and accuracy of load, height, and density measurements, and 2) the embankment continued to show zero differential settlement through 14 surveys over a period of 20 days and three trafficking events after dissolving the geofoam.

The time-dependent breakdown of global arching and accompanying transfer of load to the center column that occurred in CSE #4 illustrates the sensitive nature of arching. The edge of the facility was 8 ft from the edge of the unit cell around the center column. Although the perimeter wall provides a better support condition than the individual columns, the fact that the wall, 8 ft away edge of the unit cell, affected the rate of load transfer to the center column is remarkable. If the support from the perimeter wall were limited to the zone within a 1H:1V sloped surface progressing up from top inside edge of the perimeter wall, the unit cell surrounding the center column would have been unsupported by the perimeter wall, but the load cell data indicates this was not the case, at least initially. Another consideration is that limited base deflections due to support from the geosynthetic near the perimeter walls, as shown in Figure 6.43, may have extended the support from perimeter walls towards the unit cell around the center column.

The hourly rainfall is plotted on a secondary axis of the load cell readings in Figure 6.36. Some of the load redistribution occurring on Sept 26 to 28 is believed to be due to rainfall surcharge and perhaps due to some downward seepage forces in the embankment. Although all of the embankments were covered in plastic, some holes were observed in the plastic covering for this test. The total rainfall from Sept 26 to Sept 28 was 2.25 in.

Additional observations from CSE #4 include:

- There was 2.9 ft of fill placed between Sept 10 and Sept 15 but the EPCs only increased by about 0.5 psi during this time (see Figure 6.35). This indicates that the majority of this new load was being transferred to the columns and not to the geofoam.
- The highest EPC stress prior to dissolving the geofoam was approximately 4.6 psi vs a calculated stress of 7.2 psi, resulting in a *SRR* of 0.64 (see Figure 6.35). *SRRs* before dissolving the geofoam will be compared to calculated results from design/analysis methods that include soft soil support in Section 7.1.
- The foil strain gages gave some useful information but experienced some of the same problems as in CSE #2. In addition to the results in Figure 6.39 and Figure 6.40, the performance of the foil strain gages in CSEs #2 and #4 is discussed further in APPENDIX A.
- The settlements measured within the unit cell shown in Figure 6.41 are relatively uniform and indicate that this embankment is above the before-trafficking (BT) critical height, and is at or above the after-trafficking (AT) critical height.

- The Sept 26 to 28 rain event also caused the rate-of-change in the geogrid strain to be altered and a redistribution of the load within the center column i.e. LC53 and LC55 increased while LC54 decreased (see Figure 6.36).
- Base deflections (as shown in Figure 6.42 and Figure 6.43) and support conditions have a significant impact on arching and load transfer. The edges of the facility at a distance of 8 ft from the unit cell around the center column had an impact on the load transfer to the center column. If the base deformations are limited, then arching can support more than what would be calculated, if only on a temporary basis. For CSEs on soft soil, if there is even a small amount of subgrade support, the critical height could be lower than would be expected based on tests without subgrade support, and the surface deformations could be reduced because of the limited base deflections.
- The average surface settlement within the unit cell around the center column was 1.2 in. on Oct 6, 20 days after dissolving the geofoam (see Figure 6.41). The differential settlement of the embankment surface was less than about 0.1 inch at this time, although it is difficult to be precise because of the rough texture of the gravel surface, the potential for movement of individual gravel particles, and the error associated with orienting the total station. Since the differential settlement is within the ability of the total station to survey elevations on gravel, CSE #4 is deemed to be above the critical height before trafficking, and at or slightly above the critical height after trafficking.

Table 6.8: Timeline and properties of CSE #4.

Date	Start Elev. (ft)	Finish Elev. (ft)	Avg Nuclear Dry Density (pcf)	Avg Moisture Content (%)
Sept 6, 2010	0.0	0.5	n/a	n/a
Sept 7, 2010	0.5	1.2	135.7	1.7
Sept 7, 2010	1.2	1.7	134.1	1.7
Sept 8, 2010	1.7	2.3	136.2	1.8
Sept 9, 2010	2.3	2.9	136.0	1.9
Sept 9, 2010	2.9	3.5	135.7	1.9
Sept 10, 2010	3.5	4.1	134.2	1.6
Sept 10, 2010	4.1	4.6	136.7	1.9
Sept 10, 2010	4.6	5.2	135.8	1.8
Sept 13, 2010	5.2	5.6	136.6	2.2
Sept 14, 2010	5.6	6.1	131.7	1.4
Sept 14, 2010	6.1	6.7	131.4	1.6
Sept 15, 2010	6.7	7.2	133.1	1.9
Sept 15, 2010	7.2	7.5	135.0	1.8
Average			135.0	1.8
Geofoam Dissolved on Sept 16, 2010				
Trafficking Day 1: Sept 23, 2010				
Trafficking Day 2: Oct 5, 2010				
Trafficking Day 3: Oct 6, 2010				



Figure 6.32: Picture of CSE #4, note instrumentation panel, settlement profiler and tubes, and total station.

Extent of embankment and ramp CSE #4

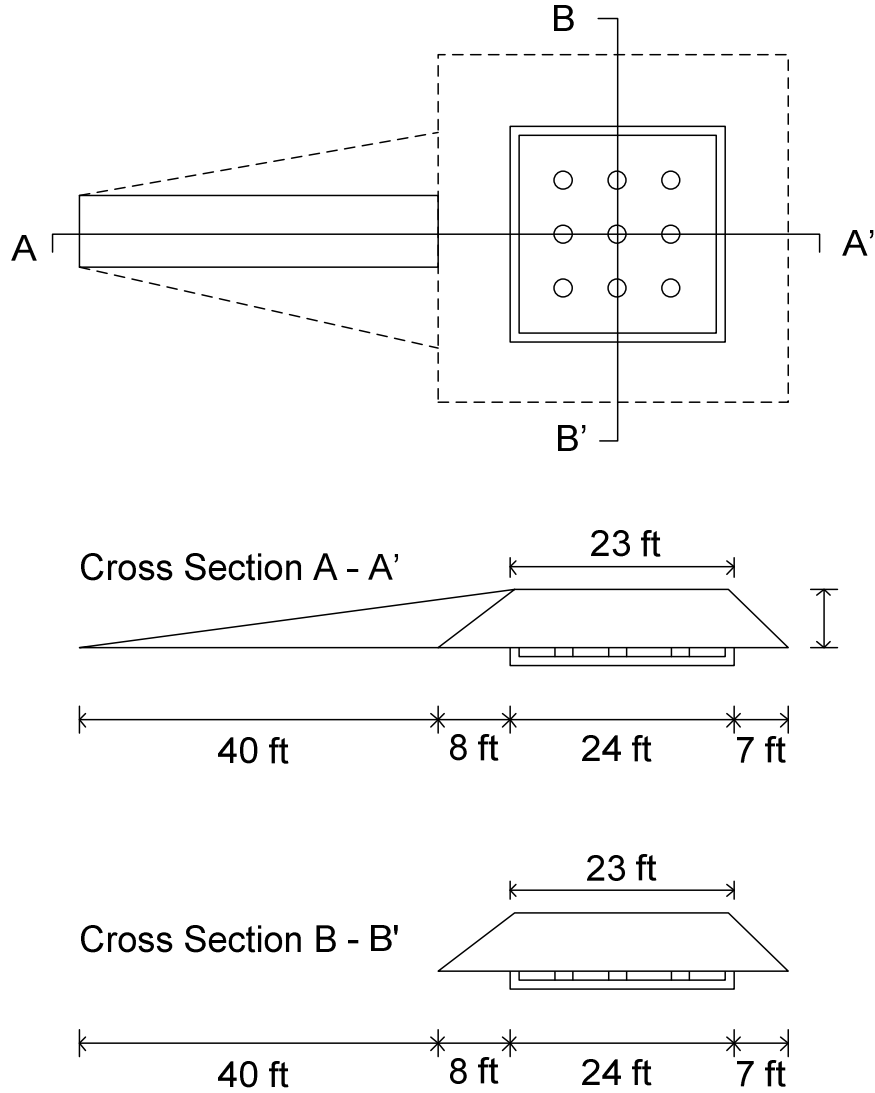


Figure 6.33: Plan and cross-section drawings of CSE #4.

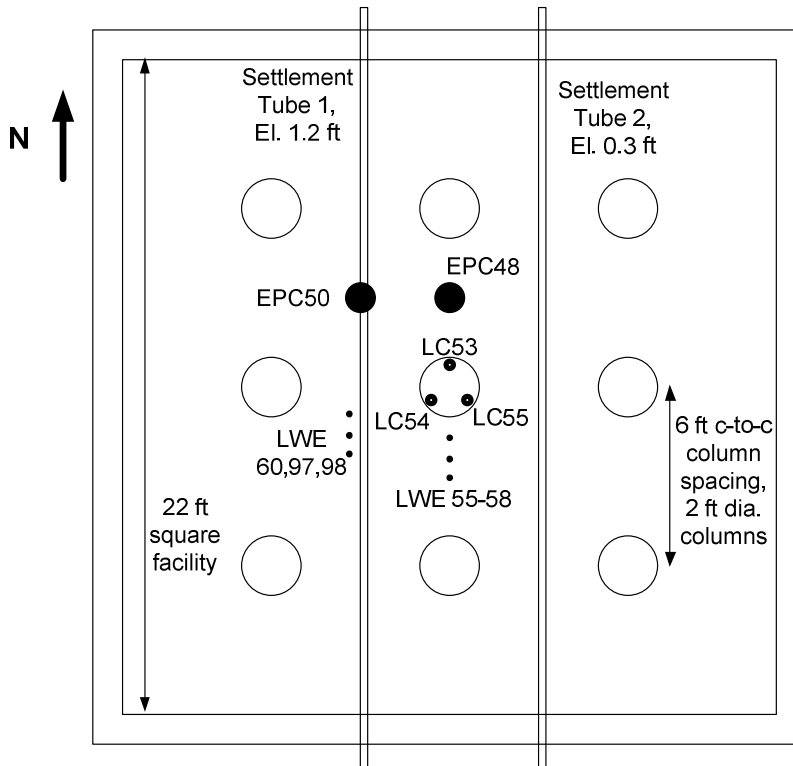


Figure 6.34: Instrumentation locations for CSE #4.

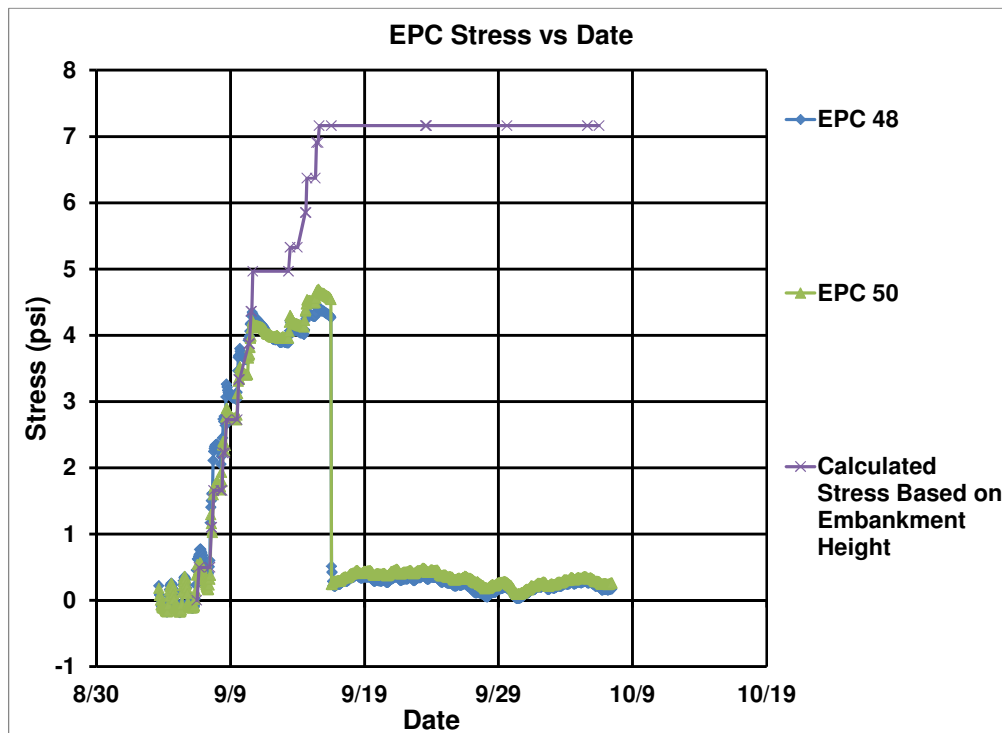


Figure 6.35: EPC data from CSE #4.

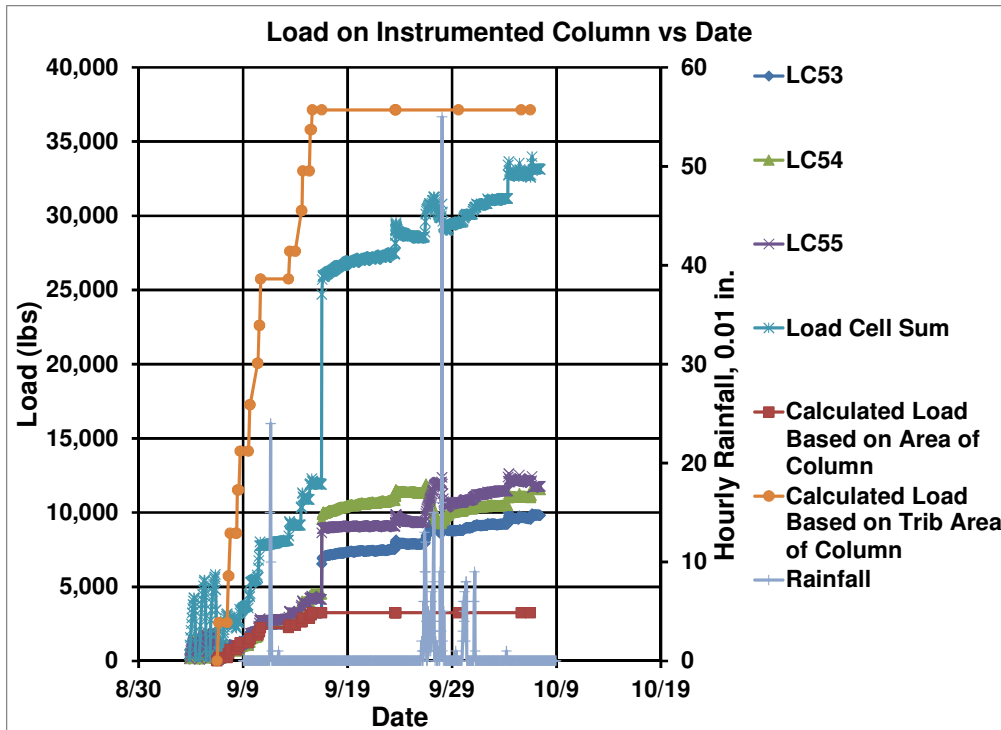


Figure 6.36: Load cell readings from CSE #4 along with hourly rainfall.

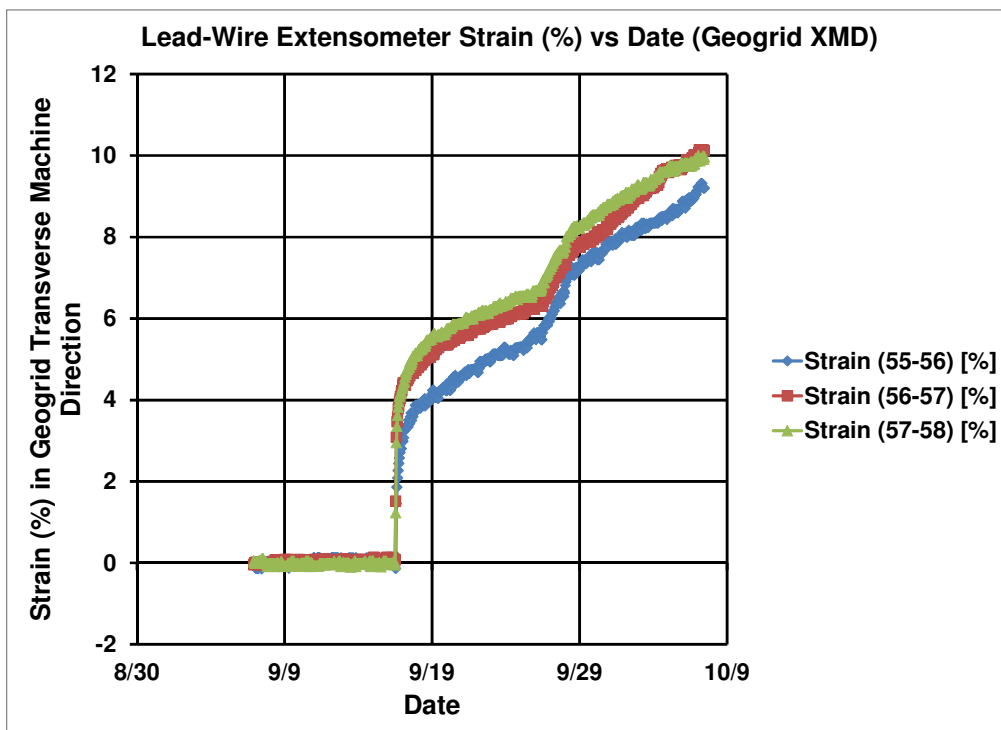


Figure 6.37: Lead-wire extensometer strain from CSE #4 (Sensors 55, 56, 57, 58).

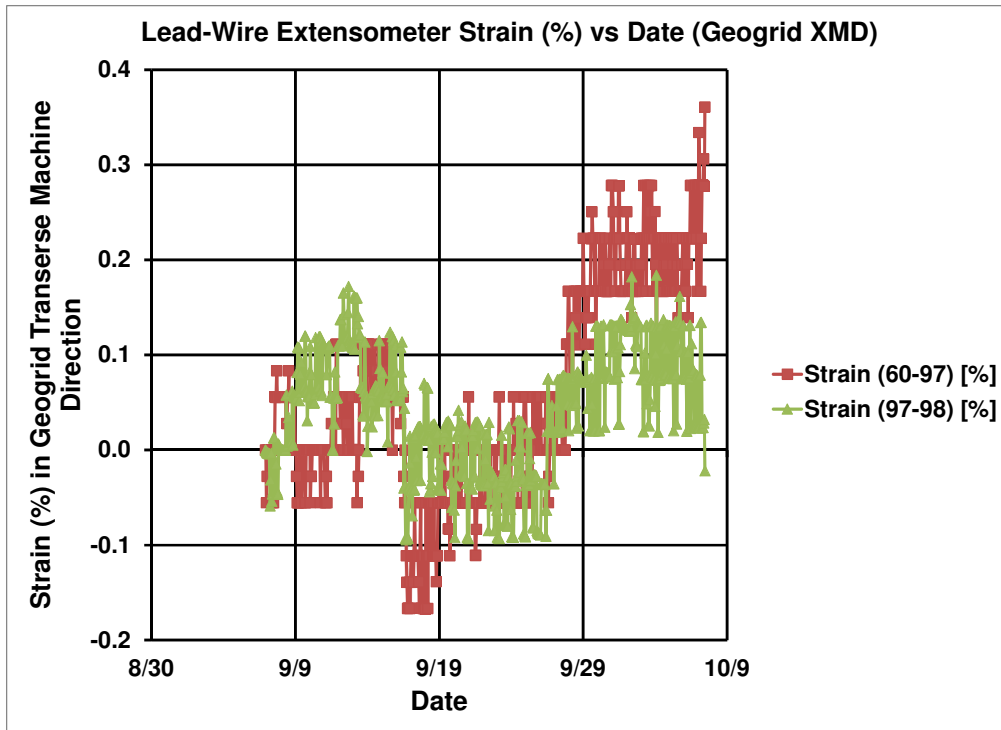


Figure 6.38: Lead-wire extensometer strain from CSE #4 (Sensors 60, 97, 98).

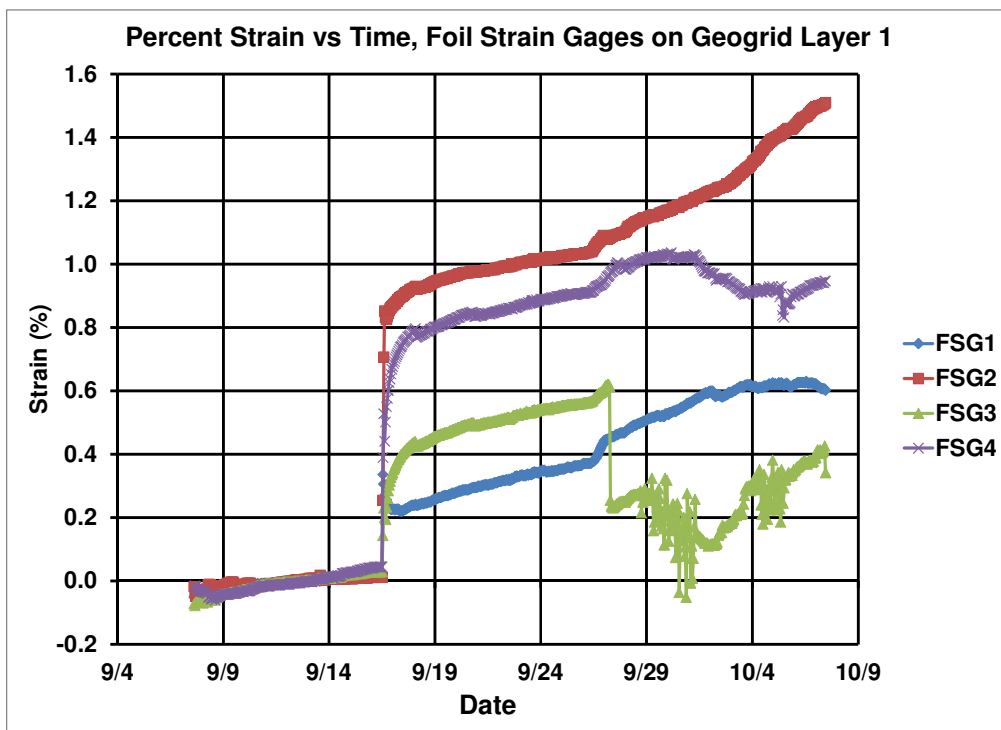


Figure 6.39: Foil strain gage data from geogrid layer #1 (Elev = 0.0) from CSE #4.

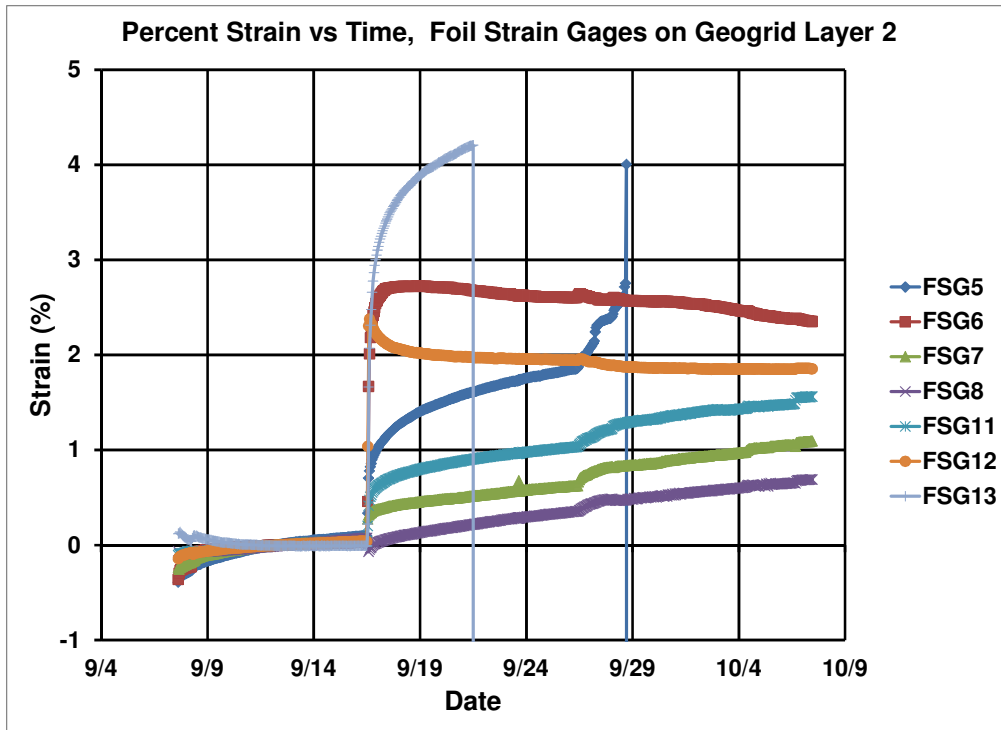


Figure 6.40: Foil strain gage data from geogrid layer #2 (Elev = 0.5 ft) from CSE #4.

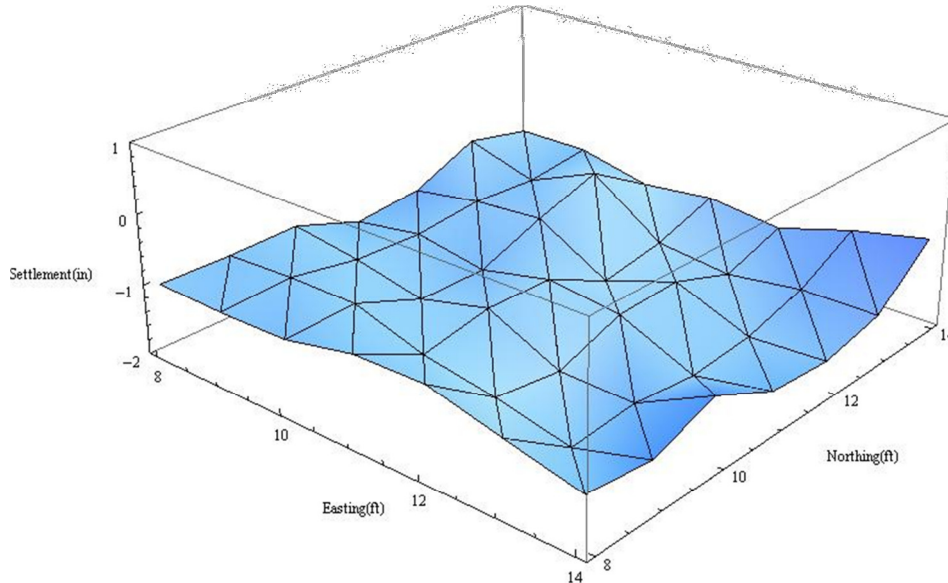


Figure 6.41: After-traffic total settlement within unit cell from CSE #4 (average settlement = 1.2 in.).

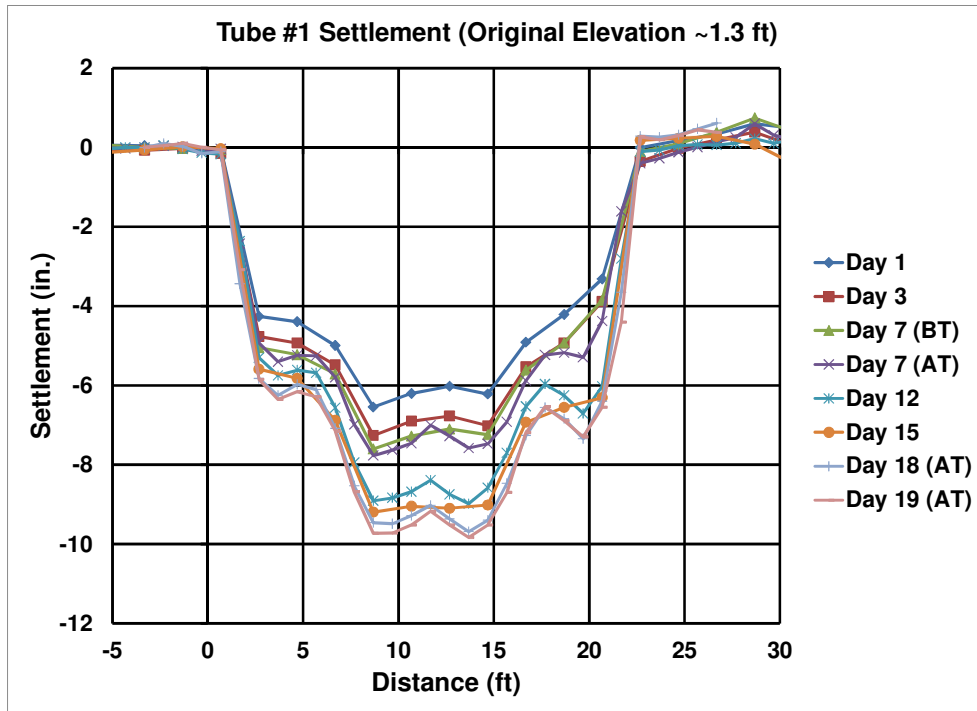


Figure 6.42: Tube #1 settlement from CSE #4 as a function of days after dissolving geofoam.

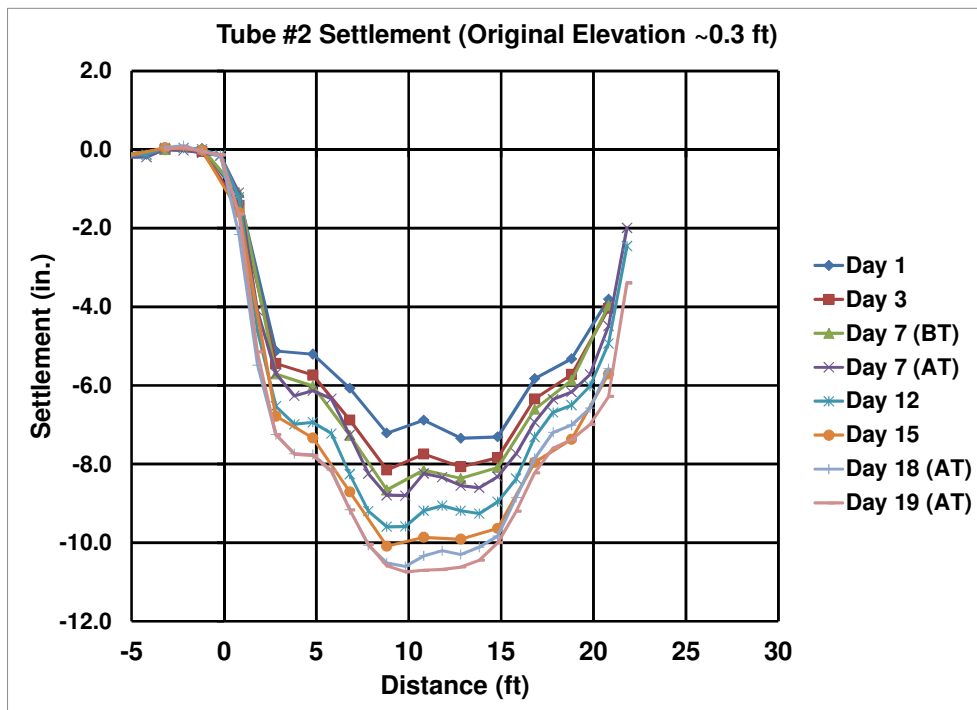


Figure 6.43: Tube #2 settlement from CSE #4 as a function of days after dissolving geofoam.

Table 6.9: Summary of surface and base settlements from CSE #4.

Settlement	BT Value (7 days after dissolving geofom)			AT Value (19 days after dissolving geofom)		
	Min	Max	Avg	Min	Max	Avg
s_{col} (in.)	n/a	n/a	0.2	n/a	n/a	1.1
$s_{soil,d}$ (in.)	0.0	0.4	0.1	0.7	1.3	1.0
$s_{soil,i}$ (in.)	0.0	0.1	0.0	0.8	1.5	1.2
$s_{base,d}$ (in.)	8.4	8.7	8.5	10.7	10.7	10.7
$s_{base,i}$ (in.)	n/a	n/a	8.2	n/a	n/a	10.6

6.7 DESCRIPTION AND RESULTS OF CSE TEST #5

The goal of CSE Test #5 was to evaluate the effect of geogrid quantity and spacing for the same column arrangement as CSEs #2 to #4. Like CSEs #2 to #4, CSE #5 contained a square array of 9 columns with 6 ft center-to-center spacing. Whereas CSEs #2 to #4 contained three layers of Tensar® BX1500 geogrid all located within the first 6 in. of the embankment, CSE #5 contained five layers of Tensar® BX1500 geogrid. The first layer was located immediately above the columns and the remaining layers were located at elevations of 6 in., 12 in., 18 in., and 24 in. The intent of CSE #5 was to model the “beam” approach to CSE design and determine if the critical height was affected given the potential for enhanced load transfer due to the confinement effect of the geogrid.

Table 6.10 contains the timeline and properties of CSE #5. Figure 6.44 shows a picture of CSE #5 upon completion of construction and Figure 6.45 shows the instrumentation locations.

The trafficking for CSE #5 was completed on November 1, 2010, but the embankment was allowed to remain in place while monitoring continued until March 2011. The instrumentation plots provide a longer-term perspective than the results from CSEs #2 to #4 as the embankment was monitored for approximately 116 days after dissolving the geofom.

Figure 6.46 to Figure 6.50 show the EPC, load cell, and strain gage data from CSE #5. Figure 6.51 contains a picture of the settlement of the embankment surface after trafficking. Figure 6.52 shows a plot of the embankment settlement after trafficking. Both Figure 6.51 and Figure 6.52 clearly show the deformations present in the embankment, and the locations of the 9 columns can be clearly seen. Figure 6.53 and Figure 6.54 show the settlement profiler data from CSE #5.

The following observations are made based on the data from CSE #5:

- After dissolving the geofoam, the load cell (Figure 6.47) and EPC (Figure 6.46) readings remained relatively constant through the 116-day monitoring period.
- The settlement profiler readings indicate that portions of the base layer of geogrid ruptured between 7 and 24 days after dissolving the geofoam (see Figure 6.54). The readings at 7 days show the typical trend with local maxima at the column locations and local minima between columns. The profile at 24 days shows a continuous deformation between the walls of the facility, indicating that the geogrid has ruptured in some places. The maximum measured strain at this point was approximately 11% which is approximately the rupture strain for the Tensar® BX1500 geogrid.
- As shown in Figure 6.54, the maximum tube #2 settlement is approximately 14 in. which suggests that there is still 2 in. or so of space between the base layer of geogrid and the slab surface (original difference was 16 in.). This is also supported by the fact that the load cell readings did not drop which would have indicated that some of the embankment was resting on the slab below.
- The strains remained relatively constant from mid-November through late February as shown in Figure 6.49 and Figure 6.50, but since the base layer of geogrid ruptured, the measured strains were probably affected by the distortions that accompanied the geogrid rupture.
- The settlements are summarized in Table 6.11. The average after-trafficking $S_{soil,i}$ and $S_{soil,d}$ were 3.2 and 6.5 in. respectively. In the 109 days that followed after taking these measurements, $S_{soil,i}$ increased by 0.2 in. to 3.4 in., and $S_{soil,d}$ increased by 1.4 in. to 7.9 in.
- The settlements in the two settlement tubes increased by 1 to 1.5 in. in the 88 days between the Day 24 and Day 112 measurements as shown in Figure 6.53 and Figure 6.54. Note that the increase in the surface settlement at the diagonal midpoints of 1.4 in. is approximately equal to the settlement increase in both of the settlement profiler tubes. The approximate equality of these base and surface settlements indicate that no arching effect remains at the diagonal midpoints for this relatively low height embankment.
- Even though the base layer of geogrid ruptured in some areas, there was not a catastrophic failure of the embankment or excessively large increases in settlements (see Figure 6.53 and Table 6.11). This indicates that CSEs with multiple layers of reinforcement are generally very robust systems.

Table 6.10: Timeline and properties of CSE #5.

Date	Start Elev. (ft)	Finish Elev. (ft)	Avg Nuclear Dry Density (pcf)	Avg Moisture Content (%)
Oct 18, 2010	0.0	0.6	137	1.1
Oct 18, 2010	0.6	1.1	140	1.9
Oct 19, 2010	1.1	1.6	135	2.9
Oct 19, 2010	1.6	2.0	136	2.1
Oct 20, 2010	2.0	2.5	138	2.8
Oct 21, 2010	2.5	3.2	137	2.5
Oct 21, 2010	3.2	3.7	138	2.3
Oct 22, 2010	3.7	4.0	137	2.1
Average			137	2.2
Geofoam Dissolved on Oct 25, 2010				
Trafficking on Nov 1, 2010				



Figure 6.44: Picture of CSE #5 upon embankment completion.

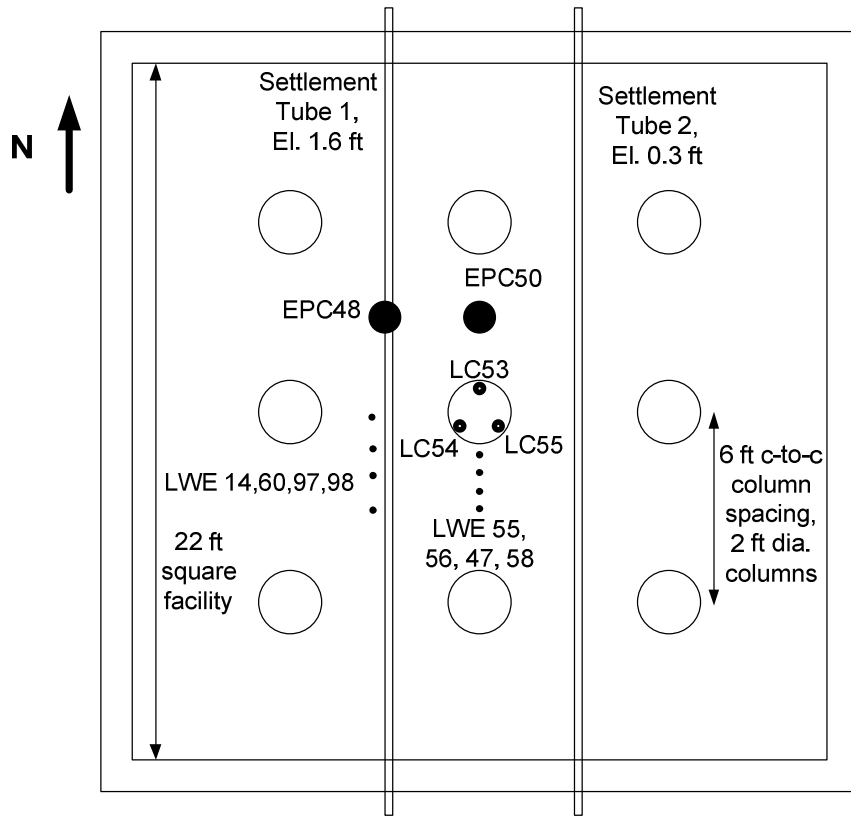


Figure 6.45: Instrumentation locations for CSE #5.

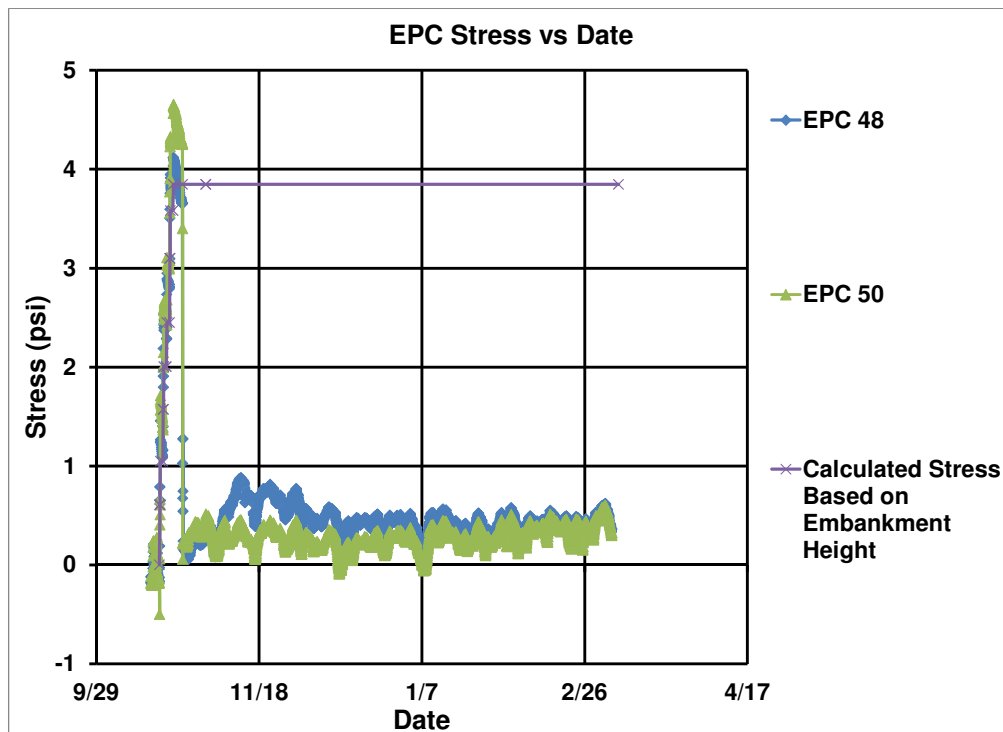


Figure 6.46: EPC data from CSE #5.

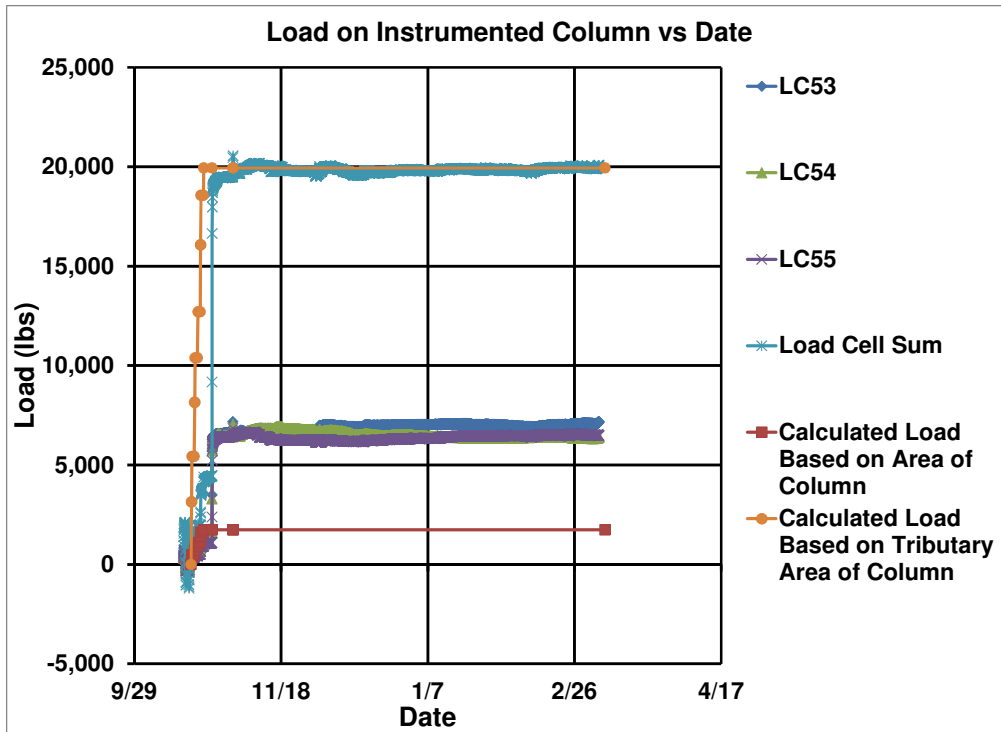


Figure 6.47: Load cell data from CSE #5.

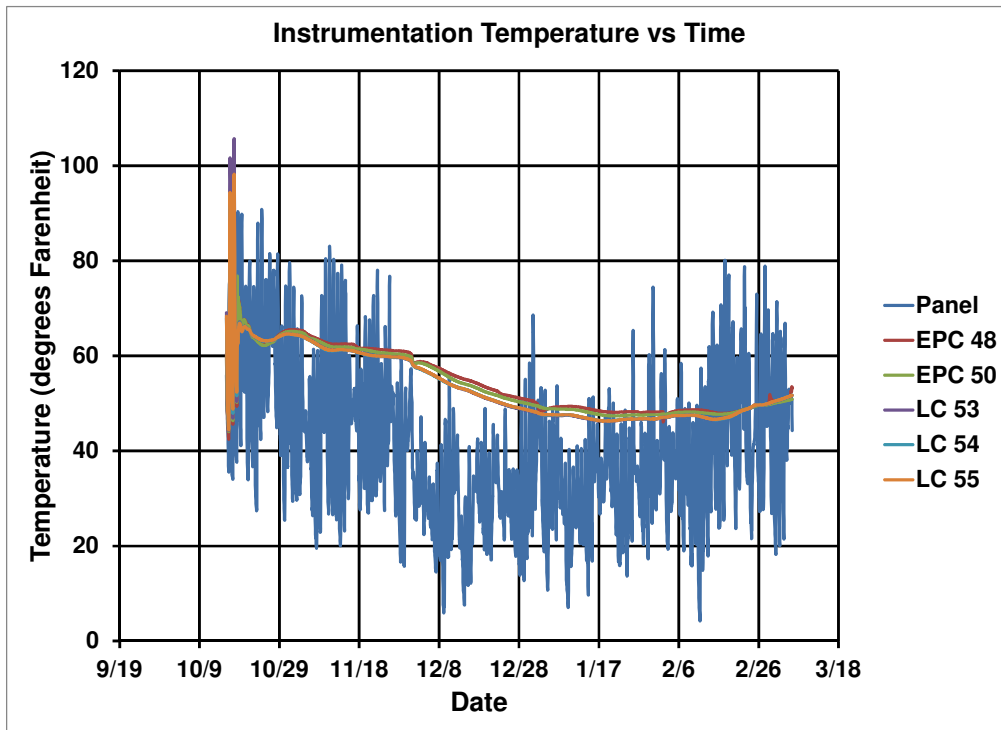


Figure 6.48: Panel, EPC, and Load Cell temperature from CSE #5.

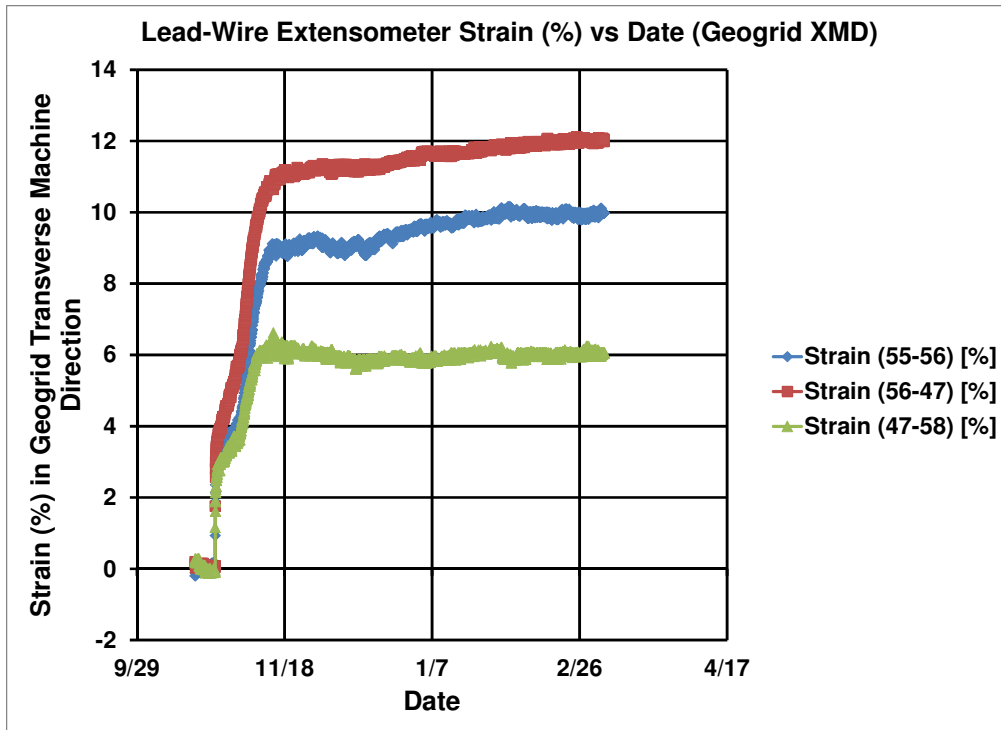


Figure 6.49: Strain data from CSE #5 (Sensors 55, 56, 47, 58).

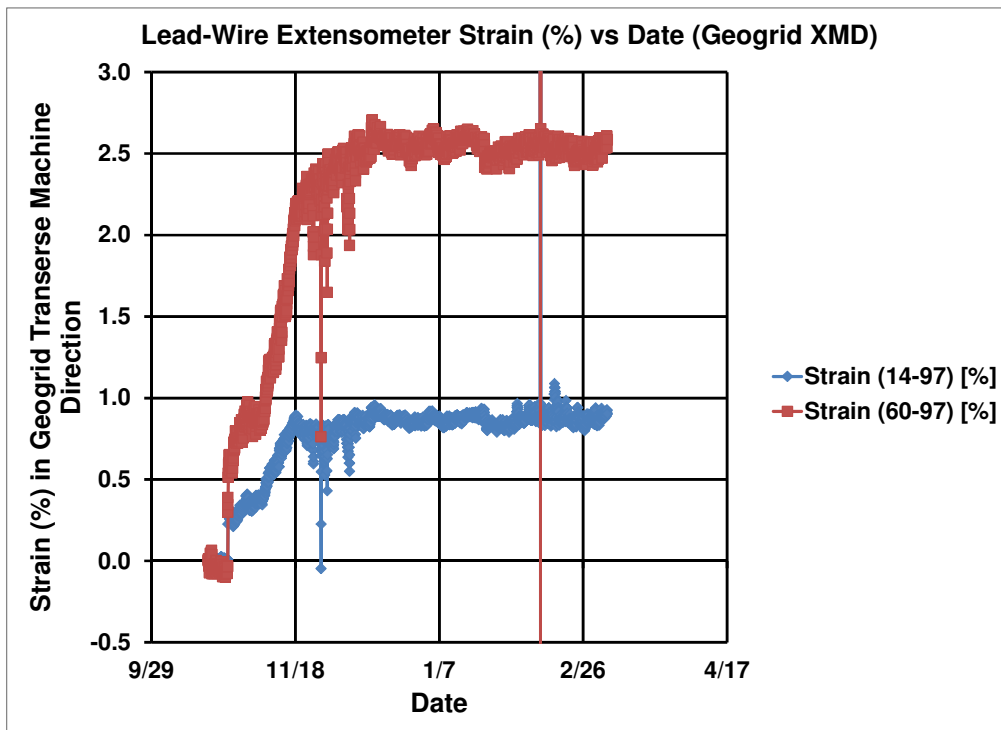


Figure 6.50: Strain from CSE #5 (Sensors 14, 97, 60).



Figure 6.51: Picture of CSE #5 differential settlement after trafficking.

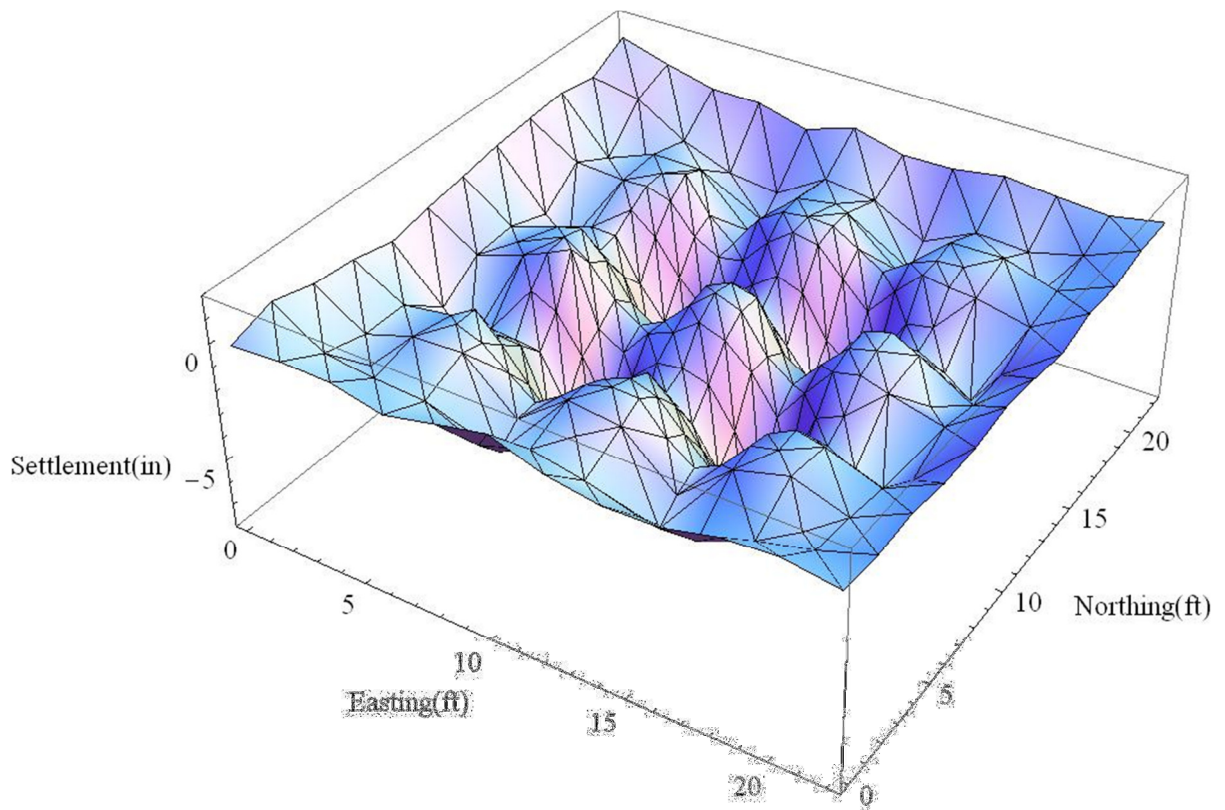


Figure 6.52: Settlement plot of CSE #5 after trafficking.

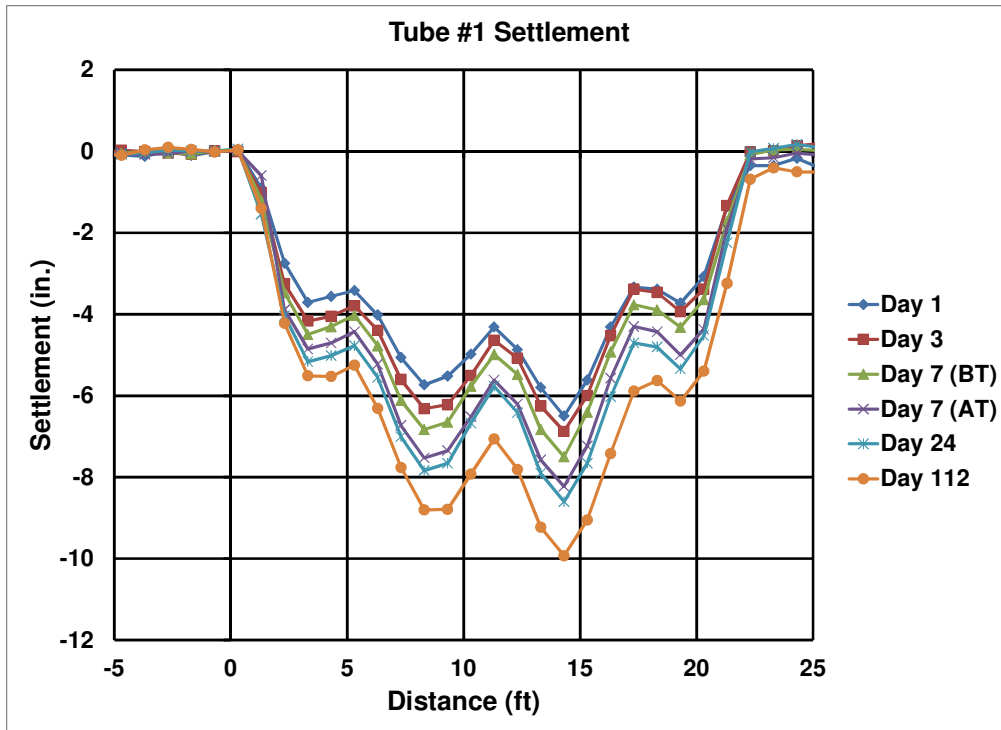


Figure 6.53: Tube #1 settlement from CSE #5.

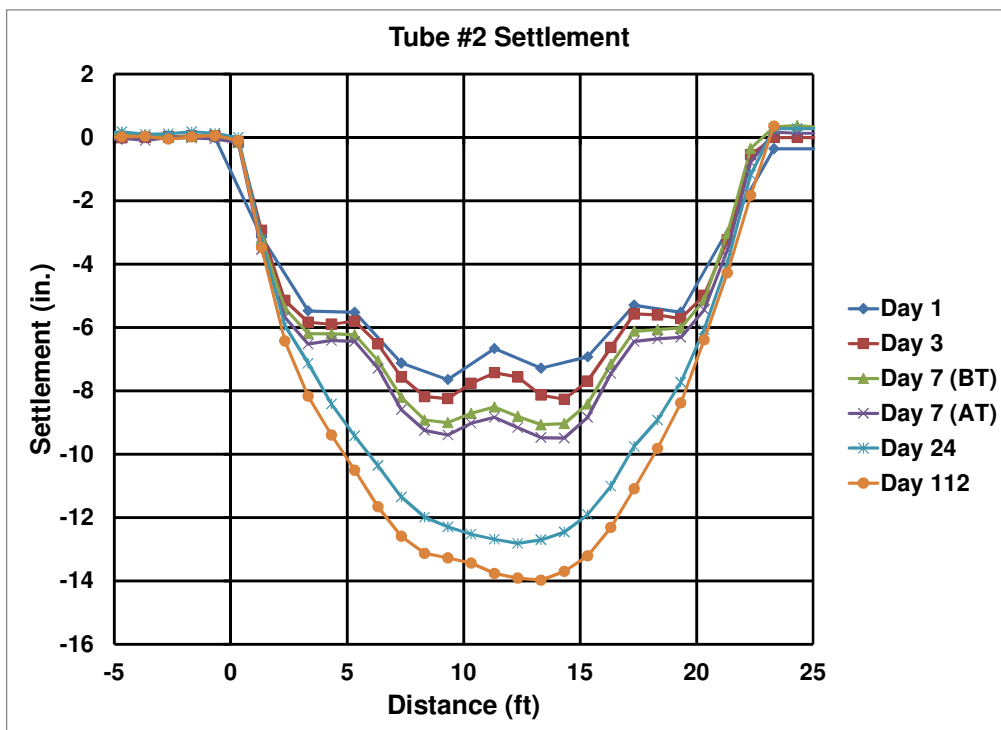


Figure 6.54: Tube #2 settlement from CSE #5.

Table 6.11: Summary of surface and base settlements from CSE #5.

Settlement	BT Value (7 days after dissolving geofoam)			AT Value (7 days after dissolving geofoam)			Long-Term (116 days after dissolving geofoam)		
	Min	Max	Avg	Min	Max	Avg	Min	Max	Avg
S_{col} (in.)	n/a	n/a	0.0	n/a	n/a	0.6	n/a	n/a	0.5
$S_{soil,d}$ (in.)	4.3	5.0	4.6	6.1	7.1	6.5	7.5	8.5	7.9
$S_{soil,i}$ (in.)	0.1	1.0	0.6	2.9	3.2	3.2	3.0	3.6	3.4
$S_{base,d}$ (in.)	9.0	9.0	9.0	9.4	9.5	9.4	Base layer of geogrid ruptured		
$S_{base,i}$ (in.)	n/a	n/a	8.5	n/a	n/a	8.8			

6.8 SUMMARY OF RESULTS AND CONCLUSIONS FROM CSE #2 TO #5

In the CSE tests, the EPC stresses and the load in the center column can each be used to calculate the SRR before dissolving the geofoam. For homogeneous fill, the stress reduction ratio is defined as:

$$SRR = \frac{\sigma_{soil}}{\gamma H + q} \quad (6.1)$$

where σ_{soil} is the stress on the soft subsoil between columns, γ is the unit weight of the fill, H is the embankment height, and q is the surcharge which is 0 for the CSE tests before traffic loading. The EPCs are located within the bottom 6 in. of fill and are essentially a direct measurement of σ_{soil} . The SRRs from the EPCs are shown in Table 6.12 for the CSE tests, in order of increasing height. The EPC values are averaged over a period of time leading up to dissolving the geofoam, EPC_i and EPC_d are the EPC stresses measured at the locations of $S_{soil,i}$ and $S_{soil,d}$ respectively as shown in Figure 6.10, and SRR_i and SRR_d are the stress reduction ratios calculated from EPC_i and EPC_d respectively. Note that the SRR_i and SRR_d are very similar for each embankment, and that, as expected, the SRR values decrease with increasing embankment height.

The load on the central column can be used to calculate the pile efficacy which can be converted to an SRR using the area replacement ratio. The column or pile efficacy, E , can be defined as:

$$E = \frac{\sigma_{col} a_s}{\gamma H + q} \quad (6.2)$$

where σ_{col} is the stress in the column (load in column divided by column area) and a_s is the area replacement ratio defined as:

$$a_s = \frac{A_{col}}{A_{unitcell}} = \frac{A_{col}}{A_{col} + A_{soil}} \quad (6.3)$$

where A_{col} is the column cross-sectional area and A_{soil} is the cross-sectional area of soil within the unit cell. The pile efficacy can then be used to calculate the SRR according to:

$$SRR = \frac{1 - E}{1 - a_s} \quad (6.4)$$

Table 6.12 also includes the *SRRs* calculated from the column loads before dissolving the geofoam. Like the EPC stresses, the column loads are averaged over a period of time prior to dissolving the geofoam. The column *SRRs* are similar in magnitude to the EPC *SRRs*. In general, both the column *SRRs* and EPC *SRRs* show a trend of decreasing *SRR* with increasing embankment height. The variation in the column *SRR* from CSE #2 is believed to be due to experimental scatter. The *SRRs* from both the EPCs and the column loads will be compared with methods that incorporate soft soil support in Section 7.1.

Table 6.12: Calculated SRRs from CSEs #2 to #5 from EPCs and load cells before dissolving geofoam.

CSE #	<i>H</i> (ft)	Avg Base EPC _{<i>i</i>} (psi)	Avg Base EPC _{<i>d</i>} (psi)	γH (psi)	EPC SRR _{<i>i</i>}	EPC SRR _{<i>d</i>}	Avg Col. Load (lbs)	Calc. Col. Load (lbs)	Column Efficacy <i>E</i>	Column SRR
5	4.0	4.2	3.7	3.9	1.09	0.96	4,470	19,940	0.22	0.85
2	5.1	4.0	3.9	4.9	0.81	0.79	8,680	25,570	0.34	0.72
3	6.2	4.3	4.2	6.0	0.70	0.70	8,580	31,000	0.28	0.79
4	7.5	4.3	4.6	7.2	0.60	0.64	11,960	37,140	0.32	0.74

Table 6.13 contains a summary of the geogrid strains and EPC stresses after dissolving the geofoam for CSEs #2 to #5, again ordered according to embankment height. Note that s is the column center-to-center spacing, d_c is the column diameter, and H is the embankment height. Figure 6.55 shows the locations of the strain measurements “Between Columns” and “Mid Columns”. The between-column strains are shown for as many as four time intervals after dissolving the geofoam since they varied considerably with time.

The following observations are made from the strains in Table 6.13:

- The strain measurements between columns are significantly higher than the strain measurements mid-column. This agrees with numerical modeling such as Jones et al. (2010).
- CSEs #5 and #3 show the expected trend of increasing strains with increasing embankment height, for each time interval. CSE #4 does not show this trend due to the temporary global arching from the facility walls that is believed to have occurred which limited the vertical stresses (and therefore the strains) on the geosynthetic. The strains at a time of 21 days are shown for CSE #4 which illustrates that significant strains did develop for this CSE as the vertical stresses increased with time.
- The mid-column strains are relatively constant and low in magnitude, regardless of the embankment height.
- The measured geogrid strains will be compared with methods for determining the tension in the geosynthetic in Sections 7.2.

Like in Table 6.12, the EPC readings in Table 6.13 are averaged over a period of time after dissolving the geofoam. EPC_i and EPC_d are the EPC stresses measured at the locations of $S_{soil,i}$ and $S_{soil,d}$ respectively as shown in Figure 6.10. Note that the EPC stresses after dissolving the geofoam, regardless of the measurement location, are extremely low. All of the EPC stresses from the four tests are less than 80 psf after dissolving the geofoam. The measured EPC stresses will be compared with methods for determining the vertical stress on the geosynthetic in Section 7.3.

Table 6.13: Geogrid strains and EPC stresses after dissolving geofoam.

CSE	Base Geogrid Strain Btwn Col's (%) at time after pumping in geofoam dissolver					Base Geogrid Strain Mid Col's (%)	Avg Base EPC_i (psf)	Avg Base EPC_d (psf)
	4 hr	24 hr	7 day	14 day	21 day			
#5	2.0–3.0	2.9–3.7	3.6–5.4	5.9–9.6	n/a**	0.4 - 0.9	45	65
#2	n/a*	n/a*	n/a*	n/a**	n/a**	0.6 - 0.8	0	75
#3	4.4–4.7	6.0–6.1	7.5–8.4	n/a**	n/a**	0.4 - 0.6	45	68
#4	2.3–3.9	3.6–4.9	5.1–6.3	7.6–8.7	9.2–10.1	0.6 - 1.5	35	48

*due to the location of the wires from the lead-wire extensometers, the actual strains in the geogrid from test #2 are believed to be significantly lower than the measured strains which are not reported here

**embankments #2 and #3 did not remain in place for 14 days; the base layer of geogrid ruptured in CSE #5 prior to 21 days, so the 14 and 21 day strains are not available for these tests

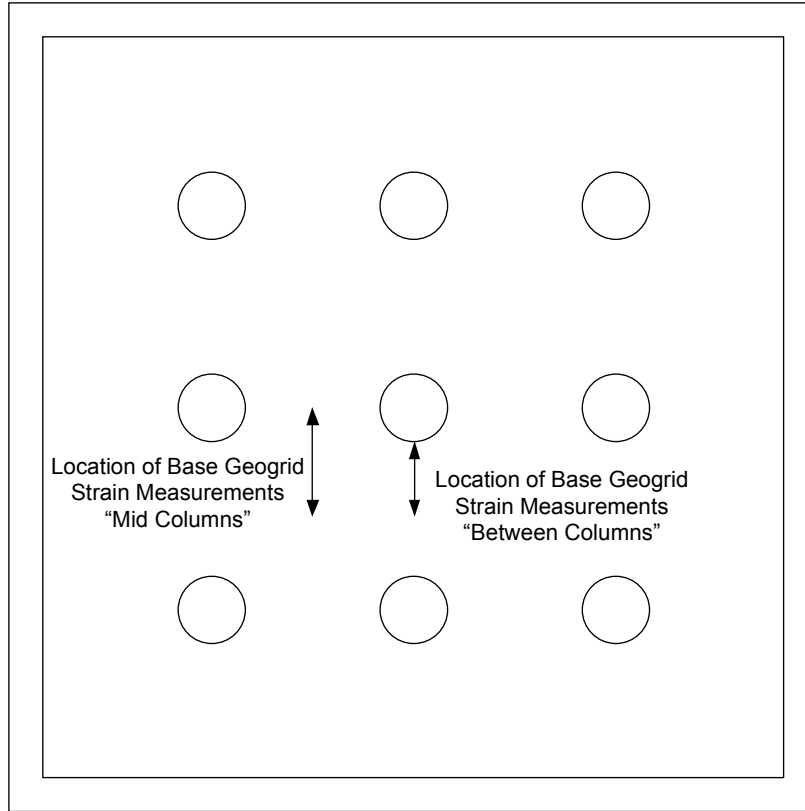


Figure 6.55: Locations of geogrid strain measurements reported in Table 6.13.

Table 6.14 and Table 6.15 summarize the average before-trafficking and after-trafficking settlements from CSEs #2 to #5. Recall that S_{col} is defined as the surface settlement above the center column, $S_{soil,d}$ is the surface settlement at the unit cell perimeter at the centroid of four columns, $S_{soil,i}$ is the surface settlement on the unit cell perimeter directly between two columns (see Figure 6.10), $S_{base,d}$ and $S_{base,i}$ are the settlements at the base of the embankment corresponding to the surface locations of $S_{soil,d}$ and $S_{soil,i}$ respectively, the differential settlements are defined as $DS_d = S_{soil,d} - S_{col}$ and $DS_i = S_{soil,i} - S_{col}$, and the differential settlement ratios are defined as $DSBR_d = DS_d/S_{base,d}$ and $DSBR_i = DS_i/S_{base,i}$.

The following observations are made from Table 6.14: Summary of average CSE settlements before trafficking (BT). Table 6.14 and Table 6.15:

- The settlements above the center column (S_{col}) are relatively low in both the before- and after-trafficking cases for all embankment heights. The after-trafficking column settlements are higher on average than the before-trafficking column settlements since the trafficking process induces some additional settlement above the center column. The low column settlements may be due, in part, to the fact that the geogrid limits the deflection of the base of the embankment in the vicinity of the column as compared to locations farther from

the column. The increase in column load due to the compression of the geofoam and compaction of new material during construction may also contribute to the low settlements.

- $S_{soil,d}$ and DS_d show the general trend of decreasing with increasing embankment height. The decrease in differential settlement with increasing embankment height is logical as the embankment height approaches the critical height, which is the minimum embankment height with zero differential settlement.
- $S_{soil,i}$ and DS_i show the general trend of decreasing with increasing embankment height, but the trend is not as pronounced as for $S_{soil,d}$ and DS_d . The magnitudes of $S_{soil,i}$ and DS_i are less than the magnitudes of $S_{soil,d}$ and DS_d due to the better support condition directly between two columns as opposed to a location at the centroid of four columns.
- Both $S_{base,d}$ and $S_{base,i}$ show the general trend of increasing with increasing embankment height. The trend of increasing base settlement with increasing embankment height is logical due to the higher vertical stresses for higher embankment heights. The exceptions to this trend are the base settlements before trafficking for CSE #4 which may be due to the time-dependent global arching discussed in Section 6.6 that may have been present.
- Since $S_{soil,d}$, DS_d , $S_{soil,i}$ and DS_i decrease with increasing embankment height, and $S_{base,d}$ and $S_{base,i}$ increase with increasing embankment height, both $DSBR_d$ and $DSBR_i$ decrease with increasing embankment height. The magnitudes of $DSBR_i$ are smaller than the magnitudes of $DSBR_d$ due to the better support condition.

Table 6.14: Summary of average CSE settlements before trafficking (BT).

CSE #	H (ft)	S_{col} (in.)	$S_{soil,d}$ (in.)	DS_d (in.)	$S_{soil,i}$ (in.)	DS_i (in.)	$S_{base,d}$ (in.)	$DSBR_d$	$S_{base,i}$ (in.)	$DSBR_i$
5	4.0	0.0	4.6	4.6	0.6	0.6	9.0	0.51	8.5	0.07
2	5.1	0.6	2.5	1.9	0.9	0.3	9.1	0.21	8.1	0.04
3	6.2	0.1	1.0	0.9	0.4	0.3	10.3	0.09	9.7	0.03
4	7.5	0.2	0.1	0.0	0.0	0.0	8.5	0.00	8.2	0.00

Table 6.15: Summary of average CSE settlements after trafficking (AT).

CSE #	H (ft)	S_{col} (in.)	$S_{soil,d}$ (in.)	DS_d (in.)	$S_{soil,i}$ (in.)	DS_i (in.)	$S_{base,d}$ (in.)	$DSBR_d$	$S_{base,i}$ (in.)	$DSBR_i$
5	4.0	0.6	6.5	5.9	3.2	2.6	9.4	0.63	8.8	0.30
2	5.1	0.6	4.4	3.8	1.6	1.0	9.5	0.40	8.9	0.11
3	6.2	0.0	2.9	2.9	1.2	1.2	10.8	0.27	10.2	0.12
4	7.5	1.1	1.0	0.0	1.2	0.0	10.7	0.00	10.6	0.00

Authors such as McGuire (2011) have shown that the maximum differential settlement is a relatively linear function of the embankment height for a given column diameter and spacing. Figure 6.56 shows a plot of maximum differential settlement (DS_d) versus embankment height for CSEs #2 to #5 for both the before- and after-trafficking cases. Both trends are approximately linear and a regression of the before-trafficking data reveals an R^2 of 0.96. A linear regression of the after-trafficking data results in a critical height that is above 7.5 ft. However, CSE #4 was constructed at 7.5 ft and is believed to be at or above the critical height. Consequently, the trendline shown for the after-trafficking data is fixed at an intercept of $H = 7.5$ ft and the same slope is used that was determined by the regression of the before-trafficking data. Note that the slope from the before-trafficking data shows good agreement with the after-trafficking data.

Figure 6.56 shows a before-trafficking critical height, $H_{crit,BT}$, of 6.5 ft and an after-trafficking critical height, $H_{crit,AT}$, of 7.5 ft for a square array of 2 ft diameter columns with 6 ft center-to-center spacing. The slope of the linear trendline is approximately 1.78:1 inches per foot.

The trendline of the differential base settlement ratio ($DSBR_d$) with normalized embankment height (H/d_c) is shown in Figure 6.57. Note that the trend of normalized differential settlement versus normalized embankment height is also linear. The linear trend of the normalized data enables comparison with bench-scale results from McGuire (2011) and future full-scale test data.

A linear regression of the after-trafficking data in Figure 6.57 results in an R^2 of 0.99. The slope from the after-trafficking regression is used to develop the equation for the before-trafficking data with the intercept from the critical height determined from Figure 6.56.

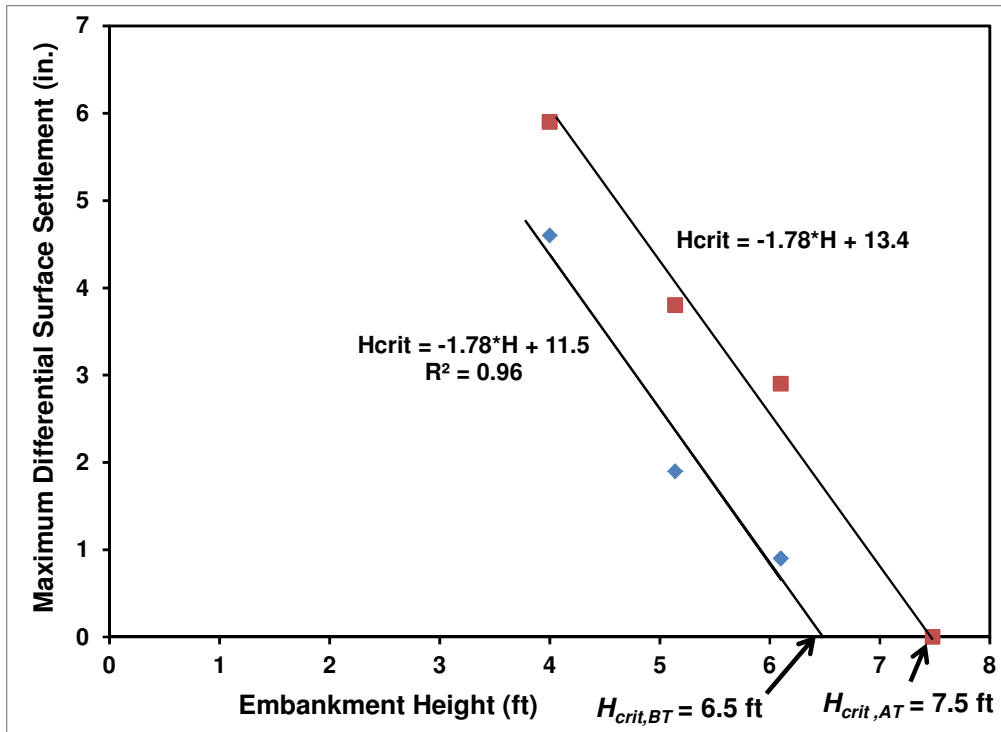


Figure 6.56: Maximum differential settlement vs embankment height (CSEs #2 to #5).

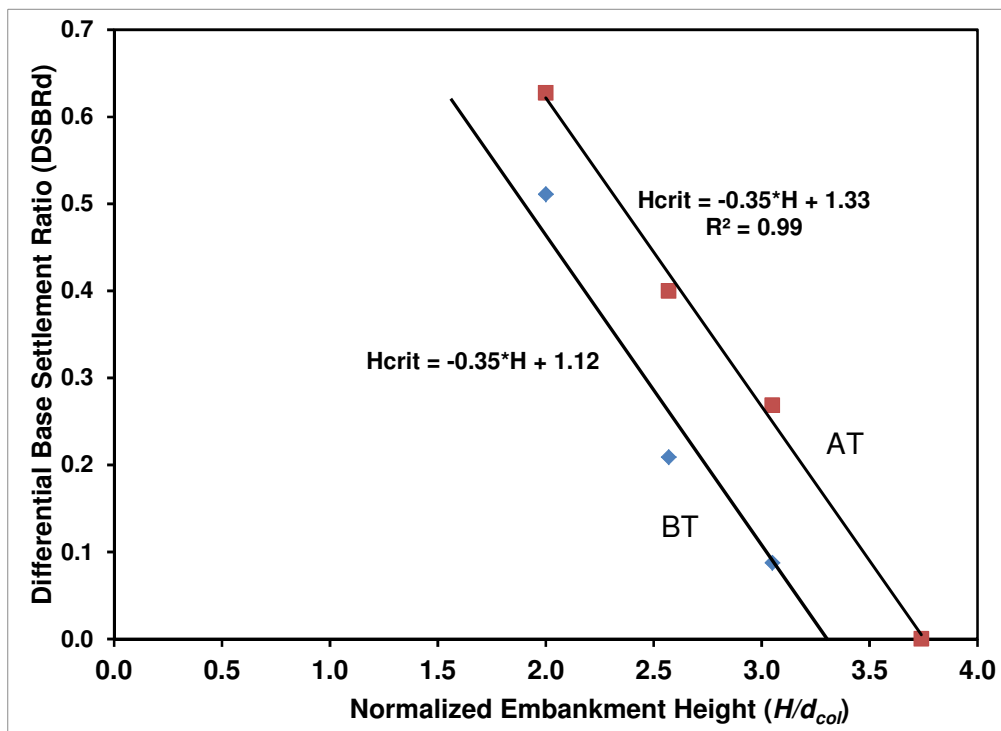


Figure 6.57: $DSBR_d$ vs normalized embankment height (CSEs #2 to #5).

The key results and conclusions from the CSE tests are listed below.

- Prior to dissolving the geofoam, the EPC stresses are generally below the calculated stresses and the load in the center column is above the calculated load based on the cross-sectional area of the column (see EPC plots from CSEs #2 to #5 in Figure 6.14, Figure 6.26, Figure 6.35, and Figure 6.46; see load cell plots in Figure 6.15, Figure 6.27, Figure 6.36, and Figure 6.47). This indicates that there is arching occurring within the fill prior to dissolving the geofoam due to the difference in compressibility of the columns and geofoam.
- In many cases, the measured EPC stress decreased slightly and the load in the center column increased slightly with time after a lift of gravel was placed (see EPC plots from CSEs #2 to #5 in Figure 6.14, Figure 6.26, Figure 6.35, and Figure 6.46). This is consistent with slight compression of the geofoam with time and load redistribution to the columns.
- The CSE tests illustrate the importance of the soft soil support. Minimal surface settlements, base settlements, and geogrid strains were measured before dissolving the geofoam. Dissolving the geofoam to remove embankment support induced significant surface settlements, base settlements, and geogrid strains for some embankment heights (see Table 6.13 and Table 6.14). The modulus of the geofoam used in the CSE tests is comparable to the modulus of normally-consolidated clay at shallow depths. For example, a typical geofoam modulus of 62,000 psf at 1% strain from the CSE tests is comparable to the modulus of normally consolidated clay at depths of 8 to 12 ft assuming that $E = 500 * s_u$, and s_u increases at 10 to 15 psf per foot of depth. Soft soils extend to much greater depths than the 16 in. of geofoam and therefore significantly more settlements can occur. In an actual CSE, the depth of influence of the embankment stress is limited by the arching in the embankment fill, the support of the geosynthetic reinforcement, and also the transfer of vertical stress from the soft soil to the columns via shear stresses at the interface between the columns and soft soil.
- After dissolving the geofoam, loads in the center column are roughly equal to the calculated loads which indicate complete dissolution of the geofoam (see Figure 6.15, Figure 6.27, Figure 6.36, and Figure 6.47). The exception to this trend is CSE #4 which reached approximately 90% of the calculated load.
- The load cells generally have similar readings which indicate the load on the center column is relatively uniform (i.e. not eccentric—see Figure 6.15, Figure 6.27, Figure 6.36, and Figure 6.47).

- Foil strain gages provided some useful information, but they experienced significant problems such as electrical malfunctions, drift, and debonding at low strains (see Figure 6.18, Figure 6.39, Figure 6.40, and APPENDIX A).
- Except for CSE #2, the lead-wire extensometers performed well and the measured strains between columns are consistent with the settlement between columns from the settlement profiler. This is discussed in further detail in Section 7.2.
- Based on observations made during the CSE testing, the gravel on the surface of embankments is relatively loose after removing the geofoam support for embankments lower than the critical height. This is consistent with the BS8006 (1995) recommendation to use the large-strain friction angle for design and analysis of CSEs.
- The before-trafficking settlements were measured 7 to 10 days after dissolving the geofoam. The before-trafficking critical height, $H_{crit,BT}$, for a square array of 2 ft diameter columns with 6 ft center-to-center spacing, WVDOT Class 1 gravel fill, and 3 layers of BX1500 placed low within the embankment, is estimated to be 6.5 ft.
- At 7 to 10 days, the embankment was trafficked with a skid-steer loader weighing approximately 4,000 lbs and with 35 psi tire pressure. The after-trafficking critical height, $H_{crit,AT}$, for this loading is estimated to be 7.5 ft for this column arrangement, fill type, and geosynthetic details.
- Increased time and heavier traffic loads might increase the after-trafficking critical height.
- The use of 5 layers of BX1500 spaced 6 in. apart vertically did not provide a response significantly different from the response for embankments with 3 layers of BX1500 located low within the embankment. This would suggest that the confinement effect of the geogrid is minimal for this application when the subgrade support is reduced to zero, and that the primary benefit of geosynthetic reinforcement in a CSE is through the tension developed in the reinforcement due to the vertical loads. The results of this study suggest that the reinforcement should be located relatively low within the embankment for maximum effectiveness.
- Since the confining effect is minimal based on the results of this study, the critical height is expected to be approximately the same when other types of geosynthetics are used (geotextile, uniaxial geogrid, etc.) but where the total stiffness of the geosynthetic is approximately the same. Stiffer geosynthetics may limit base settlements and may therefore reduce the critical height. The potential confining effect of the geogrid and the variability of critical height with type of geosynthetic require further study beyond the CSE tests described here.

CHAPTER 7 ANALYSIS OF CSE TEST RESULTS

7.1 COMPARISON OF STRESS REDUCTION RATIOS BEFORE DISSOLVING GEOFOAM

Authors such as Stewart and Filz (2005) emphasize the importance of soft soil support in the performance of CSEs. Prior to being dissolved, the geofoam in the CSE tests provides support to the embankment, and analysis procedures that have a mechanism for including soft soil support can be compared to the stress-reduction ratios (SRRs) from the EPCs and load cells in Table 6.12.

Based on the stress-strain curves for the geofoam tested in the lab (see Table 5.4 and Figure 5.3), a modulus can be calculated. This modulus can be used as an input variable to CSE design methods where soft soil support is considered, and the predicted SRRs from the design methods can be compared to measured SRRs from the field tests.

From Table 2.3, the CSE design and analysis methods that incorporate soft soil support are the Adapted Terzaghi Method, Cao et al. Method, Chen et al. Method, Filz and Smith Method, and the Kempfert Method. The method used in the Adapted Terzaghi Method is a total stress method presented by Russell et al. (2003). Since it is a total stress method and the consolidation of clays is inherently an effective stress problem, this method is not considered further. The Cao et al. Method has limitations discussed by Filz and Smith (2007) and is not considered further. The Chen et al. Method shows promise according to results presented by Chen et al. (2010), however, it requires solution of 17 nonlinear equations, and the method is impractical to implement without a pre-developed software tool. In the Kempfert et al. (2004a) method for incorporating the soft soil support, the modulus of subgrade reaction of the subsoil does not affect the vertical stress on the geosynthetic reinforcement or subgrade which ignores the fact that a stiffer subgrade will carry a higher percentage of the vertical stress. These considerations leave the Filz and Smith (2006) method using the GeogridBridge workbook which is employed in the following comparisons.

From Table 5.4, the average geofoam compressive stresses at 1% and 5% strain for the geofoam used in CSE tests #2 - #5 are 4.3 psi and 14.3 psi respectively. These values result in moduli at 1% and 5% strain of 61,900 psf and 41,200 psf respectively. For analysis with GeogridBridge, the modulus at 1% strain is used since it corresponds to the approximate compressive strain in the geofoam during the field tests. For example, an SRR of 0.75 for an embankment height of 6 ft with unit weight of 138 pcf results in a

stress of 4.3 psi which is equal to the average geofoam strength at 1% strain. Table 7.1 shows the parameters used in the GeogridBridge analysis.

Table 7.1: properties used in GeogridBridge soft soil support analysis.

Parameter	Value
Embankment height (ft)	4.0, 5.1, 6.1, and 7.5
Embankment unit weight (pcf)	138
Embankment friction angle (deg)	45
Foundation layer thickness (ft)	1.33
Foundation total unit weight (pcf)	1.0
Foundation Young's modulus (psf)	61,900
Foundation Poisson's ratio	0.05
Foundation lateral earth pressure coefficient	0.5
Interface friction between foundation soil and column (deg)	0
Combined geogrid stiffness (lb/ft)	72,000
Column center-to-center spacing (ft)	6
Column diameter (ft)	2

Figure 7.1 shows a comparison of the measured *SRRs* from CSEs #2 to #5 with the *SRRs* calculated from the GeogridBridge workbook. The *SRRs* calculated from GeogridBridge compare quite favorably to the measured *SRRs*. Filz and Smith (2006) also show that the *SRRs* from the GeogridBridge spreadsheet compare reasonably well with *SRRs* from axisymmetric and 3D FLAC analysis.

The *SRRs* at the upper right-hand corner of Figure 7.1 are from CSE #5, the lowest-height embankment with $H = 4.0$ ft. From Figure 6.46, the EPC readings were decreasing at the time the geofoam was dissolved, so the instrumentation had not reached equilibrium when the geofoam dissolver was pumped in to dissolve the geofoam. Waiting longer before pumping in the geofoam dissolver would have the effect of reducing the EPC readings and they may show better agreement with GeogridBridge for this test.

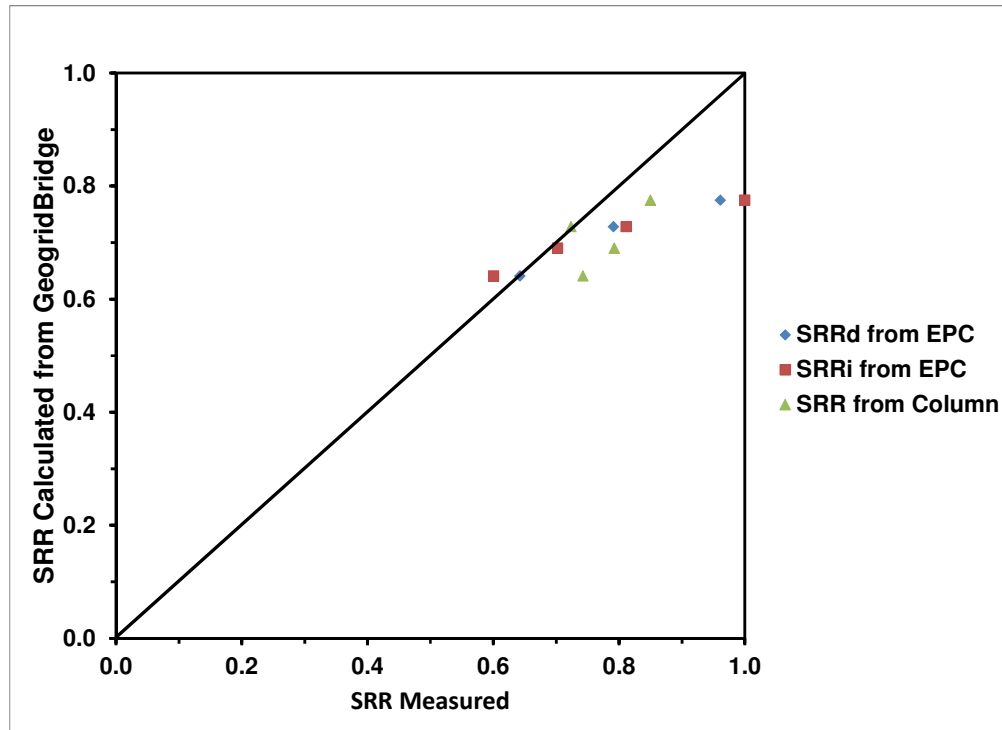


Figure 7.1: SRRs measured in CSE tests versus SRRs calculated with GeogridBridge.

7.2 COMPARISON OF DATA TO METHODS FOR DETERMINING THE TENSION/STRAIN IN THE GEOSYNTHETIC

As discussed in Chapter 2, there are three primary methods for determining the tension and strain in the geosynthetic reinforcement for a given vertical load: the Parabolic Method, the Tensioned Membrane Method, and the Kempfert et al. (2004) or EGGO 6.9 (2004) Method. It is important to note that some design methods assume a strain of 5% or 6% when using these methods, but it is possible to calculate the tension without assuming a strain, since strain and tension are related by $\varepsilon = T/J$, where J is the geosynthetic stiffness.

The range of measured base deflections between columns ($S_{base,i}$) in CSEs #2 to #5 varied from 8.1 to 9.7 in. before trafficking according to Table 6.14 and from 8.8 to 10.6 in. after trafficking according to Table 6.15. The range of measured strains for geogrid between columns from CSEs #2 to #5 varied from 3.6 to 10.1 from 7 to 21 days, as reported in Table 6.13. Table 7.2 shows the calculated strains from the Kempfert et al. (2004) Method, an exact solution to the Parabolic Method (Giroud 1995), the Parabolic Method approximation (Giroud 1995), and the Tensioned Membrane Method (Giroud et

al. 1990) for the range of deflections and strains measured in CSEs #2 to #5. Note that the diameter, d_c , of 2 ft is converted to an equivalent square width, $a = 1.77$, according to $a = 0.886*d_c$ for this analysis. Note also that the design chart for the Kempfert et al. (2004) Method is valid for strains up to 6%.

Table 7.2: Calculated strains (%) for a given deflection.

Deflection (in.)	Calculated Strain (%)			
	Kempfert et al. (2004)	Parabolic Method, Exact Solution	Parabolic Method, Small-strain Approximate Solution	Tensioned Membrane Method
6	3.2	3.6	3.7	3.7
7	4.3	4.9	5.1	5.0
8	5.7	6.3	6.6	6.5
9	n/a	7.8	8.4	8.2
10	n/a	9.6	10.4	10.1
11	n/a	11.4	12.5	12.1

Table 7.2 shows that all four methods calculate similar strains for the same deflections, with the Kempfert et al. (2004) Method producing slightly lower strains for a given deflection.

The calculated strains from each of the methods are also very close to the measured 7 to 21 day strains which fall in the range of 3.6% to 10.1% for the measured base deflections of 8.1 to 10.6 in. In general, the calculated strains tend to be slightly higher than the measured strains. Each of the methods in Table 7.2 assume that the strain in the geogrid is the same at all points in the clear span between columns. The measured strains reflect an average strain measurement between points where the lead-wire extensometers are attached to the geogrid, which were generally 4 to 6 in. apart. The strain at other locations in the geogrid, closer to the columns, may have been higher, which would result in a higher average strain across the entire clear span. The fact that the calculated strains based on the measured deflections are in good agreement, but slightly higher than, the measured strains, supports the conclusion that the measured strains and deflections from the CSE tests are consistent with one another.

In order to compare the analysis methods with the measurements in the CSE tests, it is important to determine the material properties to use in the analysis. In this case, the primary property required is the geogrid stiffness. Table 7.3 shows some of the geogrid

testing results for Tensar® BX1500 (see APPENDIX B for more detail) determined from single-rib tests with a 10% per minute strain rate, along with the values published by Tensar®. These values of strength and strain were used to determine values of the geogrid stiffness, J , for use in comparing the analytical methods with the experimental results.

Choosing the proper geogrid stiffness for analysis is extremely important. Creep testing of the Tensar® BX1500 geogrid was not completed, but time certainly is a factor in the selection of a geogrid stiffness since the CSEs remained in place for up to three weeks. The geogrid will have a lower stiffness for a longer time increment, at the same load, or for a slower strain rate. Consequently, an upper value of stiffness (35,000 plf per layer = 105,000 plf total) was selected for comparison with the strains up to 24 hours. This value seems appropriate given the strains of up to 6.1% within the first 24 hours after dissolving the geofoam and that the strain rate in the field is slower than the strain rate of 10% per minute in the lab. A lower value of stiffness was selected for the 7 to 14 day strains (16,000 per layer = 48,000 plf total) which seems more appropriate given the larger strains of up to 9.6% and the slower strain rate in the field. Note that the geogrid strains in the field were measured in the geogrid XMD.

Table 7.3: Values of geogrid stiffness used to determine approximate value for analysis.

Property	Average Measured Value 10% per min strain rate		Tensar® Published MARV	
	MD	XMD	MD	XMD
Strength at 2% strain (plf)	668	952	580	690
J , 2% (plf)	66,800	95,200	58,000	69,000
Strength at 5% strain (plf)	1,242	1,875	1,200	1,370
J , 5% (plf)	24,840	37,500	24,000	27,400
Ultimate strength (plf) / strain %	1,966 / 14.5	2,844 / 12.7	1,850 / n/a	2,050 / n/a
J , ultimate (plf)	13,558	22,393	~12,759	~16,141
Rapid-loading XMD stiffness used for comparison with strain measurements \leq 24 hrs after dissolving geofoam, J , (plf) 35,000 per layer, 105,000 plf total				
Longer-term, high-strain XMD stiffness used for comparison with strain measurements 7 to 14 days after dissolving geofoam, J , (plf) 16,000 per layer, 48,000 plf total				

Figure 7.2 and Figure 7.3 show the calculated strains at 4 – 24 hrs and 7 – 14 days respectively after dissolving the geofoam, as a function of the vertical stress on the geosynthetic reinforcement. Figure 7.4 shows the calculated vertical base deflections ($S_{base,i}$) at 7 – 14 days after dissolving the geofoam as a function of the vertical stress on

the geosynthetic reinforcement. Note that the base deflections were typically not measured at 24 hours or less after dissolving the geofoam so there is no plot for comparing base deflections at 24 hours or less.

The calculated strains and deflections in Figure 7.2 to Figure 7.4 are shown for the following five methods:

- Parabolic Method (approximate) with assumed strain = 5%
- Tensioned Membrane Method with assumed strain = 5%
- Parabolic Method (approximate) with stress-strain compatibility
- Tensioned Membrane Method with stress-strain compatibility
- Kempfert et al. (2004) Method, which incorporates stress-strain compatibility

Embankment heights in CSEs #2 to #5 ranged from 4.0 to 7.5 ft resulting in vertical overburden stresses from 548 to 1027 psf for a unit weight of 137 pcf if no arching occurs. After dissolving the geofoam, the vertical stress on the geosynthetic reinforcement should decrease significantly due to arching. The vertical stresses shown on the x-axis in Figure 7.2, Figure 7.3, and Figure 7.4 extend to 1,000 psf, but the expected values are less than this due to arching.

Because the measured strains and deflections are consistent with one another as shown in Table 7.2 and the discussion that followed, they can be effectively used to evaluate the previous five methods for calculating the tension and strain in the geogrid. Recall that the range of measured strains between columns from CSEs #2 to #5 reported earlier in Table 6.13 were 2.0% to 6.1% at 4 to 24 hours after dissolving the geofoam and 3.6% to 9.6% from 7 to 14 days after dissolving the geofoam. The vertical deflections ($S_{base,i}$ for both AT and BT cases) at 7 – 14 days after dissolving the geofoam ranged from 8.1 in. to 10.6 in. according to Table 6.14 and Table 6.15. These ranges are shown along with the five methods in Figure 7.2, Figure 7.3, and Figure 7.4. Note that the strains on the base layer of geogrid were measured in the geogrid transverse machine direction (XMD), not the machine direction (MD).

The following observations are based on the information in Figure 7.2 and Figure 7.4:

- The measured strains and deflections in Figure 7.2, Figure 7.3, and Figure 7.4 can be significantly higher than those calculated by assuming a strain of 5% for this case with zero subgrade support. Therefore, imposing stress-strain compatibility, rather than assuming a design strain of 5% or 6%, is important.

- When vertical stresses between 200 psf and 700 psf are applied using the Parabolic Method, the range of calculated strains match the range of measured strains for both the 4 – 24 hr and 7 – 14 day data.
- When vertical stresses between 400 psf to 800 psf are applied using the Parabolic Method, the range of calculated deflections match the range of measured deflections in Figure 7.4.
- The fact that the range of vertical stresses where the Parabolic Method matches the measured data is approximately the same for both strains (200 to 700 psf) and deflections (400 to 800 psf), reinforces that the strains and deflections are consistent with one another and provides evidence that the vertical stresses on the geosynthetic reinforcement fall within the range of 400 to 700 psf.
- Only the Parabolic Method produces strains and deflections within the full range of the measured strains for reasonable values of vertical stress, for all three cases.
- For assumed strains of 5%, the Parabolic Method and Tensioned Membrane Method produce deflections that are approximately the same, but not exactly the same, due to the assumptions made in each method regarding the deformed shape of the geosynthetic.
- The Kempfert et al. (2004) Method follows approximately the same trend as the Parabolic Method. The chart used by the Kempfert et al. (2004) Method only extends to strains of 6%.
- The Tensioned Membrane Method produces does not produce strains and deflections that cover the full range of measured strains and deflections for reasonable values of the vertical load on the geosynthetic reinforcement. The Tensioned Membrane Method is unconservative for this case since the calculated strains are generally lower than the measured strains.
- The EPC stresses do not produce strains within the range of measured values using any of the three methods that impose stress-strain compatibility. This indicates that one or both of the following may be true: (1) the vertical stress on the geosynthetic is not uniform and the EPCs are located in a region of low vertical stress, or (2) the EPCs are not measuring the actual stress at their location due to disturbance and shearing within the embankment fill at their location which distorts the stress reading.

Table 7.4 summarizes the principal findings of this research regarding methods to determine the tension and strain in the geosynthetic reinforcement. The key conclusion is that the parabolic method with stress-strain compatibility is recommended for analysis and design.

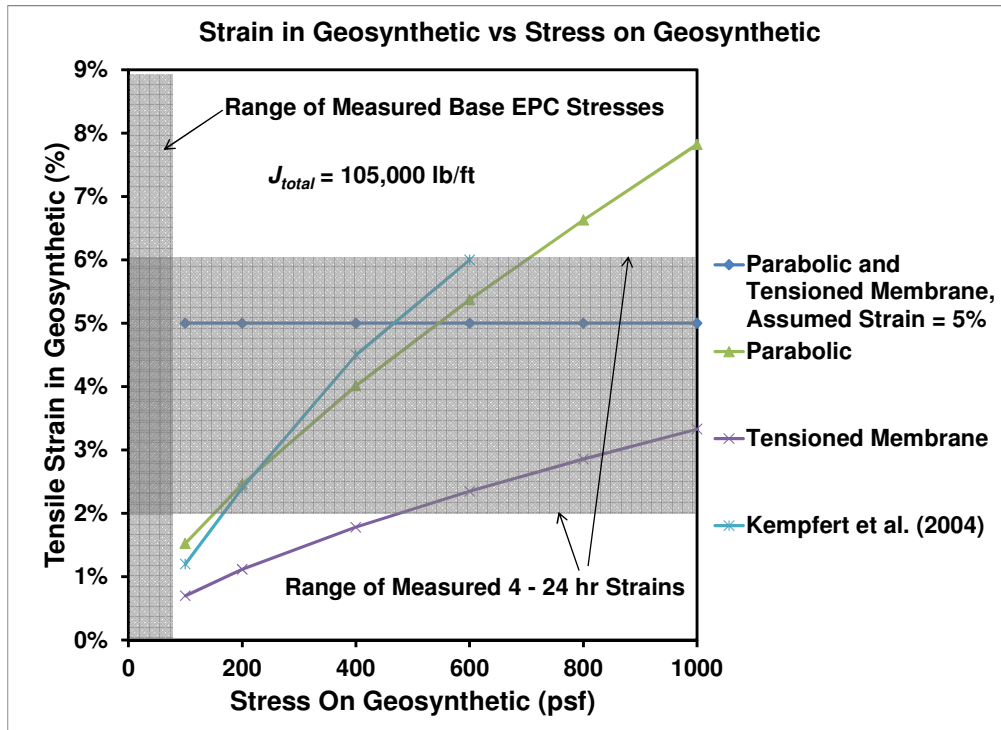


Figure 7.2: Comparison of measured and calculated strains (4 – 24 hr).

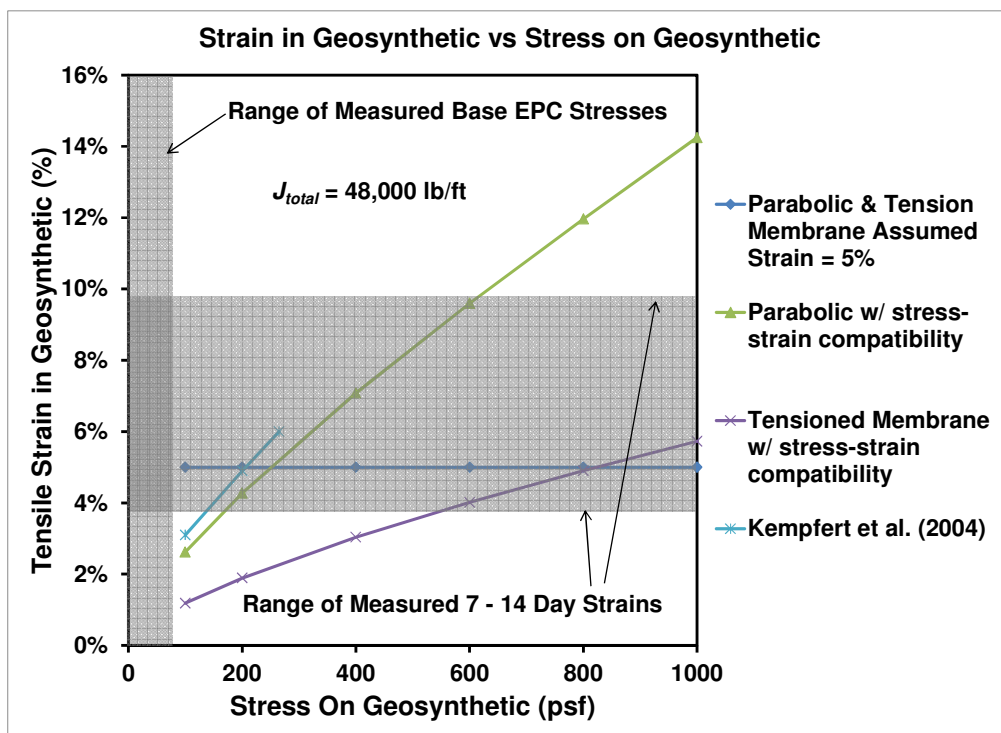


Figure 7.3: Comparison of measured and calculated strains (7 – 14 day).

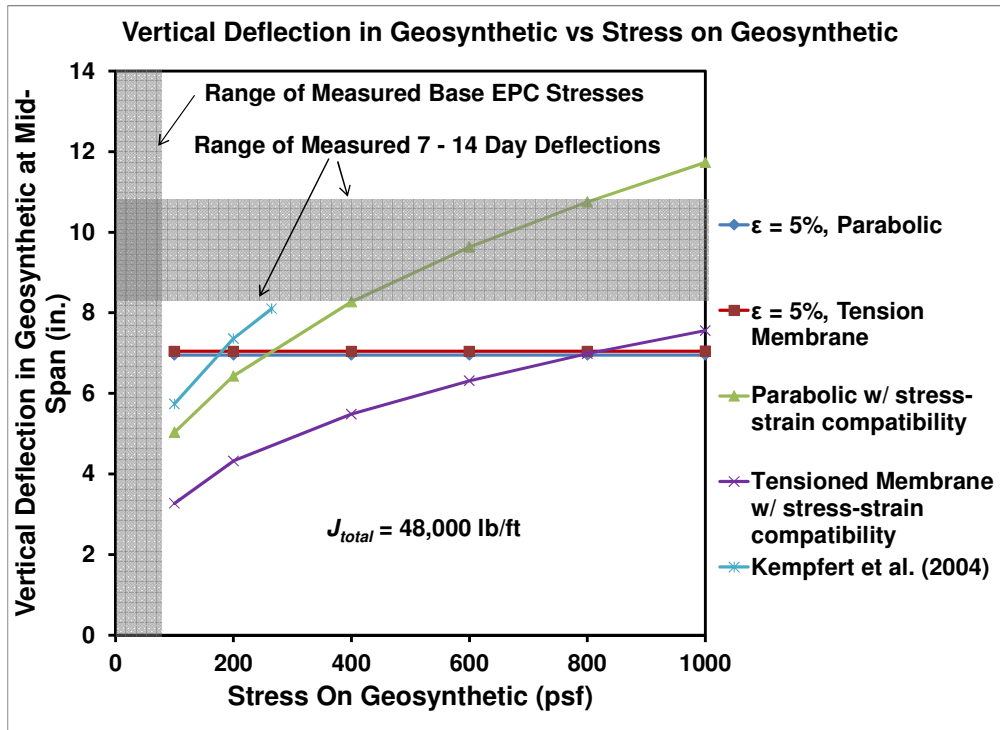


Figure 7.4: Comparison of measured and calculated vertical deflections (7 to 14 day).

Table 7.4: Recommendations and findings for design/analysis procedures to determine the tension in the geosynthetic reinforcement

Deign or Analysis Method	Method Agrees with CSE Tests?	Recommend?	Comments
Kempfert et al. (2004a) / EBGEO 6.9 (2004)	Yes	No	Reasonable method, extrapolated trend indicates agreement with CSE tests, design chart is only valid for strains up to 6%
Parabolic with stress-strain compatibility	Yes	Yes	Reasonable, easy to use method; agrees with field tests and with literature
Tensioned membrane, with stress-strain compatibility	No	No	Does not agree with field tests, unconservative

7.3 COMPARISON OF DATA TO METHODS FOR DETERMINING THE VERTICAL STRESS ON THE GEOSYNTHETIC

In the CSE tests, the earth pressure cells were generally located within the first 6 in. of gravel fill. In CSEs #2 to #4, there was one layer of geogrid below the EPCs and two layers above the EPCs at an elevation of 6 in. For CSE #5, the geogrid layers were spaced 6 in. vertically and the EPCs were located between the bottom two layers within the first 6 in. of fill. The EPC readings are therefore essentially a direct measurement of the vertical stress applied to the base layer of geogrid. However, Figure 7.2, Figure 7.3, and Figure 7.4 show that the EPC stresses do not produce strains within the range of measured strains by any reasonable method for calculating strain in the geosynthetic. The EPC readings from the CSE tests are also significantly lower than the vertical stresses predicted by most of the analysis methods used to predict the vertical stress on the geosynthetic.

There are several potential reasons why the EPC readings are not consistent with the measured strains and deflections, including the following:

- The geogrid-reinforced fill undergoes significant deflection and shear strains as the gravel dilates after the geofoam is dissolved, and significant rearrangement of the gravel particles is expected to occur in response to the change in load. In general, EPCs tend to be sensitive to the surrounding soil and bedding conditions. The rearrangement of soil particles around the EPCs as the geofoam is dissolved, and load transfer that occurred, may have had an adverse effect on the ability of the EPCs to provide accurate readings.
- Most of the design methods assume a uniform distribution of load between columns; however, the distribution of the vertical load is probably not uniform. Even if the EPCs were capable of providing accurate measurements, due to the embankment deformations (base settlements up to 10.8 in.), they may not have provided an accurate representation of the average load in the unsupported area.

Figure 7.5 illustrates the concept from the second bullet point above. The primary arch transfers the load from the embankment fill above it to the columns. It's possible that secondary arches form below the primary arch since the deflection of the geosynthetic is not uniform. The areas of the geosynthetic closer to the column deflect less and offer a better support condition and some secondary arching could occur between these regions. This phenomenon would have the effect of concentrating more of the vertical stresses on the geosynthetic closer to the columns.

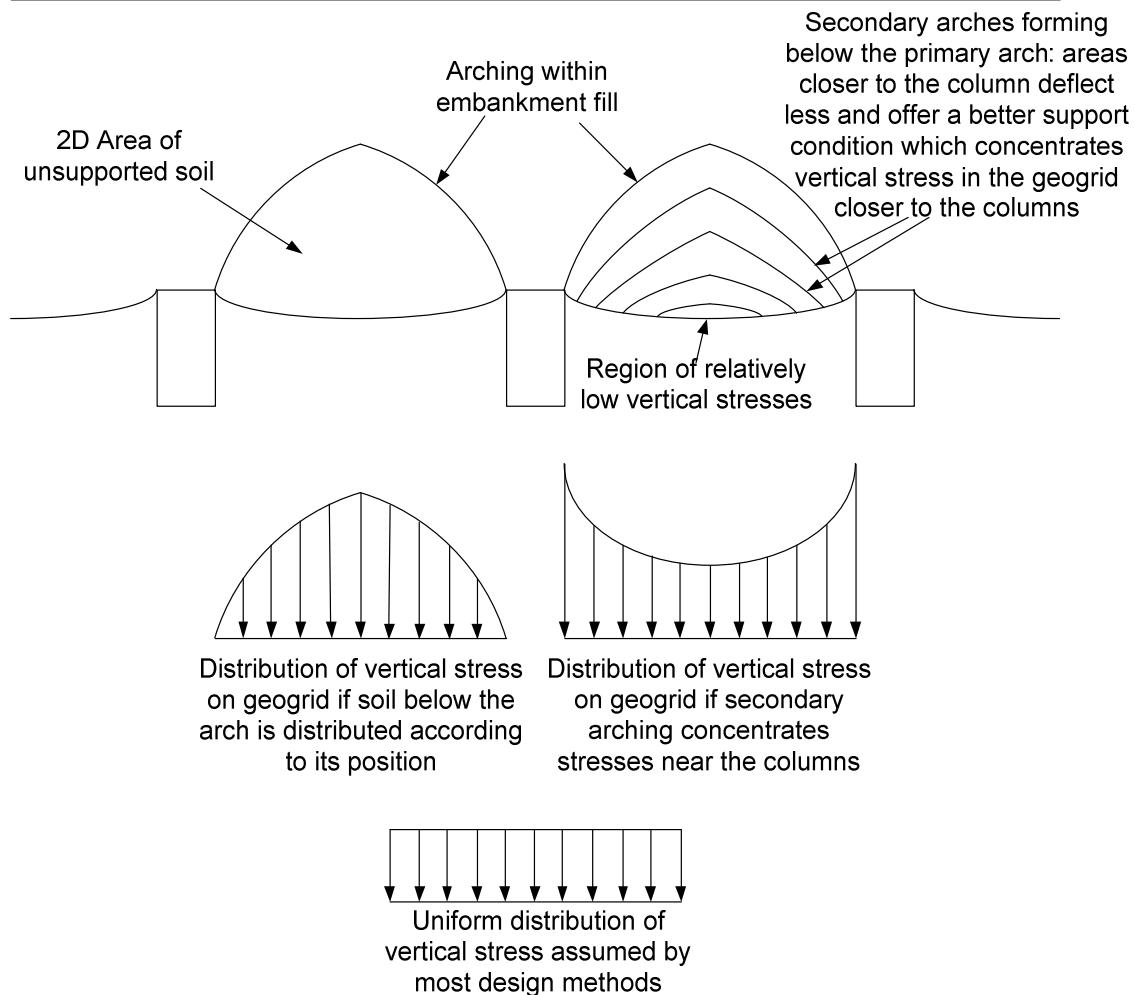


Figure 7.5: Possible distributions of vertical stress on the geosynthetic reinforcement.

Table 7.5 shows the input parameters used to calculate the vertical stress predicted by the design methods. Note that the diameter, d_c , of 2 ft is converted to an equivalent square width, $a = 1.77$, according to $a = 0.886*d_c$. Filz and Smith (2006), BS8006 (1995), and Kempfert et al. (2004) recommend this use of an equivalent square width for design/analysis of round columns.

Figure 7.6 shows the predicted vertical stresses from 10 design methods. The Cao et al. (2006) and Chen et al. (2008) methods are not shown. The EPC readings do not seem consistent with the measured strains and deflections or the predicted stresses from most design methods and are not shown. Consequently, it seems reasonable to use the range of stresses based on the strains and deflections (approximately 400 psf to 700 psf) that correspond to the Parabolic Method from Figure 7.2, Figure 7.3, and Figure 7.4. This range is shown in Figure 7.6.

Table 7.5: Parameters for comparison of EPC readings to design methods.

Parameter	Value
s (ft)	6.0
a (ft)	2.0
γ (pcf)	138
q (psf)	0
ϕ (deg)	45

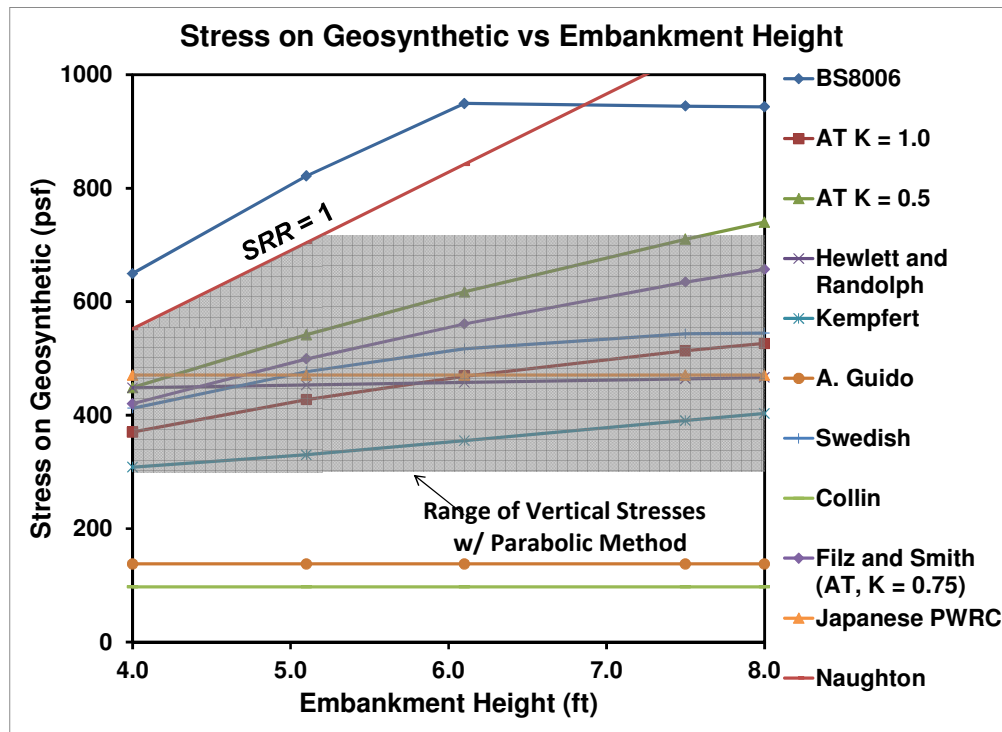


Figure 7.6: Comparison of predicted and measured vertical loads on the geosynthetic reinforcement (CSEs #2 to #5).

The following observations are made based on the information in Figure 7.6:

- The Naughton Method includes a limiting condition that $SRR = 1$ for embankments below the critical height, when the critical height is calculated according to the Naughton Method. The critical height according to the Naughton Method is 10.1 ft for the geometry and fill properties in CSEs #2 to #5 (note that the before- and after-trafficking critical heights of 6.5 ft and 7.5 ft determined from the tests and illustrated in Figure 6.56 are significantly lower than the critical height predicted by the Naughton Method). Therefore, this line represents the

overburden pressure ($SRR = 1$) in Figure 7.6. Any method plotting above this line predicts an SRR greater than unity and therefore an unreasonable value of the stress on the geosynthetic reinforcement.

- The BS8006 predicts an $SRR > 1.0$ and significantly over-predicts the vertical load on the geosynthetic reinforcement from CSEs #2 to #5.
- The Collin and Adapted Guido Methods are unconservative and significantly under-predict the vertical load on the geosynthetic reinforcement from CSEs #2 to #5.
- The Kempfert et al. (2004) Method predicts vertical stresses within the lower end of the range of those based on the Parabolic Method and the measured strains and deflections.
- The Japanese PWRC and Swedish Methods fall within the range of vertical loads from CSEs #2 to #5, they both have a fixed geometry for a given column arrangement if the embankment is above the critical height. Therefore, they may not accurately predict the vertical loads for all combinations of fill type, geosynthetic quantity and stiffness, and embankment heights.
- The Hewlett and Randolph (1988) method falls within the range of vertical stresses based on the strains and deflections using the Parabolic Method.
- The Adapted Terzaghi Method with $K = 0.5$ slightly overpredicts the vertical stresses, indicating that it is overconservative.
- Filz and Smith (Adapted Terzaghi with $K = 0.75$) and Adapted Terzaghi Method with $K = 1.0$ fall within the range of loads from CSEs #2 to #5.

Based on Figure 7.6 and the conclusions drawn from it, Table 7.6 contains the recommendations for analysis methods to calculate the vertical stresses on the geosynthetic reinforcement. Other discussion relating to the recommendations are provided below.

The Hewlett and Randolph Method assumes a domed arch shape which may not accurately model the conical shear planes extending up from the columns. Potts and Zdravkovic (2008, 2010) show that the Hewlett and Randolph Method applies to specific cases and does not accurately model all of the behavior represented in their numerical analyses.

On the other hand, the Adapted Terzaghi Method does not “over-specify” the problem by assuming a specific arch angle, a fixed volume of fill soil contributing to the vertical load, or a domed arch geometry. The Adapted Terzaghi Method calculates the reduced stress on the subsoil based on the interface properties (K , ϕ) between the stationary

(above the columns) and yielding (above the subsoil) masses of soil. Potts and Zdravkovic (2008, 2010) state that the Adapted Terzaghi Method is capable of modeling all of the behavior observed in their numerical analyses.

Based on Figure 7.6, values of K from 0.5 to 1.0 in the Adapted Terzaghi Method produce results that agree with CSEs #2 to #5. Lower values of K are more conservative for determining the load on the geosynthetic reinforcement and higher values are less conservative. Russell and Pierpoint (1997) recommend a value of 0.5, Russell et al. (2003) recommend a value of 1.0, and Filz and Smith (2006, 2007) recommend a value of 0.75 based on a numerical parameter study using methods calibrated against case histories and a bench-scale model presented by Kempfert et al. (2004a).

Potts and Zdravkovic (2010) recommend a value of $K = 1.0$ based on parametric analyses of geosynthetic reinforcement over infinitely long and circular voids using the Imperial College Finite Element Program (ICFEP). They report that a value of 1.0 is still slightly conservative based on the results of their analyses, and that the value of K is independent of properties of the fill and geosynthetic. ICFEP uses constitutive models described in Potts and Zdravkovic (1999), but the authors of this study could not find where Potts and Zdravkovic (1999) or others calibrated the ICFEP program and its constitutive models with field tests for embankments over voids.

In the author's judgment, the preponderance of evidence indicates that a K value of 0.5 (Russell and Pierpoint 1997) is unnecessarily conservative. Of all the methods shown in Figure 7.4, the Adapted Terzaghi Method with $K = 0.75$ is closest to the mid-range of the best estimates of vertical pressure from the CSE tests. Consequently, a K value of 0.75 is recommended for CSE design. Nevertheless, if additional data is collected in the future to support a different K value, such as the value of 1.0 recommended by Russell et al. (1997) and Potts and Zdravkovic (2010), then the K value for CSE design could be modified as appropriate.

Table 7.6: Recommendations and findings for design/analysis procedures to determine the load on the geosynthetic reinforcement.

Deign or Analysis Method	Method Agrees with CSE Tests?	Recommend?	Comments
Adapted Guido	No	No	Predicted stresses on geosynthetic are too low
Adapted Terzaghi	Yes	Yes	Reasonable arching method, agrees with field tests in this study ($K = 0.75$ to 1.0) and numerical modeling/case histories from literature; currently applies only to square column arrangements; Section 8.1.1 of this study presents a formulation for generalized geometry and two layers of fill
BS8006	No	No	Inconsistent, stresses on geosynthetic are too high
Cao et al.	Unknown	No	Difficult to use, other limitations documented in Filz and Smith (2007)
Chen et al.	Unknown	No	Method agrees with instrumented case histories in Chen et al. (2008, 2010), very difficult to use since no publically available software exists to the author's knowledge
Collin	No	No	Predicted stresses on geosynthetic are too low, other aspects of the procedure were incorporated into the recommended design procedure in Section 8.2
Filz & Smith	Yes	Yes	Agrees with field tests in this study, uses Adapted Terzaghi Method with $K = 0.75$; currently only applies to square column arrangements
Hewlett & Randolph	Yes	No	Rational arching method, agrees with field tests although loads are somewhat low, agrees with some numerical modeling/case histories from literature

Japanese PWRC Method	Yes	No	Simplistic, provides one load regardless of embankment height
Kempfert (EBGEO)	Yes	No	Reasonable method, difficult to use since design documents are in German and design charts vs formulas
Naughton	No	No	Disagrees with field tests, trend of increased vertical stress on geosynthetic for stronger soil seems incorrect
Swedish	Yes	No	Original method provides one arch angle for all soils; newer SINTEF procedures state that the arch angle should be calibrated but provides limited guidance on how to do the calibration

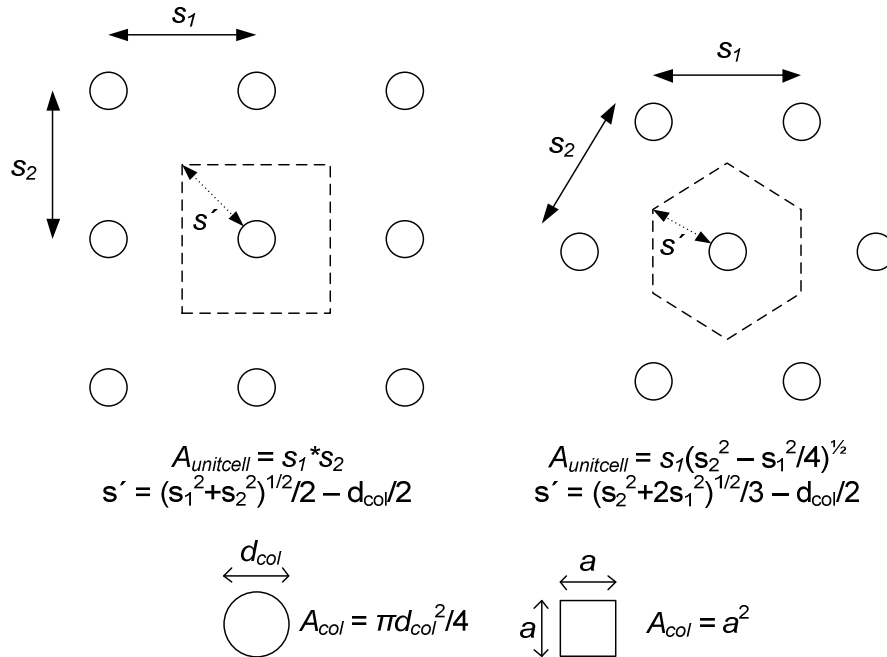
7.4 OBSERVATIONS FOR CRITICAL HEIGHT

McGuire (2011) is a work in-progress which contains an extensive review of the literature pertaining to the critical height for CSEs and bench-scale testing to investigate the influences of column arrangement and fill density on critical height. The full dissertation for McGuire (2011) at Virginia Tech will be available later in 2011 on the Virginia Tech Library's electronic thesis and dissertation website at <http://www.lib.vt.edu/find/byformat/etds.html>.

McGuire (2011) completed a series of bench-scale tests using five combinations of column diameter and spacing. The findings of McGuire (2011) suggest that the critical height, H_{crit} , is equal to:

$$H_{crit} = 1.15s' + 1.438d_{col} \quad (7.1)$$

where d_{col} is the column diameter and s' is defined in Figure 7.7. Using Equation (7.1), a dimensionless plot of H_{crit}/d_{col} vs s'/d_{col} can be created as shown in Figure 7.8. The agreement between the before-trafficking critical height from this study with the McGuire (2011) data is quite good as shown in Figure 7.8. Note that the bench-scale testing by McGuire (2011) is not subject to any trafficking or surcharge loading. The normalized after-trafficking critical height from the current study plots slightly above the McGuire (2011) trendline, which is reasonable given the additional trafficking loads that were applied.



To convert between square and round columns, an equal area conversion is recommended where $a = 0.886 * d_{col}$

Figure 7.7: Unit cell geometries and definition of s' .

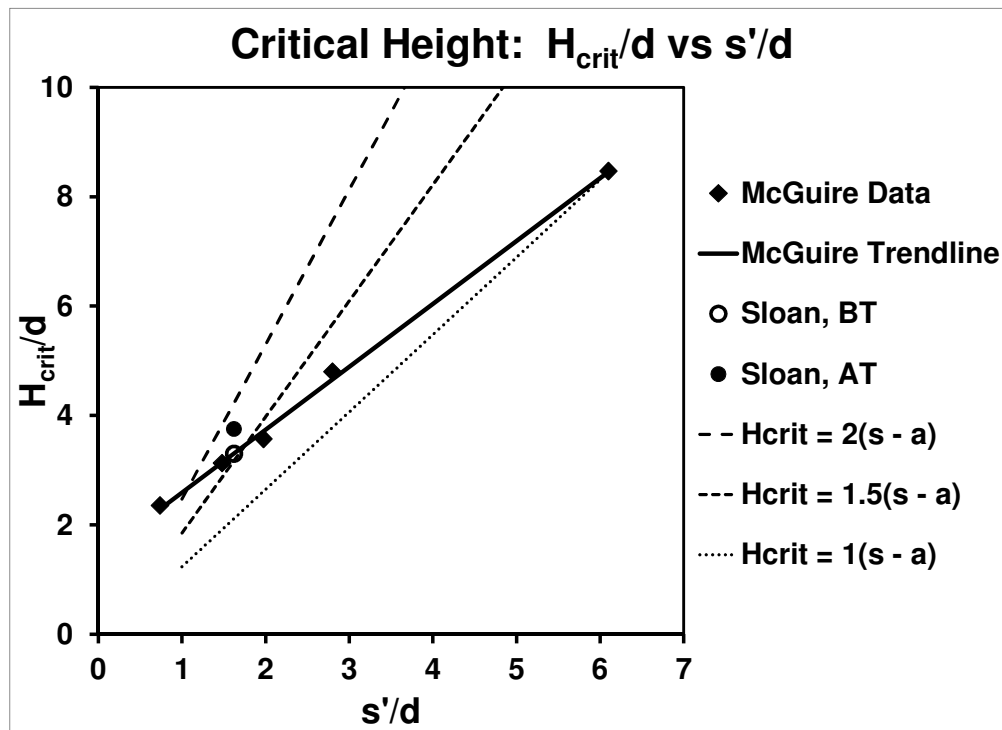


Figure 7.8: Comparison of critical height from McGuire (2011) and the current study.

Figure 7.8 also shows the critical height as a function of the clear span, $s - a$. The before-trafficking critical height from the current study shows good agreement with the $H_{crit} = 1.5(s - a)$ trendline and the after-trafficking critical height falls between the $H_{crit} = 1.5(s - a)$ and $H_{crit} = 2(s - a)$ trendlines.

Typically the embankment height, H , for a CSE will be fixed based on the elevation of the current subgrade and the required elevation of the completed road or highway. Therefore, it is helpful to determine the minimum column spacing required to ensure that there is no differential settlement at the embankment surface. Since $H \leq H_{crit}$, Equation (7.1) can be rearranged for this purpose such that:

$$s' \leq 0.87H_{crit} + 1.25d \quad (7.2)$$

A suitable combination of spacing, s , and column diameter, d , or width, a , for a given column arrangement (e.g. equilateral triangular) can then be found which produce the s' less than or equal to the value in Equation (7.2).

Note that the critical height results from the current study were determined from the worst-case scenario for subgrade support, since all of the support was removed by dissolving the geofoam. The embankments were subjected to traffic loading which resulted in an increase in the critical height.

Most column-supported embankments, even on the poorest soils, will have some subgrade support. Therefore, the relationship determined by McGuire (2011) is recommended. If the designer believes that subgrade support will be entirely lacking, then the spacing can be reduced to provide a margin of safety for the critical height.

7.5 TOTAL SETTLEMENT MAGNITUDE FOR EMBANKMENTS ABOVE THE CRITICAL HEIGHT

One of the important considerations for CSEs is the ability to predict the total settlement for embankments constructed above the critical height. Russell et al. (2003) present a method for calculating the total settlement at the surface of the embankment, d_s , for square columns in a square arrangement which can be expressed as,

$$SBR_{tot} = \frac{d_s}{d_b} = \frac{(s^2 - a^2)}{2s^2} \quad (7.3)$$

where SBR_{tot} is the ratio of surface settlement to base deflections for embankments above the critical height and d_b is the maximum base deflection. The expression assumes that the average base deflection is equal to half of the maximum base deflection ($d_b/2$) and that there is no volume change within the embankment fill. This is generally conservative since a well-compacted granular embankment fill will dilate during shearing, as well as expand due to the reduction in vertical stress in the area underlain by soft soil. An equivalent relationship for a square arrangement of round columns, as used in the CSE tests, is:

$$SBR_{tot} = \frac{\left(s^2 - \frac{\pi d_c^2}{4}\right)}{2s^2} \quad (7.4)$$

As reported in Section 6.6, there was essentially zero differential settlement measured for CSE #4 in both the before and after trafficking cases. Twenty days after dissolving the geofoam and following three trafficking events, the total settlement within the unit cell for CSE #4 averaged 1.2 in. The maximum base settlement was 10.7 in. resulting in an SBR_{tot} of 0.11. The calculated SBR_{tot} from Russell et al. (2003) based on Equation (7.4) is 0.49, which illustrates the large degree of conservatism in the Russell et al. (2003) method. These results are summarized in Table 7.7.

Table 7.7: Summary of measured and predicted values of settlement ratios for embankments above the critical height.

Method	SBR_{tot}
Measured, CSE #4	0.11
Russell et al. (2003) Predicted	0.49

CHAPTER 8

CSE DESIGN IMPROVEMENTS AND RECOMMENDATIONS

8.1 DESIGN IMPROVEMENTS

The following design improvements are presented in the sections that follow:

- Generalization of the Adapted Terzaghi Method of Arching to any combination of column and unit cell geometry, and two layers of fill (Section 8.1.1).
- Development of the Parabolic Method for tension/strain in the geosynthetic for equilateral triangular arrangements (Section 8.1.2).
- Comparison of numerical modeling results from Filz and Plaut (2009) to the Parabolic Method for predicting the strain in the geosynthetic reinforcement (Section 8.1.3).

8.1.1 Generalized Formulation of the Adapted Terzaghi Method of Arching

The Adapted Terzaghi Method captures the relevant parameters of a frictional material: unit weight, lateral earth pressure coefficient, and strength (friction angle). Russell and Pierpoint (1997) note that the Adapted Terzaghi Method of calculating the SRR for column supported embankments performs reasonably well when compared to three-dimensional numerical analyses and instrumented case histories. Filz and Smith (2006) note that the Adapted Terzaghi Method is simple and provides reasonably good agreement with numerical analyses. The Adapted Terzaghi Method also shows good agreement with the results of the field tests in this study as shown in Section 7.3.

Limitations of the Adapted Terzaghi Method of calculating SRR for column-supported embankments, as it is presented in Russell and Pierpoint (1997) and Russell et al. (2003), are that it applies to a square arrangement of square columns and that it applies for only one type of fill material. Some methods of CSE design include the use of a select fill material and multiple layers of geosynthetic reinforcement to provide additional strength and stiffness in the bridging or load transfer platform (LTP) layer. The select fill materials often have significantly higher friction angles than the minimum friction angles required by the procedures. As reported in Section 5.1.1, Duncan et al. (2007) found peak friction angles from 48 to 59 degrees and large-strain (8% to 10%) friction angles of 46 to 54 degrees for a well-graded crushed limestone specified as 21B in VDOT (2007). Multiple layers of geogrid reinforcement may also provide additional confinement and stiffening to the select fill material, as reported by Collin (2004) and Wachman et al.

(2010). In addition to square layouts, column arrangements may also be rectangular, equilateral triangular, or isosceles triangular/offset square.

Given that the Adapted Terzaghi method of arching shows reasonable agreement with numerical studies, instrumented case histories, and the field tests in this study, it will be helpful to generalize the formulation for other column and unit cell geometries and multiple layers of embankment fill. Sloan et al. (2011) presents a generalized formulation of the Adapted Terzaghi Method which is summarized here.

Figure 8.1 shows a cross-section view of a column-supported embankment with two layers of fill soil. In the Adapted Terzaghi Method, the key geometrical parameters are the area of yielding soil, perimeter of the unit cell column, and the height of the embankment. In the generalized formulation, the area of the yielding soil in plan view is expressed as A_{soil} , where,

$$A_{soil} = A_{unitcell} - A_{column} \quad (8.1)$$

where $A_{unitcell}$ is the total area of the unit cell and A_{column} is the area of the column within the unit cell. Figure 8.2 shows some potential unit cell geometries and column shapes along with the corresponding values of $A_{unitcell}$, A_{column} , and column perimeter, p . Examples of possible column layouts include square, rectangular, equilateral triangular, and isosceles triangular. Potential column shapes include square, circular, and diamond (rotated square). Other geometries are also possible using the generalized definition of the parameters above.

The generalized formulation allows for two layers of fill soil with properties of each layer defined as: $H_{1,2}$ = layer thickness, $\gamma_{1,2}$ = layer unit weight, $K_{1,2}$ = layer lateral earth pressure coefficient, and $\phi_{1,2}$ = layer friction angle. The embankment may have a surcharge, q . To simplify the expression for SRR, the following parameter can be defined, as in the report by Filz and Smith (2006):

$$\alpha_{1,2} = \frac{pK_{1,2} \tan \phi_{1,2}}{A_{soil}} \quad (8.2)$$

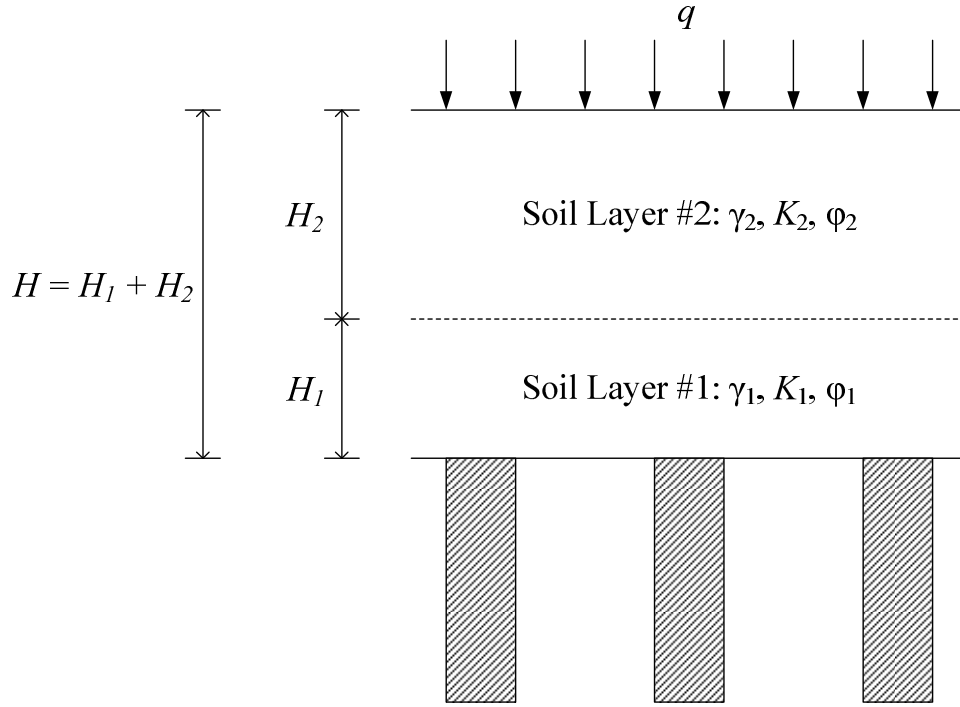


Figure 8.1: Cross-sectional geometry for generalized Adapted Terzaghi Method.

In this formulation of the generalized Adapted Terzaghi Method, for $\alpha_{1,2} \neq 0$, the stress on the subsoil, σ_{soil} is equal to,

$$\sigma_{soil} = \frac{\gamma_1}{\alpha_1} (1 - e^{-\alpha_1 H_1}) + \frac{\gamma_2}{\alpha_2} e^{-\alpha_1 H_1} (1 - e^{-\alpha_2 H_2}) + q e^{-\alpha_1 H_1} e^{-\alpha_2 H_2} \quad (8.3)$$

and the stress reduction ratio, SRR , is equal to,

$$SRR = \frac{\sigma_{soil}}{\gamma_1 H_1 + \gamma_2 H_2 + q} \quad (8.4)$$

Since the embankment settles uniformly above the critical height, it seems appropriate to limit the shearing within the embankment to the soil below the critical height. The critical height, H_{crit} , can be determined from Equation (7.1) or another suitable relationship. For $H_{crit} \geq H_1 + H_2$, or for no limits on the vertical shearing, Equation (8.3) is used. To limit the vertical shearing to the soil below the critical height, for $H_1 \leq H_{crit} \leq H_1 + H_2$,

$$\begin{aligned} \sigma_{soil} = & \frac{\gamma_1}{\alpha_1} (1 - e^{-\alpha_1 H_1}) + \frac{\gamma_2}{\alpha_2} e^{-\alpha_1 H_1} [1 - e^{-\alpha_2 (H_{crit} - H_1)}] \\ & + [q + (H_1 + H_2 - H_{crit}) \gamma_2] e^{-\alpha_1 H_1} e^{-\alpha_2 (H_{crit} - H_1)} \end{aligned} \quad (8.5)$$

To limit the vertical shearing to the soil below the critical height, for $H_1 \geq H_{crit}$,

$$\sigma_{soil} = \frac{\gamma_1}{\alpha_1} (1 - e^{-\alpha_1 H_{crit}}) + [q + (H_1 - H_{crit})\gamma_1 + H_2\gamma_2]e^{-\alpha_1 H_{crit}} \quad (8.6)$$

Equations (8.5) and (8.6) can also be used with Equation (8.4) to find the *SRR*.

This generalized formulation for *SRR* applies to any combination of column and unit cell geometries, and it allows the unit weight, friction angle, height, and lateral earth pressure coefficient to be varied independently for up to two layers of embankment fill. Note that for $H_1 = 0$ or $H_2 = 0$, the equation degenerates to the formulation provided in Russell and Pierpoint (1997). This generalized method has the following advantages:

- It applies to any column arrangement and column cross-section by using the area of the unit cell and perimeter distance of the column.
- It applies to two layers of embankment fill which allows it to:
 - account for higher quality select fill material in a load transfer platform or bridging layer by increasing the friction angle of this layer.
 - account for compaction-induced lateral earth pressures and lateral confining effect of the geogrid in a load transfer platform or bridging layer by increasing the lateral earth pressure coefficient in this layer.
- It limits vertical shearing within the embankment to the embankment fill below the critical height, which is conservative for design, and seems appropriate since the soil above the critical height settles uniformly.

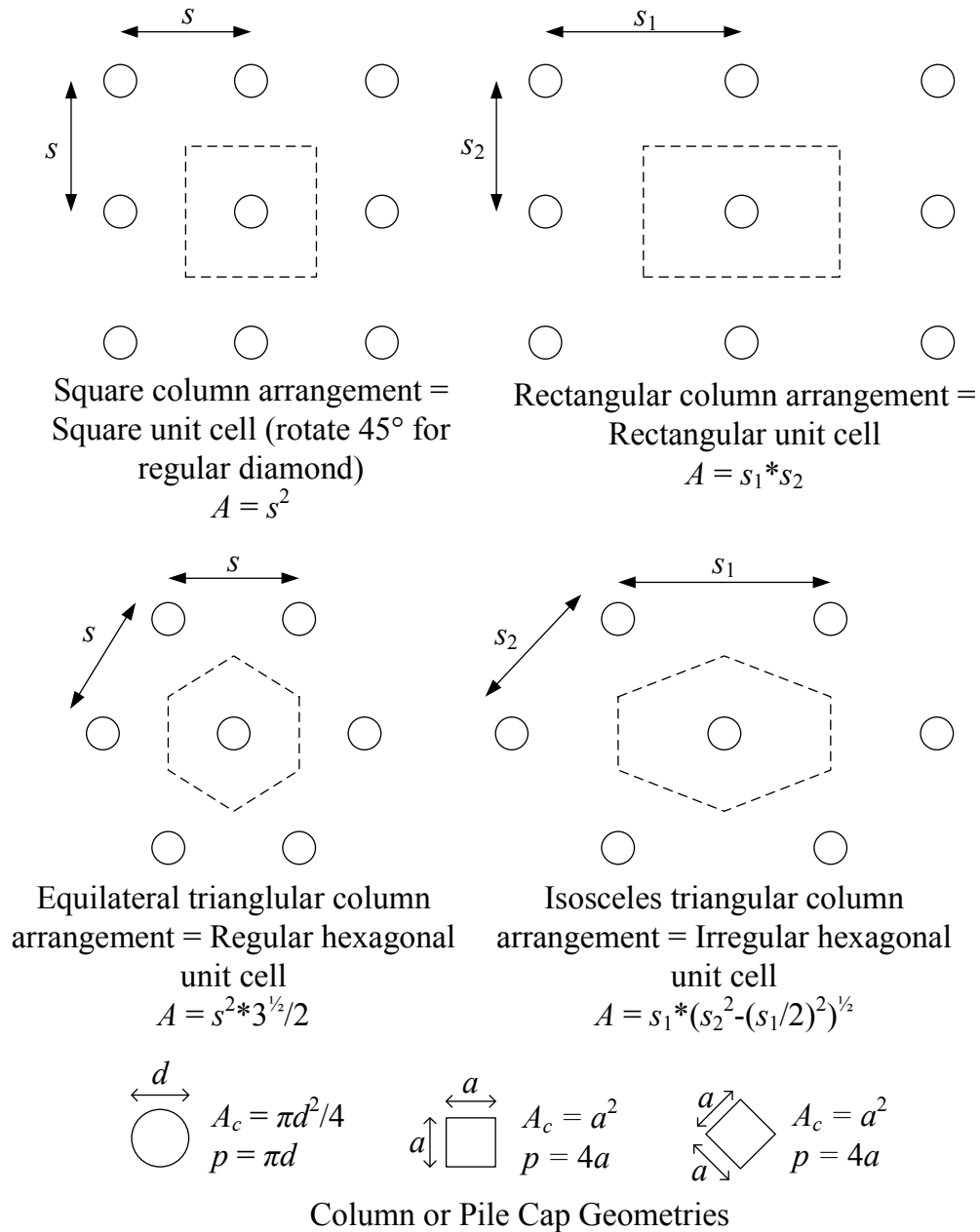


Figure 8.2: Plan view of CSE unit cell and column/pile areas.

8.1.2 Parabolic Method for Other Column Arrangements

The Parabolic Method for square column arrangements shows good agreement with the CSE tests in this study. As it is currently presented in BS8006 (1995), Rogbeck et al. (1998, 2003), and others, the method only applies to square column arrangements of square columns. Given its accuracy with published numerical modeling in the literature and with the instrumented CSEs in this study, it will be helpful to adapt the Parabolic Method for generalized column arrangements and cross-sectional areas.

For development of the generalized Parabolic Method, it is helpful to consider two types of geosynthetic reinforcement. The first case considers a radially-isotropic geosynthetic reinforcement which has relatively uniform strength in all directions. This is illustrated conceptually in Figure 8.3. One example of such a geosynthetic is the Tensar® TriAx® Geogrid. This type of geosynthetic is well-suited to equilateral triangular arrangements since the radially-isotropic geosynthetic has strength in the direction of a 60 degree line of columns whereas a biaxial geosynthetic does not.

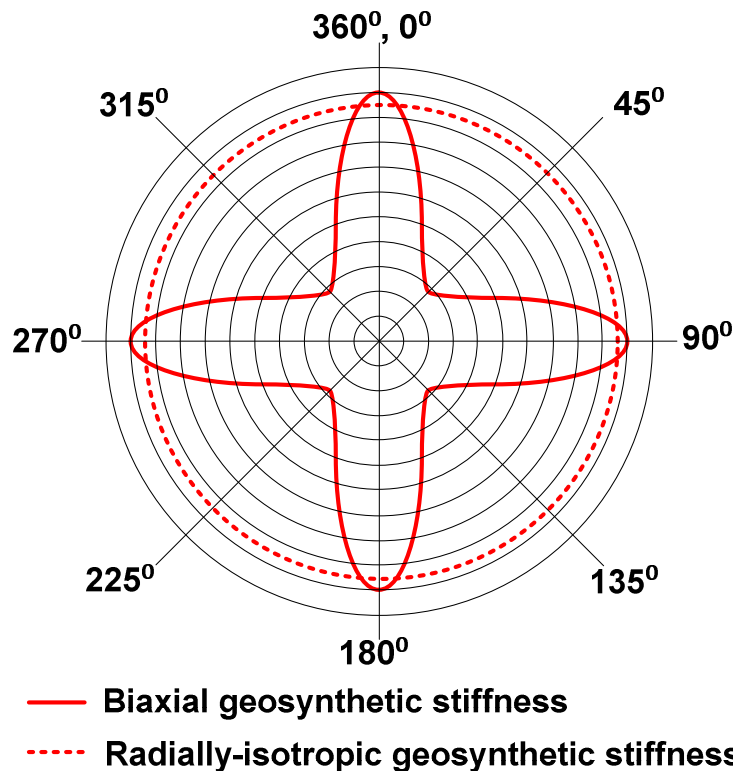


Figure 8.3: Conceptual illustration of biaxial and radially-isotropic geosynthetic stiffness.

The second case considers a biaxial geogrid which has significant strength in two directions which are perpendicular to one another, but limited strength in diagonal

directions (see Figure 8.3). Note that for a biaxial geosynthetic with the roll direction parallel to the unit cell perimeter of a square array of columns, the strong directions of the geosynthetic are always aligned with the columns where the tensile stresses and strains will be highest. This will not be the case for a biaxial geosynthetic and triangular arrangements. Therefore, the method to calculate the strain in the geosynthetic reinforcement should take this into account.

These two cases are presented in the subsections that follow.

8.1.2a Axisymmetric Parabolic Method with Radially-Isotropic Reinforcement

For a square array of square columns, the contributing area to the load on the geosynthetic reinforcement extends from the two column centroids to the adjacent centroids of the square unit cells, subtracting the inclusive area of the columns themselves. This contributing area, A_p , is equal to $(s^2 - a^2)/2$ as shown in Figure 8.4. Similarly, the area contributing to the load on the geosynthetic reinforcement can be determined for an axisymmetric approach as shown in Figure 8.5.

The variables from Figure 8.5 are defined as follows: A_p is the area contributing to the vertical load on the geosynthetic reinforcement, d_c is the column diameter, D is the diameter of the axisymmetric unit cell, p is the vertical stress that acts on the geosynthetic reinforcement over the clear span, T is the tension in the geosynthetic reinforcement, and T_h and T_v are the horizontal and vertical components of the tension in the geosynthetic reinforcement respectively.

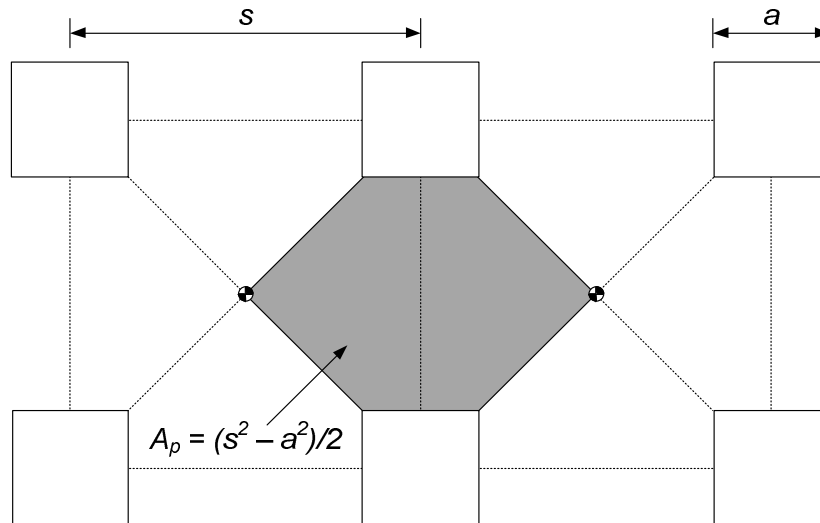


Figure 8.4: Area contributing to the load on the geosynthetic reinforcement in the Parabolic Method for a square arrangement of square columns.

Axisymmetric Parabolic Method

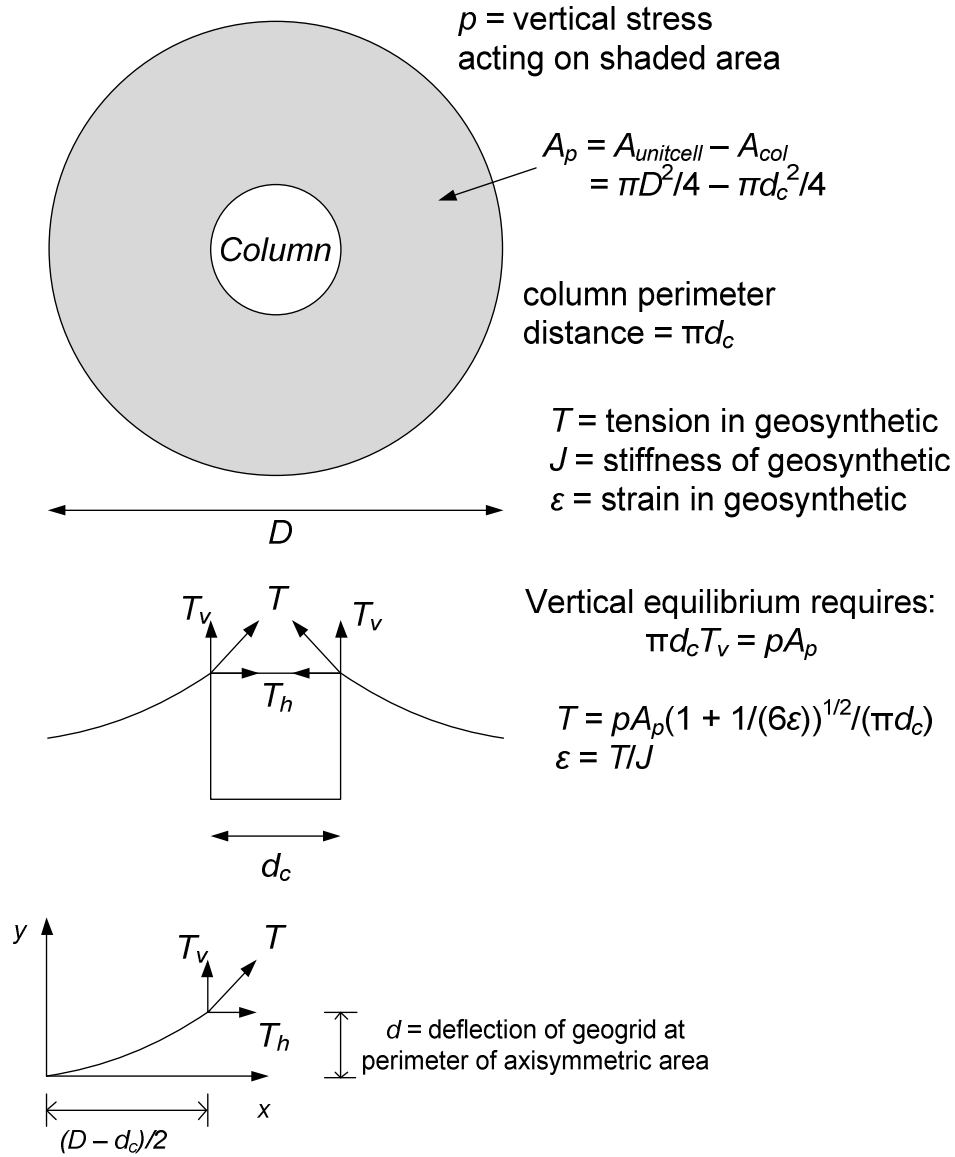


Figure 8.5: Definition sketch for Axisymmetric Parabolic Method with radially-isotropic reinforcement.

Vertical equilibrium requires that,

$$\pi d_c T_v = \rho A_p \quad (8.7)$$

The general form of a parabola is $y = kx^2$ and for $x = (D - d_c)/2$, $d = k(D - d_c)^2/4$, so $k = 4d/(D - d_c)^2$, where d is the deflection at the mid-span between columns. For

the coordinate system in Figure 8.5, m is equal to the derivative of y at $x = (D - d_c)/2$, so,

$$m = 2kx = 2 \left(\frac{4d}{(D - d_c)^2} \right) \left(\frac{D - d_c}{2} \right) = \frac{4d}{(D - d_c)} \quad (8.8)$$

Using similar triangles,

$$\frac{T}{T_v} = \frac{\sqrt{1 + m^2}}{m} \quad (8.9)$$

Substituting Equations (8.7), (8.8), and (8.9) yields,

$$T = \frac{pA_p}{\pi d_c} \sqrt{1 + \frac{(D - d_c)^2}{16d^2}} \quad (8.10)$$

According to Giroud (1995), for a parabolic deformation and small strains, the strain in the reinforcement is approximately equal to

$$\varepsilon \approx \frac{8d^2}{3(D - d_c)^2} \quad (8.11)$$

so $d^2 \approx 3(D - d_c)^2 \varepsilon / 8$ which yields,

$$T = \frac{pA_p}{\pi d_c} \sqrt{1 + \frac{1}{6\varepsilon}} \quad (8.12)$$

based on the small strain assumption of Giroud (1995).

Imposing stress-strain compatibility ($\varepsilon = T/J$) yields the following cubic equation which can be solved for the tension, T ,

$$6T^3 - 6T \left(\frac{pA_p}{\pi d_c} \right)^2 - J \left(\frac{pA_p}{\pi d_c} \right)^2 = 0 \quad (8.13)$$

where $A_p = \pi D^2/4 - \pi d_c^2/4$ for an axisymmetric approach. Such an approach is useful for an equilateral triangular arrangement of columns where the axisymmetric unit cell closely approximates the hexagonal unit cell, and can be applied by finding an equivalent

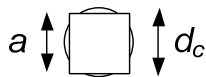
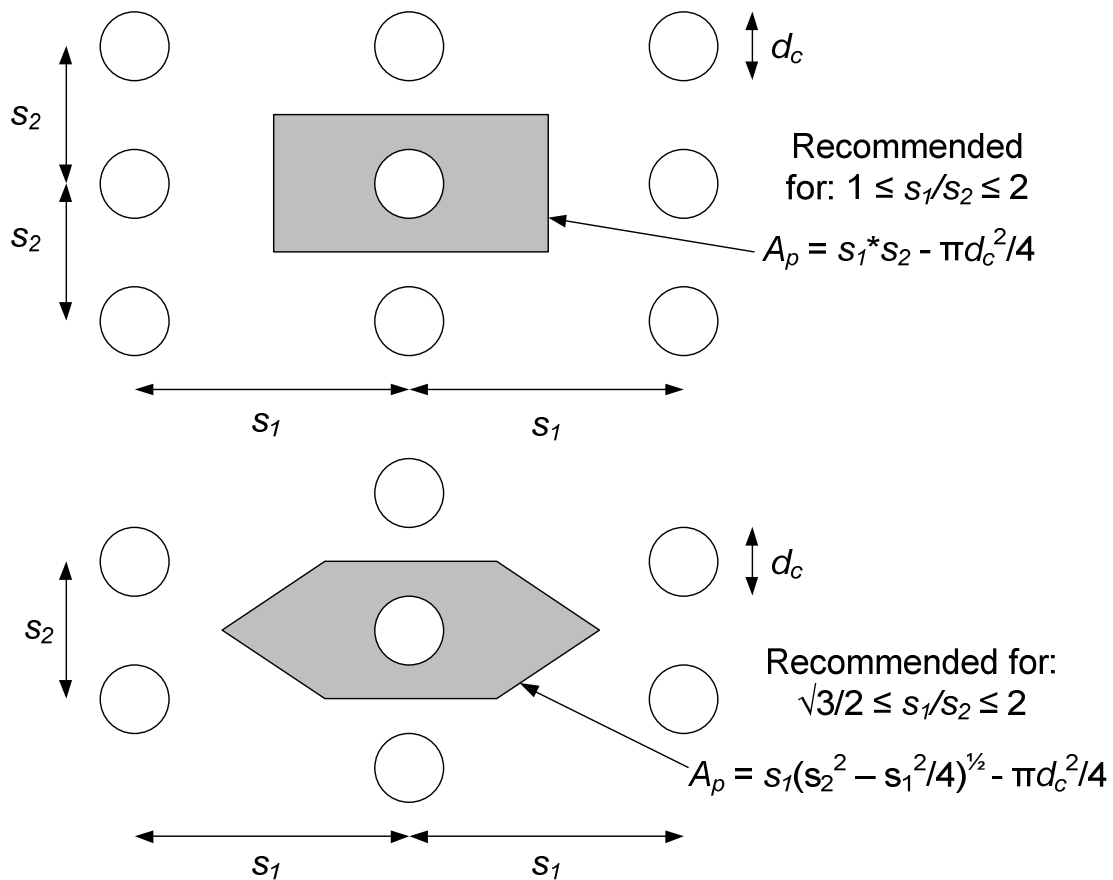
axisymmetric diameter $D = 1.05*s$, where s is the center-to-center column spacing for an equilateral triangular array of columns.

This axisymmetric approach may also be applicable for radially-isotropic geosynthetics and column arrangements other than equilateral triangular as well. The axisymmetric approach seems compatible with the behavior of radially-isotropic geosynthetics and may be applicable to rectangular or isosceles triangular arrangements, provided that the ratio of the longer span to the shorter span does not exceed a minimum value.

Figure 8.6 shows the geometries for square/rectangular and triangular layouts which are recommended for use with the axisymmetric parabolic method. In reality, the strains may be slightly higher in the longer span for rectangles and isosceles triangles. The axisymmetric properties of the radially-isotropic geosynthetic will tend to mute this effect when $s_1/s_2 \leq 2.0$. The alternative is a tessellation approach where areas are assigned to the longer and shorter clear spans for rectangles and isosceles triangles. Comparisons of the axisymmetric approach to a tessellation approach showed that the axisymmetric approach showed reasonable agreement with the tessellation approach for the strain in the longer of the two clear spans for rectangular and isosceles triangular column arrays. The axisymmetric approach of Figure 8.5 and Figure 8.6 is simpler to use and is recommended for square, rectangular, and triangular column arrangements with radially-isotropic geosynthetics for $s_1/s_2 \leq 2.0$.

Square/Rectangular and Triangular Geometries

For radially-isotropic geosynthetic and axisymmetric approach



If columns are square, use equal area approach where $d_c = 1.13 * a$

Tension/Strain Equations:
 $T = p A_p (1 + 1/(6\varepsilon))^{1/2} / (\pi d_c)$
 $\varepsilon = T/J$

For stress-strain compatibility, use:
 $6T^3 - 6T(pA_p/(\pi d_c))^2 - J(pA_p/(\pi d_c))^2 = 0$

Figure 8.6: Square/rectangular and triangular geometries for radially-isotropic geosynthetics and the axisymmetric parabolic method.

8.1.2b Parabolic Method for Triangular Column Arrangements and Bidirectional Geosynthetic

Figure 8.7 shows the definition sketch for the Parabolic Method for triangular column arrangements and bidirectional geogynthetic reinforcement. The variables that apply to

this situation are: A_p is the area contributing to the vertical load on the geosynthetic reinforcement for an unknown column arrangement, p is the vertical load applied over A_p , $c_{1,2}$ are the clear spans between columns, $w_{1,2}$ are the equivalent vertical line loads that act on the geosynthetic reinforcement over the clear spans, and where $T_{1,2}$, $\varepsilon_{1,2}$, $J_{1,2}$, and $d_{1,2}$ are the tensions, strains, stiffnesses, and mid-span deflections in the geosynthetic reinforcement in the 1,2 directions. Vertical equilibrium requires that:

$$w_1 c_1 + w_2 c_2 = p A_p \quad (8.14)$$

Following a similar process as in Section 8.1.2a, it can be shown that:

$$T_{1,2} = w_{1,2} \frac{c_{1,2}}{2a} \sqrt{1 + \frac{1}{6\varepsilon_{1,2}}} \quad (8.15)$$

Imposing stress-strain compatibility requires that:

$$\varepsilon_{1,2} = \frac{T_{1,2}}{J_{1,2}} \quad (8.16)$$

The deflections, $d_{1,2}$, are equal at the midspans, $c_1/2$ and $c_2/2$, and making the small-strain assumption if Giroud (1995) yields:

$$\varepsilon_1 c_1^2 = \varepsilon_2 c_2^2 \quad (8.17)$$

Equations (8.14) to (8.17) represent 6 equations that can be used to solve for the 6 unknowns: $T_{1,2}$, $w_{1,2}$, and $\varepsilon_{1,2}$. Substitution of Equations (8.15) to (8.17) into Equation (8.14) yields:

$$\frac{2aT_1}{\sqrt{1 + \frac{J_1}{6T_1}}} + \frac{2aT_1 \frac{J_2}{J_1} \left(\frac{c_1}{c_2}\right)^2}{\sqrt{1 + \frac{J_1 c_2^2}{6T_1 c_1^2}}} - p A_p = 0 \quad (8.18)$$

which can be solved for T_1 . T_2 can then be found according to:

$$T_2 = T_1 \frac{J_2}{J_1} \left(\frac{c_1}{c_2}\right)^2 \quad (8.19)$$

which results from (8.16) and (8.17). The resulting strains in the T_1 and T_2 directions can be calculated according to Equation (8.16).

Case #2: biaxial geosynthetic with equilateral or isosceles triangular column arrangement

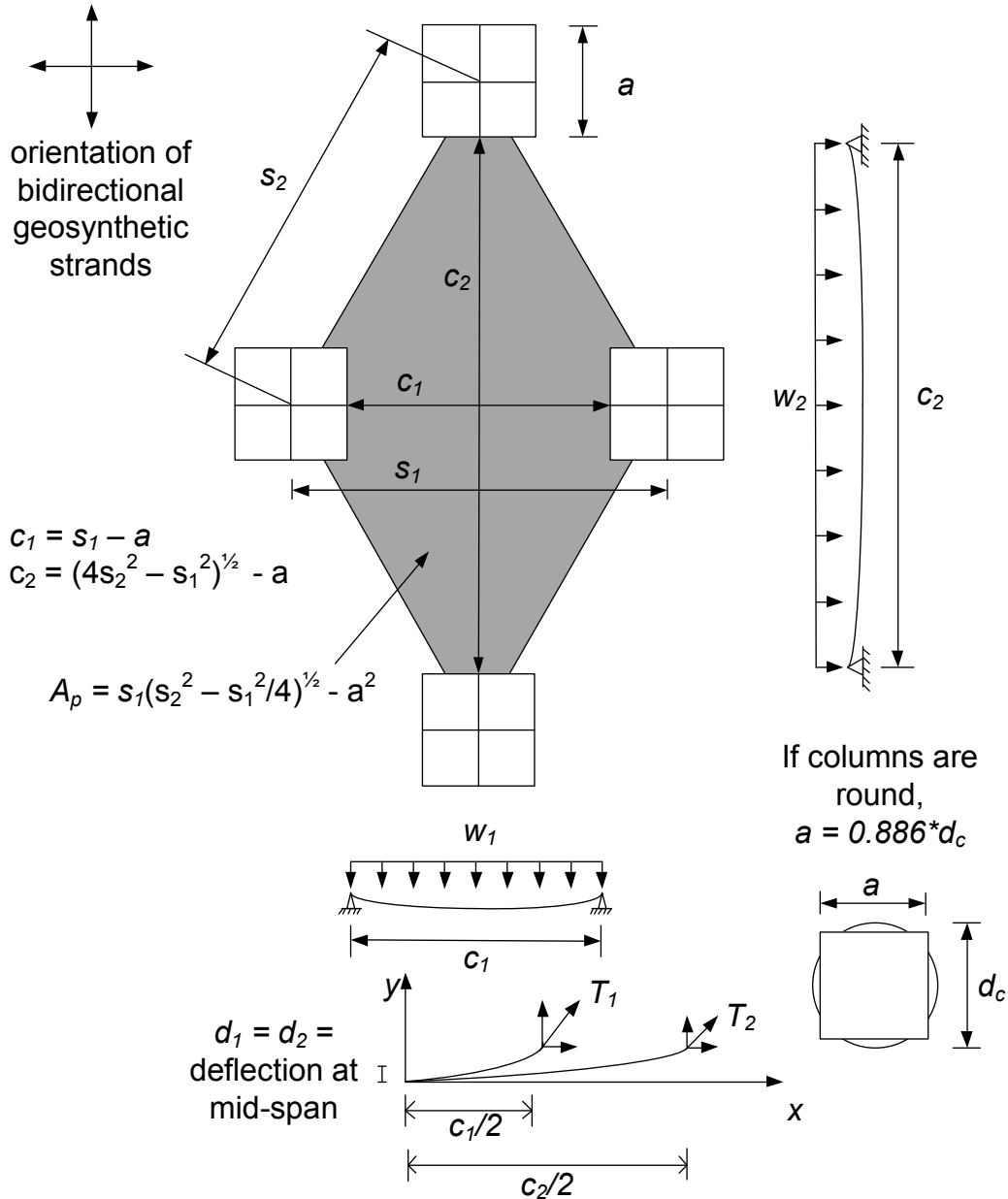


Figure 8.7: Diagram of triangular column arrangements with biaxial geogrid.

Note that this method is conservative for T_1 which will be the greater of the two tensions. If 3 or more layers of geogrid are used and the roll directions are offset 45 degrees to either side, then the axisymmetric approach may be appropriate for biaxial geogrids and triangular column arrays.

8.1.3 Comparison of Parabolic Method with Numerical Modeling

Filz and Plaut (2009) contains summary results from three types of numerical analyses investigating the geosynthetic strains and deflections for column-supported embankments. The first analysis method is a 3D membrane model described further by Jones (2007) and Jones et al. (2009). The second model is a 3D cable-net model described further by Halvordson (2007) and Halvordson et al. (2007). The third model is an axisymmetric membrane model described in Plaut and Filz (2010).

In order to represent the arching that occurs with a CSE, all three models incorporate vertical pressures on the geosynthetic, with higher pressures on the area underlain by columns and lower pressures acting down on the area underlain by soil. Support under the geosynthetic is represented by linear springs with stiff springs in the areas underlain by the pile caps, and softer springs representing the soil support. The geosynthetic properties are linear, elastic, and isotropic, with a Poisson's ratio equal to zero for membrane representations.

Filz and Plaut (2009) contain a summary table for 16 cases where strains and deflections were calculated for the specified geometry, loads, and geosynthetic properties. Of these 16 cases, 11 are for square arrangements of square columns and the strains can be compared directly to the strains calculated by the Parabolic Method as in BS8006 (1995) and others. One of the cases contains a square array of columns with the geosynthetic strains oriented at 45 degrees to the sides of the square. This case can be used to compare with the strain calculated from the triangular Parabolic Method developed in Section 8.1.2. Since the orientation is a rotated square, $c_1 = c_2$, $T_1 = T_2$, and $J_1 = J_2$. Figure 8.8 and Figure 8.9 contain the results for these two cases.

The strains from the Parabolic Method as in BS8006 (1995) compare quite well to the strains computed from the numerical analyses. This adds further support for the accuracy of the Parabolic Method for square columns in a square arrangement as in BS8006 (1995). Although there is only one case for comparison, the strain from the triangular Parabolic Method also compares well with the strain calculated from numerical analysis.

Several other conclusions from Filz and Plaut (2009) which have implications for design of CSEs are listed below:

- Peaks in geosynthetic strain occur at the corners of square pile caps and at the edges of round pile caps.

- Maximum geosynthetic strains are smaller for round pile caps than for square pile caps at the same area replacement ratio.
- Maximum geosynthetic strains are smaller for the geosynthetic orientation with strands parallel to the diagonals of the unit cell than for the orientation with strands parallel to the pile cap layout, for the case of square pile caps.
- Maximum deflections and strains increase with increasing values of the load on the geosynthetic reinforcement, and with decreasing values of the subsoil stiffness, area replacement ratio, and geogrid stiffness.
- The net vertical load on the geosynthetic reinforcement increases with increasing values of vertical load on the geosynthetic, area replacement ratio, and geosynthetic stiffness, and with decreasing values of subsoil stiffness.

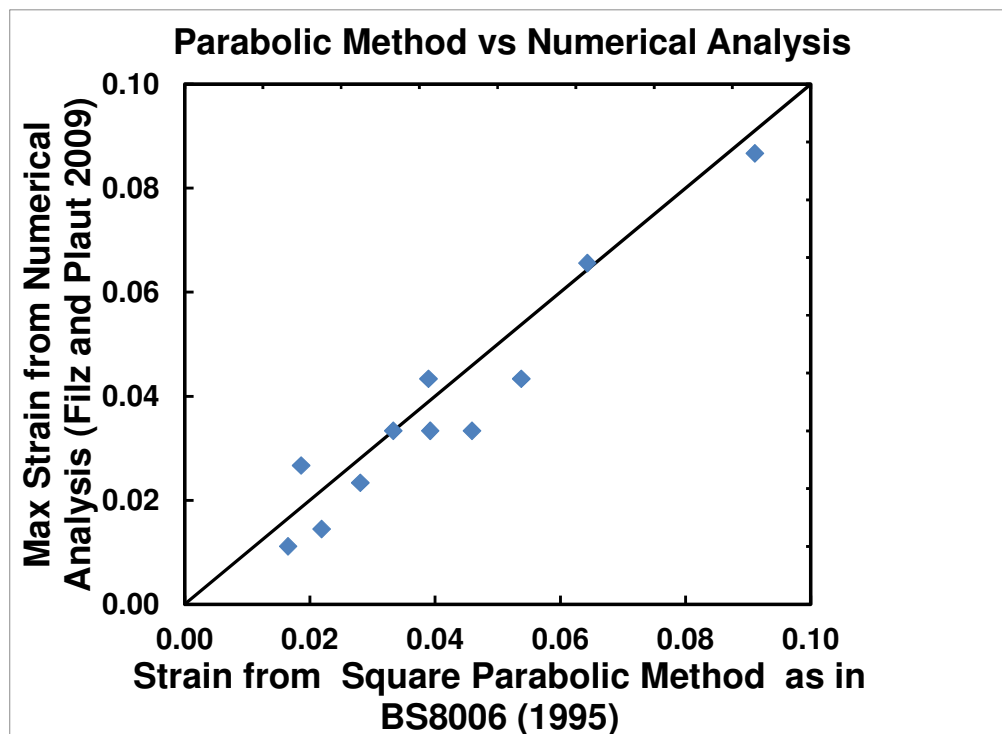


Figure 8.8: Strain from numerical analyses (Filz and Plaut 2009) compared to strain from the Parabolic Method for square column arrangements.

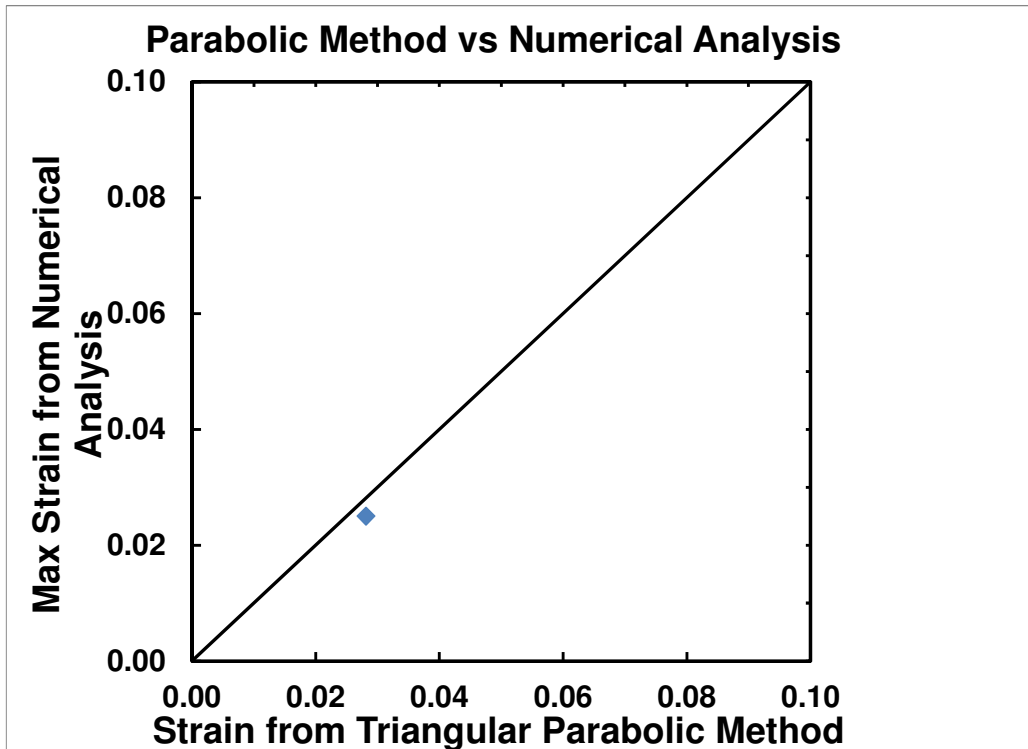


Figure 8.9: Strain from numerical analyses (Filz and Plaut 2009) compared to strain from the Parabolic Method for triangular column arrangements

8.2 RECOMMENDED DESIGN PROCEDURE

The following procedure is recommended based on a review of the available literature, documented case histories, and the CSE tests reported in this document. In this method, the terms “bridging layer” and “load transfer platform (LTP)” are used interchangeably, since they both refer to a geosynthetic-reinforced select fill layer within the CSE. Figure 8.10, Figure 8.11, Figure 8.12, and Figure 8.13 illustrate the parameters used in the design procedure and Table 8.1 provides information used in the procedure.

1. Collect project information, including the required embankment height, H , the traffic surcharge loading, q , and the maximum allowable post-construction embankment settlement, S . The embankment height will be determined by elevation of the existing subgrade and the required final elevation of the finished road surface. Typically, $q = 250$ to 300 psf, but q may vary depending on the application. According to Elias et al. (2006b), the CSE technology reduces post-construction settlements of the embankment surface to typically less than 2 to 4 in. (50 to 100 mm). The allowable total settlement will depend on the type of

application, the embankment height, and the embankment fill properties. An allowable total settlement of 3 in. (75 mm) is recommended here and in the SHRP2 guide specification.

2. Collect subsurface information, including stratigraphy, field test data, laboratory test results, and ground water information. Develop subsurface profile(s) for design.
3. Given the embankment height, surcharge loading, and the subsurface profile (depth and soil type), select the preliminary column type(s) based on the typical column capacities, lengths, and diameters in Table 2 below. The columns should be designed to carry the entire embankment load, which results in an allowable column load, $q_{all,col}$, of:

$$q_{all,col} = A_{unitcell}(\gamma H + q)$$

where $A_{unitcell}$ is the tributary area of the column (area of the unit cell) from Figure 8.11, γ is the unit weight of the embankment fill, H is the embankment height, and q is the embankment dead and live load surcharge. The approximate embankment heights, H , in Table 2 were determined by substituting the $q_{all,col}$ from Table 2, $\gamma = 135$ pcf, $q = 250$ psf, and $A_{unitcell} =$ values shown in the column heading into the equation above and solving for H . Note that the approximate heights in Table 2 are based on the allowable column loads ONLY, and the criteria in Step 3a/b below must still be applied to determine the minimum acceptable layer thicknesses and the total embankment height for a given column spacing. For example, Vibro-Concrete Columns with an allowable column capacity of 250 kips and a column tributary area of 64 ft² results in a maximum embankment height of 27 ft; however, a height as low as 10 ft may not be acceptable once the criteria from 3a/b are applied. Table 2 is intended to be a guide for preliminary column selection. The column selection and column design will be finalized in Step 6, and several iterations may be required.

If an upper layer of competent soil is present, then credit may be given to help satisfy the critical height requirement in a. below. Competent soils are defined as having a relative density of medium dense (compact) or above ($D_r > 40\%$, $N > 10$ blows/ft) for cohesionless soils, and a consistency of medium-stiff or above ($s_u = 500$ psf) for clays. A conservative, low average, of the competent soil thickness, t , should be used in the criteria below. In this method, the effective column diameter is increased based on the transfer of vertical stresses from the competent

layer to the column based on a 4:1 slope as illustrated in Figure 8.12. This load transfer has the effect of increasing the pile width by $0.5t$.

In conjunction with selecting the preliminary column type(s), select trial values of the maximum center-to-center column spacing, s , of columns in a square/rectangular or triangular array and the minimum column diameter, d_{col} , or pile cap width, a , to satisfy the following criteria:

- a. The embankment height, H , must be greater than the critical height, H_{crit} . The critical height is the minimum height at which there is zero differential settlement for a given column diameter, spacing, and arrangement. Based on the results of the field-scale tests in this study, there is agreement with the relationship for H_{crit} developed by McGuire (2011), $H_{crit} = 1.15s' + 1.438d_{col}$, and there is also agreement for a more conventional relationship of $H_{crit} = 1.5(s - a)$. The most conservative of these two relationships is recommended (largest predicted critical height) as noted below:

$$H > H_{crit} = \max \begin{cases} 1.5(s - a - 0.5t) \\ 0.81s + 0.97a \end{cases}$$

Generally, the embankment height, H , is fixed by the existing subgrade elevation and the required road or highway elevation and the minimum column center-to-center spacing, s , can be found according to:

$$s \leq \min \begin{cases} 0.67H + a + 0.5t \\ 1.23H - 1.20a \end{cases}$$

for a given column width, a , and competent layer thickness, t .

- b. $s - a \leq 10$ ft (3 m) according to Collin (2004) and Elias et al. (2006b).

Note that an equivalent area conversion between d_{col} and a , such that $a = 0.886d_{col}$, is recommended when applying criteria a. and b. The recommendations presented here, which are based on formula originally developed for square columns or pile caps, should also be safe for round columns or pile caps when the equal area conversion is applied.

4. Choose the select fill for the bridging layer. Collin (2004) and Elias et al. (2006b) recommend an effective friction angle of at least 35°. The gradation requirements are as follows:

Size	% Passing
200 mm (4 in.)	100
4.75 mm (No. 4)	70-15
0.425 mm (No. 40)	60-10
0.075 mm (No. 200)	15-5

Due to the wide range of acceptable gradations for the criteria above, and the desire for a well-graded material to provide strength and promote arching, the select fill should also have:

$$c_c = \frac{D_{30}^2}{D_{60}D_{10}} = 1 \text{ to } 3, \text{ and } c_u = \frac{D_{60}}{D_{10}} > 4$$

where c_c and c_u are the coefficients of curvature and uniformity, respectively, determined from the gradation curve. Reinforced fill material passing the No. 40 sieve shall have a liquid limit less than 40 and a plasticity index less than 20.

Estimate the values of unit weight, friction angle, modulus, and Poisson's ratio for this material. When selecting the friction angle, the large-strain effective stress friction angle should be used for design. Large-strain friction angles for select gravel fill can be quite large. For example, triaxial tests by Duncan et al. (2007) on VDOT 21B produced peak friction angles that varied from 48 to 58 degrees and occurred at axial strains of 2% to 5% for confining pressures from 6 to 30 psi. At the same confining pressures, the friction angles at axial strains of 8% to 11% were only slightly smaller and varied from 46 to 53 degrees.

The minimum thickness of the bridging layer/LTP fill, H_b , should satisfy the larger of the two following criteria:

- a. $H_b \geq 2 \text{ ft.}$
- b. $H_b \geq 0.5(s - a).$

5. Determine the embankment fill material that will be used above the bridging layer. This may be any suitable material for embankment construction. Estimate the values of unit weight, friction angle, modulus, and Poisson's ratio for this material.
6. Design the columns or piles to be able to carry the entire load from the embankment and surcharge with an adequate factor of safety. Thus, each column should be designed to carry an allowable load of $(\gamma H + q)A_{unitcell}$ where $A_{unitcell}$ is defined in Figure 8.11 based on the square or equilateral triangular column arrangement.

Multiple column types may be suitable for a particular set of project conditions, and the column cost may be the determining factor in the column selection process. Design, QC/QA, specification, and cost estimating guidance for aggregate columns, vibro-concrete columns, combined soil stabilization with vertical columns (CSV), continuous flight auger (CFA) piles, geotextile encased columns (GEC), deep mixing methods (DMM), and jet grout columns is provided in the SHRP2 R02 "Guidance and Selection System" under the respective technology categories. Some additional information on column design, including traditional piles, is provided below.

- a. The design of concrete, steel, and timber piling is well established. Design guidelines have been developed by FHWA and may be found in *Design and Construction of Driven Pile Foundations* (FHWA HI-97-013 and 014).
- b. For the design of timber piles, the reader is also referred to *Timber Pile Design and Construction Manual*, Timber Piling Council.
- c. Deep mixing method columns, aggregate columns, and geotextile encased columns are addressed in *Ground Improvement Methods* (FHWA-NHI-06-020) in addition to the SHRP2 R02 guidance.
- d. Guidelines for design of continuous flight auger (CFA) piles, drilled displacement piles, and screw piles are found in FHWA *Geotechnical Engineering Circular No. 8* available online at: <http://www.fhwa.dot.gov/engineering/geotech/pubs/gec8/>.

If CSEs are used in potentially liquefiable soils in a seismic area for support of embankments or structures, the cyclic stresses caused by ground shaking will be shared between the columns and the untreated matrix soil. By virtue of their greater stiffness, the columns will attract a greater proportion of the cyclic shear stresses than given simply by the replacement ratio (the ratio of the treated area in plan to the total plan area). To maintain structural integrity and ensure satisfactory performance requires a design that prevents horizontal shear failure in aggregate columns or combined shear and bending failures in cemented columns and walls. Analysis of this complex soil-structure problem is usually site and project specific and requires input from someone with prior knowledge and experience.

Whether the matrix soil will liquefy with the columns in place can be assessed in terms of the reduced shear stress and strain that it is subjected to after accounting for that carried by the columns. A very conservative (high) estimate of the reduced shear stress will be given by the seismically-induced horizontal shear stress in the untreated ground multiplied by (1 - replacement ratio).

7. Select a suitable layer or layers of geosynthetic reinforcement using the Microsoft Excel spreadsheet GeogridBridge, which is available online by searching for "GeogridBridge" at: <http://vtrc.viriniadot.org/PUBS.aspx>. The spreadsheet was originally developed by Filz and Smith (2006) and updated by Sloan et al. (2011). A brief description of the analysis procedure is included in this document following this design procedure. Currently the workbook will function for square column arrangements only, but the workbook is being updated to support other column arrangements in accordance with the final version of this design guidance. This procedure was selected based on analysis of available information in the literature and the results of field tests conducted for SHRP2 R02. The SHRP2 R02 design development project document for Column Supported Embankments can be accessed within the SHRP2 R02 Guidance and Selection System for more information and a review of other design/analysis procedures.

The workbook will calculate the tension in the geosynthetic, T_{pp} , due to the embankment vertical loads. The geosynthetic reinforcement should be selected to satisfy the following criteria:

- a. The creep-limited strength of the geosynthetic at 5% strain, $T_{cr@5\% \epsilon}$ shall be less than the required strength, T_g .

$$T_{cr@5\% \epsilon} \geq T_g$$

where, $T_g = T_{rp}$ if the reinforcement is design to carry vertical stresses only; if the reinforcement is also designed to carry the lateral spreading loads, then $T_g = T_{rp} + T_{ls}$ (see 8a below).

- b. The required tension shall be less than the allowable long-term geosynthetic tensile strength of the combined layers of geosynthetic reinforcement after applying appropriate reduction factors for durability, installation damage, creep, and an overall factor of safety, i.e.

$$T_g \leq T_a = \frac{T_{ult}}{RF_D \times RF_{ID} \times RF_{CR} \times FS_{UNC}}$$

where, T_a = allowable tensile strength of geosynthetic

T_{ult} = ultimate tensile strength from single or multi-rib tensile strength tests (ASTM D 6637) for geogrids or wide width tensile strength tests (ASTM D 4595) for geotextiles

$T_g = T_{rp}$ if the reinforcement is design to carry vertical stresses only; if the reinforcement is also designed to carry the lateral spreading loads, then $T_g = T_{rp} + T_{ls}$ (see 8a below)

RF_D = Durability reduction factor is dependent on the susceptibility of the geosynthetic to attack by microorganisms, chemicals, thermal oxidation, hydrolysis and stress cracking. The typical range is from 1.1 to 2.0.

RF_{ID} = Installation damage reduction factor can range from 1.05 to 3.0, depending on backfill gradation and product mass per unit weight.

RF_{CR} = Creep reduction factor is the ratio of the ultimate strength (T_{ult}) to the creep limited strength obtained from laboratory creep tests for each product, and can vary typically from 1.65 to 5.0.

FS_{UNC} = Overall factor of safety or load factor reduction to account for uncertainties in the geometry of the structure, fill properties, reinforcement properties, and externally applied loads. For load transfer platforms a minimum overall factor of safety of 1.5 is typical.

Guidelines for determining specific values for the reduction factors (RF_D , RF_{ID} , RF_{CR}) used in design are found in *Mechanically Stabilized*

Earth Walls and Reinforced Soil Slopes (FHWA NHI-00-043). Values for some manufacturers and products are established by the National Transportation Product Evaluation Program (NTPEP) and can be found online at:

http://www.ntpep.org/ContentManagement/PageBody.asp?PAGE_ID=26

As of January 2011, the site contained reports for the following manufacturers and product lines: ACE Geosynthetics, Miragrad XT Geogrid, Synteen SF Geogrid, Luckenhaus Raugrid Geogrid, Maccaferri Macgrid, Tensar UX-MSE/UX-HS Geogrid, Linear Composites ParaWeb/ParaLink and ParaGrid, and Strata SG Geogrid. If NTPEP reduction factors are not available for the manufacturer and type of geosynthetic proposed by the Design Engineer, then the values used should be those recommended by the geosynthetic manufacturer supported by laboratory testing in accordance with the procedures described in *Mechanically Stabilized Earth Walls and Reinforced Soil Slopes* (FHWA NHI-00-043), and as approved by the Engineer.

8. Calculate the tension in the geosynthetic reinforcement due to the tendency of the embankment to spread laterally and also the required bond length at the embankment sideslopes, as in BS8006 (1995) and the papers by Collin (2004) and Rogbeck et al. (2003). There are two ways to design the geosynthetic reinforcement to resist the lateral spreading forces: 1) design an additional layer(s) of reinforcement solely to resist the lateral spreading forces, or 2) add the tension due to lateral spreading to the tension induced by the vertical embankment loads and design the geosynthetic reinforcement to resist the total tension. Option 1 is the preferred method since the lateral spreading forces only occur in one direction, perpendicular to the axis of the embankment, and therefore the geosynthetic can be chosen and oriented for this purpose (e.g. a uniaxial geogrid).

- a. The tension in the reinforcement due to lateral spreading, T_{ls} , is equal to:

$$T_{ls} = \frac{1}{2} K_a \gamma H^2 + q K_a H$$

where: K_a = active earth pressure coefficient of the embankment fill

γ = unit weight of embankment fill

H = full embankment height

q = embankment surcharge

If Option 1 above is used, then the geosynthetic should be chosen to resist T_{ls} with suitable reduction factors and a factor of safety as in Section 7b. If the geosynthetic reinforcement is designed to handle the embankment vertical loads and lateral spreading forces, then the total tension in the geosynthetic reinforcement perpendicular to the axis of the embankment is $T_g = T_{ls} + T_{rp}$, and the tension in the geosynthetic reinforcement parallel to the embankment centerline is $T_g = T_{rp}$.

- b. The minimum length, L_e , of reinforcement necessary to develop the required strength of the reinforcement without the sideslope of the embankment sliding across the reinforcement (see Figure 8.13) is determined by:

$$L_e \geq \frac{T_{ls}FS}{\gamma h \alpha_1 \tan \varphi_1}$$

where: α_1 = coefficient of interaction for sliding between the reinforcement and fill above the reinforcement

φ_1 = friction angle of the embankment fill above the reinforcement

FS = factor of safety for lateral sliding development length (recommend a minimum of 1.3)

γ = unit weight of embankment fill

h = average height of the embankment above the reinforcement length L_e

Note that the distance L_e begins at the crest of the embankment and extends a minimum distance, L_e , toward the toe of the embankment as shown in Figure 8.13.

- c. The minimum bond length of the reinforcement due to pullout forces, L_b , as shown in Figure 8.13, is determined by:

$$L_b \geq \frac{(T_{ls} + T_{rp})FS}{\gamma h (\alpha_1 \tan \varphi_1 + \alpha_2 \tan \varphi_2)}$$

where: α_1 = coefficient of interaction for sliding between the reinforcement and fill above the reinforcement
 φ_1 = friction angle of soil above the reinforcement
 α_2 = coefficient of interaction for sliding between the geosynthetic reinforcement and embankment fill
 φ_2 = friction angle of soil below the reinforcement
 FS = factor of safety for lateral sliding development length (recommend a minimum of 1.3)
 γ = unit weight of embankment fill
 h = average height of the embankment above the reinforcement length L_b

9. Calculate the average embankment settlement, S , as the sum of the embankment compliance, S_E , the compression of the columns, S_C , and the compression of underlying material, S_U , if significant. The sum of S_E and S_C is calculated in the GeogridBridge workbook or can be calculated by hand based on the column type using the design guidance for each column type listed in step 6. The value of S_U can be determined using the approach of Broms (1991), in which the embankment load is transferred to the bottom of the columns and the load is distributed with depth using a 1H:2V load spread below the bottom of the columns. The embankment settlement, S , determined this way represents the average settlement of the pavement surface. The differential settlement of the pavement surface should be small if the criteria and details in steps 3 and 4 are properly addressed. If a significant time period elapses between the mid-point of embankment construction and pavement placement, Janbu's (1963) method can be used to estimate the portion of the embankment settlement that occurs before the pavement is constructed. The GeogridBridge workbook computes this settlement and subtracts it from the total embankment settlement to obtain the post-construction settlement of the pavement.
10. If the embankment settlement is too large, the design process should be repeated using a closer column spacing, a larger area replacement ratio, stiffer geosynthetic reinforcement, stiffer columns, and/or a preload.
11. Develop the geosynthetic details:
 - a. There are two options to reduce or eliminate abrasion between the columns and the base layer of geosynthetic reinforcement:

- i. Sections of non-woven geotextile, with a minimum weight of 8 oz., may be cut and placed over the column tops or pile caps and subgrade soil with the lowest layer of geosynthetic reinforcement placed directly on top of the non-woven geotextile. This method can be applied in any case, and it is the preferred method if the subgrade is weak and mixing of the reinforced fill and subgrade soil will occur without the non-woven geotextile at the interface to separate the fill and subgrade soil.
 - ii. Where the subgrade is strong enough to prevent mixing of materials, the bottom layer of geosynthetic may be placed on a lift of compacted bridging layer material at an elevation 6 in. above the top of the columns or pile caps.
- b. Each additional layer of geosynthetic above the base layer, should be separated from the underlying layer of geosynthetic by a 6 to 12 in. lift of compacted bridging layer material.
- c. If biaxial or radially-isotropic geosynthetic reinforcement is used, the base layer of geosynthetic should be placed with the roll direction parallel to the axis of the embankment. The roll directions should be alternated for each additional layer of geosynthetic reinforcement so that the overlying layer is placed perpendicular to the layer beneath it. A minimum of two layers of geosynthetic are recommended so that the strong direction of the geosynthetic occurs in two different directions (since biaxial geosynthetics have slightly different properties in the machine and cross-machine directions) and so the overlaps occur in two different directions when the layers are placed perpendicular to one another. If uniaxial geosynthetics are used, then two perpendicular layers may be used to act as one biaxial layer.
- d. Adjacent layers of geogrid reinforcement should be overlapped sufficiently to transfer tension from one roll to the next. A minimum overlap of 3 ft is recommended. If geotextiles are used the seam between adjacent rolls should be sewn and the strength of the seam will govern the design strength of the geosynthetic.
- e. The roll width should be wide enough so that the entire roll width does not fall between columns, i.e. some portion of every roll falls on top of a

column. To meet this criteria, the roll width should be selected such that $w - v \geq s$, where w = geosynthetic roll width, v = geosynthetic overlap, and s = column center-to-center spacing.

12. Determine the extent of the columns required across the embankment width. The lateral extent of the column system across the width of the embankment should extend a sufficient distance beyond the crest of the embankment to ensure stability with an adequate factor of safety (recommend a minimum of 1.3) and that any differential settlement will not extend to the embankment crest.

As a preliminary check, BS8006 (1995) recommends the maximum horizontal distance between the outer edge of the pile cap or column and the toe of the embankment, L_p , (see Figure 8.13) be calculated as follows:

$$L_p = H(n - \tan \theta_p)$$

Where: H = embankment height

n = sideslope of the embankment (i.e. nH:1V slope)

θ_p = angle from the vertical between the outer edge of the outside pile cap and the crest of the embankment, typically $\theta_p = 45 - \frac{\phi}{2}$

ϕ = friction angle of the embankment fill

More detailed stability checks should be performed as follows:

- a. There are several approaches that may be used to check the edge stability of the embankment sideslopes outside the columns. The computer software developed for FHWA for the design of both reinforced and non-reinforced slopes and embankments, ReSSA, is an excellent tool for checking edge stability. Other commercial software may be used to check local stability of the embankment outside the columns, as well as global stability.
- b. Global stability analysis recommendations are based on the column type and whether geosynthetic reinforcement for lateral spreading is included:

- i. Global stability for embankments on driven piles. The piles in a column supported embankment are designed to carry the full vertical embankment load and are generally not designed to carry any lateral forces. Generally, the geosynthetic reinforcement, if used, is designed to carry the additional tension due to the tendency of the embankment to spread laterally, as in step 8 above. For this case, global stability is not an issue. In cases where geosynthetics are not used, battered piles may be used to resist these lateral forces. Global stability analysis of pile-supported embankments, without reinforcement, can be performed according to the method in BS8006 (1995). This method is also summarized by Collin (2004), Elias et al. (2006b), and Filz and Navin (2006).
 - ii. Global stability for embankments on stone columns without geosynthetic reinforcement for lateral spreading. Filz and Navin (2006) summarize the Circular Sliding Surface Method from Aboshi et al. (1979), the Average Strength Parameter Method from Goughnour (1991), and the Profile Method from Barksdale and Bachus (1983). The Profile Method is recommended for use with commercial slope stability software.
 - iii. Global stability for embankments on deep mixing method and vibro-concrete columns without geosynthetic reinforcement for lateral spreading. Key references include the SHRP2 R02 documentation for these technologies, as well as the reports by FHWA (2011), Filz and Navin (2006), and Filz and Templeton (2011).
 - iv. For guidance on incorporating the benefit of geosynthetic reinforcement in the overall stability of the CSE, see *Mechanically Stabilized Earth Walls and Reinforced Soil Slopes* (FHWA/NHI-00-043).
13. Prepare construction drawings and specifications. Guidance for QC/QA and specifications for CSEs is provided in separate documents located within the SHRP2 R02 Guidance and Selection System.

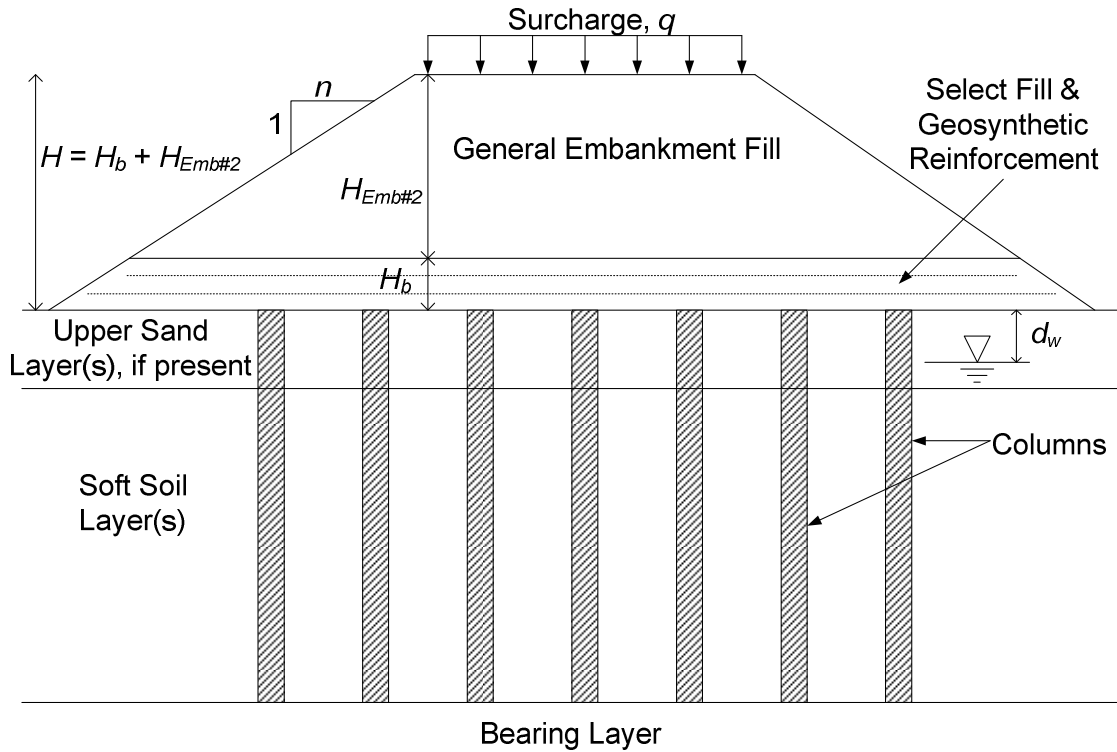
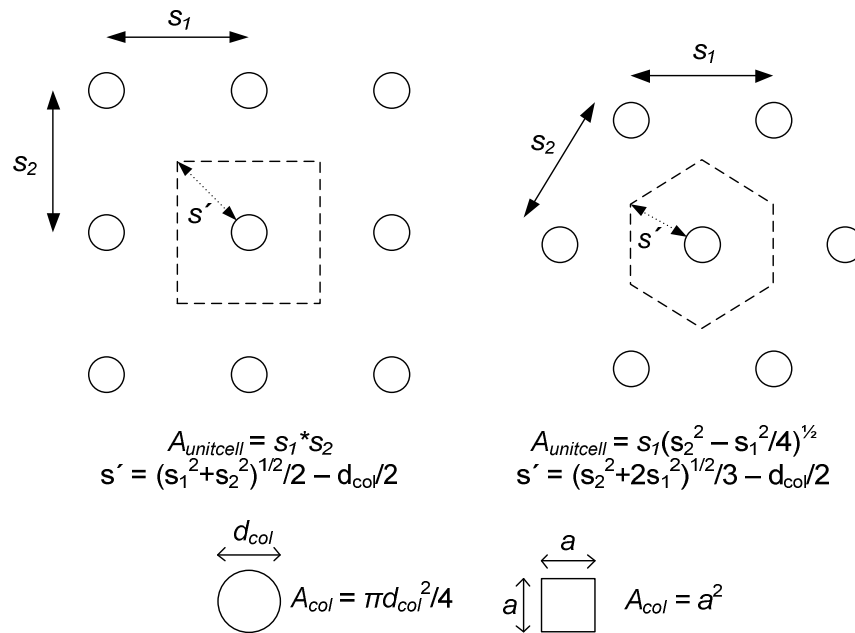


Figure 8.10: Definition sketch for a geosynthetic reinforced column supported embankment.



To convert between square and round columns, an equal area conversion is recommended where $a = 0.886 * d_{col}$

Figure 8.11: Column geometries (round or square) and unit cell areas for square/rectangular or triangular arrangements.

Table 8.1: Column types, capacities, lengths, diameters and approximate embankment heights based on column capacity and spacing.

Column Type	Typical Range of Allowable Capacity (kip)	Approximate Values of H (ft) to Produce the Allowable Column Capacity for $q = 250$ psf and $\gamma = 135$ pcf (values of A in ft^2)*				Typical Lengths (ft)	Typical Column Diameter or Width (in.)**
		$A = 16$	$A = 36$	$A = 64$	$A = 100$		
CSV	6-13	4	-	-	-	10-30	5-6
Timber piles	20-110	9-50	6-21	8-11	-	15-65	12-22
Stone columns	20-110	9-50	6-21	8-11	-	10-35	18-47
Geotextile encased column	65-135	19-61	12-26	8-14	-	10-35	30-60
Geopier rammed aggregate pier	50-150	22-66	9-28	8-15	-	10-35	24-36
Augered piles	75-250	35-114	14-50	8-27	4-17	15-80	12-24
Vibro-concrete columns	100-250	44-114	19-50	10-27	6-17	10-35	18-24
Pre-cast concrete piles	90-225	40-102	17-44	9-24	5-15	30-50	0-24
Deep mixing method (DMM) columns	90-270	40-123	17-54	9-29	5-18	30-100	24-120
Shells driven without mandrel	110-300	50-139	21-61	11-33	6-21	15-80	12-18
Cast-in-place concrete shell (mandrel driven)	90-315	40-144	17-63	9-35	5-21	10-130	8-18
Steel H piles	90-450	40-206	17-91	9-50	5-31	15-100	6-12
Steel pipe piles	180-550	81-258	35-114	19-63	11-40	30-130	8-48

*cells highlighted in gray do not meet the criteria in 3a and the values are not reported

**pile caps may be added for some column types to satisfy the requirements from Step 3a and 3b

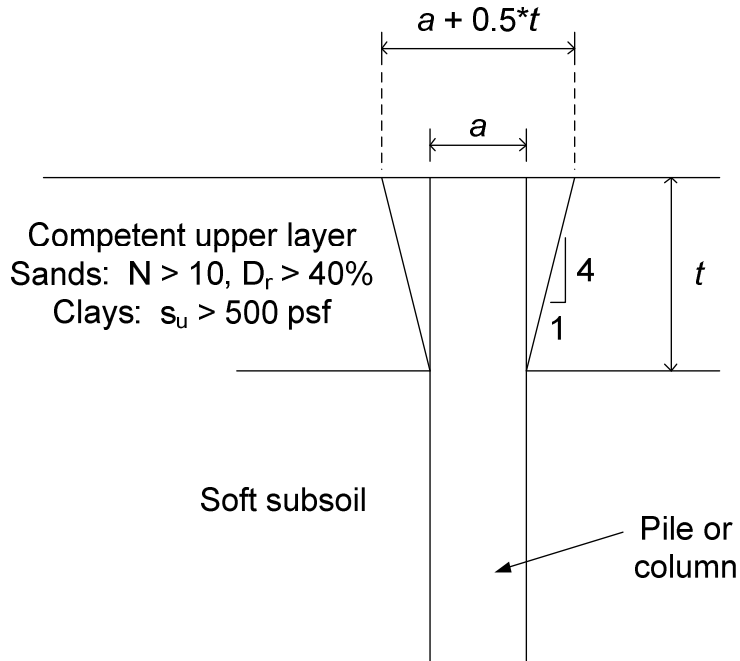


Figure 8.12: Effective column width for competent upper layer.

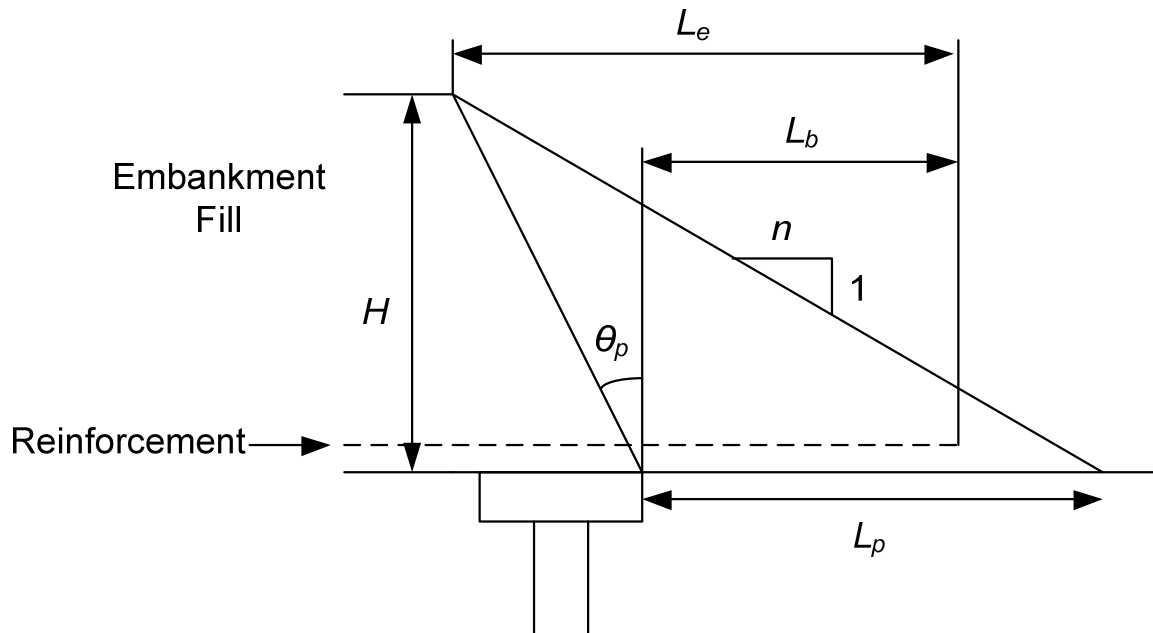


Figure 8.13: Definition of L_e , L_b , and L_p .

CHAPTER 9

QC/QA AND SPECIFICATIONS FOR CSE

9.1 QUALITY CONTROL AND QUALITY ASSURANCE

QC/QA for a column supported embankment project should include verification of the properties and placement of the LTP fill, embankment fill, and the geosynthetic reinforcement. Although not covered in this document, industry standard QC/QA procedures for the type of column or pile used for embankment support should be followed.

Pre-production embankment test sections should be considered only on very large projects or where a performance approach specification is used. For large projects, design validation is particularly useful, because a test section may lead to a more economical design. However, as more knowledge of column supported embankments is gained through case histories, numerical modeling, and the embankment tests for this SHRP2 R02 project, a need for test embankment sections, even for large projects, may be reduced.

If a performance approach specification is used, then monitoring of the embankment test section will serve as the basis for an acceptable design. Typically, the acceptance criteria for performance approach specifications are based on maximum allowable total and/or differential settlement criteria.

Whether or not a test section is constructed, settlement and/or lateral displacement monitoring should be included to verify that the embankment performs as expected.

Geosynthetics testing and verification should include:

- Documentation of the manufacturer, model number, lot number, and roll number for each roll of geosynthetic reinforcement used.
- Verification of the following properties of the geosynthetic according to the manufacturer's certified test results: ultimate strength per ASTM D 6637 (geogrid) or ASTM D 4595 (geotextile), creep resistance per ASTM D5262, durability, coefficient of interaction for sliding per ASTM 5321 [see complete list of geotextile properties and test methods compiled by Holtz et al. (2007) Table 1-4, pages 1-12 to 1-14].

- Inspection of each roll to verify that it is undamaged prior to covering with fill material.
- Verification that storage and shipment is such that the geosynthetic does not receive prolonged exposure to ultraviolet radiation prior to covering.
- Observation to verify removal of deleterious materials prior to placement of geosynthetic reinforcement.
- Observation of geosynthetic placement to verify it is taut, unless sagging is prescribed by the design method, and construction notes to enhance arching in the embankment fill.
- Observation to verify that equipment is not operated directly on the geosynthetic and minimum fill thickness is placed before equipment is operated over geosynthetic; equipment should not make sharp turns.
- Observation to verify there are no large piles of fill material on top of the LTP which may cause a local bearing capacity failure.
- Observation to verify proper orientation, overlap, and elevation within the embankment.
- Verification that, if geotextile seams are specified, the seams should be placed up and every stitch should be inspected.

A recommended “Geosynthetic Field Inspection Checklist” is included in Table 1-5 on page 1-25 of Holtz et al. (2007). Construction procedures for reinforced embankments are contained in Section 7.8 (pages 7-45 to 7-52) of Holtz et al. (2007), and although it is written for the general category of reinforced embankments, much of it applies to column supported embankments.

Verification for the LTP and embankment fill should include:

- Gradation testing for all fill material(s) to verify it meets the specified gradation (frequency of testing determined by state DOT recommendations typical for embankment fill projects).
- Atterberg limits testing to verify liquid limit and plasticity index are below the specified maximum values (frequency of testing determined by state DOT recommendations typical for embankment fill projects).
- Modified Proctor compaction testing to determine the maximum dry unit weight and the optimum moisture content (for use in calculating relative compaction and determining the allowable range of moisture contents), or minimum and maximum density tests (for use in calculating relative density for granular fill placement).

- In situ density testing with nuclear gage, sand cone, balloon densometer, or other reliable method to verify the specified relative density is met; the specific method of density testing and frequency should follow guidelines typical of the DOT in the state where the project is located.
- Observation to verify that the maximum compacted lift thickness is not exceeded (recommend 12 inches for large compaction equipment and 6 inches for hand operated equipment).

The following monitoring is recommended:

- Surface survey to confirm the finished embankment elevation, followed by periodic resurvey to quantify total and differential settlements.
- Settlement plates at the elevation of the geosynthetic reinforcement should be considered to monitor settlement during and after construction.
- Inclined meters at the embankment toe should be considered to monitor lateral displacement.

The following QC/QA methods are described further below: embankment test section, geosynthetics verification, testing of embankment fill materials, and monitoring. Further guidance for QC/QA can be found in reports by Elias et al. (2006b), FHWA (2004), and Holtz et al. (2007).

9.1.1 QC/QA Method Description: Embankment Test Section

Elias et al. (2006b) and FHWA (2004) include provisions in a performance specification for an embankment test section. The test section requires a minimum of four rows of columns in each direction. It requires settlement plates to be installed to monitor settlement of the subgrade and monitoring of total and differential settlement at the surface of the test section. A specified surcharge is placed on the test embankment. The contractor's design is considered acceptable if the measured surface settlements between columns are less than the specified amount. This method is suited to a performance-type specification where the contractor demonstrates the performance of the design. It could also be used to verify the contractor's ability to construct the owner's design and also verify performance for other types of specifications.

Piezometers, inclinometers, strain gauges on geosynthetic reinforcement, load cells on columns, pressure cells in the embankment fill or soft soil, surveying, and other techniques can be used to provide information about the performance of the column supported test embankment.

Wachman and Labuz (2008) describe the use of strain gauges on the columns and geosynthetic reinforcement, as well as settlement plates and earth pressure cells within the embankment. Measurements were used to verify design assumptions during and after construction.

9.1.2 QC/QA Method Description: Geosynthetics Verification

In general, this method involves verification that the geosynthetics (if used) satisfy the required specifications. This should include verification of the manufacturer, model number, lot number, and manufacturer's test data for the geosynthetic. It may also include independent testing of samples of the geosynthetic taken from the construction site. Some other specific verification methods relating to the geosynthetic reinforcement are discussed below.

Holtz et al. (2007) present and describe specifications and construction techniques for reinforced embankments, some of which apply to column supported embankments. Stumps and debris should be removed prior to placement of the geosynthetic reinforcement. The geosynthetic reinforcement should be pulled taut prior to placement of fill material on top to ensure that there is no sagging, unless sagging is required by the design method and specifications as a means to promote arching within the embankment fill and develop the tensile forces within the geosynthetic.

If a geosynthetic is used, the contractor should provide a manufacturer's certificate of compliance to the Engineer which includes the following information about each roll of material to be used (Holtz et al. 2007): manufacturer's name and current address, full product name, geosynthetic structure including fiber/yarn type if applicable, polymer type(s), roll number, and certified test results. Seams in geotextiles should be sewn as required with all seams placed up and every stitch inspected. The geosynthetic should be inspected for holes, rips, or tears. Defective material should be replaced or repaired. Geosynthetic roll identification, storage, and handling should be in conformance to ASTM D 4873. The geosynthetic should be covered during shipment and storage such that it is protected from ultraviolet radiation including sunlight, site construction damage, precipitation, chemicals, flames including welding sparks, temperatures in excess of 70 Celsius, and other environmental conditions that may damage the physical properties of the geosynthetic. Table 1-5 of Holtz et al. (2007) on page 1-25 contains a geosynthetic field installation checklist.

Proper orientation and overlap of geosynthetic (placement details) should be verified. No changes to the reinforcement details (orientation, layout, overlap, type, elevation, etc.) should be made without approval of the engineer. Remove slack and wrinkles from the geosynthetic prior to placing fill. Equipment should not be allowed directly on the geosynthetic. FHWA (2004) and Elias et al. (2006) recommend a minimum fill of 150 mm (6 in.) above the geosynthetic before it is trafficked by equipment. Vehicle turning should be kept to a minimum so as not to damage the geosynthetic. The geosynthetic should be unrolled smoothly, without dragging. It should be examined for damage before covering with fill material. The height of individual fill piles on the geosynthetic should be limited to avoid a local bearing capacity failure. The geosynthetic should be covered within 48 hours of placement.

Geosynthetics should meet the required ultimate strength (ASTM D 6637), creep limited strength, and coefficient of interaction for direct sliding (ASTM 5321). Some designs may call for placement of an additional sacrificial geosynthetic layer over columns to protect the reinforcement geosynthetic.

9.1.3 QC/QA Method Summary: Testing of Embankment Fill Materials

The primary test method for the load transfer platform soil and the embankment fill is density testing, either by nuclear gauge, sand cone, balloon densometer, or other method. This is then compared with the specified relative compaction or relative density from Proctor tests or minimum and maximum density tests. The moisture content can also be checked at the same time the density testing is completed. The gradation of the material should be verified by submittal from the contractor with recent test results from an independent laboratory. Samples can also be taken from the site and verified by the owner/agency or at the contractor's expense, if so specified in the contract documents. In some cases, triaxial or direct shear testing may be performed to determine the shear strength of the fill material(s).

According to Rogbeck et al. (2003), the load transfer platform and embankment fill should be monitored for moisture content, density, grain size distribution, Atterberg limits, shear strength, and organic content.

A lift thickness may be specified. Elias et al. (2006b) recommend a maximum uncompacted thickness per lift of 250 mm (10 in.) for heavy compaction equipment and a maximum uncompacted thickness per lift of 150 mm (6 in.) for hand-operated equipment.

According to FHWA (2004), LTP fill should be compacted to 95% of the modified Proctor (ASTM D 1557) maximum dry unit weight at a moisture content no more than 2 percent above or below optimum. The test method, frequency, and verification of material specifications and compaction should be stated in the specifications.

9.1.4 QC/QA Method Summary: Monitoring

The QC/QA category of monitoring differs from the monitoring that occurs on an embankment test section in two regards: (1) the monitoring is performed on the production embankment, and (2) the density and types of instrumentation are significantly reduced. The category of monitoring involves the measurement of vertical and lateral movements, primarily at the embankment surface to ensure that there is no detrimental differential settlement and that stability is maintained. Whereas the instrumentation on an embankment test section may include load cells, pressure cells, strain gages, and piezometers, the monitoring for the production embankment typically includes only periodic surveys of the embankment surface and perhaps the use of inclinometers.

Elias et al. (2006b) provide a performance specification where the contractor is responsible for the design. Payment is based on successfully limiting total settlement and/or differential settlement, as determined by post-construction monitoring, to values not greater than the specified amounts.

9.2 CSE PERFORMANCE GUIDE SPECIFICATION

Commentary: The following specification is provided as a guide for the installation of column-supported embankments. This specification deals solely with the design and construction of the embankment above the tops of the columns. A separate specification section for the column type or a general column performance specification should be included in the Contract Documents in addition to this CSE specification or should be integrated into this CSE specification.

Although this specification does not include the columns, successful column installation is crucial to the success of a CSE project. Items to consider incorporating in the column specification which affect CSE performance include, but are not limited to: required verticality of the column, tolerance for horizontal placement of the column, tolerance for the elevation of the column top, roughness of the column top, achieving minimum column diameter/width and strength requirements, column QC/QA requirements to include materials sampling & testing/load testing/core sampling/integrity testing, etc. All column

performance requirements should be measured and verified prior to placement of any geosynthetic reinforcement or fill material.

Care should also be taken when integrating the embankment fill, base course, and pavement specification sections into the complete specification package. Just as the columns are important to CSE performance, the placement and properties of the materials above the CSE bridging layer/load transfer platform can also have a significant impact on CSE performance, particularly on the embankment total and differential settlement requirements in Section 7.4. The timing of the completion embankment construction and the start of paving operations may have an impact on the total and/or differential settlement measured on the pavement surface. The contractor may elect to allow a period of time (2 to 4 weeks) for some of the embankment settlement to occur, before re-leveling the embankment with new material, and constructing the pavement section. Note that there are two options for confirming the differential settlement requirements in Section 7.4. The first method is based on traditional survey techniques and the second is based on the International Roughness Index (IRI) of the pavement.

Guidance on specifications for soil improvement column types (sand compaction piles, aggregate columns, vibro-concrete columns, combined soil stabilization with vertical columns or CSV, continuous flight auger piles, geotextile encased columns, deep mixing method columns, and jet grout columns) may be found under the specific technology within the SHRP2 R02 Guidance and Selection System. Guidance on specifications for traditional pile types can be found in “Design and Construction of Driven Pile Foundations” (FHWA DTFH61-97-D-00025).

This specification should be modified as appropriate for the particular requirements of the project. Items in the specification which contain commentary are shown in italicized text. Blanks (_____) are provided where the owner/engineer may need to provide further information.

1.0 Description and Objectives.

- 1.1. Project Description: The work shall consist of designing and constructing a column-supported embankment (CSE) as indicated on the plans and drawings. [Insert a brief description of the overall project, new road/highway or expansion of existing road/highway, etc., if desired]. The design concept of the CSE involves constructing a pattern of columns using an approved soil improvement technique or traditional concrete, steel, or timber piles [The Owner/Engineer may elect to restrict the choice of column types based on the site conditions. If so,

this should be stated here]. The columns are constructed to bear on a firm strata [Insert a description of the strata along with the commonly accepted geologic name of the strata, if desired. In some CSE applications, floating columns of increasing length are installed to provide a transitional settlement profile up to the structural CSE. If floating columns are desired or deemed necessary by the Engineer based on the CSE application, this should be stated here.]. The CSE shall be designed to efficiently distribute the embankment load plus any surcharge live and dead loads onto the columns.

The number of columns, their spacing, their diameter and depth shall be determined by the CSE Contractor and as approved by the Engineer. The thickness of select fill and general embankment fill materials, number of reinforcement layers, type of reinforcement, and properties of the geosynthetic reinforcement shall be determined by the CSE designer/installer and as approved by the Engineer. The column type shall be determined by the CSE Contractor and as approved by the Engineer. It shall be the Contractor's responsibility to determine and implement the system to ensure that the specified performance required by this specification is achieved.

- 1.2. Project Objectives and Design Requirements: The CSE system shall safely transfer the weight of the embankment and roadway loading, with a suitable factor of safety, to an adequate bearing layer. The system shall be designed as an end bearing system. Frictional resistance based on the penetration length into the bearing layer may be included in the column design, if applicable, depending on the column type. The CSE system shall be designed according to FHWA guidelines [also insert references to State guidance if applicable].
- 1.3. Prior to submitting the bid, the Contractor shall review the available subsurface information and visit the site to assess site geometry, equipment access conditions, and location of existing structures and above ground utilities and facilities.

2.0 References.

- 2.1. FHWA NHI-06-020 *Ground Improvement Methods: Reference Manual – Volumes I & II*
- 2.2. FHWA DTFH61-97-D-00025 *Design and Construction of Driven Pile Foundations*
- 2.3. AASHTO R 43-07 *Standard Practice for Determination of International Roughness Index (IRI) to Quantify Roughness of Pavements*
- 2.4. ASTM C 136 / AASHTO T 27 *Standard Test Method for Sieve Analysis of Fine and Coarse Aggregates*

- 2.5. ASTM C 117 / AASHTO T 11 *Materials Finer than 75- μ m (No. 200) Sieve in Mineral Aggregates by Washing*
- 2.6. ASTM D4318 / AASHTO T 89 & T90 *Standard Test Methods for Liquid Limit, Plastic Limit, and Plasticity Index of Soils*
- 2.7. ASTM D 1557 *Standard Test Methods for Laboratory Compaction Characteristics of Soil Using Modified Effort*
- 2.8. ASTM D2487 *Standard Practice for Classification of Soils for Engineering Purposes (Unified Soil Classification System)*
- 2.9. ASTM D 6637 *Standard Test Method for Determining Tensile Properties of Geogrids by the Single or Multi-Rib Tensile Method*
- 2.10. ASTM D 4595 *Standard Test Method for Tensile Properties of Geotextiles by the Wide-Width Strip Method*
- 2.11. ASTM D 5262 *Standard Test Method for Evaluating the Unconfined Tension Creep and Creep Rupture Behavior of Geosynthetics*
- 2.12. ASTM E 950 *Standard Test Method for Measuring the Longitudinal Profile of Traveled Surfaces with an Accelerometer Established Inertial Profiling Reference*

3.0 Definitions.

- 3.1. Bidder: An individual, firm, or corporation submitting a proposal for the proposed work.
- 3.2. Contractor: The individual, firm, joint venture, or company contracting with the Owner to perform work.
- 3.3. Design Engineer: The Contractor's licensed Professional Engineer in the State where the project is located per State Statutes, that performs the CSE design.
- 3.4. Engineer: The Owner's project engineer or project manager.
- 3.5. Inspector: The Owner's field representative on the project site.
- 3.6. Owner: Agency responsible for the project.
- 3.7. Plans: The drawings provided by the Owner for bidding purposes.
- 3.8. Proposal (Bid, Bid Proposal). The offer of a bidder to perform the work and to furnish the labor and materials at the prices quoted.
- 3.9. Specifications: The directions, provisions, and requirements contained herein, together with all stipulations contained in the Contract Documents, setting out or relating to the method and manner of performing the work, or to the quantities and qualities of materials and labor to be furnished under the Contract.
- 3.10. Working Drawings: Drawings submitted by the Contractor detailing the CSE work.

4.0 Minimum Contractor Qualifications.

- 4.1. The Contractor constructing the Column Supported Embankment shall have a minimum 5+ years experience installing geosynthetic reinforcement and the column type submitted in the Contractor's bid proposal.
- 4.2. The Contractor shall provide documentation for three recent, successful projects completed with these general site conditions and improvement criteria. The Contractor shall provide names and contact information of individuals who can attest to the adequacy of the work performed. This information shall be submitted in the Contractor's bid proposal.
- 4.3. The Contractor must assign a Project Manager who has been responsible for the CSE work on at least three (3) projects. The Project Manager shall have been in full-time employment of the Contractor for at least two of those projects (provide reference list; minimum number of years/projects in bid proposal). A Design Engineer that is a consultant cannot be the Project Manager.
- 4.4. The CSE shall be designed by the Design Engineer, a Professional Engineer licensed in the State of _____ with experience in the design of at least three successfully completed CSE projects over the past five years. The Design Engineer may be either an employee of the Contractor or a separate Consultant Design Engineer meeting the stated experience requirements.
- 4.5. The Contractor must assign a full-time Project Superintendent with at least three (3) years experience in CSE construction and who has been responsible for a minimum of three (3) CSE projects (provide reference list, years/projects in bid proposal).
- 4.6. Written requests for substitution of these key personnel must be submitted prior to personnel changes. Documentation must be submitted to the Owner that demonstrates that the substitute meets the requirements listed above. Substitution may not be made until written approval is provided by the Owner.

5.0 Equipment.

- 5.1. The equipment required for column installation will vary depending on the column type. Equipment for column installation should meet FHWA criteria for the type of column selected. *[If the owner/engineer restricts the column type, then equipment requirements for one or more column types may be inserted here].*
- 5.2. Equipment for fill and geosynthetic placement shall not cause excessive loads or settlement to the soft ground between columns.

6.0 Materials.

6.1. The select fill shall meet the following gradation requirements:

Size	% Passing
200 mm (4 in.)	100
4.75 mm (No. 4)	70-15
0.425 mm (No. 40)	60-0
0.075 mm (No. 200)	15-0

The select fill shall also have:

$$c_c = \frac{D_{30}^2}{D_{60}D_{10}} = 1 \text{ to } 3, \text{ and } c_u = \frac{D_{60}}{D_{10}} > 4$$

Select fill material passing the No. 40 sieve shall have a liquid limit less than 40 and a plasticity index less than 20.

- 6.2. General embankment fill shall be free from frozen, organic, and otherwise deleterious materials. The gradation (ASTM C 136 / AASHTO T 27 and ASTM C 117 / AASHTO T 11) and Atterberg limits (ASTM D4318 / AASHTO T89 & T90) shall be submitted to the Engineer for approval.
- 6.3. The allowable strength of the geosynthetic (T_a) must be equal to or greater than the required strength (T_g). Allowable tensile strength T_a of the geosynthetic shall be determined using a reduction factor approach to account for creep rupture strength and degradation mechanisms of the reinforcement.

The allowable long-term geosynthetic design tensile strength T_a is:

$$T_g \leq T_a = \frac{T_{ult}}{RF_D \times RF_{ID} \times RF_{CR} \times FS_{UNC}}$$

where, T_a = allowable tensile strength of geosynthetic

T_{ult} = ultimate tensile strength from single or multi-rib tensile strength tests (ASTM D 6637) for geogrids or wide width tensile strength tests (ASTM D 4595) for geotextiles

RF_D = Durability reduction factor is dependent on the susceptibility of the geosynthetic to attack by microorganisms, chemicals, thermal oxidation, hydrolysis and stress cracking. The typical range is from 1.1 to 2.0.

RF_{ID} = Installation damage reduction factor can range from 1.05 to 3.0, depending on backfill gradation and product mass per unit weight.

RF_{CR} = Creep reduction factor is the ratio of the ultimate strength (T_{ult}) to the creep limited strength obtained from laboratory creep tests for each product, and can vary typically from 1.65 to 5.0.

FS_{UNC} = Overall factor of safety or load factor reduction to account for uncertainties in the geometry of the structure, fill properties, reinforcement properties, and externally applied loads. For load transfer platforms, a minimum overall factor of safety of 1.5 is typical.

The specific values for the reduction factors (RF_D , RF_{ID} , RF_{CR}) used in design shall be those established by the National Transportation Product Evaluation Program (NTPEP) and can be found online at: http://www.ntpep.org/ContentManagement/PageBody.asp?PAGE_ID=26. If NTPEP reduction factors are not available for the manufacturer and type of geosynthetic proposed by the Design Engineer, then the values used shall be those recommended by the geosynthetic manufacturer, supported by laboratory testing and as approved by the Engineer.

- 6.4. In addition to the long term allowable strength requirement, there is a serviceability requirement. For serviceability, the geosynthetic must have a creep limited strength at a strain of 5% ($T_{cr@5\%e}$) according to ASTM D 5262 that is equal to or greater than the required strength.

$$T_{cr@5\%e} \geq T_g$$

7.0 Design Requirements.

- 7.1. Available information developed by the Owner, or by the Owner's duly authorized representative (Engineer) includes the following items:

7.1.1. Plans prepared by _____, dated _____.

7.1.2. Geotechnical report No.(s) _____ titled _____, dated _____.

7.2. Columns Requirements

7.2.1. The columns shall be designed to carry the entire vertical load from the embankment and surcharge from the pavement and traffic, with an adequate factor of safety.

7.2.2. The columns shall be designed in accordance with FHWA recommendations for the chosen column type. The column specification is found in Section _____.

- 7.3. The column-supported embankment shall be designed in accordance with FHWA recommendations and/or with numerical stress-strain analysis. The following variables are used in the criteria below: s = column center-to-center spacing, a =

column width, H = embankment height, a_s = area replacement ratio (column area divided by column tributary area). At a minimum, the following criteria shall be satisfied:

- 7.3.1. The clear span between columns shall be less than or equal to the embankment height ($s - a \leq H$) and the clear span shall not exceed 10 ft (3 m) [$s - a \leq 10$ ft (3 m)].
- 7.3.2. The minimum thickness of select fill for the bridging layer (load transfer platform) shall be the larger of 2 ft or $0.5(s - a)$.
- 7.4. The performance requirements for the Column Supported Embankment are as follows:
 - 7.4.1. The total settlement at any point on the surface of the embankment shall not exceed 3 inches.
 - 7.4.2. Differential Settlement [*choose one of the following from 7.4.2.1 or 7.4.2.2. Also choose section*]:
 - 7.4.2.1. The maximum allowable differential settlement shall be 1 inch per 100 feet.
 - 7.4.2.2. Alternate pavement roughness performance criteria for measuring differential settlement: each pavement section shall have an International Roughness Index (IRI) of _____ in/mile (see table below for further guidance) measured 30 to 60 days after completion of paving in accordance with ASTM E 950 and AASHTO R 43-07.

Condition Term	IRI Rating (inches/mile)		Interstate and NHS Ride Quality
	Interstate	Other	
Very Good	< 60	< 60	0 – 170 is Acceptable; Less than Acceptable > 170
Good	60 – 94	60 – 94	
Fair	95 – 119	95 – 170	
Mediocre	120 – 170	171 – 220	
Poor	> 170	> 220	

Table adapted from FHWA’s “1999 Status of the Nation’s Highways, Bridges, and Transit: Conditions and Performance Report”

- 7.4.3. Local stability at the embankment sideslopes and global stability of the Column Supported Embankment shall be achieved with an adequate factor of safety of at least 1.3 [*or other value depending on project performance requirements*].
- 7.5. The CSE system and construction processes shall not cause any additional loading, detrimental settlement, or damage to adjacent facilities or embankments [*allowable tolerances for lateral or vertical movements can be inserted here, if*

applicable]. Monitoring of adjacent facilities and/or embankments noted in the Plans shall be completed in accordance with paragraph 9.6.1.

7.6. [*Insert environmental restrictions, if applicable (noise, vibration and emissions restrictions, air or water pollution constraints, known areas of subsurface contamination, presence of archeologically sensitive areas, etc.)*.]

7.7. [*Refer to known locations of utilities which may interfere with CSE construction as shown on the Plans.*]

8.0 Submittals.

8.1. Following award of the contract and prior to the start of construction, the Contractor shall submit to the Engineer for his approval, all required details, specifications, drawings, construction sequence, design calculations, quality control plan, monitoring plan, and any other required information for the Column Supported Embankment system. The Engineer has the right to require changes as he/she deems necessary to satisfy the performance specification of the Column Supported Embankment with no additional cost to the Owner. The Contractor shall allow a minimum of 30 days for the review of the initial submission and shall also account for the subsequent review and approval process which will depend on the accuracy and quality of the submission documents.

8.2. The following shall be submitted to the Engineer at least 30 days prior to beginning work:

8.2.1. Proposed CSE construction sequence and schedule.

8.2.2. Working drawings and design to the Engineer for review and approval prior to starting of the work indicating the embankment details (material types, elevations, geosynthetic reinforcement, etc), column type, column layout, column size, spacing of columns, column top elevations, and the depth of columns as proposed to achieve the criteria outlined in this specification and the contract plans. The Contractor shall be responsible for providing all lines and grades for columns, including locations of all utilities and survey markers.

8.2.3. [*Column load tests (and/or other performance measure such as materials sampling and testing, core sampling and testing, integrity testing, etc.) are recommended for the ground improvement columns or piles. These performance requirements should be clearly stated in the column specification in Section _____.*]

8.2.4. Gradation, Atterberg limits, and the resulting USCS classification for all fill materials used.

8.2.5. The Contractor shall submit a certificate stating that the reinforcement meets the design requirements for ultimate strength, creep, durability,

installation damage, and coefficient of interaction for sliding in accordance with the design submittal.

- 8.2.6. A detailed written procedure of plans to protect adjacent facilities and embankments from damage, including design calculations [*include this provision if necessary*].
- 8.3. Approval of the proposed design and construction methodologies shall not relieve the Contractor of the responsibility for the safety of the method or equipment used or the responsibility of carrying out the work in full accordance with the requirements of the Contract Documents.
- 8.4. The Contractor shall submit as-built drawings to the Owner no-later-than 30 days following completion of construction. [*Insert as-built requirements here to include electronic and/or hard-copy requirements*].

9.0 Embankment Construction and QC/QA Requirements.

- 9.1. Pre-Construction Meeting: A pre-construction meeting shall be held prior to mobilizing equipment to the project site. At the meeting, the column installation means/methods, observation, acceptance/rejection procedures, testing, and CSE construction procedures shall be discussed and formalized.
- 9.2. Working Drawings
 - 9.2.1. The Contractor shall provide working drawings which shall show the location of each column, as well as the top and bottom elevations. Each column shall be identified with a reference number. The working drawings shall also provide detail on the select fill, geosynthetic reinforcement, and general embankment fill.
 - 9.2.2. An approved set of working drawings and contract specifications shall be on-site at all times during construction of the load transfer platform.
- 9.3. Site Preparation
 - 9.3.1. The Contractor shall ensure a firm base on which heavy equipment can be operated safely under its own power.
 - 9.3.2. The Contractor shall accurately locate the limits of column installation and embankment extents in accordance with the contract plans.
 - 9.3.3. The Contractor shall exercise caution to avoid settlement or damage to existing facilities and settlement, undermining, or instability to existing embankments.
 - 9.3.4. Stability of all the temporary sheeting and/or temporary slopes, if used to facilitate installation of the columns and/or embankment, is the responsibility of the Contractor. The Contractor shall be responsible for any damage caused by his activities at no additional cost to the Owner.

- 9.3.5. The Contractor shall exercise caution and account for the temporary instability that may be caused by ground improvement (if used) until the ground improvement features gain strength with time.
- 9.4. Select Fill Placement and QC/QA Requirements
- 9.4.1. No geosynthetic reinforcement or fill materials shall be placed prior to satisfying the column performance criteria, unless the fill material is required as a working platform for column installation.
- 9.4.2. Instrumentation for performance measurements and instrumentation for monitoring of existing structures and embankments (if required) shall be installed prior to placement of any select fill or geosynthetic reinforcement.
- 9.4.3. Prior to construction of the load transfer platform, the Contractor shall prepare subgrade, and remove any deleterious materials such as tree roots. The foundation soil shall be observed and approved by the Design Engineer and the Engineer or Inspector prior to placement of select reinforced fill.
- 9.4.4. If cementitious ground improvement methods are used, placement of fill material shall not start until the columns have gained adequate strength to support the fill materials and fill installation and construction equipment.
- 9.4.5. Select reinforced fill shall be placed in horizontal layers not exceeding 250 mm (10 in.) in uncompacted thickness for heavy compaction equipment. For zones where compaction is accomplished with hand-operated compaction equipment, fill shall be placed in horizontal layers not exceeding 150 mm (6 in.) in uncompacted thickness.
- 9.4.6. Select reinforced fill shall be compacted to a minimum 95% maximum dry density, as determined in accordance with ASTM D-1557 (modified proctor) at a moisture content no more than 2 percent above or below optimum. This may not be achievable for the first lift of fill because of the weak subgrade between columns, however, subsequent lifts should meet the minimum requirements.
- 9.4.7. Test methods and frequency, and verification of material specifications and compaction, shall be the responsibility of the State.
- 9.5. Geosynthetic Reinforcement Placement and QC/QA Requirements
- 9.5.1. The reinforcement shall be placed at the locations and elevations shown on the Contractors working drawings. No changes to the geosynthetic reinforcement layout, including, but not limited to length, reinforcement type (*i.e.*, strength), direction of reinforcement, or elevation shall be made without the explicit written approval of the Engineer.
- 9.5.2. Construction equipment shall not be operated directly on the geosynthetic reinforcement. A minimum fill thickness of 150 mm (6 in.) is required for operation of vehicles over the reinforcement. Turning of vehicles should be

kept to a minimum to prevent tracks or tires from displacing the fill and/or geosynthetic reinforcement.

- 9.5.3. Minimum overlap of adjacent rolls of reinforcement shall be per the construction Plans or as approved in the Working Drawings.
 - 9.5.4. Each roll of geosynthetic reinforcement should be inspected to ensure that it is undamaged prior to covering with fill material.
 - 9.5.5. Care shall be taken to prevent excessive mud, wet concrete, epoxy, or other deleterious materials from coming in contact with and affixing to the geogrid materials.
 - 9.5.6. Geosynthetic reinforcement shall be stored at temperatures above -20 degrees F (-29 degrees C).
 - 9.5.7. Geosynthetic reinforcement shall not be left directly exposed to sunlight for a period longer than recommended by the manufacturer or one month whichever is shorter.
 - 9.5.8. Any roll or portion of a roll of geosynthetic damaged before, during, and/or after installation shall be replaced.
 - 9.5.9. Large piles of fill material shall not be placed on the geosynthetic reinforcement.
 - 9.5.10. If geotextile seams are specified, the seams should be placed up and every stitch should be inspected.
 - 9.5.11. The Contractor shall remove slack and wrinkles from the geosynthetic prior to placing fill.
 - 9.5.12. The Contractor shall submit the lot numbers and roll numbers along with their locations within the embankment for all geosynthetic reinforcement.
- 9.6. Monitoring Requirements
- 9.6.1. Monitoring of adjacent facilities/embankments [*facilities requiring monitoring should be noted on the Owner's Plans put out for bid*].
 - 9.6.1.1. Identify and permanently mark settlement monitoring locations using paint, concrete nails, concrete embedded brass caps or other accepted survey practice method a minimum of 14 calendar days prior to commencing any construction work.
 - 9.6.1.2. Measure the elevations of the settlement monitoring locations at least twice between their installation and the commencement of construction.
 - 9.6.1.3. Measure elevations of settlement monitoring locations during daylight hours and at the convenience of the property owner. Make prior arrangements with the property owner to allow access to the property to identify monitoring locations and make measurements.

- 9.6.1.4. Measure elevations of the settlement monitoring locations at least weekly after construction has begun. Continue measurements until the Design Engineer determines that the measurements can be discontinued and as approved by the Owner's Engineer.
- 9.6.1.5. Provide report of measurements within 24 hours of measurement to the Engineer for review.
- 9.6.1.6. Remove settlement location monitoring identifying materials and restore locations to their original condition when settlement measurements are discontinued at final Owner acceptance.
- 9.6.2. Monitoring of CSE performance:
- 9.6.2.1. Inclinerometers shall be installed by the Contractor at reasonable intervals, but at a minimum spacing of _____ ft along both embankment toes to monitor lateral movements. Inclinerometer locations shall be included in the design submittals in accordance with paragraph 8.1 and as approved by the Engineer. Inclinerometers shall be monitored at a time interval submitted by the Contractor and as approved by the Engineer and shall demonstrate tolerable lateral movements given the embankment conditions as determined by the Design Engineer and as approved by the Owner's Engineer.
- 9.6.2.2. Surface Settlement Monitoring [*use this section if the criteria in 7.4.2.1 is used*].
- 9.6.2.2.1. The contractor shall identify and permanently mark embankment settlement monitoring locations on the pavement surface using paint, concrete nails, concrete embedded brass caps or other accepted survey practice method within 48 hours of pavement completion. The Contractor shall submit the survey locations in accordance with paragraph 8.1 and shall ensure an adequate number of survey points on the embankment surface above and between the column locations. At a minimum, the Contractor shall provide two survey points for every ___ ft along the embankment alignment, with one survey point located above a column and one survey point located at the centroid of a unit cell formed by the centers of adjacent columns. The pairs of survey points shall be staggered to provide coverage of both sides of the embankment.
- 9.6.2.2.2. The Contractor shall monitor the embankment for a period of _____ days [*recommend 30 to 60 days*] and the performance criteria in paragraph 7.4 shall be satisfied prior to processing the final payment.

9.6.2.2.3. The Contractor shall measure elevations of the settlement monitoring locations at least weekly and provide a report of measurements within 24 hours of measurement to the Engineer for review. The report shall provide the data in reduced and tabulated or plotted form to show a direct comparison between the measured values and the performance criteria. The report shall clearly indicate whether each measurement satisfies the total and differential settlement criteria in paragraph 7.4.

9.6.2.3. Surface Settlement Monitoring [*use this section if the criteria in 7.4.2.2 is selected*] Pavement roughness performance criteria for measuring differential settlement: each pavement section shall have an International Roughness Index (IRI) of _____ in/mile in accordance with Section 7.4.2.2 measured _____ days [*recommend 30 to 60 days*] after completion of paving in accordance with ASTM E 950 and AASHTO R 43-07. The IRI measurement as a performance measure of differential settlement shall be in addition to any other IRI measurements required in the pavement specification section, unless a single IRI measurement can be used to satisfy both requirements. If the definition of multiple pavement sections are warranted based on the size of the project, the location of the pavement sections shall be submitted to the Engineer for approval.

9.6.2.3.1. Roughness data collection should be performed when the pavement is in stable condition. Data should not be collected during winter (frost/freeze or freeze/thaw) or wet base conditions. Data collection should be performed during good weather conditions when wind conditions will not affect equipment stability and on dry pavement. All equipment manufacturers' recommended procedures should be observed. The following general practice rules shall be met:
Temperature: between 40 and 100 F;
Wind: data collection shall not be performed when wind conditions affect the stability of the equipment/vehicle; and
Surface: data collection shall be performed when the roadway surface is dry.

9.6.2.3.2. Data should only be collected at the speeds that correspond to the manufacturer's recommended speed range. Constant speeds should be maintained for all measurements within specified ranges.

9.6.2.3.3. Roughness measurements should be taken over the entire length of the roadway section. However, in order to achieve equipment and speed stability, a minimum run-in length, consistent with the manufacture's specification, may be required prior to the beginning of the measurement area.

9.6.2.4. For quality control and performance measurement, and as recommended by the Design Engineer, the Contractor may elect to install piezometers in the soft soil, load cells or strain gauges on columns, settlement plates and/or earth pressure cells within the embankment fill, and/or strain gauges on the geosynthetic. The plan for installation of this instrumentation shall be submitted in accordance with paragraph 8.1 and approved by the Engineer prior to placement.

10.0 Acceptance Criteria: The Column Supported Embankment is considered acceptable when the embankment construction and QC/QA requirements are completed in accordance with Section 9, compliance with the performance criteria from paragraph 7.4 is demonstrated, and no damage to adjacent facilities is found or compensation is made for damaged caused or damage is repaired at Contractor's expense.

11.0 Measurement: The Column-Supported Embankment shall be measured on a lump sum basis.

12.0 Payment.

12.1. All cost in connection with design, equipment, mobilization and demolization, material, and labor for the construction of the Column Supported Embankment, including soil aggregate and the geosynthetic reinforcements as required in this specification, shall be paid as a Lump Sum. *[if the column specification is combined with this embankment specification, then revise wording to include cost of the columns as well].*

12.2. Separate payment will not be made for site preparation, dewatering, temporary works to facilitate construction, etc. Include all the anticipated cost in price bid item for "Column Supported Embankment."

12.3. *[The Owner/Engineer should specify how the payment will be distributed. Progress payments may be required on larger projects but may not be required on smaller projects. One option for payment distribution, if required, is the following: 10% payment will be made upon submission and acceptance of Column Supported Embankment working drawings. 65% payment will be made upon complete installation of Column Supported Embankment. 25% payment will be made upon acceptance of Column Supported Embankment performance based on reading of geotechnical field instrumentation data and completion of geotechnical field instrumentation monitoring program.]*

CHAPTER 10

SUMMARY, CONCLUSIONS, AND RECOMMENDATIONS

10.1 SUMMARY OF WORK ACCOMPLISHED

The following summarizes the work accomplished in this study.

- An introduction and technology overview of CSEs was provided in Chapter 1 and Chapter 2.
- Existing CSE design procedures were described and ranked in Chapter 3, based on information available in the literature.
- A CSE test facility, as described in Chapter 4, was constructed.
- The materials, equipment, and test procedures used in the CSE tests were described in Chapter 5. To the author's knowledge, this is the first documented use of geof foam for temporary support.
- A series of five instrumented, full-scale, CSE tests were conducted. The tests were described and the results were presented in Chapter 6.
- The results of the CSE tests were analyzed and compared with existing analysis procedures in Chapter 7.
- A generalized formulation of the Adapted Terzaghi Method from Sloan et al. (2011) was presented in Section 8.1.1.
- Two new Parabolic Methods for triangular column arrangements were presented in Section 8.1.2. The first is an axisymmetric approach with radially-isotropic geosynthetic reinforcement and the second is for triangular column arrays with biaxial geosynthetic reinforcement.
- Results of numerical analyses by Filz and Plaut (2009) were compared with results from square and triangular Parabolic Methods in Section 8.1.3. Eleven cases with square column arrangements and one case with an isosceles triangular arrangement and biaxial geogrid were compared. The parabolic methods show good agreement with the maximum strains from the numerical analyses by Filz and Plaut (2009), for the twelve cases presented.
- The recommended CSE design procedure, based on the results of the CSE tests and information in the literature, was presented in Section 8.2. The design recommendations were incorporated into an updated version of the Geogridbridge workbook originally developed by Filz and Smith (2006).
- Recommended QC/QA procedures and a recommended performance specification for CSEs was presented in Chapter 9.

10.2 CONCLUSIONS

The primary conclusions of this study are:

- The critical height for 6.0 ft center-to-center spacing of 2.0 ft diameter columns in a square array, with three layers of Tensar® BX1500 polypropylene geogrid, was shown to be approximately 6.5 ft before trafficking.
- The before-trafficking critical height agrees with the predictions from the bench-scale tests, as expressed in an equation developed by McGuire (2011).
- The addition of two more layers of Tensar® BX1500 geogrid (5 layers total) in a “beam” arrangement did not have a significant impact on the critical height for this column diameter and spacing.
- The critical height after trafficking with a Bobcat skid-steer loader was shown to be approximately 7.5 ft, which is 1.0 ft higher than the before-trafficking case. Thus, the application of vehicle loads to the embankment surface can increase the critical height significantly.
- The Parabolic Method for determining the tension and strain in the geosynthetic reinforcement shows good agreement with the CSE test results. The Kempfert et al. (2004) Method for determining the tension and strain in the geosynthetic reinforcement appears to show a similar trend as the Parabolic Method for this configuration; however, their design chart is only valid for strains up to 6% for the geometry of the CSE tests in this study. The Tension Membrane Method for determining the tension and strain in the geosynthetic reinforcement does not show good agreement with the CSE test results and is unconservative.
- The Adapted Terzaghi Method (Russell and Pierpoint 1997, Russell et al. 2003, Sloan et al. 2011), Hewlett and Randolph (1988) Method, and Filz and Smith (2006, 2007) Method show good agreement with the CSE test results. The other arching methods from Chapter 3 do not show good agreement with the CSE test results.
- The Filz and Smith (2006, 2007) Method shows good agreement with the stress-reduction ratios measured before the geofam was dissolved when the modulus from the geofam unconfined compressive strength tests is used in the GeogridBridge workbook as the soft soil modulus.

10.3 SUMMARY OF RECOMMENDATIONS FOR CSE DESIGN

A full design procedure is found in Chapter 8. Important design recommendations are summarized below.

- The Adapted Terzaghi method with $K = 0.5$ to 1.0 is the recommended method for determining the load on the geosynthetic. Unless future data indicates that a different value should be used, a K value of 0.75 is recommended. Filz and Smith (2006, 2007) and Sloan et al. (2011) contain the equations for 2 layers of fill.
- The fill within a CSE can undergo significant shear strains. The large-strain friction angle should be used for design.
- The Parabolic Method is the recommended method for determining the tension in the geosynthetic. Stress-strain compatibility should be imposed using $\varepsilon = T/J$ rather than assuming a strain of 5% or 6%.
- Soft soil support has an important impact on CSE performance, and it should be included in the CSE design and analysis.
- The overall recommended design procedure is contained in the GeogridBridge spreadsheet described by Filz and Smith (2006, 2007). The spreadsheet uses the Adapted Terzaghi Method for calculating the stress on the geosynthetic reinforcement, the Parabolic Method for determining the tension and strain in the geosynthetic reinforcement, load-displacement compatibility principles for incorporating the support provided by soft soils, and other features described fully in Filz and Smith (2006). The spreadsheet has been updated to allow triangular arrangements in addition to square arrangements. The recommended design procedure using the GeogridBridge spreadsheet is in Chapter 8 of this document.

10.4 RECOMMENDATIONS FOR FURTHER RESEARCH

The following items relating to CSE design and performance should be investigated further:

- Future CSE field tests should be conducted to further evaluate the effect of column diameter and spacing on critical height. The before-trafficking results of the field tests in this study compare well with the bench-scale results of McGuire (2011). Other combinations of column diameter and spacing should be evaluated to determine how the before-trafficking results compare with McGuire (2011). A series of at least two tests, but preferably three tests, for two other combinations of column diameter and spacing (4 to 6 new tests) is recommended. The current

study plus the two additional configurations will yield 3 data points for comparison with the 5 bench-scale configurations tested by McGuire (2011). The after-trafficking critical height in the current study is higher than the critical height predicted by the McGuire (2011) which was determined in bench-scale tests where trafficking is not possible. The field tests with two additional configurations will enable an accurate determination for both the before and after-trafficking cases.

- In future CSE tests, the spacing between the perimeter wall and the outermost 8 columns should be 1.1 to 1.2 times the clear span between columns, particular for higher embankment heights, to avoid boundary effects from the facility walls.
- In future CSE tests, the foil strain gages should not be used due to the length of time required to prepare the geogrid, glue the gages, and establish the electrical connections required for data collection. The gages also debonded at strains lower than the manufacturer's limit. The time investment in the foil strain gages did not seem to be worth the data collected from them.
- Future field tests should be conducted using triangular column arrangements.
- State DOT CSE projects should be instrumented to further study the effect of soft soil support on CSE performance.
- An advanced constitutive model (beyond Mohr-Coulomb linear-elastic, perfectly-plastic) and/or discrete element modeling should be completed for the CSE tests in this study. Ideally, a model could be calibrated to accurately predict the settlements and critical height for the column arrangement and spacing in this study. A advanced constitutive model or discrete element model is recommended due to the difficulty in modeling the geogrid elements (Smith 2005) and the difficulty in achieving reasonable agreement with measured settlement (McGuire 2011) when using a continuum approach. If successful, the model could be used to complete a parametric study and evaluate other configurations of column diameter and spacing.
- Numerical analyses should be conducted to evaluate whether the presence of a competent upper layer and lateral pile capacity within this layer is sufficient to reduce or eliminate the need for geosynthetic reinforcement to resist lateral spreading. The pile capacity may not be as large as would be calculated using customary procedures for laterally loaded piles if the piles and supporting ground move as an integral unit.
- CSEs that are adequately designed with geosynthetic reinforcement to carry the lateral spreading forces and with columns to transfer the embankment load to a bearing layer may or may not require further stability analysis. The presence of the reinforcement and columns may eliminate the need for stability analysis. On

the other hand, some global failure mechanisms may still be possible depending on the strength of the reinforcement, soft soil, and columns. Numerical analysis should investigate the need for further stability analysis when CSEs are adequately designed with geosynthetic reinforcement to resist the lateral spreading stresses.

- Numerical modeling should be accomplished to further assess the Parabolic Method for equilateral triangular arrangements. The method shows good agreement for one analysis contained in Filz and Plaut (2009), but should be evaluated further.
- Further numerical and/or experimental research should be performed to develop criteria for reduction in LTP thickness and/or reduction in critical height for competent soil at the subgrade level.

REFERENCES

- Abdulah, C.H., and Edil, T.B. (2007a). "Behaviour of geogrid-reinforced load transfer platforms for embankment on rammed aggregate piers." *Geosynthetics International*. 14(3): 141-153.
- Abdulah, C.H., and Edil, T.B. (2007b). "Numerical analysis of catenary load transfer platform for Geopier-supported embankment." *GSP 173 Advances in Measurement and Modeling of Soil Behavior*.
- Almeida, M.S.S., Ehrlich, M., Spotti, A.P., and Marques, M.E.S. (2007). "Embankment supported on piles with biaxial geogrids." *Geotechnical Engineering*. 160: 185-192.
- Batista, I.S., Coutinho, R.Q., and Whittle, A.J. (2008). "A case study on the performance of embankments on treated soft ground." *GeoAmericas 2008 Conference*, IFAI, Cancun.
- Bell, A.L., Jenner, C.G., Maddison, J.D., and Vignoles, J. (1994). "Embankment supported using geogrids with vibro concrete columns." *Proc. Fifth International Conference on Geotextiles, Geomembranes, and Related Products*. Singapore. 335-338.
- Bergado, D.T., Jamsawang, P., Tanchaisawat, T., and Lai, Y.P. (2008). "Performance of reinforced load transfer platforms for embankments supported by deep cement mixing piles." *GeoCongress 2008*: 628-637.
- Blume, K., Alexiew, D., Glotzl, F. (2006). "The new federal (Autobahn) A26 in Germany with geosynthetic reinforced embankments on soft soils." *Proceedings of the 8th International Conference on Geosynthetics*, Yokohama, Japan, pp 912-916.
- Brandl, H., Gartung, E., Verspohl, J., and Alexiew, D. (1997). Performance of a geogrid reinforced railway embankment on piles. *Proc. of the Fourteenth Int. Conf. On Soil Mechanics and Foundation Engineering*, Hamburg, 6-12 Sept, Vol. 3, 1731-1736.
- Brandon, T.L., Al-Qadi, I.L., Lacina, B.A., and Bhutta, S.A. (1996). "Construction and instrumentation of geosynthetically stabilized secondary road test sections." *Transportation Research Board Record 1534*.
- British Standards Institution. BS8006 (1995). Code of Practice for Strengthened/Reinforced Soils and Other Fills. London, U.K.
- Cain, W. (1916). *Earth Pressure, Retaining Walls and Bins*, New York, John Wiley and Sons, Inc.
- Camp, W.M., and Siegel, T.C. (2006). "Failure of a column-supported embankment over soft ground." *Proceedings of the 4th International Conference on Soft Soils Engineering*, Vancouver, Canada.
- Cao, W.P., Chen, Y.M., and Chen, R.P. (2006). "An analytical model of piled reinforced embankments based on the principle of minimum potential energy." *GSP 151: Advances in Earth Structures: Research to Practice*. ASCE, 217-224.
- Carlsson, B. (1987). "Reinforced soil, principles for calculation." Terratema AB, Linköping. (In Swedish).
- Chen, R.P., Chen, Y.M., Han, J., and Xu, Z.Z. (2008a). "A theoretical solution for pile-supported embankments on soft soils under one-dimensional compression." *Canadian Geotechnical Journal*, 45: 611-623.

- Chen, Yun-min., Wei-ping, C., and Chen, Ren-peng, (2008b), "An experimental investigation of soil arching within basal reinforced and unreinforced piled embankments". *Geotextiles and Geomembranes* doi:10.1016.
- Chen, R.P., Chen, Y.M., Wang, S.H., and Xu, Z.Z. (2009). "Theoretical study and field tests on pile-supported embankments over soft ground." *Proceedings, US-China Workshop on Ground Improvement Technologies*. ASCE.
- Clara, R.A., Marigliano, A.C.G., and Solimo, H.N. (2009). "Density, viscosity, and refractive index in the range (283.15 to 353.15) K and vapor pressure of α -pinene, d-limonene, (\pm)-linalool, and citral over the pressure range 1.0 kPa atmospheric pressure." *J. Chem. Eng. Data*. 54:1087-1090.
- Chen, R.P., Xu, Z.Z., Chen, Y.M., Ling, D.S., and Zhu, B. (2010). "Field tests on pile-supported embankments over soft ground." *ASCE Journal of Geotechnical and Geoenvironmental Engineering*. 136(6): 777-785.
- Collin, J.G. (2004). "Column supported embankment design considerations." 52nd Annual Geotechnical Engineering Conference- University of Minnesota.
- Collin, J.G. (2007). "U.S. state-of-practice for the design of geosynthetic reinforced load transfer platforms in column supported embankments." *GeoDenver 2007*.
- Collin, J.G., Watson, C.H., and Han, J. (2005). "Column-supported embankment solves time constrain for new road construction." *GSP 131 Contemporary Issues in Foundation Engineering*.
- Collin, J.G., Han, J., and Huang, J. (2006). *Design Recommendations for Column Supported Embankments*. FHWA-HRT-.
- Cuelho, E.V., Christopher, B.R., and Perkins, B.R. (2008). "Small strain and displacement monitoring methods for geosynthetics under monotonic and cyclic loading." *GeoAmericas 2008 Conference, IFAI, Cancun*.
- Dove, J.E., Badillo, B.E., Decker, J.B., Sommerville, J.T., Mauldon, M. and Ware, E. M. (2008). "Remote Characterization of Rock Exposures using Terrestrial LiDAR." *In: Characterization, Monitoring and Modeling of Geosystems*, Geotechnical Special Publication 179, American Society of Civil Engineers, pp. 484-491.
- Dumas, C., Cannon, R.R., Lwin, M.M., Mansukhani, S., McLain, K.W., Pelnik III, T.W., Porbaha, A., Putcha, S., Brown, D., Short, R.D., Macnab, A., and Christopher, B.R. (Report Facilitator) (2003) *Innovative Technology for Accelerated Construction of Bridge and Embankment Foundations*, FHWA-PL-03-014, Federal Highway Administration, U.S. Department of Transportation, Washington, D.C., 90 p.
- Duncan, J.M., Brandon, T., Jian, W., Smith, G., Park, Y., Griffith, T., Corton, J., and Ryan, E. (2007). "Densities and friction angles of granular materials with standard gradations 21b and #57." Report of a testing program performed by the Virginia Tech Center for Geotechnical Practice and Research. 92 p.
- EBGEO 6.9 (2004). *German Recommendations for Geosynthetic Reinforcement*.
- Ellis, E., and Aslam, R. (2009a). "Arching in piled embankments: comparison of centrifuge tests and predictive methods – part 1 of 2." *Ground Engineering*, June.
- Ellis, E., and Aslam, R. (2009b). "Arching in piled embankments: comparison of centrifuge tests and predictive methods – part 2 of 2." *Ground Engineering*, July.
- FHWA (2004). *Ground Improvement Method- Technical Summary #7: Column Supported Embankments*. NHI Course No. 132034. FHWA NHI-04-001.

- FHWA (2011). "Design guide for levee and floodwall stability using deep-mixed shear walls."
- Filz, G.M. and Navin, M.P. (2006). "Stability of column-supported embankments." Virginia Department of Transportation, VTRC 06-CR13.
- Filz, G.M., and Smith, M.E. (2006). "Design of Bridging Layers in Geosynthetic-Reinforced, Column-Supported Embankments," Virginia Transportation Research Council, Charlottesville, Virginia, 46 p.
- Filz, G. M. and Smith, M. E. (2007). "Net vertical loads on geosynthetic reinforcement in column-supported embankments." GeoDenver 2007, GSP-172: Soil Improvement.
- Filz, G.F., and Plaut, R.H. (2009). "Practical implications of numerical analyses of geosynthetic reinforcement in column-supported embankments." *Advances in Ground Improvement: Research to Practice in the United States and China* (GSP 188).
- Filz, G.M., and Templeton, E. (2011). "Design guide for levee and floodwall stability using deep-mixed shear walls."
- Fluet, J.E., Christopher, B.R. and Slaters, A.R., (1986). "Geosynthetic stress-strain response under embankment loading conditions", Proceedings of the Third International Conference on Geotextiles, Vol 1, Vienna, Austria, Apr 1986, pp. 175-180.
- Forsman, J., Honkala, A., and Smura, M. (1999). "Hertsby case: a column stabilized and geotextile reinforced road embankment on soft subsoil." *Dry mix method for deep soil stabilization*, H. Bredenberg, G. Holm, and B.B. Broms, eds., Balkema, Rotterdam, The Netherlands, 263-268.
- Forsman, J. (2002). Geovahvistetutkimus, koerakenteiden loppuraportti 1996-2001 [Georeinforcement-project, final report of test structures 1996-2001], Tiehallinto, Helsinki, Finland (in Finnish).
- Gabr, M.A., Robinson, B., Collin, J.G., and Berg, R.R. (2006). *Promoting Geosynthetics Use on Federal Lands Highway Projects*. FHWA-CFL/TD-06-009.
- Gartung, E., Verspohl, J., Alexiew, D., and Bergmair, F. (1996). "Geogrid reinforced railway embankment on piles – monitoring." *Geosynthetics: Applications, Design and Construction*, DeGroot, Den Hoedt and Termaat (eds). Balkema, Rotterdam.
- Giroud, J.P. (1995). Determination of geosynthetic strain due to deflection, *Geosynthetics International*, Vol. 2, No. 3, pp. 635-641
- Giroud, J.P., Bonaparte, R., Beech, J.F., and Gross, B.A. (1990). Design of soil layer – geosynthetic systems overlying voids, *Geotextile and Geomembranes*, Vol 9, pp. 11-50.
- Guido, V.A., Knueppel, J.D., and Sweeny, M.A. (1987). "Plate loading tests on geogrid-reinforced earth slabs." *Geosynthetics '87 Conference*, New Orleans, 216-225.
- Habib, H.A.A., Brugman, M.H.A., and Uijting, B.G.J. (2002). "Widening of Road N247 founded on a geogrid reinforced mattress on piles." Proceedings, 7th International Conference on Geosynthetics, Delmas, Gourc and Girard (eds). Swets & Zeitlinger, Lisse, 369-372.

- Halvordson, K.A. (2007). “Three-dimensional analysis of geogrid reinforcement used in pile-supported embankments.” Masters Thesis, Virginia Polytechnic Institute and State University.
- Halvordson, K.A., Plaut, R.H., and Filz, G.M. (2010). “Analysis of geosynthetic reinforcement in pile-supported embankments. Part II: 3D cable-net model.” *Geosynthetics International*. 17(2): 68-76.
- Han, J. (1999). “Design and construction of embankments on geosynthetic reinforced platforms supported by piles.” Invited Speaker, ASCE/PaDOT Geotechnical Seminar, Hershey, PA, Apr. 14-16.
- Han, J. and Gabr, M.A. (2002). “Numerical analysis of geosynthetic-reinforced and pile-supported earth platforms over soft soil.” *Journal of Geotechnical and Geoenvironmental Engineering*, 128(1), 44-53.
- Han, J., and Huang, J. (2005). “Development of design charts for geosynthetically reinforced embankments on deep mixed columns.” FHWA National Deep Mixing (NDM) Research Program, Project No: NDM 202.
- Hewlett, W.J. and Randolph, M.F. (1988). “Analysis of piled embankments.” *Ground Engineering*. 21(3): 12-18.
- Horgan, G.J. and Sarsby, R.W. (2002). “The arching effect of soils over voids and piles incorporating geosynthetic reinforcement.” *Geosynthetics – 7th ICG*, 373.
- Hossain, M.D.S. and Rao, K.N. (2006). “Performance evaluation and numerical modeling of embankment over soft clayey soil improved with Chemico-Pile.” TRB2006 Session: Performance and Quality Assessment of Column Supported Embankments.
- Huang, J., Han, J. and Oztoprak, S. (2009). “Coupled mechanical and hydraulic modeling of geosynthetic-reinforced column-supported embankments.” *J. of Geotechnical and Geoenvironmental Engineering*, ASCE: 1011-1021.
- Jenner, C. G., Austin, R.A. and Buckland, D. (1998). “Embankment support over piles using geogrids.” *Proceedings of 6th International Conference on Geosynthetics*, Vol. 1, Rowe, R.K. (ed.), Atlanta, Georgia, March, 763-766.
- John, N. W. M. *Geotextiles*. Blackie & Son Ltd., Glasgow and London, 1987.
- Jones, B.M. (2008). “Reinforcement used in column-supported embankments.” Masters Thesis, Virginia Polytechnic Institute and State University.
- Jones, B.M., Plaut, R.H., and Filz, G.M. (2010). “Analysis of geosynthetic reinforcement in pile-supported embankments. Part I: 3D plate model.” *Geosynthetics International*. 17(2): 59-67.
- Jones, C.J.F.P., Lawson, C.R., and Ayres, D.J. (1990). “Geotextile reinforced pile embankments.” *Geotextile, geomembranes and related products*, Den Hoedt (Ed.), Balkema, Rotterdam: 155-160.
- Kempfert, H.-G., Gobel, C., Alexiew, D. and Heitz, C. (2004a) “German recommendations for reinforced embankments on pile-similar elements.” *EuroGeo3 - Third European Geosynthetics Conference, Geotechnical Engineering with Geosynthetics*, pp. 279-284.
- Kempfert, H.-G., Heitz, C., and Raithel, M. (2004b). “Geogrid reinforced railway embankment on piles, Railway Hamburg—Berlin Germany.” ICGGE.

- Kempton, G. and Naughton, P. (2002). "Piled embankments with basal reinforcement: development of design methods and state of the art." Proc. XV Italian Conference on Geosynthetics, Bologna, Italy.
- Lambrechts, J.R., Ganse, M.A., and Layhee, C.A. (2003). "Soil mixing to stabilize organic clay for I-95 widening, Alexandria, VA." *Proceedings of the 3rd International Conference on Grouting and Ground Treatment*: 575-585.
- Lambrechts, J. R. and Layhee, C. A. (2003). "Stability Analyses of Deep Soil Mix Buttresses in Organic Clay for I-95 Widening, Alexandria, VA." *Proceedings 12th Panamerican Conference on Soil Mechanics and Geotechnical Engineering*: 2097-2104.
- Le Hello, B. and Villard, P. (2009). "Embankments reinforced by piles and geosynthetics—Numerical and experimental studies dealing with the transfer of load on the soil embankment." *Engineering Geology*, Elsevier, 106: 78-91.
- Liu, H.L., Ng, C.W.W., and Fei, K. (2007). "Performance of a geogrid-reinforced and pile-supported highway embankment over soft clay: Case study." *Journal of Geotechnical and Geoenvironmental Engineering*, 133(12), 1483-1493.
- Love, J. and Milligan, G. (2003). "Design methods for basally reinforced pile supported embankments over soft ground". *Ground Engineering*, March, Thomas Telford, pp. 39-43.
- Low, B.K., Tang, S.K., and Choa, V. (1994). "Arching in piled embankments." *Journal of Geotechnical Engineering*, 120:11, 1917-1938.
- McGuire, M. (2011). *Deformation Based Design of Geotechnical Composite Foundation Systems Incorporating Columnar Support with or without Geosynthetic Reinforcement*. PhD Dissertation in progress, Blacksburg, VA.
- McGuire, M.P., and Filz, G.M. (2008). "Quantitative comparison of theories for geosynthetic reinforcement of column-supported embankments," GeoAmericas 2008 Conference, IFAI, Cancun.
- Miki, H. (1997). "Design of deep mixing method of stabilization with low improvement ratio." 1st Seminar on Ground Improvement in Highways, Thailand Department of Highways, Ministry of Transport and Communications and Japan International Cooperation Agency (JICA), 197-204.
- Mitchell, J.M., and Soga, K. (2005). *Fundamentals of soil behavior*. John Wiley and Sons, Inc. Hoboken, New Jersey.
- Naughton, P. J. (2007). "The significance of critical height in the design of piled embankments." GeoDenver 2007, GSP-172: Soil Improvement.
- Navin, M. P. (2005). *Stability of Embankments Founded on Soft Soil Improved with Deep-Mixing-Method Columns*, Ph.D. dissertation, Blacksburg, VA.
- Noguchi, T., Miyashita, M., Inagaki, Y., and Watanabe, H. (1998). "A new recycling system for expanded polystyrene using a natural solvent. Part 1. A new recycling technique." *Paching Technology and Science*, 11:19-27.
- Oh, Y. I. and Shin, E. C. (2007). "Reinforced and arching effect of geogrid-reinforced and pile-supported embankment on marine soft ground." *Marine Georesources and Geotechnology*, 25, 97-118.
- Ohde, J. (1938). Zur Theorie des Erddruckes unter besonderer Berücksichtigung der Erddruck Verteilung, *Die Bautechnik*, Vol 16, pp 150-761.

- Plaut, R. H., and Filz, G.M. (2010). "Analysis of geosynthetic reinforcement in pile-supported embankments. Part III: Axisymmetric model." *Geosynthetics International*. 17(2): 77-85.
- Raithel, M., Kirchner, A., Kempfert, H.-G. (2008). "Pile-supported embankments on soft ground for a high speed railway – load transfer, distribution and concentration by different construction methods."
- Potts, D.M., and Zdravkovic, L. (1999). *Finite Element Analysis in Geotechnical Engineering: Theory*. Thomas Telford, London, UK.
- Potts, V.J., and Zdravkovic, L. (2008). "Finite element analysis of arching behaviour in soils." Proceedings of The 12th International Conference of International Association for Computer Methods and Advances in Geomechanics (IACMAG). Goa, India.
- Potts, V.J., and Zdravkovic, L. (2010). "Finite-element study of arching behavior in reinforced soils." *Ground Improvement*. I63(G14): 217-229.
- Rogbeck, Y., Alen, C., Franzen, G., Kjeld, A., Oden, K., Rathmayer, H., Want, A., and Oiseth, E. (2003). "Nordic guidelines for reinforced soils and fills." Nordic Geosynthetic Group of the Nordic Geotechnical Societies, Nordic Industrial Fund.
- Rogbeck, Y., Gustavsson, S., Sodergren, I., and Lindquist, D. (1998). "Reinforced Piled Embankments in Sweden - Design Aspects." *Proceedings, Sixth International Conference on Geosynthetics*, 755-62.
- Rowe, K.R., and Li, A.L. (2003). "Insights from case histories: reinforced embankments and retaining walls." Keynote Lecture. Landmarks in Earth Reinforcement. Swets & Zeithlinger, Lisse, pp 803-829.
- Russell, D., and Pierpoint, N. (1997) "An assessment of design methods for piled embankments." *Ground Engineering*, Vol. 30, No. 11, November, pp. 39-44.
- Russell, D., Naughton, P.J. and G. Kempton, G. (2003). "A new design procedure for piled embankments." *Proceedings of the 56th Canadian Geotechnical Conference and 2003 NAGS Conference*, Vol. 1, Winnipeg, MB, September – October 2003, pp. 858-865.
- Serridge, C.J. and Synac, O. (2007). "Ground improvement solutions for motorway widening schemes and new highway embankment construction over soft ground." *Ground Improvement*. 11(4): 219-228.
- Shiells, D. P., Pelnik III, T.W., and Filz, G.M. (2003). "Deep mixing: an owner's perspective." *Grouting and Ground Treatment, Proceedings of the 3rd International Conference*, ASCE Special Publication No. 120, New Orleans: 489-500.
- Shin, C., and Chase, G. G. (2005). "Nanofibers from recycle waste expanded polystyrene using natural solvent." *Polymer Bulletin* 55:209-215.
- Sloan, J.A., Filz, G.M., and Collin, J.G. (2011). "A generalized formulation of the Adapted Terzaghi Method of arching in column-supported embankments." *Proceedings of GeoFrontiers 2011*. ASCE. 798 – 805.
- Smith, M. E. (2005). Design of Bridging Layers in Geosynthetic-Reinforced Column-Supported Embankments, Doctoral Dissertation, Virginia Tech, Blacksburg, Virginia.

- Smith, M.E., and Filz, G.M. (2007). "Axisymmetric numerical modeling of a unit cell in geosynthetic-reinforced, column-supported embankments," *Geosynthetics International*, 14(1), 13-22.
- Stewart, M. E., Navin, M. P., and Filz, G. M. (2004). "Analysis of a column-supported test embankment at the I-95/Route 1 interchange." *Geotrans 2004*, 1337-1346.
- Svano, G, Ilstad, T., Eiksund, G., and Watn, A. (2000). "Alternative calculation principle for design of piled embankments with base reinforcement." *Proceedings of the 4th GIGS, Helsinki*, 542-548.
- Terzaghi, K. (1943). *Theoretical Soil Mechanics*.
- van Eekelen, S.J.M, Bezuijen, A., Oung, O. (2003). "Arching in piled embankments; experiments and design calculations." *Foundations: Innovations, observations, design and practice*, Thomas Telford, London, 2003, 885-894.
- van Eekelen, S., Bezuijen, A., Alexiew, D. (2008a). "Piled embankments in The Netherlands, a full-scale test, comparing 2 years of measurements with design calculations." *Proceedings, EuroGeo4*, Edinburgh, UK Chapter, International Geosynthetics Society.
- van Eekelen, S. and Bezuijen, A. (2008b). "Design of piled embankments considering the basic starting points of the British Standard BS8006." *Proceedings, EuroGeo4*, Edinburgh, UK Chapter, International Geosynthetics Society.
- Villard, P, Le Hello, B., Chew, S.H., Nancey, A., Delmas, Ph, Loke, K.H., and Mannsbart, G. (2004). "Use of high-strength geotextiles over piles – results from a full-scale test." *Proceedings of the 3rd European Geosynthetics Conference*, Munich, Germany, Vol. 1, 295-298.
- Virginia Department of Transportation (2007). *Road and Bridge Specifications, Section 208, Subbase and Aggregate Base Material*. p. 142.
- Virginia Test Method (VTM) 25. *Dry Preparation, and Mechanical Analysis of Soils, Select Material, Subbase, and Aggregate Bases-* (Soils Lab). November 1, 2000.
- Vishay Micro-Measurements Instruction Bulletin B-137. *Strain Gage Applications with M-Bond AE-10, AE-15, and GA-2 Adhesive Systems*.
- Vishay Micro-Measurements Instruction Bulletin B-147. *Application of M-Coat J Protective Coating*.
- Vollmy, A. (1937). *Eigebettete rohre*, Mitt. Inst. Baustatik, Eidgen. Tech. Hochschule, Zurich, Mitt. No. 9.
- Wachman, G., and Labuz, J.F. (2008). "TH 241 column-supported embankment." Minnesota Department of Transportation, CTS #08-11.
- Wachman, G.S., Biolzi, L, and Labuz, J.F. (2010). "Structural behavior of a pile-supported embankment." *Journal of Geotechnical and Geoenvironmental Engineering*, ASCE, Vol. 136, No. 1, 26 – 34.
- Wang, B., Li, K., Shi, B., Wei, G. (2009). "Test on application of distributed fiber optic sensing technique into soil slope monitoring." *Landslides*. 6:61-68.
- Warren, K.A., Brooks, J.A., and Howard, I.L. (2005). "Survivability of foil strain gages mounted on geosynthetics under full-scale construction loads." *GRI-18 Geosynthetics Research and Development in Progress*, ASCE.
- Warren, K.A., Brooks, J.A., and Howard, I.L. (2006). "Foil strain gage attachment techniques for geotextile and geogrid." ASCE GeoCongress.

- Warren, K.A., Christopher, B., and Howard, I.L. (2010). "Installation and calibration of strain gages, extensometers, and inductance coils on geosynthetics." Publication TBD.
- West Virginia Division of Highways. (2000). Standard Specifications: Roads and Bridges. Division 300, Section 307: Crushed Aggregate Base Course.
- Whyte, D. (2005). "The overriding aspects of the design of geosynthetic-reinforced pile supported embankments." GSP-131: Contemporary Issues in Foundation Engineering.
- Young, L.W., Minton, M.N., Collin, J.G, Drooff, E., (2004). "Vibro-concrete columns and geosynthetic reinforced load transfer platform solve difficult foundation problem." 22nd World Road Congress.
- Young, L.M., Milton, M.N., Collin, J.G., and Drooff, E.R. (2008) "Vibro-Concrete Columns and Geosynthetic Load Transfer Platform Solve Difficult Foundation Problem", Pan American Geosynthetic Conference, Cancun, Mexico, March 2008.
- Zaeske, D., (2001) "Zur Wirkungsweise von unbewehrten und bewehrten mineralischen Tragschichten über pfahlartigen Gründungselementen." Schriftenreihe Geotechnik, Universität GhKassel, Heft 10.
- Zanzinger, H. and Gartung, E. (2002) "Performance of a geogrid reinforced railway embankment on piles." *Geosynthetics-7th ICG-Delmas*, Gourc & Girard, Swets & Zeitlinger, Lisse 381- 386.

APPENDIX A: FOIL STRAIN GAGE CALIBRATION

Purpose of using Foil Strain Gages in the Column Supported Embankments

Using a 16-channel multiplexer, up to 16 foil strain gages can be installed on the geogrid in each column supported embankment (CSE) test to measure strains at 16 specific locations and orientations. The foil strain gages measure strain at a specific point, whereas lead-wire extensometers, which were also used in the tests, measure an average strain over the distance between attachment points. Compared to lead-wire extensometers, foil strain gages have two distinct advantages. The first advantage is that strains can be measured at 16 different locations, compared to the 6 locations that were possible using draw-wire extensometers. The second advantage is that the foil strain gages can be oriented in any direction on the geogrid. Lead-wire extensometers have to be oriented such that the lead wires run straight out of the embankment to instrumentation located outside the CSE, whereas the wires leading from the foil strain gages can be run in any direction without affecting the measured strains. These advantages make foil strain gages a useful tool to measure the strain of the geogrid reinforcement in the CSE tests.

Compared to lead-wire extensometers, foil strain gages do have limitations when used to measure strains of geogrid. Unlike the lead-wire extensometers, which can be prepared and installed onsite, considerable time is needed to prepare the geogrid layers, bond the gages to the geogrid, apply a protective coating to the gages, and then transport and install the instrumented geogrid onsite. Also, unlike the lead-wire extensometers, the foil strain gages have the potential to debond from the geogrid as the geogrid is loaded, and the readings may be prone to drift with no change in loading.

Due to the advantages and disadvantages for each strain measuring device, both lead-wire extensometers and foil strain gages were used as instrumentation within two of the test embankments.

Previous Use of Foil Strain Gages on Projects

The use of foil strain gages on geosynthetics has been documented in several instrumented roadway tests, including by Brandon et al. (1996), Warren et al. (2005), and Wachman and Labuz (2008). Noted survivability rates of these gages ranged from approximately 28% (Brandon et al. 1996) to 50% (Wachman and Labuz 2008) through the duration of each project. It was noted by Brandon et al. (1996) that most of the gages failed during construction or shortly after construction of the flexible pavement sections. Due to the

high number of gages that survived, the attachment techniques used by Warren et al. (2006) were further considered.

Foil strain gages were installed under seventeen full scale test sections under low-volume, flexible pavement in the project described by Warren et al. (2005). In one section of this research project, testing was conducted to determine the best method to protect the longevity of the strain gages underneath a roadway during and after construction. While data providing the exact strain measurements were not reported for either of the reinforcement materials, it was noted that the strain gages continued to perform under a significant amount of construction traffic. Information regarding the method used to install the stain gages was not provided within this paper. However, Warren et al. (2006) details installation methods for foil strain gages on both geogrid and geotextile. Installation techniques described by Warren et al. (2006) generally follow the minimum standard installation techniques described by Vishay Micro-Measurements, from whom we obtained the strain gages used on this project.

Determining Strains from Foil Strain Gages

Strains are determined with foil strain gages by measuring the amount of voltage returned in response to an input voltage is applied to the circuit. The output voltage changes as the gage elongates because the resistance within the circuit changes as the circuit length increases and the diameter of the conductors decreases. Therefore, if the input voltage is held constant as the gage is elongated, then strains can be determined by relating the output voltage to the length of the gage. The gage is combined with three other resistors in a Wheatstone bridge.

Based on information provided in Vishay's Tech Note TN-507-1, the equation for determining strain from output voltage is provided in Equation 1 shown below.

$$\epsilon \times 10^{-3} = \frac{4 \frac{E_o}{E}}{F \left(1 - .002 \frac{E_o}{E} \right)} \quad (A1)$$

where: E_o = Output Voltage in mV

E = input voltage in V

F = gage factor

ϵ = strain in microstrain $\left(\frac{in}{in \times 10^6} \right)$

Note that this equation provides the measured strain at the specific location of the strain gage and is not the average strain across a specified length of geogrid. Due to the manufacturing process of polypropylene geogrid (punched and drawn), the strength and stiffness varies significantly from location to location on the geogrid. The ribs have strained the most during the manufacturing process and have a locally higher modulus due to strain hardening. The junctions have strained the least and have a locally lower modulus. In addition, the cross-sectional area of polypropylene differs at different locations. Therefore, the gage placement is key, and the calibration factor is dependent on the gage location, whether it is centrally located between junctions or closer to one junction. A calibration factor needs to be applied to the calculated strain to determine the average strain of the geogrid. A description of the procedure used to determine the calibration factor is provided in the section titled Calibration of Foil Strain Gages.

Composition of Strain Gage Circuits

For each strain gage glued to a rib of geogrid, two external terminals were also glued to separate, adjacent ribs. Small lengths of polyurethane coated, 134-AWP copper wire were connected the strain gage to the external terminals. The small lengths of wire were approximately 1 inch in total length, but when strain relief was bent into the wire, the length decreased to approximately ½ inch. An approximate 45-foot length of 22 AWG, coated wire was connected to each strain gage circuit. This 45-foot, 22 AWG, coated wire ran out of the embankment to a bridge completion module located within the waterproof multiplexer housing. Bridge completion modules used in the embankments were Vishay Micro-Measurements type MR1-120-133 external bridge completion modules. The bridge completion modules were connected to a dedicated 16-channel multiplexer with 22 AWG copper wire, which was connected to a Micro-1000 datalogger. A diagram showing the connections used to complete the required circuitry is provided as an attachment to this memorandum.

Initial Testing for Use of Foil Strain Gage

Prior to implementing the foil strain gages in the field, 16 gages were installed and tested on geogrid samples in the lab. These 16 samples were tested to determine a method for installing these gages onto rolls of geogrid and to ensure that the instrumentation was working correctly. Strain gages used in these initial tests were Vishay Micro-Measurements type EP-08-230DS-120 gages. Samples were tested in general accordance with ASTM D6637-01 Method A (Single Rib Specimen Testing). Samples were tested using an Instron 4411, constant rate of strain testing machine. The configuration of the testing machine is shown in Figure A1 below.



Figure A1: Instron 4411 – constant rate of strain geogrid tensile testing machine.

Deviations from this standard testing procedure included testing the samples at a low, constant rate of strain (approximately 1% strain per minute) to provide a longer time until failure, and consequently more points of comparison between the machine strain and the strain measured with the strain gauges. Times from the Instron load frame and the datalogger were synchronized to compare strain measurements. All of the instrumented geogrid samples were tested in the direction transverse to the machine roll direction on BX1500 polypropylene geogrid. Tests were completed at an approximate displacement rate of 0.10 inches/minute.

Revisions to the Vishay's installation method were made over the course of these 16 initial tests. Revisions include prewiring the gages prior to gluing the gages to the geogrid, abrading the geogrid at a 45 degree angle to the rib, and using dead weight to hold the gage in place as the glue cured. The revised procedure was employed to install the foil strain gages for embankment 2. A generalized listing of this procedure is provided in the section titled "General Procedure for Installing Foil Strain Gages on Polypropylene Geogrid".

General Procedure for Installing Foil Strain Gages on Polypropylene Geogrid

Detailed instructions for installing foil strain gages on samples are provided in Vishay Micro-Measurements Instruction Bulletins B-137-16 and B-147-5 dated February 4, 2005 and January 31, 2005 respectively. A generalized 13-step procedure used in this study is provided here.

- 1. Pre-wire the gage by soldering 134-AWP copper wire to the ends of the gage.*
- 2. Abrade each location where strain gage is to be attached using 400 grit sand paper. Abrasions to the geogrid should cross-hatched at an approximate 45 degree angle to the geogrid rib.*

3. *Neutralize and condition each location after abrading in accordance with Vishay's written instructions detailed in Vishay Micro-Measurements Instruction Bulletin B-137-16.*
4. *Using clear tape to move the prewired strain gage and 2 bondable terminals, place each strain gage and terminal at the desired abraded location.*
5. *Place a small amount of M-Bond GA-2 adhesive resin pre-mixed with M-Bond Type 10-A on the grid where the gages and terminals will be located. A small amount of glue should be placed under each gage and terminal as well.*
6. *Press the gages and terminals into the glue, making sure that there are no air bubbles underneath the gages and terminals.*
7. *Place a small piece of rubber below the geogrid underneath each location where a gage and terminal are located. A complementary piece of rubber should be placed on top of each strain gage and each terminal. These pieces of rubber are placed to evenly distribute the weight applied on top of the gages and terminals while the glue cures. An example a rubber piece below the geogrid is shown in Figure A2 below.*

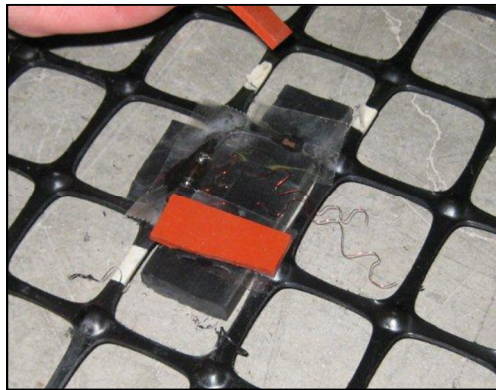


Figure A2: Example of rubber distribution system below a geogrid layer.

8. *Apply a weight on top of the gages and terminals to keep them in place until the glue cures (approximately 24 hours).*
9. *Remove the weights and tape from each gage and terminal. Connect the strain gages to the terminals with short lengths of wire. Connect a 45-foot length of 22 AWG wire to each completed strain gage circuit. This wire will be connected to the bridge completion module at a later time. An example of a strain gage connected to the terminals, with strain gage relief, is shown in Figure A3 below.*

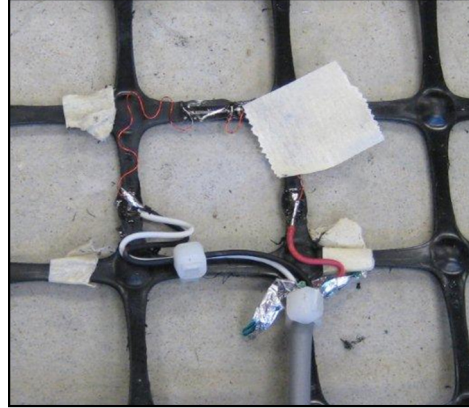


Figure A3: Strain gage connected to external terminals with strain relief.

10. Apply a liberal amount of M-COAT J-3 polysulfide protective coating to each completed circuit, and allow the coating to dry for approximately 24 hours. An example of a strain gage circuit coated in this protective material is shown in Figure 4 below.

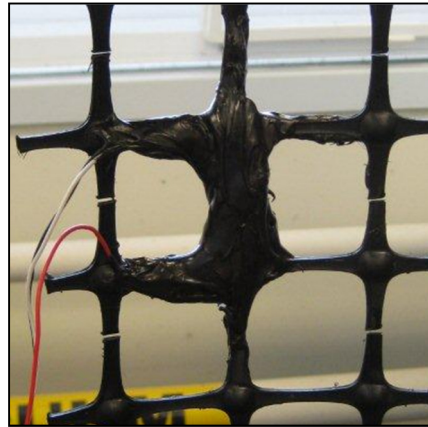


Figure A4: Strain gage encased in M-Coat J-3 Protective Coating.

11. Wrap each completed circuit in electrical tape. An example of a circuit encased in the protective coating wrapped in electrical tape is shown in Figure 5 below.

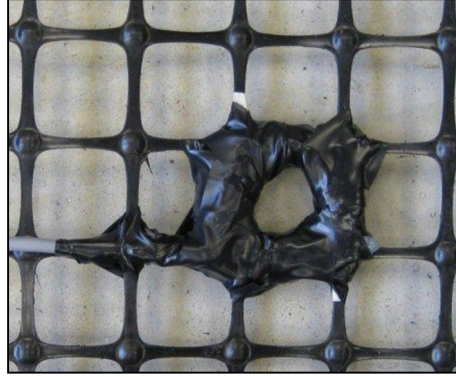


Figure A5: Strain gage encased in protective coating and wrapped in electrical tape.

12. Transport the layers of geogrid to the project site and complete the circuits to the data logger using an external bridge completion module.
13. Carefully place fill on top of the circuits in a manner that will not puncture the protective coating or tape.

Calibration of Foil Strain Gages

Due to the manufacturing process of polypropylene geogrid, local strength and stiffnesses vary significantly along the length of a rib. Because of this difference, the strain measured by a foil strain gage must be calibrated in order to determine the average strain for the entire length of the specimen. A generalized equation to determine the average strain is given in Equation (A2) shown below.

$$\varepsilon_{machine} = CF * \varepsilon_{FSG} \quad (A2)$$

where: $\varepsilon_{machine}$ = Average strain over entire sample as measured by tensile testing machine

CF = Calibration Factor

ε_{FSG} = Strain measured by foil strain gage

Samples were tested in general accordance with ASTM D6637-01 using an Instron 4411, constant rate of strain testing machine. Strains measured by the foil strain gages attached to the geogrid samples were compared to strains measured by the machine. A calibration factor can be determined for any value of strain measured by both the testing apparatus and the foil strain gage. An average calibration factor for a sample was determined by averaging the calibration factors over a range of strains measured by the machine. Typically, this range was over the entire range that the foil strain gage remained bonded to the geogrid sample (i.e.: 0% strain to the strain at debonding). In some cases however, the strains measured by the foil strain gages did not closely match up over the entire

range of the measurements. In these cases, the calibration factor for the sample was determined over a smaller range of strains (i.e.: 2% strain to the strain at debonding). Specific details for calibration testing for each embankment are provided in the sections below.

Foil Strain Gage Calibration Testing for Embankment 2

Samples were prepared and tested following the generalized procedure up to the application of the protective coating system. Calibration factors for these tests were 1.37 and 1.22. After these tests, 3 additional samples were prepared with the protective coating applied to the test sample. Results from these tests were comparable to the results from two of the previous, non-coated samples, with calibration factors of 1.11, 1.34, and 1.25. These results indicated that the protective coating system did not change the overall stiffness of the geogrid samples. ***Based on the results of these 5 tests, a calibration factor of 1.25 was developed for strain gages used in embankment 2.*** Results of the laboratory calibration tests, as well as applied load versus strain charts, are provided in Figures A6 to A10.

Foil Strain Gage Calibration Testing for Embankment 4

Due to an approximate 2 month lead time required to produce the strain gages in Embankment 2, different types of strain gages were used to instrument the geogrid in Embankment 4. The general purpose strain gages used in Embankment 4 are Vishay Micro-Measurements type EP-08-125AD-120. The installation of these gages was completed following the same general procedure as listed above with the exception that excess material was trimmed from each of the gages prior to the installation of these gages on the geogrid. The 125AD gages are wider than the 230DS gages and some of the excess backing material was trimmed so the gages fit on the geogrid ribs.

A total of eight gages were installed onto geogrid samples and tested to determine a calibration factor for the type EP-08-125AD-120 gages. Three of these tests were omitted from consideration because the corrected data produced from the strain gage did not match the data produced from the testing machine. This difference is most likely to have been caused by the gage not completely bonding to the geogrid sample. Results from the remaining tests varied, with calibration factors of 1.40, 1.72, 1.28, 1.30, and 1.31. **Based on the results of these tests, a calibration factor of 1.40 was developed for the strain gages used in embankment 4.** Results of these 5 tests, as well as applied load versus strain charts, are provided in Figures A11 to A15.

Performance of Foil Strain Gages in the Embankments

Foil strain gages were installed onto layers of geogrid for each of two CSE tests using the generalized procedure listed above. In general, the foil strain gages tended to debond more quickly in the field compared to the tested samples in the lab. The following sections describe the performances of the strain gages in both embankments.

Performance of Foil Strain Gages in Embankment 2

Sixteen EP-08-230DS-120 gages were installed on two layers of Tensar® BX1500 geogrid reinforcement from June 30 to July 2, 2010. These geogrid layers were cut from roll number 310725A, lot number 056. Seven strain gages were installed on the lowest layer (directly on top of columns) and 9 gages were installed on the second layer (6 in. above columns). One strain gage on each layer was observed to be installed improperly after the dead weight was removed. Wiring for these two gages was therefore not completed. After completion of the circuitry wiring, each of the remaining gages were coated in Vishay's M-COAT J-3 polysulfide protective coating system and loosely wrapped in electrical tape. Both layers were transported and installed into embankment 2 on July 19, 2010.

After installation, it was determined that three of the gages (two gages from the first layer and one gage from the second layer) were not functioning properly. These gages were disconnected from the datalogger, and no further data was collected from them. After construction of the embankment was completed and prior to the foam dissolver being introduced underneath the embankment, it was observed that 4 of the remaining 11 gages had either electrical problems producing drift within the data or the gages seemed to partially debond from the geogrid. These problems caused the data collected from these gages to be deemed unreliable. 5 of the remaining gages debonded quickly after the introduction to the foam dissolver underneath the embankment. Debonding occurred at corrected strains ranging from 1.4% to 5.2%. At the time of the demolition of the embankment, the remaining two gages had approximate strains ranging from 1.1% to 1.7%. Diagrams showing the locations of the foil strain gages and charts showing the performance of the strain gages corresponding to each CSE test are shown in Chapter 6.

Performance of Foil Strain Gages in Embankment 4

Sixteen gages were installed on two layers of BX1500 grid reinforcement on July 30, 2010. Four of the gages were installed on the first layer of geogrid and 12 gages were installed on the second layer. The specific lot and roll number for these two sheets of geogrid are not known, as the roll was not labeled for shipping. After the weight was removed from each of the gages, it was observed that 2 of the gages did not bond to the geogrid.

Circuitry was completed on the remaining 14 gages on August 18, 2010. These gages were then coated using Vishay’s M-COAT J-3 polysulfide protective coating system and wrapped in electrical tape from August 19 to August 20, 2010. Both layers were transported and installed in embankment 2 on September 7, 2010. Only 13 gages were connected to the data logger in the field due to the limited number of working bridge completion modules.

Based on data collected after the layers of geogrid were placed and installed, it was determined that two of the gages on the second layer were not working. These two gages were disconnected from the datalogger and were not further considered. Two gages debonded from the second layer of the geogrid at the time the foam dissolver was introduced underneath the test embankment. These gages debonded at approximate corrected strains of 2.8% and 3.2%. Five of the remaining nine gages debonded at some point prior to demolition of the embankment. These gages debonded at approximate corrected strains ranging from 0.7% to 5.1%. At the time of the demolition of the embankment, the remaining four gages had approximate strains ranging from 0.8% to 1.9%. Diagrams showing the location of the foil strain gages and charts showing the performance of the strain gages corresponding to each CSE test are shown in Chapter 6.

Performance Summary of Foil Strain Gages used in the Embankments

The following table provides a summary of the performance of the foil strain gages.

Table A1: Summary of foil strain gage performance in CSEs #2 and #4.

CSE Test	Number of Gages Installed	Gage Problems Experienced				Remaining Functional Gages
		Improper Gage Gluing or Bonding	Gages with Electrical Problem After Installation	Gages Experiencing Drift	Gages That Debonded During Testing	
2	16	2	5	2	5	2
4	16	2	2	0	7	4*
*Note: One gage from Embankment 4 not connected due to limited number of working bridge completion modules.						

These results compare closely to the results presented by Brandon et al. (1996), in which only 28% of the gages survived. Like the results of Brandon et al. (1996), the gages that failed typically failed during construction or shortly thereafter.

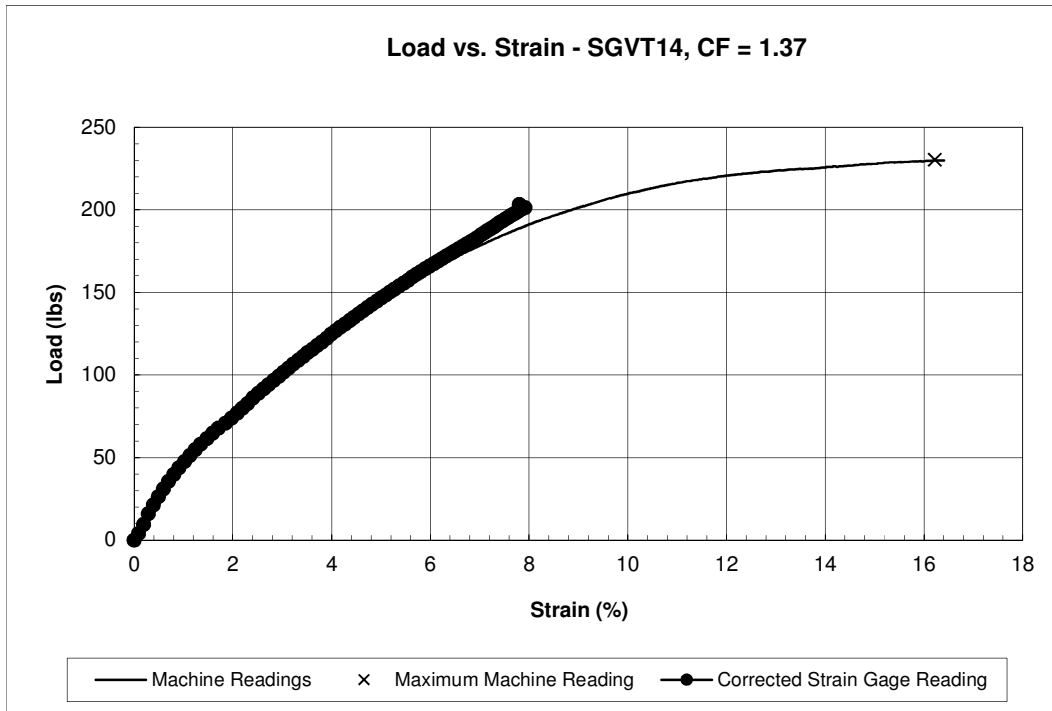


Figure A6: Calibration of EP-230DS foil strain gages for CSE #2.

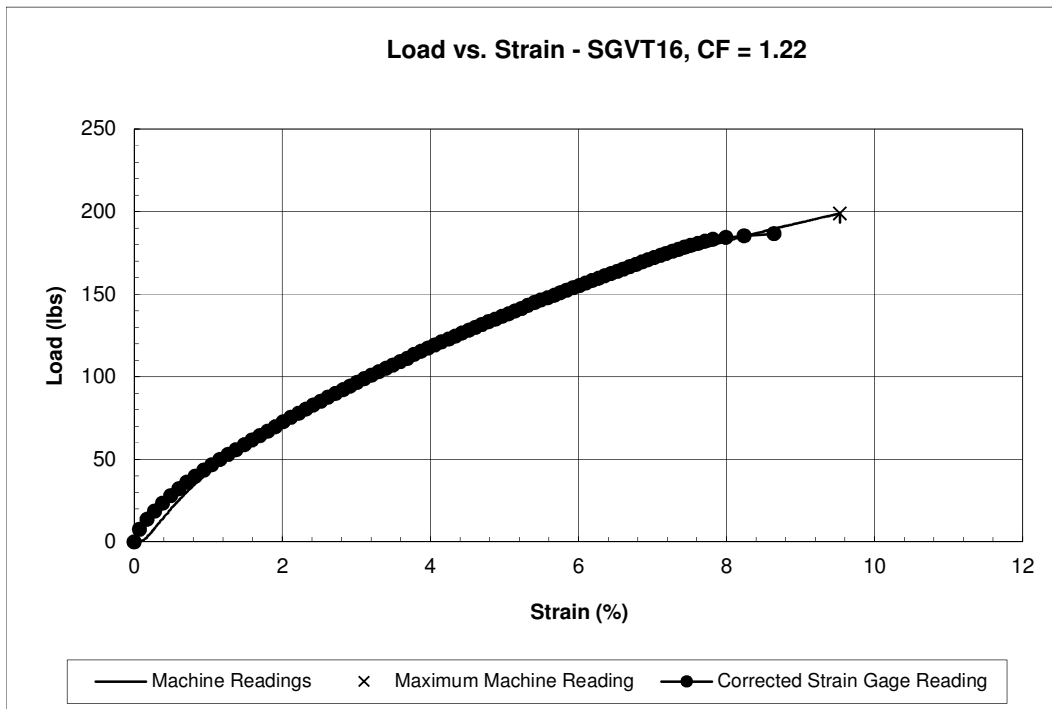


Figure A7: Calibration of EP-230DS foil strain gages for CSE #2.

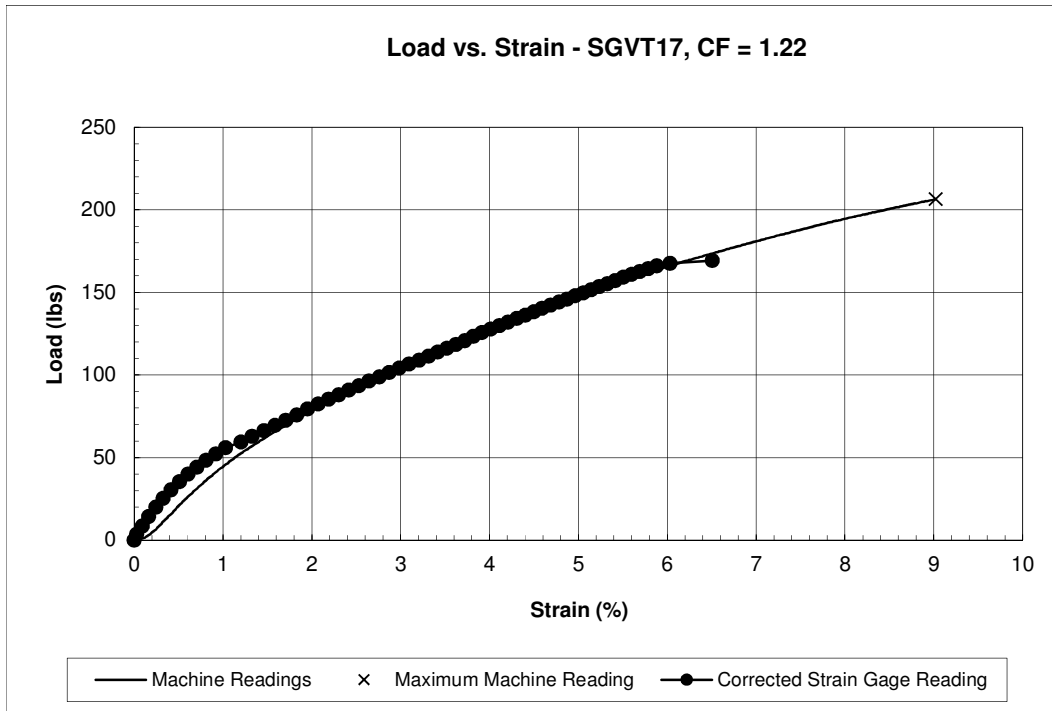


Figure A8: Calibration of EP-230DS foil strain gages for CSE #2.

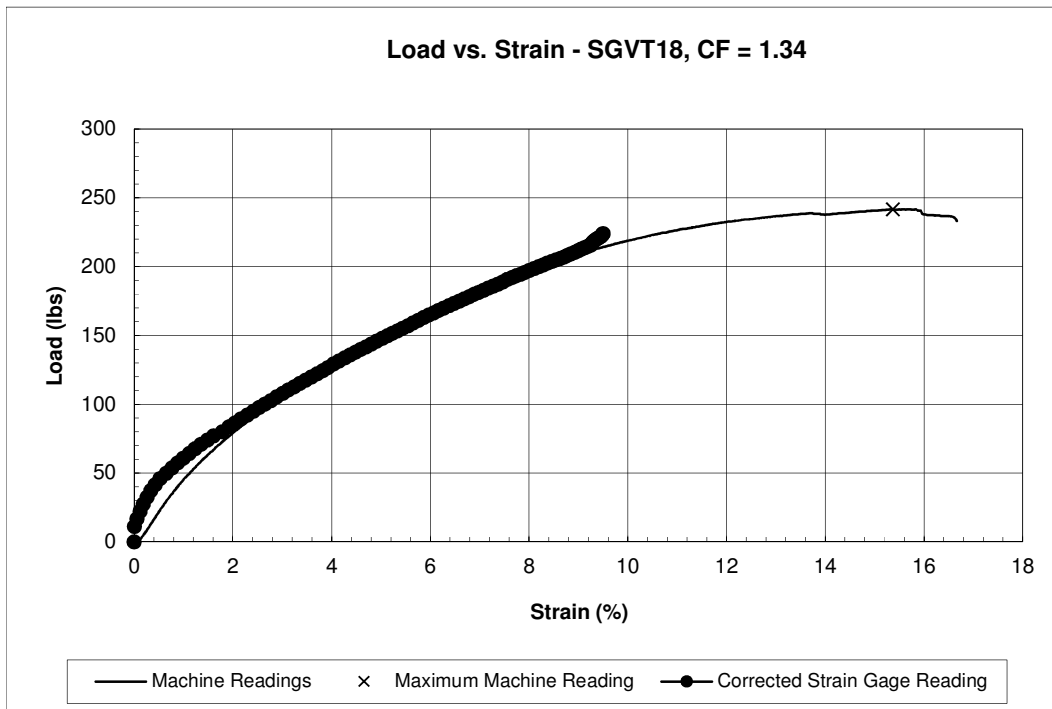
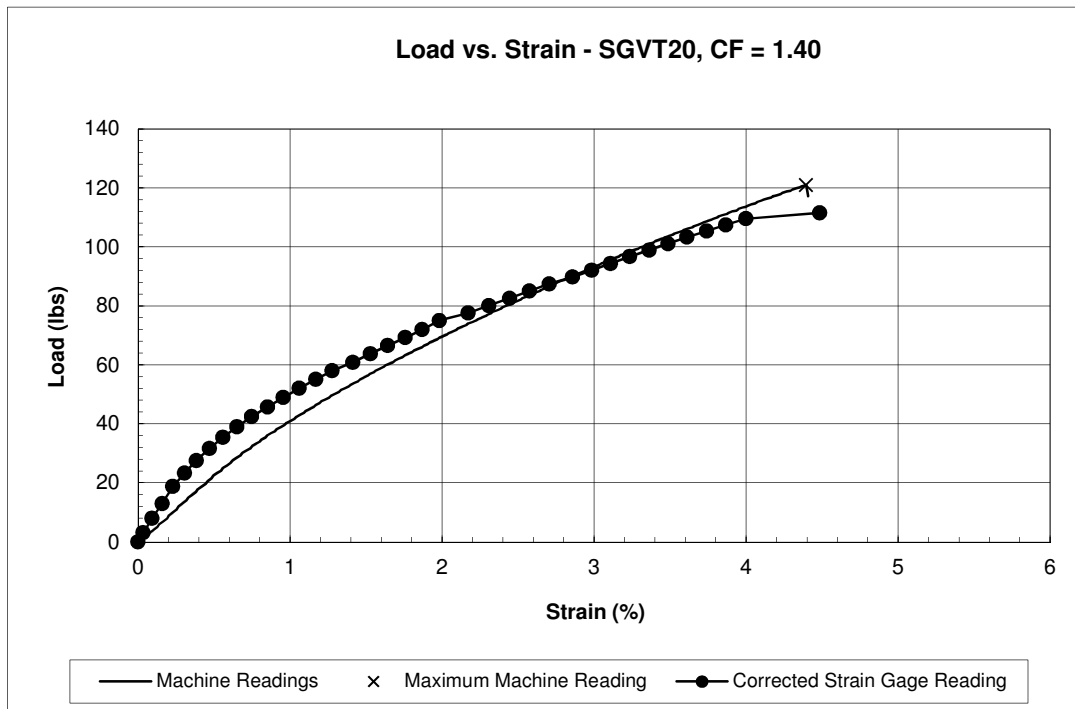
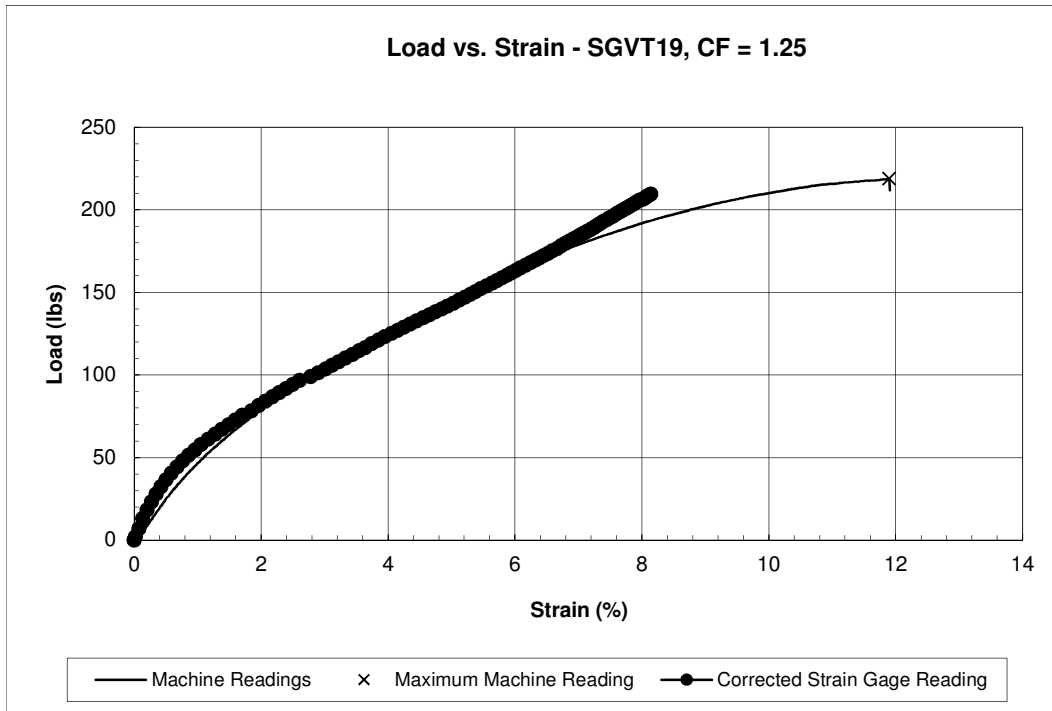


Figure A9: Calibration of EP-230DS foil strain gages for CSE #2.



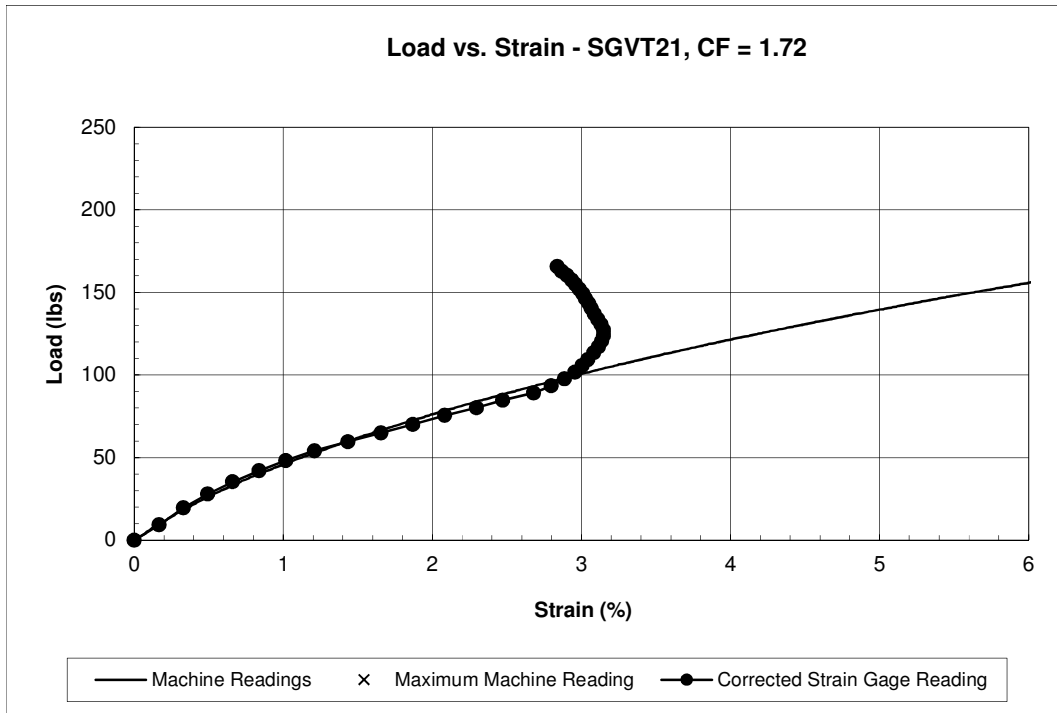


Figure A12: Calibration of EP-125AD foil strain gages for CSE #4.

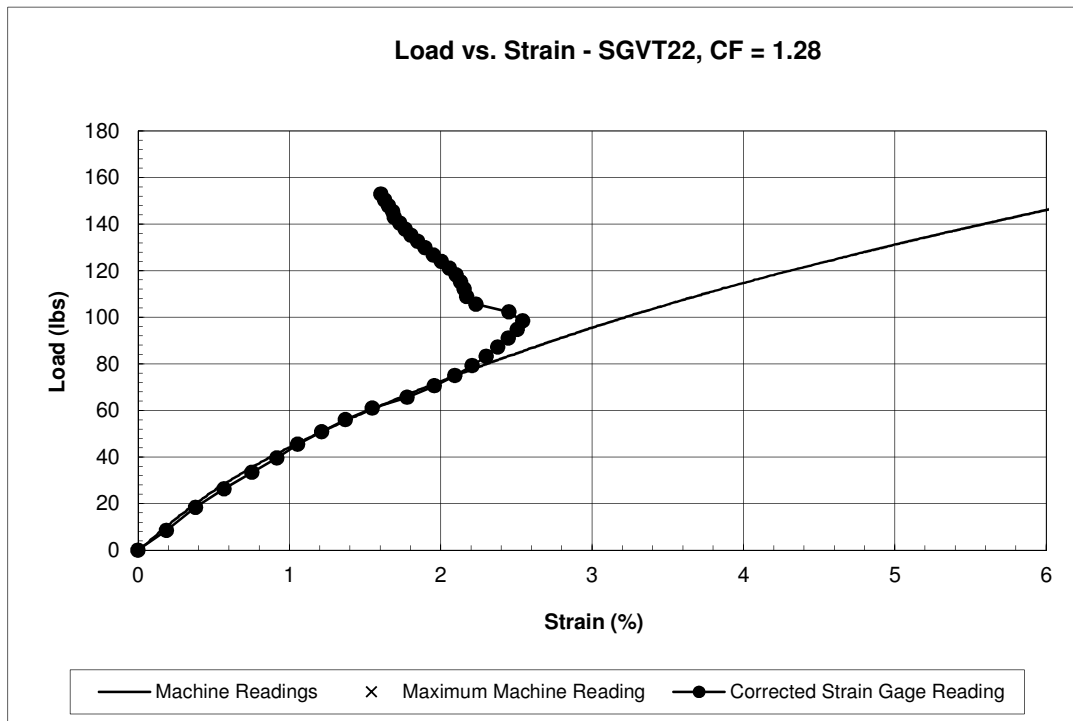


Figure A13: Calibration of EP-125AD foil strain gages for CSE #4.

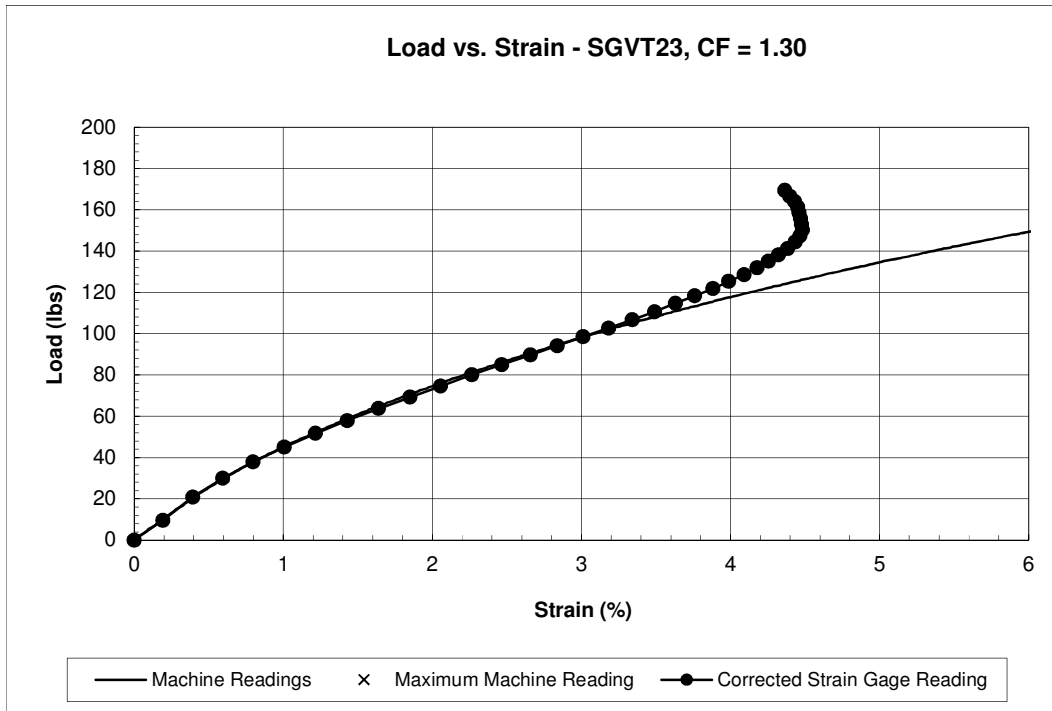


Figure A14: Calibration of EP-125AD foil strain gages for CSE #4.

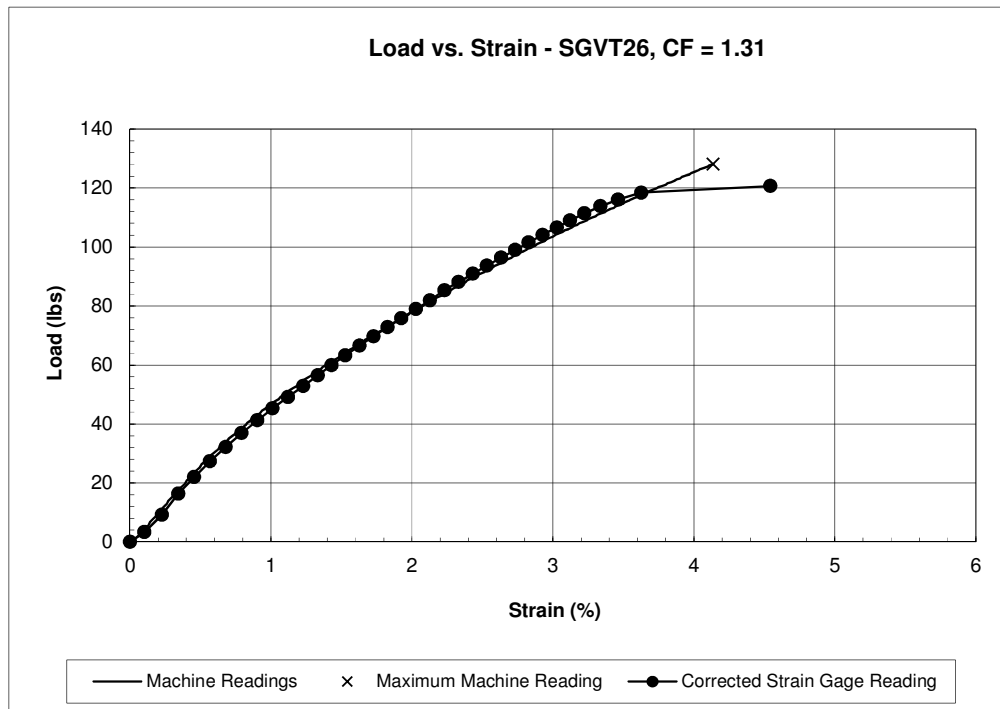


Figure A15: Calibration of EP-125AD foil strain gages for CSE #4.

APPENDIX B: GEOGRID TESTING

This appendix provides a summary of the results of tensile strength testing of geogrid samples used as reinforcement in compacted gravel fill for research on Column Supported Embankments for the SHRP2 R02 project. Tensile strength testing was conducted on selected geogrid samples from CSEs #1 through #5 to determine accurate strengths for use in future analysis.

Sampling/Testing Procedure

Testing of geogrid samples was completed in general accordance with ASTM D6637-01 Method A (Single Rib Specimen Testing). Samples were allowed to equalize to the testing atmosphere for approximate periods of 24 hours or more prior to testing. Samples were trimmed to lengths ranging from approximately 12 to 13 inches long and three ribs wide. The outermost ribs were cut in accordance with ASTM D 6637 and the tensile strength on the central ribs was measured. Samples were tested using an Instron 4411, constant rate of strain testing machine. A picture showing the configuration of the testing machine is shown in Figure B1 below.



Figure B1: Instron 4411, constant rate of strain testing machine.

Samples were held in the machine using 1-inch by 2 inch, screw side action, smooth-faced clamps. A strain rate of 10% per minute was applied to each of the samples until rupture. Applied load and displacement data was collected by the testing machine at intervals of approximately one second during testing.

Geogrid samples used in these tests were collected from the remainder of rolls of geogrid used in the construction of the test embankments. Material type, lot number, roll number, embankment number, and lift number are shown in Table B1 below. Specific lot and roll numbers of the rolls used in Embankments 2 and 3 are not known because the delivered

rolls were not labeled with this information. Tables B2 (machine direction) and B3 (transverse machine direction) show the average strengths and strains for each roll of geogrid tested.

Table B1: List of Geogrid Rolls Tested for Tensile Strength

Roll ID	Tensar® Material Type	Embankment and Lift Number, if known
Lot 310731, Roll 011	BX1500	1, Lift 1
Lot 112440, Roll 010	BX1500	1, Lift 2
Embankment 2, Lift 1	BX1500	2, Lift 1
Embankment 2, Lift 2	BX1500	2, Lift 2
Embankment 3, Lift 2	BX1500	3, Lift 2
Lot 113008, Roll 011	BX1500	4
Lot 310730	BX1500	4
Lot 310720, Roll 032	BX1500	5
Lot 310720, Roll 036	BX1500	5
Lot 310720, Roll 03X	BX1500	5
Lot 113184, Roll 096	BX1200	1
Embankment 1, Lift 4	BX1200	1, Lift 4
Embankment 1, Lift 5	BX1100	1, Lift 5

Five samples were tested in both the machine and transverse directions for each roll. An additional sample was tested if a sample was observed to slip during the test or if the sample ruptured prematurely compared to other samples of similar material type. Results of samples that slipped or ruptured at strengths well below accepted strengths at the measured strains were omitted and were not considered in calculating average roll values per ASTM Standard D6637-01.

Testing Results

Data from each of the tests completed was interpreted to determine strengths per unit length at 2% elongation, 5% elongation, the ultimate tensile strength, and strength at rupture. The strain at the ultimate tensile strength and the strain at rupture were also recorded. Strengths per unit length were determined by multiplying the applied load by the number of ribs per unit length in the direction perpendicular to loading. This number varied by material type and direction. The approximate number of ribs used to determine these strengths are listed in Table B4 shown below.

Table B2: Summary of geogrid testing, machine direction.

Test Name	Machine Direction						
	Maximum Load (lbs)	Strength per Unit Length at 2% Elongation (plf)	Strength per Unit Length at 5% Elongation (plf)	Ultimate Strength per Unit Length (plf)	Strain at Ultimate Strength (%)	Strength at Rupture (plf)	Strain at Rupture (%)
MARVs for BX1500	--	580	1200	1850	--	--	--
MARVs for BX1200	--	410	810	1310	--	--	--
MARVs for BX1100	--	280	580	850	--	--	--
BX1500, Lot 310731, Roll 011	220	618	1211	1933	18.7	1798	25.8
BX1500, Lot 112440, Roll 010	231	653	1254	2032	15.2	2020	16.2
Emb 2, Lift 1	215	655	1233	1884	14.7	1862	16.4
Emb 2, Lift 2	214	576	1164	1882	14.3	1797	15.8
Emb 3, Lift 2	219	640	1219	1922	14.4	1880	18.3
BX1500, Lot 113008, Roll 011	235	703	1332	2063	13.3	2030	15.3
BX 1500, Lot 310730	225	667	1288	1980	12.9	1976	13.8
BX1500 Lot 310720 Roll 032	226	589	1208	1988	16.4	1977	17.6
BX1500 Lot 310720 Roll 036	224	603	1208	1965	16.1	1932	17.3
BX1500 Lot 310720 Roll 03X	216	628	1200	1900	15.9	1881	17.6
BX1200, Lot 113184, Roll 096	200	711	1348	2042	14.1	2023	16.6
Emb 1 Lift 4	194	487	947	1512	14.5	1471	22.1
Emb 1 Lift 5	128	369	704	1012	11.8	991	12.5

Table B3: Summary of geogrid testing, transverse machine direction.

Test Name	Transverse Machine Direction						
	Maximum Load (lbs)	Strength per Unit Length at 2% Elongation (plf)	Strength per Unit Length at 5% Elongation (plf)	Ultimate Strength per Unit Length (plf)	Strain at Ultimate Strength (%)	Strength at Rupture (plf)	Strain at Rupture (%)
MARVs¹ for BX1500	--	690	1370	2050	--	--	--
MARVs for BX1200	--	620	1340	1970	--	--	--
MARVs for BX1100	--	450	920	1300	--	--	--
BX1500, Lot 310731, Roll 011	231	972	1821	2849	13.7	2840	14.5
BX1500, Lot 112440, Roll 010	218	982	1777	2693	24.1	2623	24.7
Emb 2, Lift 1	220	950	1788	2716	12.6	2696	13.1
Emb 2, Lift 2	221	964	1839	2734	12.1	2603	12.7
Emb 3, Lift 2	220	978	1884	2722	11.3	2694	11.7
BX1500, Lot 113008, Roll 011	232	951	1844	2865	13.4	2819	15.0
BX 1500, Lot 310730	230	997	1919	2842	12.4	2807	12.8
BX1500 Lot 310720 Roll 032	229	932	1849	2832	12.9	2810	13.5
BX1500 Lot 310720 Roll 036	231	666	1752	2862	12.1	2838	12.5
BX1500 Lot 310720 Roll 03X	237	1036	1955	2932	13.6	2836	14.6
BX1200, Lot 113184, Roll 096	200	711	1348	2042	14.1	2023	16.6
Emb 1 Lift 4	205	683	1335	2097	15.2	2095	16.3
Emb 1 Lift 5	139	479	963	1404	12.1	1390	13.6

Table B4: Approximate Number of Ribs per Linear Foot for Material Type and Testing Direction

Material Type	Transverse Direction	Machine Direction
BX1500	12.4	8.78
BX1200	10.2	7.80
BX1100	10.2	7.92

In general, failure occurred by rupture of the geogrid sample at a junction point as shown in Figure B2 below. The specific junction where the rupture occurred varies by test but always occurred between the clamp faces. While it may not be seen within the picture shown below, fraying of ribs was typically observed.

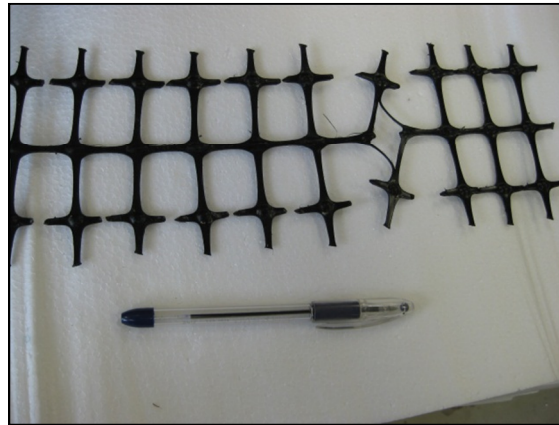


Figure B2: Example of ruptured geogrid sample.

The following sections provide summaries of testing completed for the three material types tested (BX1500, BX1200, and BX1100).

Interpretation of Testing Results

Average strengths for each of the rolls tested exceeded the unit strengths published by Tensar® for 2% elongation, 5% elongation and ultimate unit strength. This behavior is generally expected since the strengths published by Tensar® are Minimum Average Roll Values (MARV) and individual sample tests should generally be higher than the MARVs. Based on documentation provided by Tensar®, MARVs are determined by averaging the strength values from many sample rolls of a specific type of geogrid and subtracting two standard deviations from this strength.

While the average of each roll of geogrid exceeded the MARVs, the differences between average strengths in this study and the corresponding MARVs varied with each strain

level and each roll. The percent increase in strength above the MARVs at 2% elongation, 5% elongation, and ultimate strengths were calculated for each roll tested. The equation for Percent Increase in Strength is shown below.

$$\text{Percent Increase in Strength (\%)} = \frac{\text{Measured Value} - \text{Tensar MARV}}{\text{Tensar MARV}} \times 100\%$$

Values of average percent increase in strength for each of the specific rolls tested are provided in Tables A7 through A12. A summary of the average percent increase in strength for each of the strengths listed in the MARVs for each material type is listed in Table B5.

Table B5: Summary of Average Percent Increase in Strength above MARV for Each Material Type Tested

Material Type	Designated Strength	Transverse Direction	Machine Direction
BX1500	2% Strain	38.0%	9.7%
	5% Strain	36.9%	3.5%
	Ultimate Strength	38.7%	6.3%
BX1200	2% Strain	12.4%	16.7%
	5% Strain	0.3%	17.7%
	Ultimate Strength	5.0%	18.4%
BX1100	2% Strain	6.5%	31.8%
	5% Strain	4.7%	21.4%
	Ultimate Strength	8.0%	19.0%

The somewhat erratic variations in percent increase in strength listed in Table B5 may be due to imperfections in each roll caused by the manufacturing process or damage to samples caused by the clamping force used to hold the samples in place and not allow the samples to slip.